

RSC Medicinal Chemistry

Accepted Manuscript

This article can be cited before page numbers have been issued, to do this please use: A. Amaya-Flórez, J. R.-Galindo, E. Sanchez-Yocue, A. Ruiz-Martinez, J. S. Serrano-García, A. Romo-Pérez, P. Cano-Sánchez, V. Reyes-Marquez, R. Le Lagadec and D. Morales-Morales, *RSC Med. Chem.*, 2025, DOI: 10.1039/D5MD00178A.



This is an Accepted Manuscript, which has been through the Royal Society of Chemistry peer review process and has been accepted for publication.

Accepted Manuscripts are published online shortly after acceptance, before technical editing, formatting and proof reading. Using this free service, authors can make their results available to the community, in citable form, before we publish the edited article. We will replace this Accepted Manuscript with the edited and formatted Advance Article as soon as it is available.

You can find more information about Accepted Manuscripts in the [Information for Authors](#).

Please note that technical editing may introduce minor changes to the text and/or graphics, which may alter content. The journal's standard [Terms & Conditions](#) and the [Ethical guidelines](#) still apply. In no event shall the Royal Society of Chemistry be held responsible for any errors or omissions in this Accepted Manuscript or any consequences arising from the use of any information it contains.

Cyclometalated Complexes: Promising Metallodrugs in the Battle Against Cancer

Andrés Amaya-Flórez,^a Jordi R.-Galindo,^a Elkin Sanchez-Yocue,^a Adrian Ruiz-Martinez,^a Juan S. Serrano-García,^a Adriana Romo-Pérez,^a Patricia Cano-Sanchez,^a Viviana Reyes-Marquez^b, Ronan Le Lagadec^a and David Morales-Morales^{a,*}

^a*Instituto de Química, Universidad Nacional Autónoma de México, Circuito Exterior, Ciudad de México, CP 04510, México.* ^b*Departamento de Ciencias Químico-Biológicas, Universidad de Sonora, Luis Encinas y Rosales S/N, Hermosillo 83000, Sonora, México.*

E-mail: damor@unam.mx; Fax: +52-5556162217; Tel: +52-5556224514

Abstract

Metal-based treatments are an excellent alternative as drugs for oncological treatment and research. The success of *cisplatin* and its derivatives has been a clear example of how such compounds can play an important role in cancer therapy. However, the low selectivity, side effects, and resistance associated with this drug have led to the search for new strategies to overcome these limitations. For this reason, organometallic compounds are gaining significant attention as potential antitumor agents. Compared to platinum-based drugs, these compounds often exhibit greater stability, better lipophilicity, higher selectivity, and reduced resistance in cancer cells. This review aims to illustrate the antitumor properties of cyclometalated compounds containing metals from groups 8, 9, and 10. It will also highlight various biochemical studies that attempt to explain how these compounds can enter cells, the different molecular targets, and the types of cell death they can trigger.



1. Introduction

Since the discovery of the first organometallic compound, Zeise's salt,¹ an extremely important field of research emerged that successfully bridged the areas of organic and inorganic chemistry. Organometallic compounds are characterized by the presence of a metal-carbon covalent bond, and they have been widely employed as catalysts,²⁻⁴ in the design of new materials,⁵⁻⁷ in energy technology,⁸⁻¹⁰ and in medicinal chemistry.¹¹⁻¹³ Over the years, this discipline has been honored with 13 Nobel Prizes in Chemistry, including the elucidation of the crystal structure of vitamin B12, highlighting the importance of organometallic compounds in life sciences, making them attractive for study in biology and medicine.

The first organometallic compound used as a drug was *salvarsan*, an organoarsenic compound used for the treatment of syphilis. Following, the discovery of *ferrocene* has been one of the cornerstones for the synthesis of new bioorganometallic compounds, demonstrating antimicrobial,¹⁴⁻¹⁶ antioxidant,^{17,18} and antitumor properties.^{19,20} Subsequently, another metallocene, *titanocene dichloride*, which exhibited antitumor properties was discovered and became the first organometallic compound to reach clinical trials. Due to these developments, today, many rationally designed and synthesized organometallic compounds have been created as potential cytotoxic agents for cancer treatment.

Undoubtedly, *cisplatin* has been the drug of choice for the treatment of various cancers, being the first metal-based drug approved by the Food and Drug Administration (FDA) in 1978, for the treatment of testicular, ovarian, and bladder cancers. However, due to its low selectivity and the side effects, it was necessary to improve its cytotoxic activity and selectivity.²¹⁻²⁵ As a result, platinum-based drugs have undergone three generations, of which five drugs (**Figure 1**) have been clinically approved, two globally (*carboplatin* and *oxaliplatin*) and three regionally; in Japan (*nedaplatin*) in China (*lobaplatin*) and in the North Korea (*heptaplatin*),



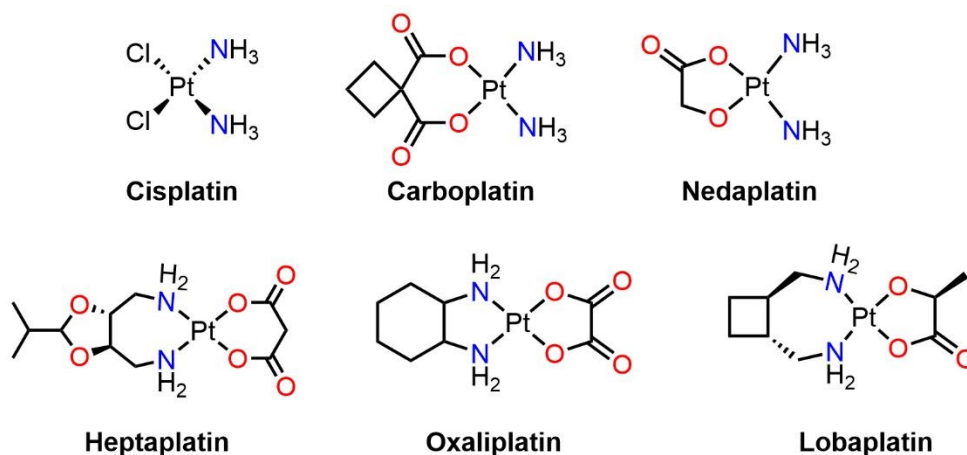


Figure 1. Platinum metallodrugs approved for cancer treatment.

It has been proved that one of the main molecular targets of platinum drugs is DNA by coordination with nucleobases.²¹ This target is non-specific for cancerous cells and could lead to resistance development and lack of tumor selectivity. Therefore, the design of new metal-based compounds should focus on biomolecules or biological processes that improve selectivity, increase cancer inhibition, and reduce side effects. These properties would be obtained by targeting specific biochemical processes related to cancer, through complex antitumor mechanisms and avoiding drug resistance.²⁶⁻²⁸

In this context, organometallic complexes exhibit great structural versatility, meaning they can adopt various geometries (usually ranging from linear to octahedral). On the other hand, versatility can be also offered by ligands and oxidation state modification, tuning intracellular properties like kinetic stability, and lipophilicity.²⁹ Depending on the type of ligand, antitumor organometallic compounds can be classified into six categories: metal arenes, metal acetylides, metal carbonyls, metal carbenes, metal cyclopentadienyls (Cp), and cyclometalated complexes (**Figure 2**).²⁶

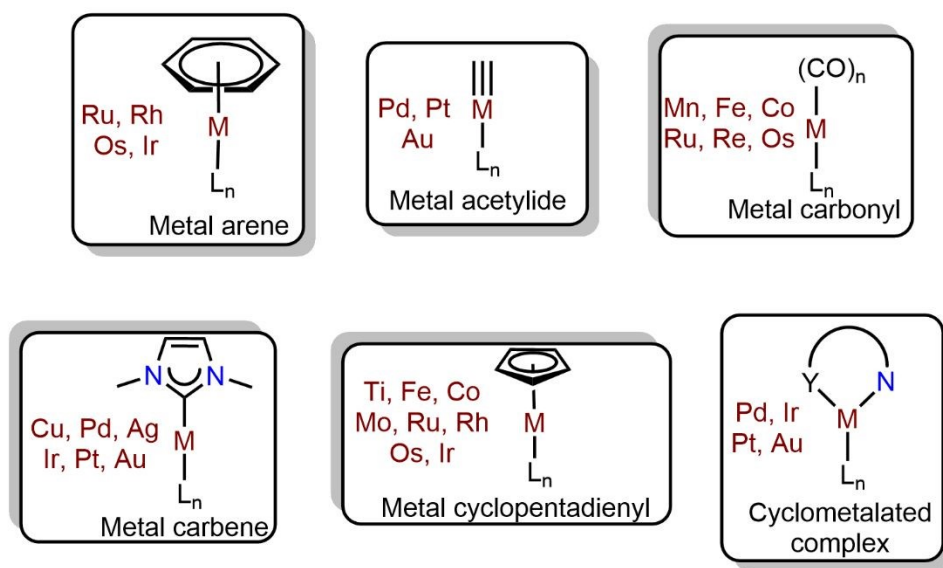
From this perspective, arene and cyclopentadienyl complexes have been among the most remarkable organometallic structures in terms of anticancer activity for various reasons. For instance, their typical geometries can be classified into two main types. On one hand, the so-called *piano-stool* structures are characterized by an aromatic ring (arenes or cyclopentadienyls) as the central component, which plays a crucial role due to its hydrophobic nature, facilitating the entry of these complexes into the cell. Additionally, they may contain monodentate ligands X and Y or a chelating X[^]Y unit, along with a leaving group Z, which is often a halogen. Modulating the electronic and steric properties of ligands X, Y, and Z allows for fine-tuning the anticancer properties of these compounds, enhancing the synergy between metal centers and ligands.^{30,31}



On the other hand, cyclopentadienyl complexes not only adopt a *piano-stool* conformation but can also form *sandwich-type* structures, such as ferrocene, enabling the functionalization of organic groups on the cyclopentadienyl moiety to improve the cytotoxic properties of these complexes.³² Along the same lines, complexes derived from N-heterocyclic carbenes (NHCs) have gained significant attention in medicinal chemistry, as they can form stable bonds with various metal centers. Moreover, the synthesis of these compounds is relatively simple compared to other organometallic structures. The stability of these complexes is influenced by the aromaticity of the NHC ligand and the nature of the substituents that can be incorporated into the ligand backbone, allowing for fine-tuning of steric, electronic, and lipophilic properties.³³

Regarding carbonyl complexes, it has been demonstrated that at low doses, CO exerts beneficial effects on physiopathological functions, preventing inflammation and oxidative stress. This has led to the development of CO-releasing molecules (CORMs), focusing on metal centers, as they provide greater molecular design flexibility, enabling control over the number and spatial arrangement of CO ligands, which in turn allows for a broader range of CO release.³⁴

As for metal acetylides, these complexes are characterized by a metal center bonded to one or more alkynyl units through a σ -bond. Such structures have attracted attention due to their unique physicochemical, photophysical, and photochemical properties, with the latter two being particularly relevant for their application in theranostic therapy.³⁵ For a more in-depth discussion on the anticancer activities of the organometallic compounds, the following references may be of great use.³⁶⁻⁴⁵



Antitumor organometallics



Figure 2. Organometallic compounds used as antitumor agents.

Finally, cyclometalated complexes have played a significant role in medicinal chemistry over the past twenty years. Unlike the previously mentioned organometallic compounds, these complexes can form bi- or tridentate chelates, which confer greater stability and allow them to coordinate with a wide variety of transition metals. Furthermore, due to the structural diversity these compounds offer, they can give rise to all five of the previously described organometallic structures. For example, a bicyclic metalated structure can form arene, cyclopentadienyl, or carbonyl-type compounds, while a tricyclic metalated structure can yield N-heterocyclic carbene or acetylide complexes as auxiliary ligands.⁴⁶⁻⁴⁸

Metals such as Fe, Ru, and Os have demonstrated superior performance compared to platinum complexes, as they have been shown to exhibit mechanisms of action distinct from cisplatin, targeting molecular sites other than DNA and activating cell death pathways different from apoptosis.⁴⁹⁻⁵¹ On the other hand, Ir and Rh have displayed remarkable photophysical and photochemical properties, making them particularly attractive for applications in photodynamic therapy (PDT) and theranostic therapy.⁵²⁻⁵⁴ Lastly, despite belonging to the same group as platinum, Ni and Pd complexes have exhibited more efficient cytotoxic properties and distinct mechanisms of action compared to cisplatin.^{55,56} Moreover, platinum itself has been a constant subject of study, aiming to develop more selective designs that enhance its specificity toward cancer cells while reducing toxicity to healthy cells.^{57,58}

Based on the discussion so far, the rich structural diversity offered by organometallic complexes makes them promising candidates for the design of new metallodrugs, enabling the disruption of cancer cell homeostasis and the activation of various cell death pathways, which allows them to be used as a unique class of therapeutic agents for cancer treatment.

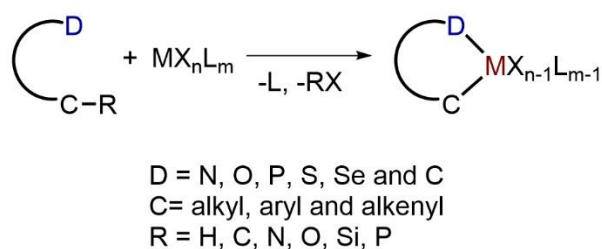
This review aims to provide an overview of the literature on the anticancer properties of bi- and tridentate cyclometalated compounds of groups 8, 9, and 10 published since 2014. This is aimed to explore the effects of these organometallic compounds from the perspective of the metal center as well as the organic ligands, and how this synergy enables great versatility in the different modes of action these complexes can offer in cancer therapy.

2. Formation and types of cyclometalated complexes with d-block metals

The formation of cyclometalated compounds occurs through the activation of a transition metal over a C-R bond to form a chelate with a σ M-C bond and a coordination bond D-M (D = N, O, P, S, Se, and C) (**Scheme 1**). This type of reaction consists of two consecutive steps: first, the coordination of



the metal center to the donor atom D, followed by the intramolecular activation of the C-R bond to close the cycle.^{59,60}



Scheme 1. Formation of cyclometalated compounds.

These types of compounds are characterized by their great thermodynamic and redox stabilities, as well as the ability to adjust the steric and electronic properties of the anionic ligands (X) or auxiliary ligands (L) to obtain compounds with enhanced lipophilic character. Depending on the type of ligand desired, cyclometalated compounds can be classified as **CD** type, which is usually mononuclear or dinuclear (Figure 3a), and **DCD** type, which bears tridentate ligands to form two metallacycles. These complexes can possess more than one carbon atom as donor atoms (**CC**, **DCC**, **CCC**) and the carbon atom is not restrictively the central atom (**DDC**). If the tridentate ligand adopts a meridional geometry around the metal center, they are known as pincer complexes (Figure 3b).⁶¹ Complexes with more than three donor atoms are less common.

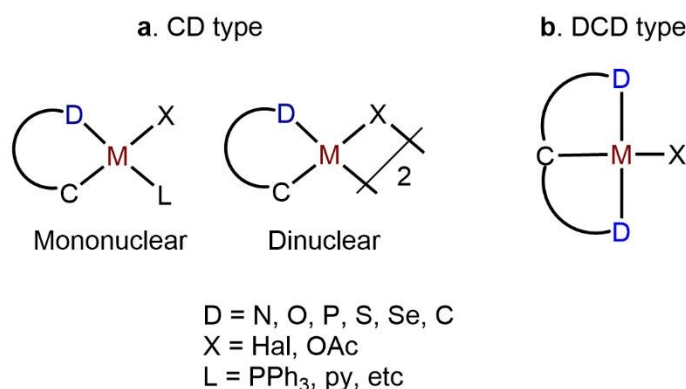


Figure 3. Types of cyclometalated compounds: **a)** CD type and **b)** DCD type.

This review will start with cyclometalated compounds from group 8 (Fe, Ru, and Os), followed by groups 9 (Rh and Ir) and 10 (Ni, Pd, and Pt).



3. Cyclometalated compounds of group 8

3.1. Iron

Iron is an essential element for human life, and it is present in important biomolecules like hemoglobin and iron-sulfur clusters (Fe-S), which are required for energy metabolism, respiration, and so on.⁶² Moreover, cancerous cells require higher iron demand due to higher mitochondrial activity. These processes can be altered with iron complexes, which would lead to reactive oxygen species (ROS) production and cell death.^{63,64} For that reason, Le Lagadec's group has synthesized a series of C^N cyclometalated Fe(III) and Fe(II) complexes (**1-Fe** and **2-Fe**) (**Figure 4**), which have been used in cytotoxicity studies.^{65,66}

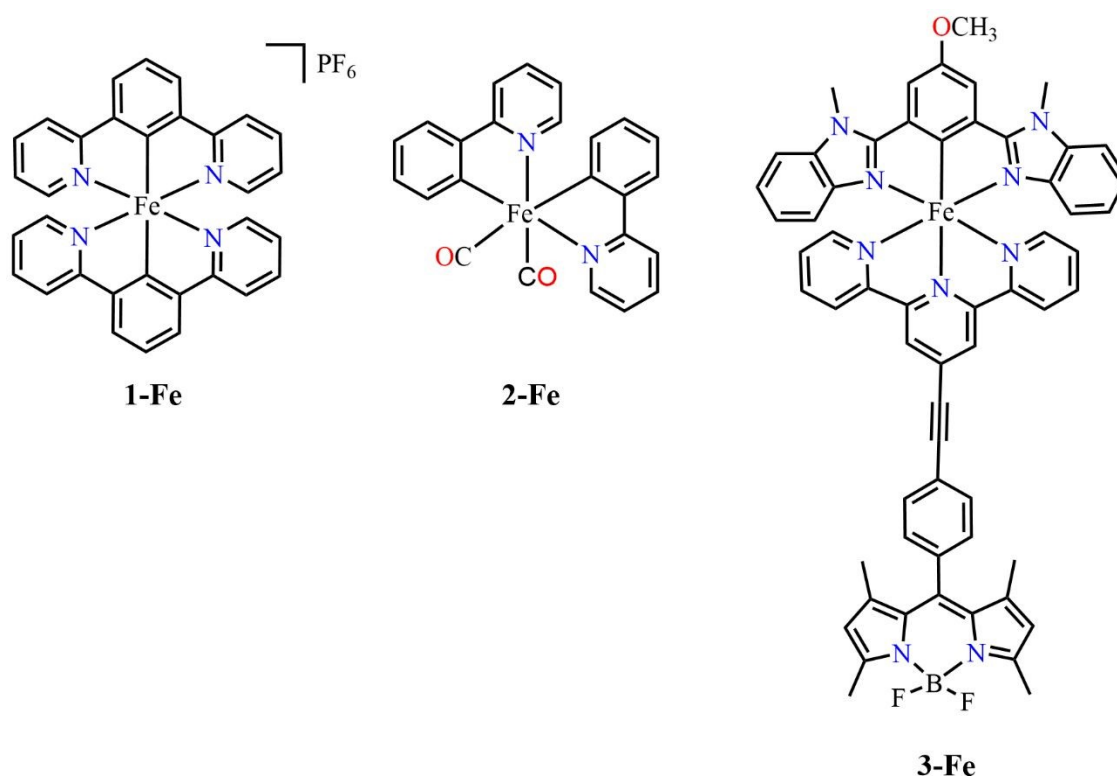


Figure 4. Cyclometalated Fe(III) (**1-Fe**) and Fe(II) (**2-Fe** and **3-Fe**) complexes evaluated in cytotoxicity studies.

1-Fe was tested on human colon cancer (HCT-15), lung cancer (SKLU-1), and two types of gastric cancer cell lines (AGS and KATO III). These cancer cell lines are distinguished by the type of p53 tumor suppressor gene they typically express. For instance, AGS expresses a wild-type p53, whereas KATO III expresses a mutated form of p53, which leads to a form of resistance in cancer cells to DNA-damaging chemotherapy. **1-Fe** was shown to be more active than *cisplatin* in all cancer cell



lines, with IC_{50} values ranging from 0.2 to 0.8 μM . Western blot assays revealed that **1-Fe** induces cell death through a pathway independent of p53 and caspase 3 but strongly induces ATF4 (Activating Transcription Factor 4) in AGS cells. Additionally, there was a reduction in the ratio of two forms of LC3 (an autophagy marker), suggesting that **1-Fe** causes cell death via a pathway involving endoplasmic reticulum (ER) stress and autophagy.⁶⁵ On the other hand, the **2-Fe** complex was tested on three gastric cancer cell lines: AGS, KATO III, and NUGC3, the latter carrying a Y220C mutation in p53 (**Table 1**).

Table 1. IC_{50} values of the **2-Fe** complex on three gastric cancer cell lines: AGS, KATO III, and NUGC3a.

Compound	IC_{50} (μM)		
	AGS	KATOIII	NUGC3
2-Fe	4.1 ± 0.6	42 ± 1.1	26 ± 1.2
<i>cisplatin</i>	29 ± 1.3	11 ± 0.9	18 ± 1.1

^a Cell viability determined by MTT assay after treatment for 48 h

Regarding the possible mechanism of action, it was found that, unlike the **1-Fe** complex, **2-Fe** does not promote an increase in ATF4 protein (a marker of the endoplasmic reticulum stress response pathway). The results indicate that **2-Fe** reduces the survival of gastric cancer cells, but the molecular mechanisms involved appear to be independent of caspase-induced apoptosis, TP53 stabilization, and ATF4 expression.⁶⁶

Tabrizi prepared a cyclometalated Fe(II) complex (**3-Fe**) that has two tridentate ligands: one of the NCN type, which corresponds to the cyclometalated ligand, and one NNN ligand, where a BODIPY fragment is attached to a meso-phenyl-4'-ethynyl-2,2':6'2"-terpyridine. Phototoxicity assays showed a higher cytotoxicity in HeLa cancer cells after irradiation at 500 nm (IC_{50} value of 1.0 μM) than that in the dark (IC_{50} value of 73 μM), yielding a phototoxicity index (PI) of 69.7. It was also observed that exhibits good absorption in HeLa cells and that its target organelle is the mitochondria.⁶⁷

3.2. Ruthenium

Many ruthenium complexes have displayed elevated cytotoxicity and selectivity against cancerous cell lines, being an attractive alternative to platinum-based drugs.⁶⁸ Ruthenium compounds can also be used as prodrugs, which are later activated inside the cell via photo-activation or ligand oxidation



for instance.⁶⁹ Ruthenium complexes such as NAMI-A, KP1019, and NKP1339 have reached clinical trials, but more investigation is needed to offer improved treatment against cancer.^{70,71}

Bipyridine and phenanthroline ligands

In recent years, Le Lagadec's group has synthesized a series of Ru(II) cyclometalated compounds (**1a-Ru** to **5b-Ru**), testing them as potential anticancer agents (**Figure 5**). Complexes **1a-Ru** to **3-Ru** were used to determine the *in vitro* cytotoxicity on two different gastric cancer cell lines, KATO III and AGS. Cytotoxicity assays using the MTT protocol were conducted both in the absence and presence of light, (**Table 2**). The coordination analog of complex **1a-Ru** (complex **3-Ru**) was included for comparison purposes. All cyclometalated compounds demonstrated greater activity in the presence of light for both cancer cell lines, being more active than *cisplatin* and the **3-Ru** compound. The highest phototoxicity index (PI) was obtained for complexes **1b-Ru** and **2b-Ru** with PI values from 2.56 to 5.70. Both compounds can produce singlet oxygen ($^1\text{O}_2$), while the **3-Ru** compound did not generate this radical. In addition, **1b-Ru** was able to damage DNA and cleave caspase 3 (an apoptosis marker) upon light irradiation.⁷²



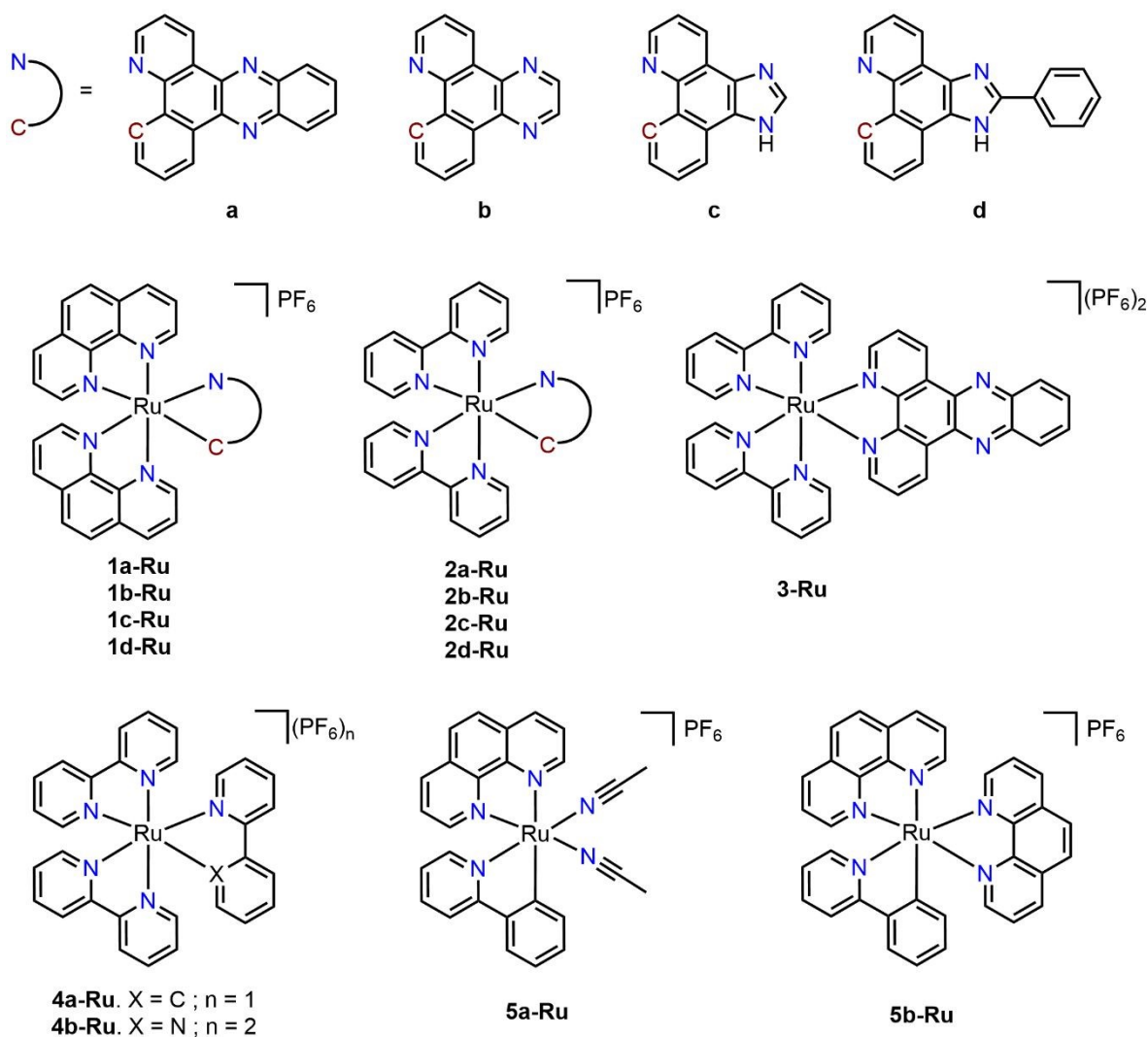


Figure 5. Cyclometalated Ru(II) complexes with bipyrindine and phenanthroline auxiliary ligands (1a-Ru – 5b-Ru).

Table 2. IC₅₀ values of the 1a-Ru to 3-Ru complexes at 48 hours under dark and light conditions^a.

Compound	IC ₅₀ (μM) KATO III			IC ₅₀ (μM) AGS		
	Dark	Light	PI ^b	Dark	Light	PI ^b
1a-Ru	0.38 ± 0.03	0.32 ± 0.05	1.19	1.30 ± 0.12	0.52 ± 0.04	2.50
1b-Ru	0.57 ± 0.04	0.10 ± 0.03	5.70	0.63 ± 0.03	0.18 ± 0.03	3.50
1d-Ru	0.46 ± 0.07	0.44 ± 0.12	1.05	0.70 ± 0.02	0.50 ± 0.07	1.40
2a-Ru	0.41 ± 0.02	0.35 ± 0.05	1.17	1.30 ± 0.10	0.75 ± 0.08	1.73
2b-Ru	0.91 ± 0.09	0.27 ± 0.06	3.37	0.87 ± 0.04	0.34 ± 0.05	2.56
2c-Ru	5.12 ± 0.02	4.89 ± 0.15	1.05	5.01 ± 0.29	3.88 ± 0.85	1.29



2d-Ru	0.52 ± 0.03	0.50 ± 0.08	1.04	0.85 ± 0.05	0.67 ± 0.09	1.27
3-Ru	100.0 ± 5.0	95.0 ± 8.0	1.05	106.00 ± 5.0	100.00 ± 3.0	1.06
cisplatin	11.0			29.00		

^a Cell viability determined by MTT assay after treatment for 48 h under dark and cells irradiated for 1 h

^b PI (Phototoxic Index) = IC₅₀ dark/IC₅₀ light

Lactate dehydrogenase (LDH) is overexpressed in cancerous cells due to high glucose consumption through glycolic metabolism. LDH activity inhibition has been considered an alternative target in cancer treatment. Thus, **4a-Ru** and **4b-Ru** complexes were tested on gastric and colon cancer cells expressing wild-type p53 (AGS and HCT116) and mutant p53 (KATO III and SW480). The assays were performed using the MTT protocol, and it was observed that the **4a-Ru** complex was the most cytotoxic in all cancer cell lines (IC₅₀ = 0.7 μM to 1.6 μM) compared to its coordination analog complex **4b-Ru** (> 200 μM). Kinetic inhibition studies of LDH demonstrated that they both inhibited the enzyme's activity. Therefore, the higher cytotoxicity of compound **4a-Ru** could be related to other interactions inside the cell.⁷³ Furthermore, through theoretical modeling, binding sites within LDH were identified where **4a-Ru** could hypothetically interact with NADH and oxamate molecules, which are key binding sites for LDH inhibition (**Figure 6a**). Therefore, the higher cytotoxicity of the **4a-Ru** compound could be related to its interactions with NADH and oxamate.

The resistance mechanisms of Ru(II) cyclometalated complexes are poorly understood in comparison with those of Pt(II) compounds. Hence, a study was conducted employing the cytotoxic compounds **5a-Ru** and **5b-Ru**. Resistance was identified from genes *ABCB1* and *EGFR*; the former is responsible for the import/export processes governing the concentration of metallodrugs inside the cell, while the latter is an EGF growth factor receptor that induces proliferative and survival pathways, causing pro-apoptotic effects and cell cycle arrest. *ABCB1* inhibition assays were carried out with inhibitors of ABC transporters (*e.g.* verapamil), revealing an increase in cytotoxicity of the complexes after treatment. Theoretical studies revealed that **5a-Ru** could have two binding modes with *ABCB1* (**Figure 6b**). In the first site (**Figure 6c**), **5a-Ru** binds within a hydrophobic environment, exhibiting π -stacking interactions with various aromatic amino acids. Similarly, in the second site (**Figure 6d**), adjacent to the first, π -stacking interactions with aromatic amino acids also predominate. This suggests that the binding of **5a-Ru** to an internal conformation of *ABCB1* is feasible even in the absence of nucleotides. This is the first study to reveal such resistance pathways.⁷⁴



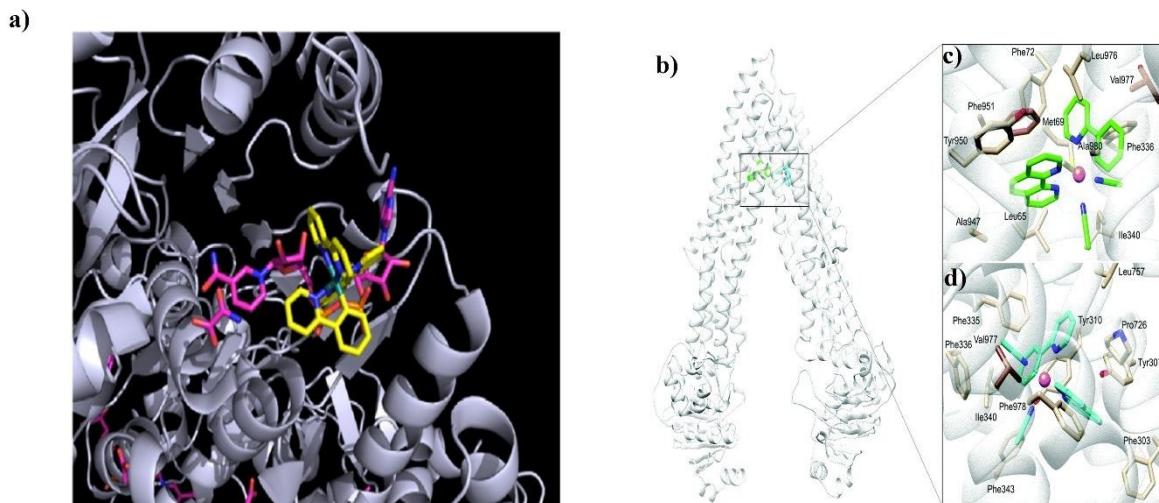


Figure 6. a) Interaction of **4a-Ru** with LDH. b) Binding modes of **5a-Ru** with ABCB1. c) and d) Binding sites of **5a-Ru**, predominantly exhibiting hydrophobic interactions. (Reproduce with permission from ref. 73 (Copyright 2016, Elsevier) and 74 (Copyright 2020, Royal Society of Chemistry)).

Furthermore, in a subsequent study, it was identified that the **5a-Ru** complex exhibits higher cytotoxicity towards gastric cancer (GC) cells compared to the drug *oxaliplatin*. On the other hand, it was established that **5a-Ru** does not induce caspase-3 cleavage nor express the p53 gene, indicating that classical DNA/p53 damage is not the main mode of action. Instead, it induces the expression of proteins such as XBP1 and CHOP, which are two central effectors of the Unfolded Protein Response (UPR) pathway. Additionally, this complex was also capable of reducing glutathione (GSH) levels, resulting in increased ROS production, which may lead to cell death. Moreover, it was confirmed that **5a-Ru** can induce cell death through caspase-independent apoptosis (**Figure 7**). *In vivo* studies conducted on mice showed that the ruthenium complex was more efficient in inhibiting tumor growth than *oxaliplatin*, to the point of eliminating the tumor in the mouse. These findings suggest that **5a-Ru** and similar compounds may bypass classical resistance mechanisms in cancer cells, such as the elevation of GSH production, GSH mutation, and alterations in the p53 pathway.⁷⁵



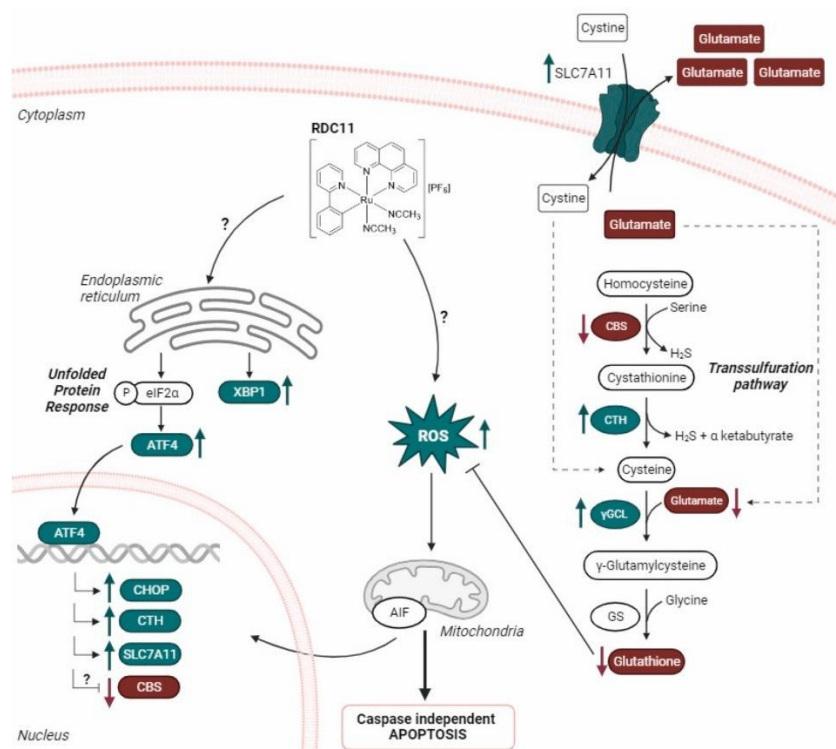


Figure 7. Plausible mechanism of action of the 5a-Ru complex, which exhibits effects on the transsulfuration pathway while evading classical resistance mechanisms. Green arrows indicate positive regulation, while red arrows indicate negative regulation. (Reproduce with permission from ref. 75, Copyright 2024, Elsevier).

McFarland group synthesized a series of cyclometalated compounds (**6a-Ru** to **9a-Ru**) bearing ligands with expanded π -systems (**Figure 8**), which were subjected to phototoxicity studies against two cancer cell lines: human melanoma (SK-MEL-28) and leukemia (HL60) (**Table 3**). Coordination analogs (**6b-Ru** to **9b-Ru**) were evaluated as well. Complexes **6a-Ru** to **8-Ru** were more cytotoxic than their coordination analogs in both cancer cell lines in the dark and after light irradiation, obtaining PI values from 5.4 to 18. For complex **9a-Ru**, PI values were 1400 and 410 for SK-MEL-28 and HL60, respectively. Additionally, **9a-Ru** was tested as a potential diagnostic agent due to its elevated light sensitivity (**Figure 9a-c**). Using differential interference contrast (DIC) microscopy and evaluating the fluorescence of **9a-Ru** under dark conditions (**Figure 9a**), visible light (**Figure 9b**), and red light (**Figure 9c**), the complex exhibited luminescence within the cell. Additionally, employing DIC microscopy (central panel) allowed for the determination of cell morphology, revealing that in darkness, **9a-Ru** is localized in the cell nucleus, whereas after exposure to visible and red light, the complex relocates to the cytoplasm. Comparing fluorescence overlays with DIC images, the green signal appears brighter in populations irradiated with visible light (**Figure 9b**). The



9b-Ru complex did not produce any detectable green or red luminescence, suggesting the importance of a σ C–Ru bond for generating these images.⁷⁶

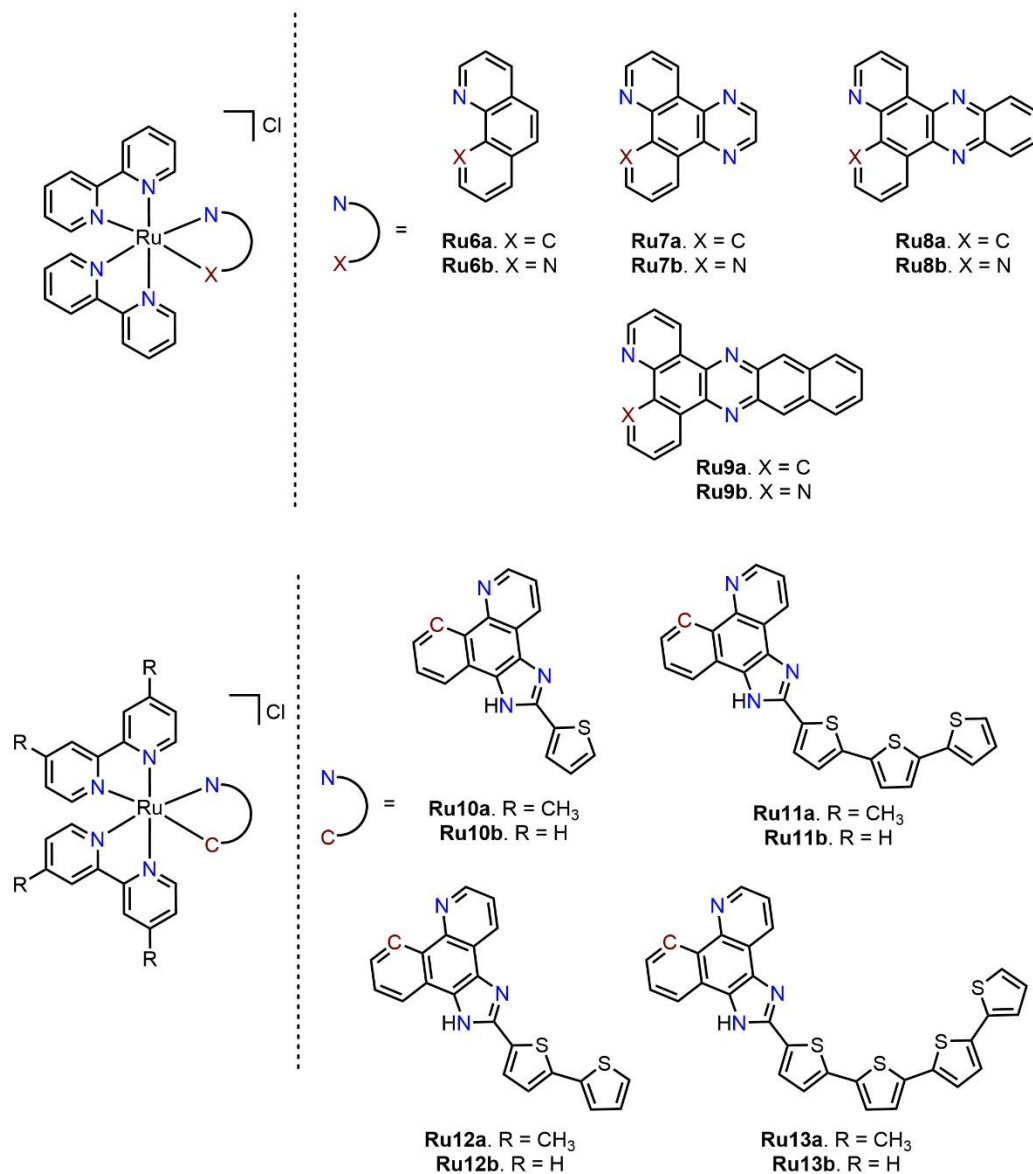
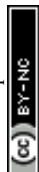


Figure 8. Cyclometalated Ru(II) complexes bearing expanded π -systems (6a-Ru - 13b-Ru).

Table 3. EC₅₀ values of the 6a-Ru – 9b-Ru complexes at 48 hours under dark and light conditions^a.

Compound	EC ₅₀ (μ M) SK-MEL-28			EC ₅₀ (μ M) HL60		
	Dark	Light	PI ^b	Dark	Light	PI ^b
6a-Ru	1.94 \pm 0.04	0.258 \pm 0.009	7.5	1.29 \pm 0.01	0.151 \pm 0.001	8.6
7a-Ru	1.16 \pm 0.01	0.142 \pm 0.002	8.3	3.06 \pm 0.10	0.167 \pm 0.003	18



8a-Ru	1.92 ± 0.02	0.208 ± 0.003	9.1	1.14 ± 0.01	0.211 ± 0.004	5.4
9a-Ru	>300	0.206 ± 0.003	1400	>300	0.741 ± 0.016	410
6b-Ru	>300	8.86 ± 0.12	34	>300	19.52 ± 1.32	15
7b-Ru	>300	237 ± 7	1.3	>300	253 ± 11	1.2
8b-Ru	>300	172.5 ± 5	1.7	>300	166 ± 4	1.8
9b-Ru	265 ± 5	0.812 ± 0.005	1500	282 ± 19	0.303 ± 0.020	930

^a Cell viability determined by MTT assay after treatment for 48 h under dark and cells irradiated for 16 h

^b PI (Phototoxic Index) = $IC_{50} \text{ dark} / IC_{50} \text{ light}$

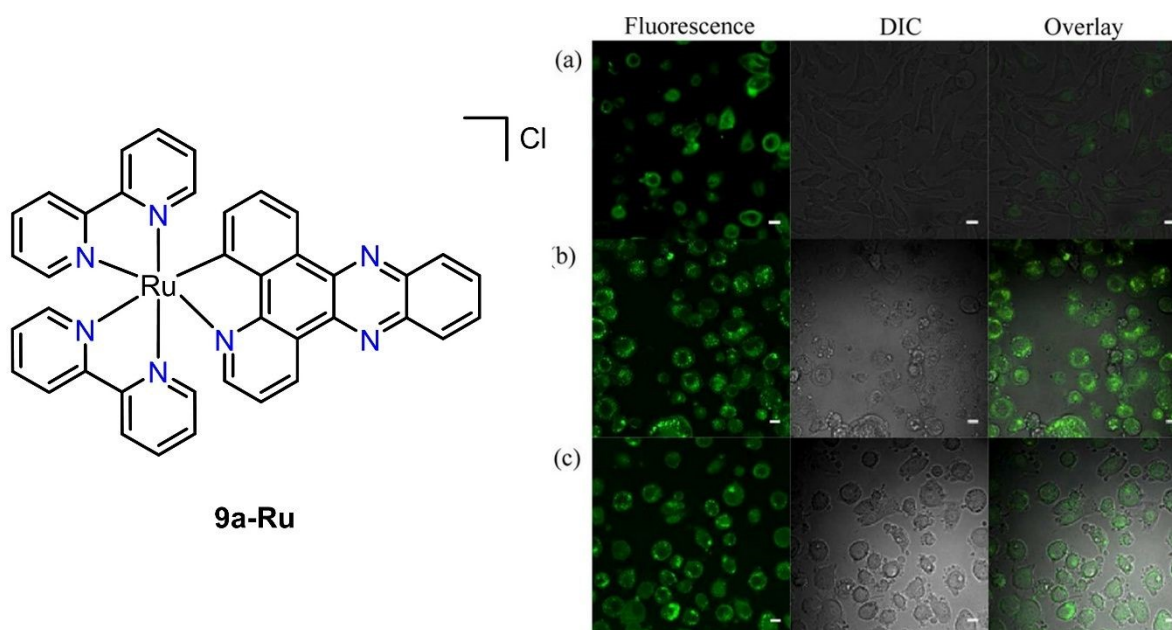


Figure 9. Comparison of the fluorescence emitted by the 9a-Ru complex in SK-MEL-28 cells under a) darkness, b) visible light, and c) red light (50 J cm^{-2}). (Reproduce with permission from ref. 76 Copyright 2015, American Chemical Society).

In another work by the McFarland group, the phototoxicity against the SK-MEL-28 cell line was evaluated with ruthenium(II) cyclometalated complexes (**10a-Ru** to **13a-Ru**, and **10b-Ru** to **13b-Ru**) using a series of α -oligothiophene derivatives, aiming to extend the π -conjugation of the ligand.^{77,78} The lipophilicity of the cyclometalated complexes increased as the number of thiophene groups increased, with **Ru13a** and **Ru13b** being the most lipophilic compounds. In the dark, these complexes were the least cytotoxic ($EC_{50} > 300 \text{ }\mu\text{M}$) compared to **10a-Ru** – **12a-Ru** and **10b-Ru** – **12b-Ru** complexes, with EC_{50} values ranging from $0.38 \text{ }\mu\text{M}$ to $19.5 \text{ }\mu\text{M}$. After irradiation, PI of **13a-Ru** and **13b-Ru** were ¹¹⁵3 and 267, respectively, while the presence of the methyl groups in the bipyridine backbone seems to play an important role.



Chen and coworkers synthesized a series of complexes based on β -carboline alkaloid-derived ligands as the cyclometalating ligand and bipyridine derivatives (**14a-Ru** – **16b-Ru**) (**Figure 10**), and their antiproliferative activity was evaluated against HeLa and BEAS-2B cells (immortalized healthy human bronchial epithelial cells) (**Table 4**). All complexes presented higher cytotoxicity against HeLa (IC_{50} 1.9 – 4.1 μ M) than *cisplatin* (IC_{50} 18.1 μ M), as well as a higher selectivity index (SI).⁷⁹

Table 4. IC_{50} values (μ M) of **14aRu-16bRu** complexes in cancerous and healthy cell lines^a

Compound	IC_{50} (μ M)		
	HeLa	BEAS-2B	SI ^b
14a-Ru	2.4 \pm 0.1	15.2 \pm 0.9	6.3
14b-Ru	2.8 \pm 0.2	16.1 \pm 1.3	5.7
15a-Ru	1.9 \pm 0.4	10.6 \pm 0.6	5.6
15b-Ru	3.4 \pm 0.3	11.2 \pm 0.5	3.3
16a-Ru	3.2 \pm 0.4	13.5 \pm 2.4	4.2
16b-Ru	4.1 \pm 0.6	14.2 \pm 1.8	3.5
<i>cisplatin</i>	18.1 \pm 0.5	13.8 \pm 0.9	0.8

^a Cell viability determined by MTT assay after treatment for 48 h

^b SI (Selectivity Index) = IC_{50} (BEAS-2B)/ IC_{50} (HeLa)

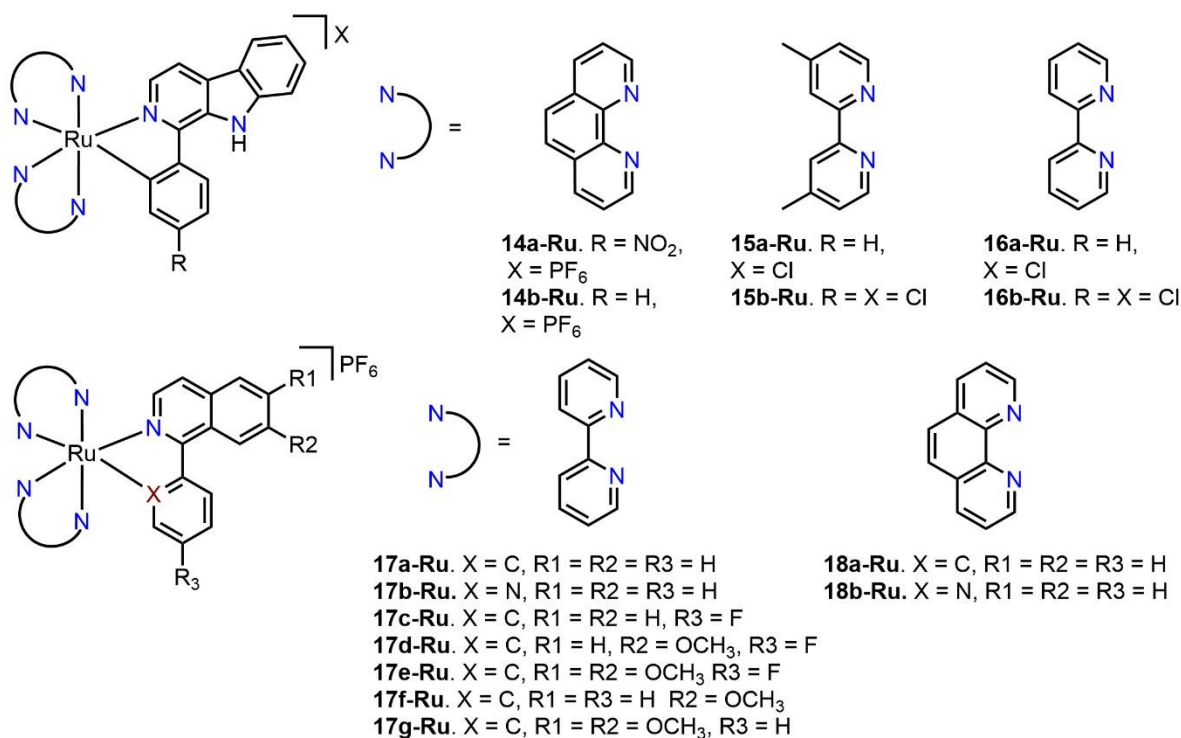


Figure 10. Ru(II) C^N compounds with cyclometalated ligands derived from β -carboline (**14a-Ru** - **16b-Ru**) and isoquinolines (**16a-Ru** - **18b-Ru**).

The Chen's group also prepared a series of complexes bearing isoquinoline and phenantroline ligands (**17a,b-Ru** and **18a,b-Ru**), and studied their cytotoxic activity towards lung cancer cell line (NCI-H460) and HBE cells (normal human bronchial epithelial cells). The cyclometalated complexes **17a-Ru** and **18a-Ru** showed higher antiproliferative activity against NCI-H460 with IC₅₀ values of $2.1 \pm 0.2 \mu\text{M}$ and $1.8 \pm 0.3 \mu\text{M}$, respectively. The selectivity indexes were 10.5 and 11.1 for **16a-Ru** and **17a-Ru** and were higher than that of *cisplatin* (SI = 0.6).⁸² Afterwards, they introduced different substituents into the backbone of the cyclometalated ligand to further enhance the cytotoxic activity of these complexes (**17a-Ru** and **17c-g-Ru**). All these complexes were subjected to MTT assays on various cancer cell lines and a healthy cell line (HBE). All the complexes exhibited high activity across all cancer cell lines, being most active in the lung adenocarcinoma cell line (A549) and *cisplatin*-resistant (A549/DDP), while also showing lower toxicity in the healthy HBE line. Complexes **17a-Ru**, **17f-Ru**, and **17g-Ru** were able to overcome *cisplatin* resistance through the PI3K/mTOR/Nrf2 signaling pathway, while the Akt/GSK-3 β /Fyn pathway was altered by complexes **17c-Ru** - **17e-Ru**.^{83,84}

The mechanisms of action of complexes **14a-Ru** - **18b-Ru** have been investigated by Chen's group based on biochemical and cytotoxic assays (**Figure 11a-e**). Thus, it was observed that all complexes caused DNA damage via ROS (**Figure 11a**), mitochondrial dysfunction (**Figure 11b**), induced apoptosis (extrinsic and intrinsic) (**Figure 11c**), and were mainly accumulated in the nucleus and mitochondria of the cancerous cells. It has been shown that the cyclometalated complexes can actively be transported into the cell via endocytosis. Cell cycle arrest was found in G0/G1 phase for complexes derived from β -carboline (**15a-Ru** - **16b-Ru**), and in the S and G2/M phases with isoquinoline ligands (**17a-Ru** and **17c-g-Ru**) (**Figure 11d**). Based on all these studies, Chen's group has proposed various mechanisms of action through which the **14a-Ru** - **18b-Ru** complexes could act on cancer cells (**Figure 11e**).

Ruthenium complexes bearing fluorinated cyclometalated ligands were prepared by the Huang group, starting from 2,4-difluorophenylpyridine (**19a-Ru**) and coumarin (**19b-Ru**) (**Figure 12**). These compounds were subjected to *in vitro* assays (under normoxia and hypoxia conditions) against HeLa cell line under light and dark conditions.⁸⁵ Under normoxia, **19b-Ru** exhibited better cytotoxicity when irradiated with white light with IC₅₀ of *ca.* $2.5 \mu\text{M}$, through the generation of hydroxyl radicals. Additionally, **19b-Ru** also demonstrated an excellent PDT (Photodynamic Therapy) effect in *in vivo* assays, almost completely inhibiting the endogenous hypoxic solid tumor in mice.



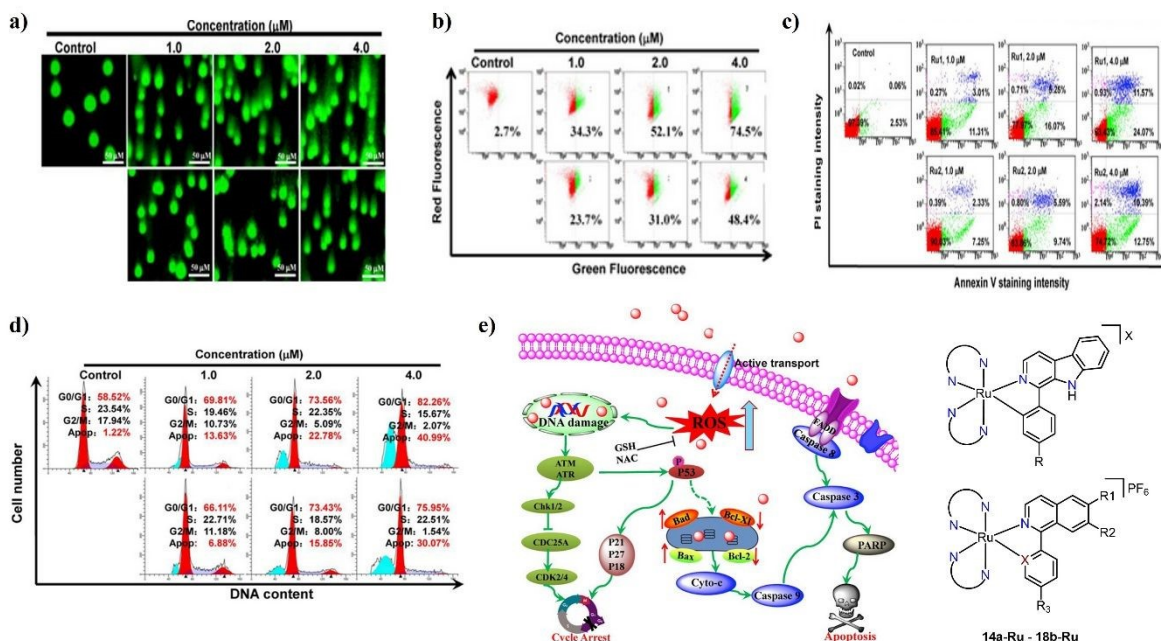
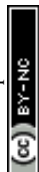


Figure 11. Schematic summary representation of the biochemical assays conducted with the **14a-Ru – 18b-Ru** compounds on different cancer cell lines: **a)** comet assays for DNA damage, **b)** mitochondrial dysfunction assessed by flow cytometry, **c)** apoptosis analysis via flow cytometry, **d)** cell cycle study using flow cytometry, and **e)** proposed mechanism of action for **14a-Ru – 18b-Ru**. (Reproduce with permission from ref. 79 Copyright 2017, Elsevier).

The cytotoxic activity of the bis-cyclometalated Ru(III) complex (**20-Ru**) was measured in breast cancer (MCF-7) and colon cancer (HT-29), showing higher activity in HT-29 ($IC_{50} = 9.2 \pm 2.3 \mu M$ at 48 h) compared to *cisplatin* ($IC_{50} = 23.0 \pm 0.6 \mu M$). Since it is a Ru(III) species, it is speculated that it can be reduced to Ru(II), being the active species responsible for carrying out biochemical processes inside the cancer cells.⁸⁶ On the other hand, **21a-c-Ru** complexes (**Figure 12**) were tested on the most aggressive breast cancer cell line, triple-negative breast cancer (MDA-MB-231), as well as drug-resistant colon cancer (SW620AD300). These complexes proved to be more active than *cisplatin* ($IC_{50} = 29.39 \pm 2.3 \mu M$) in MDA-MB-231, with IC_{50} ranging from $3.39 \mu M$ to $11.06 \mu M$, being **21a-Ru** the most active of the family ($IC_{50} = 3.39 \pm 2.4 \mu M$). However, in the SW620AD300 cell line, **21a-Ru** ($IC_{50} = 13.96 \pm 2.2 \mu M$) and **21b-Ru** ($IC_{50} = 16.19 \pm 1.7 \mu M$) were less active than *cisplatin* ($IC_{50} = 9.55 \pm 1.0 \mu M$), while **21c-Ru** was slightly more active ($IC_{50} = 9.48 \pm 0.7 \mu M$). Through cell migration studies on MDA-MB-231 cells, the inhibitory effects of **21a-Ru – 21c-Ru** were measured (**Figure 13**) to evaluate the antimetastatic activity of these complexes. After 24 hours of treatment, all complexes were able to reduce the wound closure of the intermediate space compared to the



control group. These compounds showed a preference for the cell nucleus and mitochondria, where the complexes caused a loss of mitochondrial membrane potential (MMP), resulting in ROS overload in the tumor cells, inducing apoptosis.⁸⁷

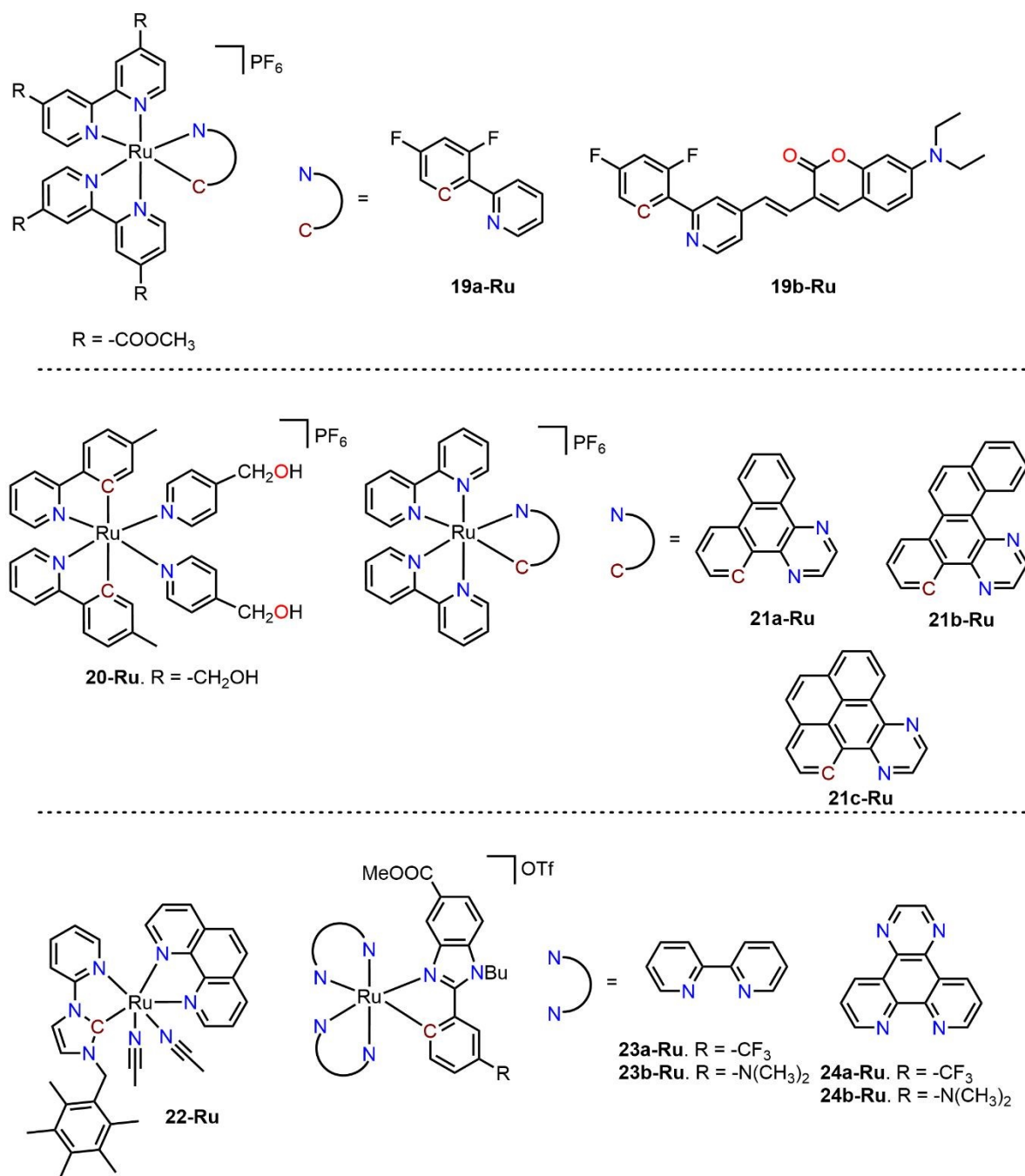


Figure 12. Cyclometalated ruthenium(II) and (III) complexes evaluated in cytotoxicity studies (**19a-Ru** - **24b-Ru**).



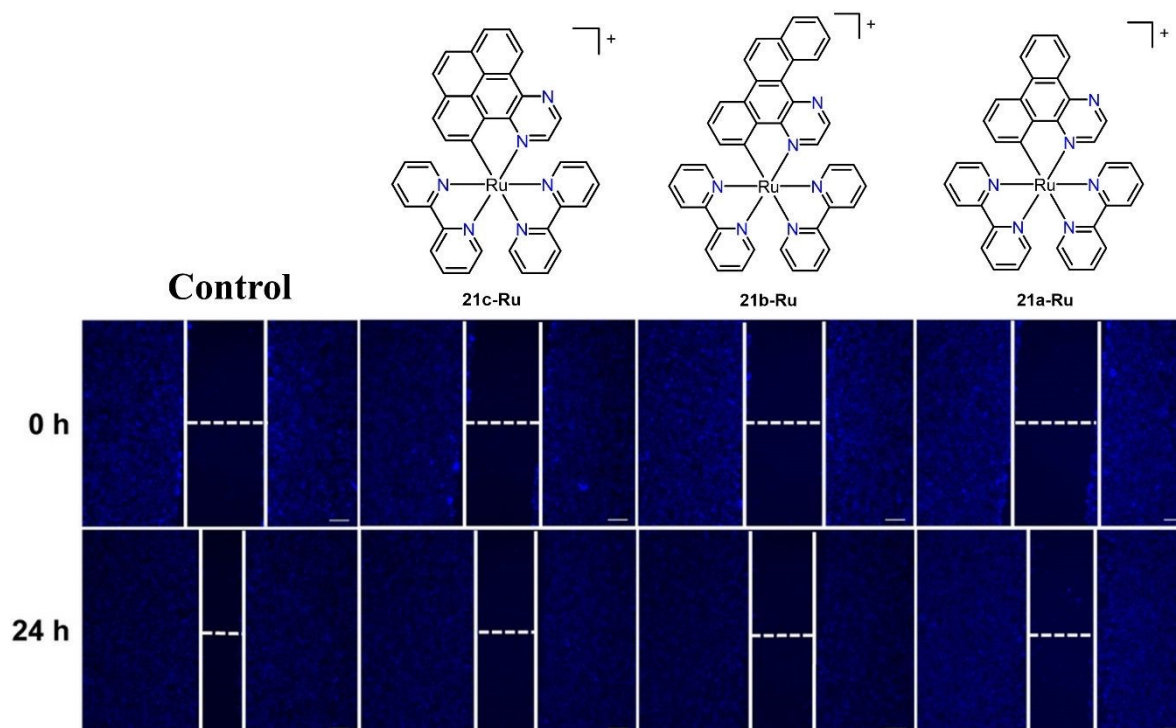


Figure 13. Study of cell migration of the **21a-Ru – 21c-Ru** complexes on MDA-MB-231 cells using the wound healing assay. (Reproduce with permission from ref. 87 Copyright 2021, Elsevier).

Complex **22-Ru** exhibited notable antiproliferative activity in the A549 cancer cell line and the *cisplatin*-resistant A549R cell line, showing an RF (resistance factor) of 2.2 compared to *cisplatin*'s RF of 3.9. Furthermore, **22-Ru** induces apoptosis and inhibits cell proliferation by arresting the cell cycle at the G2/M phase. Additionally, **22-Ru** also demonstrated significantly greater antimetastatic activity than the NAMI-A complex, even efficiently suppressing angiogenesis.⁸⁸

Although apoptosis-mediated programmed cell death is usually the most common pathway among Ru(II) C^N complexes, some of these complexes may lead to other forms of cell death. For example, **23a,b-Ru**, and **24a,b-Ru** complexes (**Figure 12**) were subjected to phototoxicity assays against HeLa, OE33, and A375 cells with IC₅₀ values ranging from 0.7 to 9.0 μM in the dark, and from 0.14 to 1.8 μM after light irradiation. Hypoxic conditions were applied to HeLa cell lines and no significant modification in the antiproliferative activity was observed for most of the complexes. The complexes showed greater retention in cell membranes, causing the appearance of membrane protrusions, indicating cell death by oncosis.⁸⁹

One of the peculiarities of ruthenium complexes is that they have shown a preference for organelles such as mitochondria and the endoplasmic reticulum (ER), unlike platinum-based compounds which



primarily accumulate in the nucleus. Complexes **25a,b-Ru** (**Figure 14**) were mainly located in the nucleus (**Figure 15e, f**), mitochondria (**Figure 15g, h**), and ER (**Figure 15a-d**) of human glioblastoma cells (A172). Compound **25a-Ru** was the most cytotoxic (IC_{50} 0.25-1.15 μ M) and presented the highest lipophilicity ($\log p_{o/w} = 2.35 \pm 0.04$).⁹⁰ On the other hand, **26a-Ru** and **27a-c-Ru** complexes were evaluated in an ovarian cancer cell line (A2780), showing main retention in the cell membrane and cytosol, with only a small amount localized in the nucleus. Anticancer effects of the complexes would be related to a decrease in MMP and ROS activation, instead of DNA interaction.⁹¹

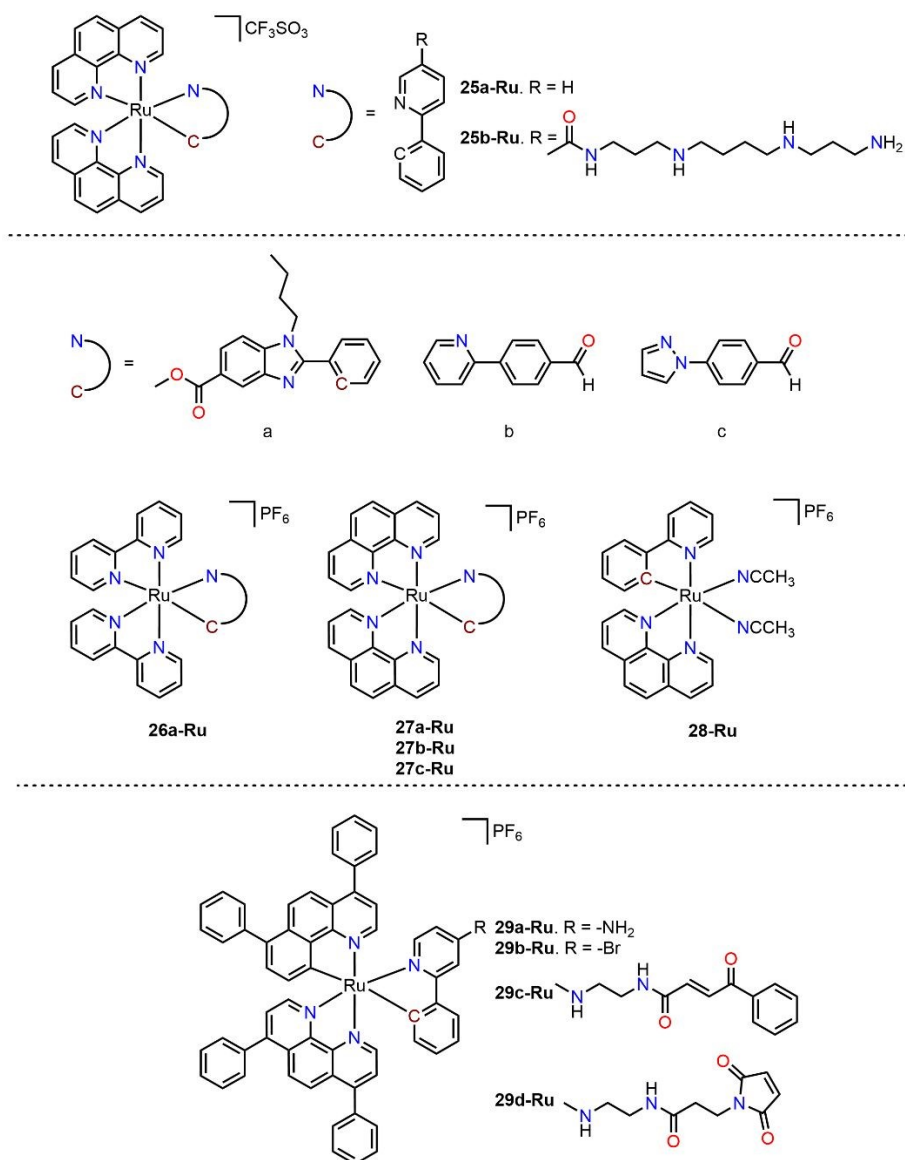


Figure 14. Ruthenium(II) complexes with different types of cyclometalated ligands (**25a-Ru** - **29d-Ru**).



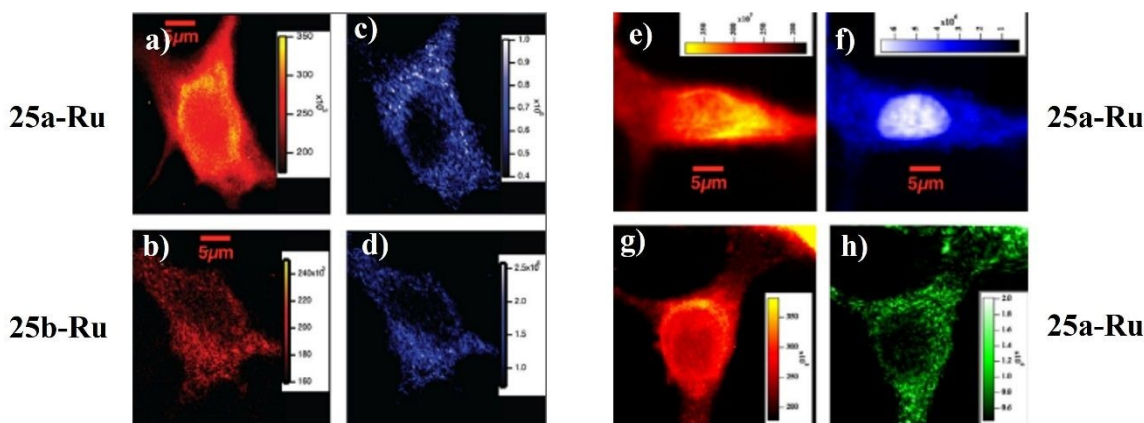


Figure 15. Accumulation of the **25a-Ru** – **25b-Ru** complexes in different organelles, such as **a-d**) ER, **e, f**) nucleus, and **g, h**) mitochondria in A172 cells, analyzed by confocal microscopy. (Reproduce with permission from ref. 90 Copyright 2014, American Chemical Society).

Similarly, Le Lagadec's and Gaiddon's groups have contributed to a better understanding of the molecular pathways affected by Ru(II) C^N cyclometalated complexes.⁹² They have evaluated the activity of complex **28-Ru** against human colorectal adenocarcinoma (HCT 116) (**Figure 14**). It was determined that this complex altered redox enzymes, affecting the metabolism of cancer cells and tumor growth *in vivo*. This alteration is primarily directed at the glucose oxidase and PHD2 redox enzymes affecting their function and altering the HIF-1 pathway, which is a master regulator of cancer cell survival and tumor angiogenesis.

Gasser *et al.*⁹³ synthesized different Ru(II) cyclometalated complexes (**29a-d-Ru**) with maleimide and benzoylacrylic derivatives as the cyclometalating ligands. The **29a-Ru** complex showed excellent phototoxic performance in the near-infrared region, being probably the first Ru(II) polypyridyl compound to date to exhibit such activity in the near-infrared range. Complex **29a-Ru** displayed a very low ¹O₂ generation, was non-toxic in the dark, and could cause cell death after light irradiation. Complexes **29c-d-Ru** were used to prepare antibody-drug conjugates (ADCs) using cetuximab (CTX), a monoclonal antibody targeting the epidermal growth factor receptor (EGFR), which is overexpressed in some tumors. These **Ru-CTX** bioconjugates were intended to selectively and efficiently target tumor cells. However, these bioconjugates showed only a mild effect on PDT activity. Despite this, these complexes are the first **Ru-CTX** conjugates reported to date, serving as an example for future modifications to potentially enhance their effects.

One of the main strategies in recent years has been the development of compounds that can target multidrug-resistant (MDR) cancer cells, a major challenge in eradicating the disease. Chao and collaborators⁹⁴⁻⁹⁷ synthesized various Ru(II) cyclometalated C^N complexes using polypyridyl



auxiliary ligands (**30-Ru** – **32-Ru**) (**Figure 16**), evaluating their activity on different cancer cell lines, including drugs resistant cells such as A549/DDP and H460/MX20 resistant to mitoxantrone (**Table 5**). Compared to *cisplatin*, **30-Ru** – **32-Ru** complexes exhibited higher antitumor activity in both the parental A549 cell line and the *cisplatin*-resistant line (A549/DDP), with RF values ranging from 0.8 to 3.3. On the other hand, the **33-Ru** complex demonstrated the ability to surpass resistance in mitoxantrone-resistant H460 cancer cells, with a low RF, making it a promising candidate, along with **30-Ru** – **32-Ru**, as potential metallodrugs in the fight against cancer. These complexes also demonstrated high lipophilicity, with preferential cellular accumulation in the nucleus (**30-Ru**, **31a-d-Ru**, and **33-Ru**) and mitochondria (**32-Ru** and **33-Ru**). Additionally, **30-Ru** and **31a-d-Ru** complexes showed the ability to intercalate with DNA, inhibiting cellular transcription and even disrupting the binding of the transcription factor NF- κ B, as observed with **30-Ru**. Meanwhile, **32-Ru** and **33-Ru** complexes exhibited high intracellular ROS production and mitochondrial damage due to the reduction in MMP. All the complexes induced apoptotic cell death in cancer cells.

A series of complexes (**34-Ru** – **36c-Ru**) synthesized by Ruiz *et al.*⁹⁸ were used in phototoxicity studies under normoxic and hypoxic conditions on the HeLa cell line. It was found that **34-Ru** and **36b-Ru** were non-toxic under dark and hypoxic conditions ($IC_{50} > 100 \mu M$), unlike under normoxic conditions ($IC_{50} = 0.71$ and $7.1 \mu M$ respectively). When irradiating the cells with green light, the complexes were more active under hypoxic conditions ($IC_{50} = 0.17$ and $0.13 \mu M$ respectively), with PI values higher than 588 for **34-Ru** and 769 for **36b-Ru**. The other complexes did not exhibit outstanding PI values, being toxic under both dark and light conditions, as well as under normoxic and hypoxic conditions.



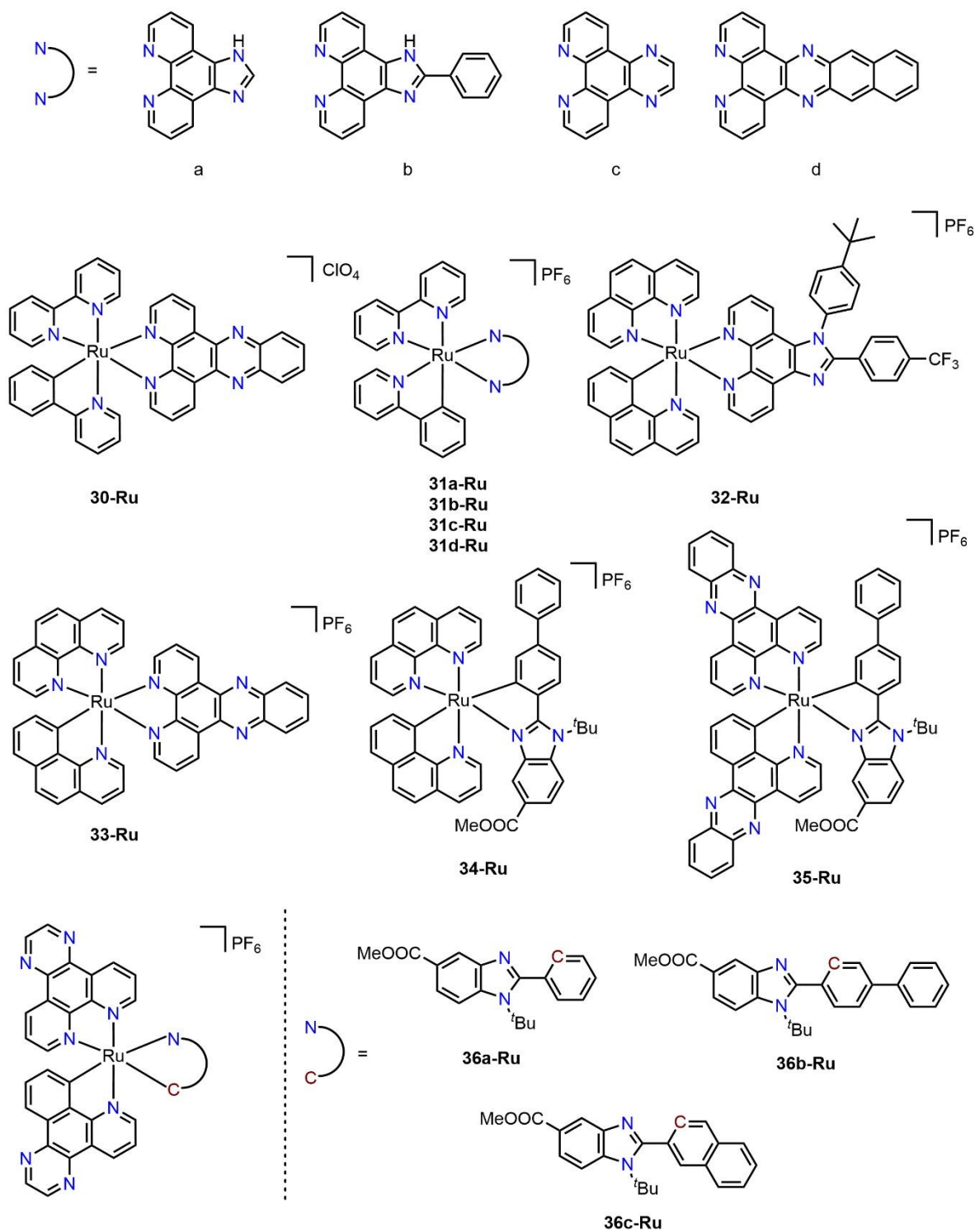


Figure 16. Ru(II) cyclometalated complexes with polypyridyl-type auxiliary ligands (**30-Ru** - **36c-Ru**).



Table 5. IC₅₀ values (μM) for **30-Ru – 33-Ru** complexes on MDR cancer cell lines^a

Compound	IC ₅₀ (μM)					
	A549	A549/DDP	RF ^b	H460	H460/MX20	RF ^c
30-Ru	1.4	2.9	2.1	-	-	-
31a-Ru	4.6	7.1	1.5	-	-	-
31b-Ru	2.5	5.2	2.1	-	-	-
31c-Ru	2.8	5.9	2.1	-	-	-
31d-Ru	1.3	4.3	3.3	-	-	-
32-Ru	1.0	0.8	0.8	-	-	-
33-Ru	-	-	-	0.67	0.70	1.0
<i>cisplatin</i>	21.3	142.5	6.7	-	-	-

^a Cell viability determined by MTT assay after treatment for 48 h

^b RF (Resistant Factor) = IC₅₀ (A2780cisR)/IC₅₀ (A2780)

^c RF (Resistant Factor) = IC₅₀ (H460/MX20)/IC₅₀ (H460)

3.2.1. Piano stool complexes

Ruiz *et al.*⁹⁹ synthesized a series of Ru(II) C^N cyclometalated complexes using different cyclometalating ligands, such as benzimidazole derivatives (**37a-g-Ru**) and C^N ligands containing non-coordinating CHO groups (**38a-Ru-39c-Ru**) (**Figure 17**). Complexes **37a-g-Ru** were tested against A2780 (human ovarian cancer), A427 (human lung cancer), HT29 (human colorectal adenocarcinoma), and A2780cisR (*cisplatin*-resistant human ovarian cancer) cell lines, as well as a human umbilical vein endothelial cell line (EA.hy926), using *cisplatin* as a positive control. All ruthenium complexes were active against all cancer cell lines, showing greater activity than *cisplatin*, as shown in **Table 6**. Additionally, all the complexes were active against the *cisplatin*-resistant cell line A2780, with RF values ranging from 0.90 to 2.4, which are lower than that of *cisplatin* (10.3). These complexes increased the caspase-3 activity, causing caspase-dependent apoptosis-mediated cell death in A2780 cells. Through an in vitro tube formation inhibition assay, the ability of the **37a-Ru – 37g-Ru** complexes to inhibit angiogenesis was studied (**Figure 18**). By analyzing three parameters total length, number of meshes (network structures or polygons), and total mesh area it was observed that the **37d-Ru** and **37g-Ru** complexes most effectively inhibited vascular tube formation, making them the most potent angiogenesis inhibitors in the EA.hy926 cell line.



In a subsequent study, Ruiz and collaborators investigated the cytotoxic activity of **38a-Ru - 39c-Ru** complexes, which exhibited higher antitumor activity than *cisplatin* against A2780cisR (resistant cell line), with RF values ranging from 0.8 to 2.2. These compounds can affect the cell cycle, halting replication in the G1/S phases, and cause a decrease in MMP and an increase in caspase 3/7 activation, inducing caspase-dependent apoptosis mediated by mitochondria (extrinsic pathway).¹⁰⁰

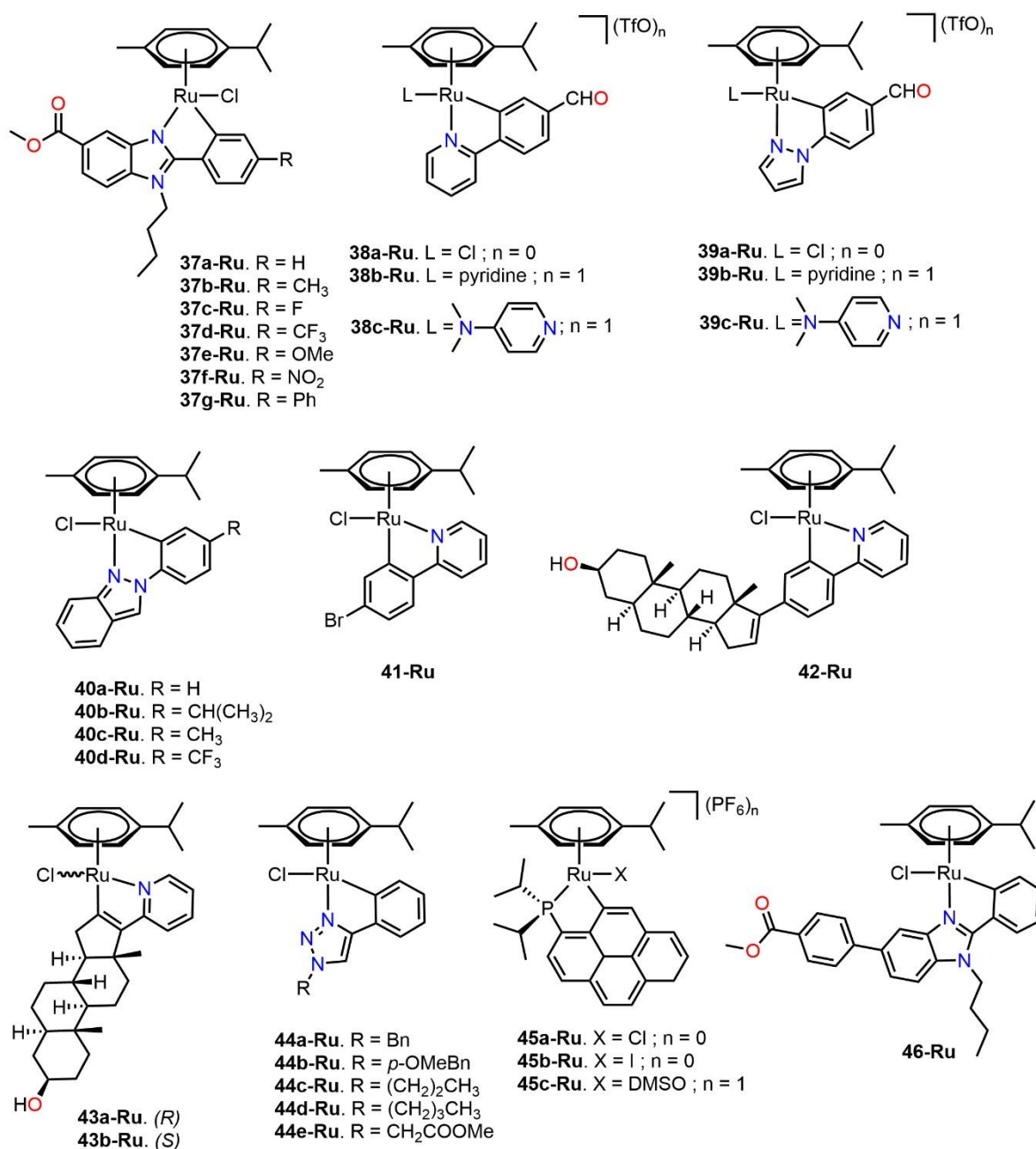


Figure 17. Cyclometalated piano stool Ru(II) C^N complexes (**37a-Ru - 46-Ru**).

Table 6. IC₅₀ of complexes **37a-g-Ru** in various cancer cell lines^a



Compound	IC ₅₀ (μM)					
	A2780	A427	HT29	A2780cisR	EA.hy926	RF ^b
37a-Ru	1.82 ± 0.35	2.58 ± 0.64	2.88 ± 0.55	2.37 ± 0.10	7.05 ± 1.07	1.3
37b-Ru	1.48 ± 0.35	2.99 ± 0.24	3.31 ± 0.04	1.46 ± 0.14	5.49 ± 1.57	0.98
37c-Ru	1.36 ± 0.07	1.85 ± 0.29	2.74 ± 0.11	3.26 ± 0.32	> 8	2.4
37d-Ru	1.24 ± 0.45	1.28 ± 0.07	1.93 ± 0.07	1.98 ± 0.23	3.35 ± 0.04	1.6
37e-Ru	1.56 ± 0.48	1.84 ± 0.60	2.76 ± 0.31	2.18 ± 0.22	5.10 ± 0.25	1.4
37f-Ru	1.30 ± 0.45	1.47 ± 0.18	2.35 ± 0.27	2.52 ± 0.16	7.21 ± 0.04	1.9
37g-Ru	1.07 ± 0.34	1.24 ± 0.07	1.99 ± 0.08	0.96 ± 0.23	1.67 ± 0.03	0.90
cisplatin	1.90 ± 0.20	6.09 ± 1.49	7 ± 0.07	19.57 ± 1.82	9.86 ± 0.64	10.3

^a Cell viability determined by crystal violet assay after treatment for 48 h

^b RF (Resistant Factor) = IC₅₀ (A2780cisR)/IC₅₀ (A2780)

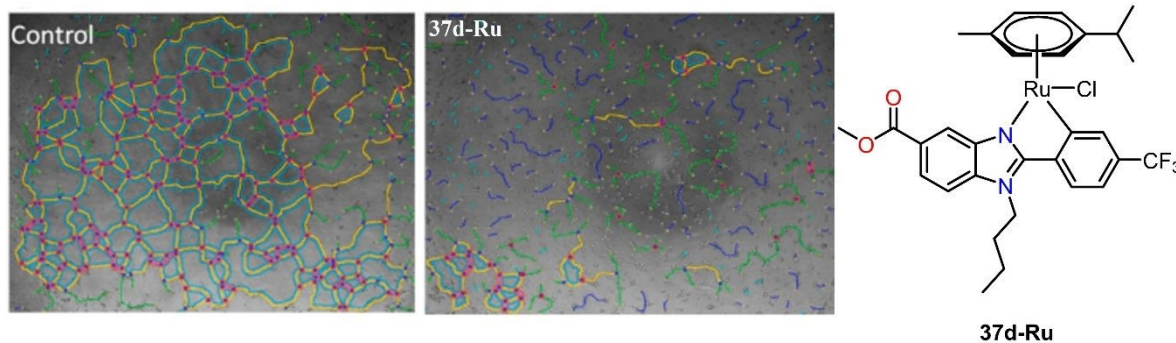


Figure 18. Effect of the **37d-Ru** complex in the tube formation assay of E.A.hy926 endothelial cells. (Reproduce with permission from ref. 99 Copyright 2015, American Chemical Society).

Chanda and collaborators initially synthesized complexes **40a,b-Ru**, but their antiproliferative activity was lower than *cisplatin*.¹⁰¹ Hence, the cyclometalated ligand was then modified to improve their cytotoxicity, yielding complexes **40c-Ru** and **40d-Ru**. As a result, **40c-Ru** complex showed high selectivity towards MDA-MB-231, MDA-MB-468 (triple negative breast cancer), and HCT-116 (human colon cancer cell) with SI (selectivity index) ranging from 20.57 to 26.75.¹⁰²

Cellular uptake of metal complexes can be improved by incorporating biomolecules like steroids into the ligands, which would later lead to higher cytotoxicity. Thus, Bräse *et al.* synthesized two cyclometalated complexes containing C[^]N ligands based on epiandrosterone (**42-Ru** and **43a,b-Ru**), as well as a cyclometalated complex without the steroid moiety (**41-Ru**). Complexes **42-Ru** and **43a,b-Ru** proved to be highly active against *cisplatin*-resistant human bladder carcinoma (RT112 cp) with RF values of 0.33 (**42-Ru**), 1.54 (**43a-Ru**), and 2.20 (**43b-Ru**), which were lower than that of



cisplatin (RF = 14). These results suggest that Ru(II) cyclometalated complexes with steroids in their structure are more cytotoxic and can attack *cisplatin*-resistant cancer cells.¹⁰³

Complexes **44a-e-Ru** bearing a cyclometalated ligand that contains a triazole have been evaluated as anticancer compounds against human non-small cell lung cancer (A549), colon adenocarcinoma (SW480), and human ovarian carcinoma (CH1/PA-1). Their anticancer activity was carried out in DMF and in DMSO as solvents. Complexes **44a-c-Ru** presented the highest antiproliferative activity against the human ovarian carcinoma cell line (CH1/PA-1) ($IC_{50} = 5.7\text{--}15\text{ }\mu\text{M}$ in DMF and $IC_{50} = 4.0\text{--}8.8\text{ }\mu\text{M}$ in DMSO).¹⁰⁴ DMSO adducts are proposed to improve the cytotoxicity of the complexes since the cytotoxicity is slightly higher in this solvent. However, more studies are required to establish the mechanism of action of these complexes.

Complexes **45a-c-Ru** were tested on the A549 cell line with time-course assays, which resulted in no significant change over time (Table 7). Nevertheless, the antiproliferative activity of all complexes was approximatively similar, being the most cytotoxic **45c-Ru** with DMSO as a ligand.¹⁰⁵

Table 7. IC_{50} values of **45a-c-Ru** complexes at different time points on the A549 cell line^a

Compound	IC_{50} (μM)			
	Day 0	Day 1	Day 2	Day 7
45a-Ru	2.26 ± 0.34	2.77 ± 0.38	4.92 ± 0.59	2.67 ± 1.61
45b-Ru	5.82 ± 1.89	5.58 ± 0.47	5.61 ± 2.16	4.32 ± 2.54
45c-Ru	1.72 ± 0.67	2.47 ± 0.57	2.56 ± 0.44	2.34 ± 0.61

^a Day zero corresponds to the first IC_{50} determination after 24 h incubation by MTT assay in DMSO.

Complex **46-Ru** displayed good antitumor activity on the human hepatoma cell line (HA22T) ($IC_{50} = 9 \pm 3.1\text{ }\mu\text{M}$) compared to *cisplatin* ($IC_{50} = 12.6 \pm 2.2\text{ }\mu\text{M}$). Additionally, the complex exhibited an increase in mitochondrial ROS production (Figure 19a) as the concentration increased, which was reflected by an increase in red fluorescence. This suggests a potential decrease in mitochondrial membrane potential (MMP), which could trigger caspase activation and lead to possible apoptosis-induced cell death. Furthermore, a study on the morphology of HA22T cells was conducted, revealing that cell morphology changed in a concentration-dependent manner (Figure 19b).¹⁰⁶



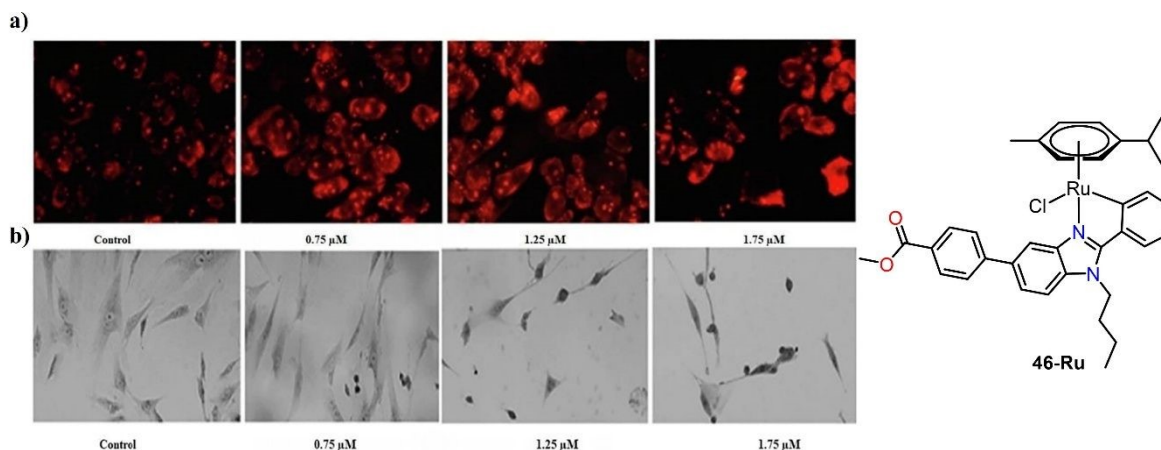


Figure 19. a) Mitochondrial superoxide generation after treatment with different concentrations of **46-Ru** and b) morphological changes in HA22T cells treated with different doses of **46-Ru**. (Reproduce with permission from ref. 106 Copyright 2023, Elsevier).

3.2.2. Pincer complexes

Hui Chao *et al.* synthesized a series of bis-tridentate pincer complexes (**47-Ru** - **48-Ru**) functionalized with organic fragments that exhibited biological synergy with the metal center. Complexes **47-Ru** and **48-Ru** (**Figure 20**) bear a functionalized anthraquinone fragment in the NNN pincer ligand. These compounds were tested on various cancer cell lines under hypoxic and normoxic conditions. The complexes showed higher cytotoxic activity compared to *cisplatin*, particularly against the *cisplatin*-resistant cancer cell line A549R (**Table 8**). The RF values of **47-Ru** and **48-Ru** were much lower than those of *cisplatin* under both normoxic and hypoxic conditions, indicating that these complexes are active in both environments. They also tested cytotoxic activity in a 3D model or MCTS (multicellular tumor spheroids) using HeLa cells to better mimic physiological conditions. In this study, the viability of the treated MCTS was assessed through fluorescence microscopy and a live/dead cell assay using the **47-Ru** and **48-Ru** complexes, with *cisplatin* as a reference (**Figure 21**). Live cells exhibited a green fluorescence, while dead cells appeared red. At 2.0 μM , **47-Ru** and **48-Ru**, as well as *cisplatin* at 60.0 μM , displayed weak green fluorescence and intense red fluorescence, indicating that the cyclometalated ruthenium complexes are more active than *cisplatin*. However, in the cellular uptake study of compound **47-Ru**, it was found that under normoxic conditions, 60% of the ruthenium was present in the nucleus and 28% in the mitochondria, while in a hypoxic environment, the accumulation of ruthenium in the mitochondria increased to 50%, while in the nucleus, it decreased to 32%. Furthermore, this complex also had the ability to inhibit the growth of hypoxia-inducible factor (HIF-1 α) in HeLa cells, which may be related to its anticancer activity in hypoxic tumors.¹⁰⁷



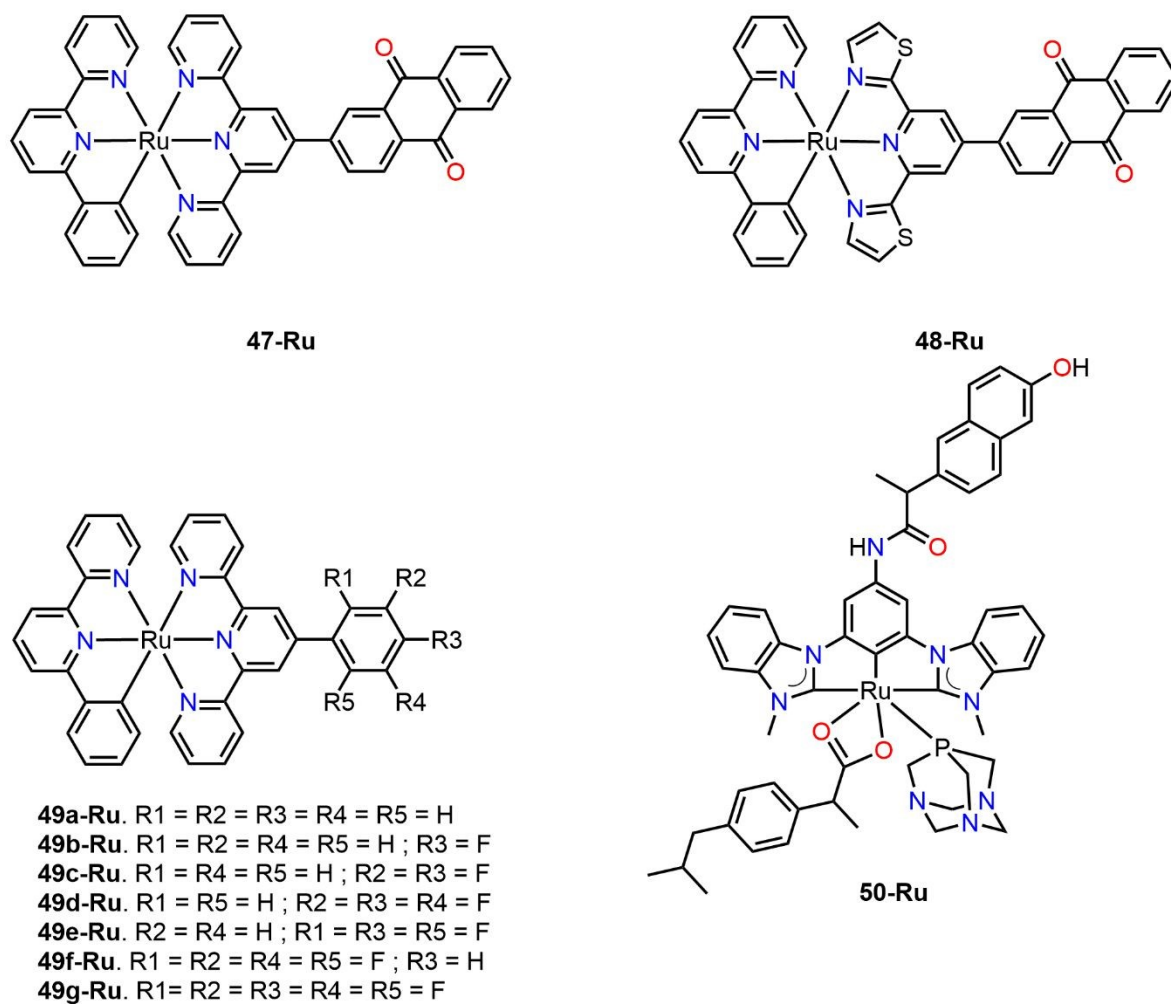


Figure 20. Pincer Ru(II) complexes (**47-Ru** - **50-Ru**).

Table 8. IC₅₀ values (μM) for complexes **47-Ru** and **48-Ru** under normoxic (20% O₂) and hypoxic (1% O₂) conditions on A549 cancer cells and *cisplatin*-resistant A549R^a

Compound	IC ₅₀ (μM)				RF _n ^b	RF _h ^c
	A549		A549R			
	normoxia	hypoxia	normoxia	hypoxia		
47-Ru	0.55 ± 0.10	0.61 ± 0.85	0.57 ± 1.23	0.60 ± 0.68	1.0	1.0
48-Ru	1.39 ± 0.21	1.86 ± 0.10	2.31 ± 0.16	2.54 ± 0.33	1.7	1.4
<i>cisplatin</i>	22.35 ± 3.18	26.31 ± 2.23	135.36 ± 11.36	150.0 ± 10.64	6.0	5.7

^a Cell viability determined by MTT assay after treatment for 48 h

^b RF (Resistance Factor in normoxia) = IC₅₀ (A549R)/IC₅₀ (A549)

^c RF (Resistance Factor in hypoxia) = IC₅₀ (A549R)/IC₅₀ (A549)



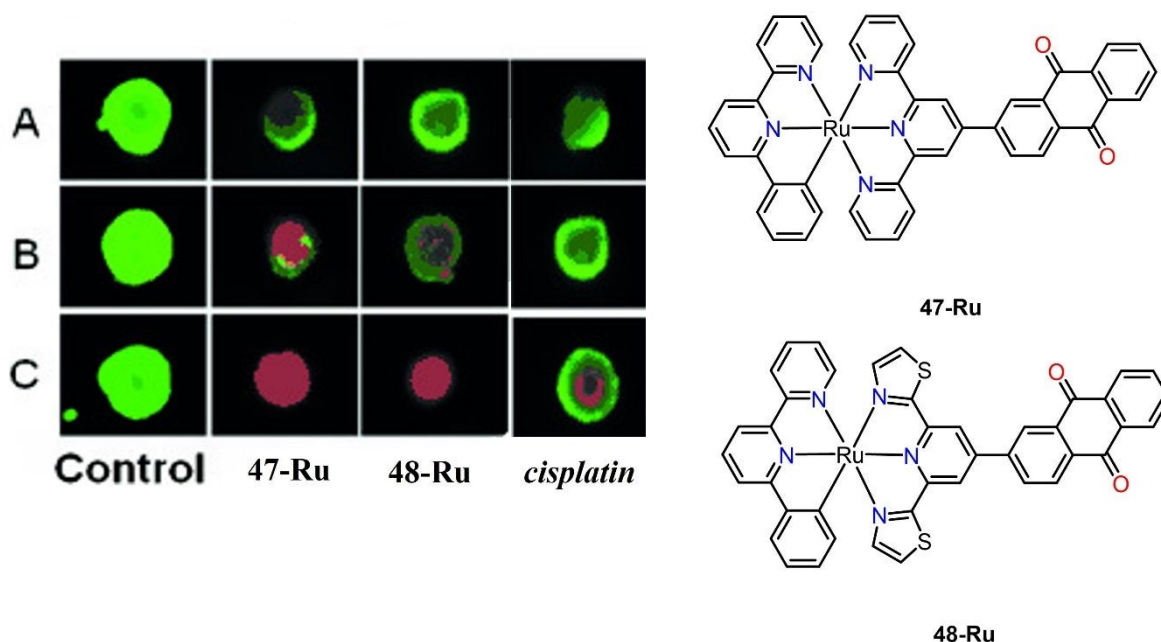


Figure 21. Inhibition of MCTS HeLa growth treated with **47-Ru**, **48-Ru**, and cisplatin analyzed by fluorescence microscopy; **A)** **47-Ru** and **48-Ru** (0.5 μM), *cisplatin* (15.0 μM), **B)** **47-Ru** and **48-Ru** (1.0 μM), *cisplatin* (30.0 μM), and **C)** **47-Ru** and **48-Ru** (2.0 μM), *cisplatin* (60.0 μM). (Reproduce with permission from ref. 107 Copyright 2015, Wiley-VCH).

On the other hand, most of the 49-Ru complexes possessed fluorine atoms incorporated into the NNN ligand, which could affect their anticancer activity. Complexes containing fluorine atoms (**49b-f-Ru**) exhibited higher cytotoxic activity compared to **49a-Ru** on A549 and A549R cancer cell lines. In addition, **49g-Ru** showed the lowest activity compared to the other cyclometalated complexes, although it had the highest number of fluorine atoms. Nonetheless, all the ruthenium complexes were more active than *cisplatin* (Table 9). Like complexes **47-Ru** and **48-Ru**, these complexes also showed a greater preference for accumulating in the nuclei and mitochondria, causing nuclear dysfunction that affected DNA replication. They also induced mitochondrial dysfunction by causing a loss in mitochondrial membrane potential (MMP), with the cell death promoted by apoptosis.¹⁰⁸

Table 9. IC₅₀ (μM) of complexes **49a-g-Ru** in cancer cell lines A549 and *cisplatin*-resistant A549^a

Compound	IC ₅₀ (μM)		
	A549	A549R	RF ^b
49a-Ru	4.71 \pm 0.14	5.53 \pm 0.20	1.2
49b-Ru	1.25 \pm 0.09	1.44 \pm 0.14	1.1
49c-Ru	2.20 \pm 0.16	3.11 \pm 0.41	1.4



49d-Ru	4.12 ± 0.33	4.54 ± 0.22	1.1
49e-Ru	2.22 ± 0.15	2.69 ± 0.09	1.2
49f-Ru	3.87 ± 0.20	3.85 ± 0.36	1.0
49g-Ru	6.12 ± 0.33	6.43 ± 0.45	1.0
cisplatin	17.2 ± 1.30	114 ± 10.1	6.6

^a Cell viability determined by MTT assay after treatment for 48 h

^b RF (Resistance Factor) = IC₅₀ (A549R)/IC₅₀ (A549)

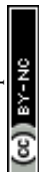
Compound **50-Ru** is a CCC pincer that contains fragments of naproxen and ibuprofen, which was tested on different cancer cell lines, and its inhibitory activity on COX enzymes responsible for inflammatory effects was also evaluated. The complex showed greater anticancer activity against the MCF-7 line (IC₅₀ = 0.91 ± 0.02 μM) compared to *cisplatin* (IC₅₀ = 2.42 ± 0.04 μM), with a selectivity index (SI) for **50-Ru** of 4.22 compared to 0.17 for *cisplatin*. Furthermore, **50-Ru** exhibited anti-inflammatory activity by inhibiting the growth of COX-1 and COX-2 isoforms, with an SI of 63.90 compared to that of ibuprofen (SI = 2.93) and the CCC pincer ligand (SI = 34.17), showing that the presence of ruthenium provides a favorable synergy in the anti-inflammatory capacity of the complex.¹⁰⁹

3.2.3. Other types of ligands

Baratta's group synthesized a series of cyclometalated Ru(II) C[^]N complexes (**51a-Ru** – **52cRu**), which were applied in cytotoxicity studies (**Figure 22**). The complexes **51a-d-Ru** were tested on two cell lines: human glioblastoma U87 MG and immortalized human cortical astrocytes (P10251-IM), using temozolomide (TMZ) as a control drug. The complexes containing a heterocyclic ring in the cyclometalating ligand (**51c-d-Ru**) exhibited the highest cytotoxic activity against U87MG, with IC₅₀ values of 1.4 and 1.7 μM, respectively. These complexes were more active than TMZ in U87 MG, which IC₅₀ was higher than 150 μM.¹¹⁰

Baratta *et al.* also tested the cytotoxic activity of ruthenium complexes bearing a cyclometalated terpyridine and different phosphine ligands (**52a-c-Ru**) on anaplastic thyroid cancer (ATC) cell lines (SW1736 and 8505C) and a healthy thyroid cell line (Nthy-ori 3-1) (**Table 10**). The complex **52a-Ru**, which has a non-chiral phosphine ligand showed the lowest cytotoxic activity, while complexes **Ru52b-c** were more active on cancer cell lines compared to *cisplatin*, suggesting that the presence of chiral centers is a viable strategy to improve the cytotoxic activity.¹¹¹

Table 10. ED₅₀ (μM) of complexes **52a-c-Ru** on ATC lines and Nthy-ori 3-1^a



Compound	ED ₅₀ (μM)		
	SW1736	8505C	Nhty-ori 3-1
52a-Ru	8.53 ± 0.98	7.73 ± 1.02	10.59 ± 1.28
52b-Ru	2.18 ± 0.16	1.95 ± 0.23	3.88 ± 0.31
52c-Ru	2.11 ± 0.11	2.06 ± 0.26	4.18 ± 0.09
cisplatin	6.40 ± 1.54	5.20 ± 1.82	11.28 ± 0.96

^a Cell viability determined by MTT assay after treatment for 72 h

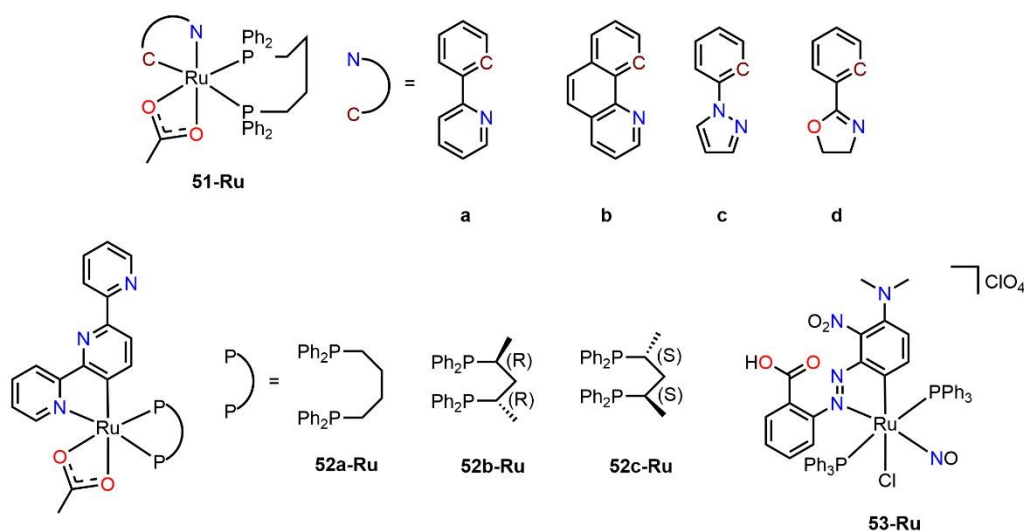


Figure 22. Phosphine bearing cyclometalated Ru(II) complexes (**51a-Ru** – **53-Ru**).

Ghosh's group synthesized a ruthenium(II) nitrosyl complex (**53-Ru**), able to release NO under visible light irradiation. This complex showed antiproliferative activity against A549 cell line to 2 μM of concentration after visible-light irradiation. Additionally, studies conducted on HeLa cell line showed that NO is responsible for cell death, suggesting that the release of NO from the cyclometalated complex is crucial.¹¹²

3.3. Osmium

Osmium complexes have been scarcely investigated in comparison with ruthenium and iron complexes. However, osmium derivatives often offer distinct features such as higher oxidation states, stronger π -back-donation, and slower ligand exchange kinetics, which would lead to different mechanisms of action against cancerous cells.^{49,113,114}

3.3.1. Phenanthroline and benzimidazole ligands

Gaiddon *et al.* conducted an evaluation of the *in vitro* and *in vivo* anticancer properties of cyclometalated **1-Os** and **2-Os** complexes (**Figure 23**), identifying the genes involved in their sensitivity/resistance by correlating their cytotoxicity with transcriptomic data from 60 cancer cell



lines. This study showed that osmium complexes, like ruthenium complexes, induce endoplasmic reticulum (ER) stress effectors, such as the transcription factor CHOP, thereby causing cellular apoptosis, which is unaffected by the p53 gene. Finally, a possible mechanism of resistance to osmium complexes was proposed, where it was observed that their cytotoxicity, compared to ruthenium, is less affected due to a higher induction of endoplasmic reticulum (ER) stress, resulting in reduced resistance and favoring cytotoxicity.⁷⁴

On the other hand, the Kašpárková group prepared six osmium complexes (**3a-Os** – **4c-Os**), with a cyclometalating ligand functionalized with benzimidazole. The complexes were more active than *cisplatin*, particularly **3b-Os**, with IC₅₀ values ranging from 0.08 to 0.45 μM against the human breast adenocarcinoma cell line (MDA-MB-231). Similarly, assays were conducted in MCTS of MDA-MB-231 cells (**Figure 24**), where complex **3b-Os** was the most active with an IC₅₀ of 0.82 μM. Additionally, **3b-Os** activated the ER stress pathway by altering calcium homeostasis, and it was confirmed through Western blot analysis by expression of several ER stress biomarkers, such as Bip, Ero1- α , IRE1 α , and CHOP.¹¹⁵

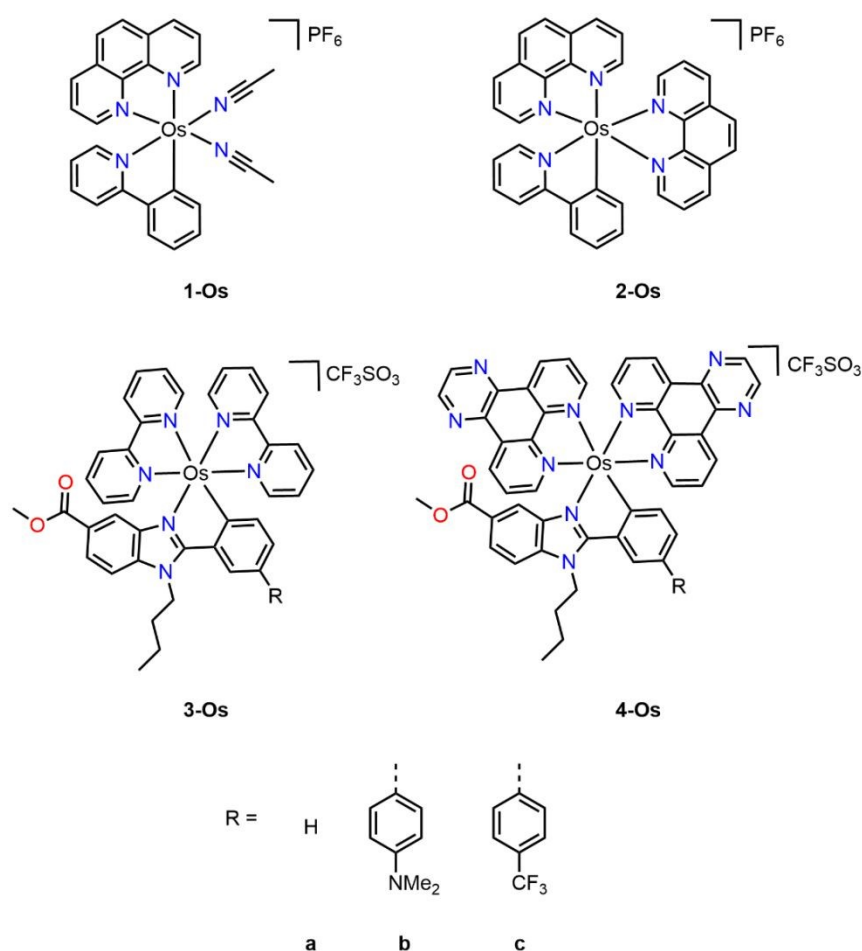


Figure 23. Osmium cyclometalated complexes with phenanthroline (**1-Os** and **2-Os**) and benzimidazole (**3-Os** - **4-Os**) ligands.

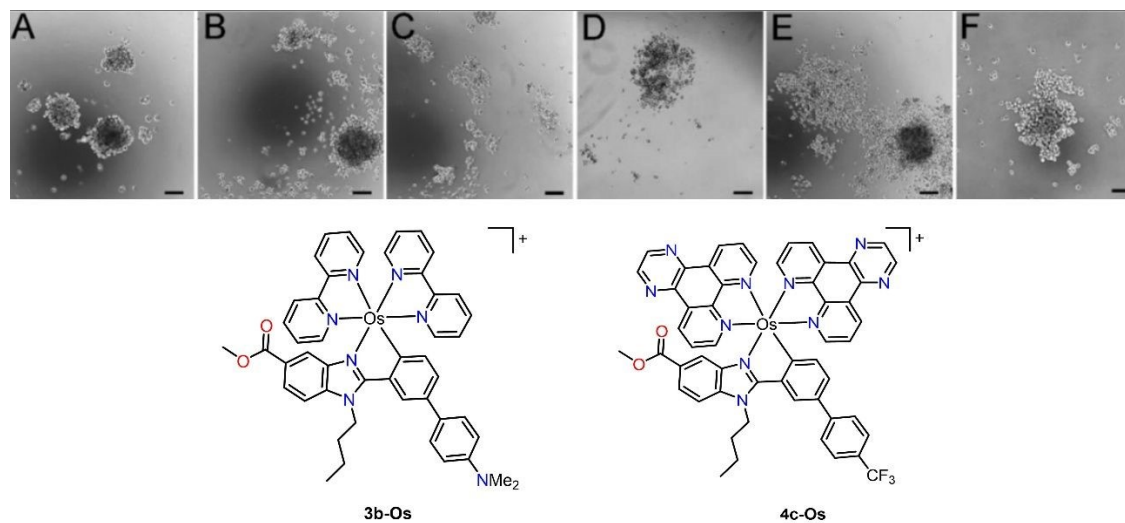


Figure 24. Images of MDA-MB-231 spheroids; A) untreated, treated with **3b-Os** B) 0.62 μM , C) 1.25 μM , and D) 2.5 μM , complex **4c-Os** E) 2.5 μM , and *cisplatin* F) 50 μM . (Reproduce with permission from ref. 115 Copyright 2023 without license, open access American Chemical Society).

3.3.2. Piano stool complexes

The Kandioller group synthesized a series of osmium complexes from 1,2,3-triazole derivatives (**5a-e-Os**) and 4-phenylthiazole (**6a-e-Os**) (**Figure 25**). For the **5a-e-Os** complexes, cytotoxicity assays were conducted against three human cancer cell lines (A549, SW480, and CH1/PA-1). The studies showed that **5a-Os** and **5b-Os** complexes were more active than *cisplatin* ($\text{IC}_{50} = 6.4 \pm 0.4 \mu\text{M}$) on the A549 lines (IC_{50} **5a-Os** = $6.0 \pm 0.4 \mu\text{M}$ and IC_{50} **5b-Os** = $5.5 \pm 0.6 \mu\text{M}$), while in the SW480 and CH1/PA-1 lines, *cisplatin* was more active than the osmium complexes. Finally, **5b-Os** was evaluated as a possible inhibitor of topoisomerase II α , an enzyme involved in regulating DNA topology and considered as a therapeutic target in cancer treatment, however, it did not present such inhibitory activity.¹⁰⁴



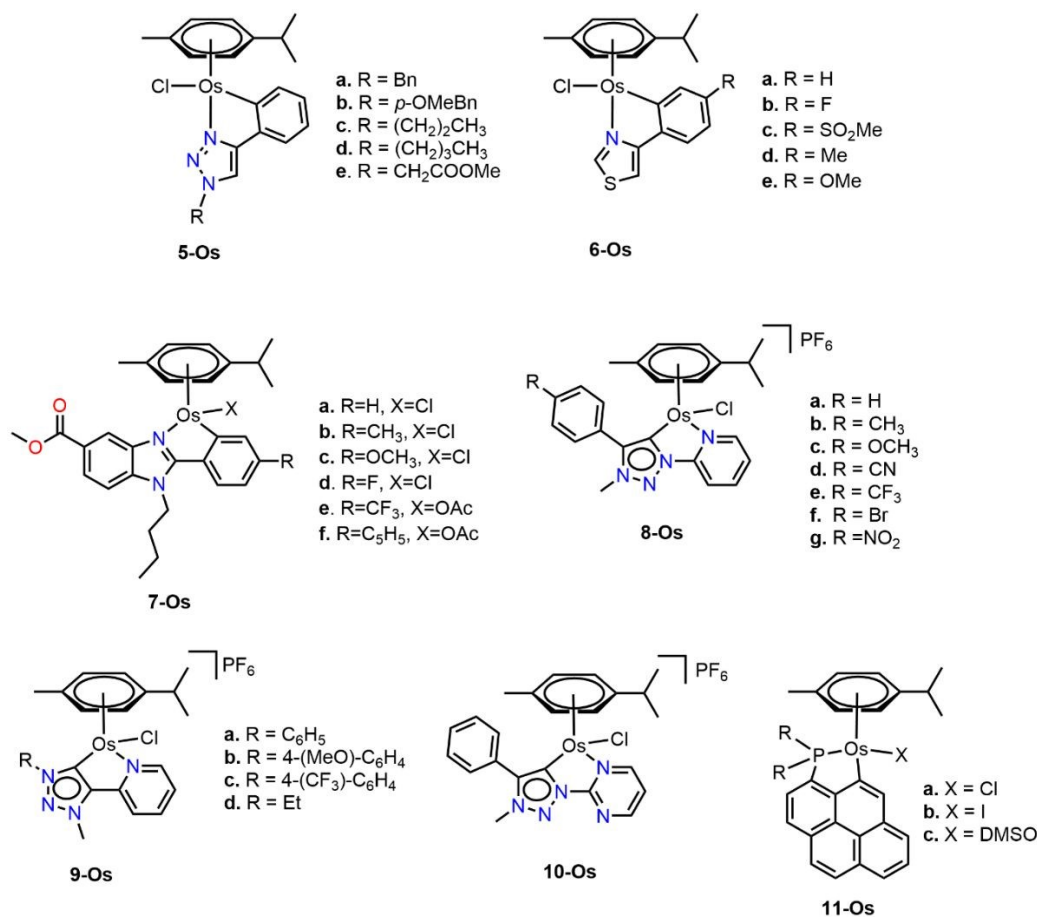


Figure 25. Piano stool cyclometalated osmium(II) complexes (**5a-11c-Os**).

Table 11. IC₅₀ (μM) of **6a-e-Os** complexes on three cancer cell lines^a

Compound	IC ₅₀ (μM)		
	A549	SW480	CH1/PA-1
6a-Os	17 ± 1	9.3 ± 1.1	3.0 ± 0.2
6b-Os	10 ± 1	7.1 ± 0.3	2.0 ± 0.4
6c-Os	10 ± 1	4.4 ± 0.5	0.83 ± 0.14
6d-Os	17 ± 1	9.3 ± 1.6	3.7 ± 0.6
6e-Os	14 ± 1	7.1 ± 1.2	2.2 ± 0.3

^a Cell viability determined by MTT assay after treatment for 96 h

In a subsequent study, **6a-e-Os** complexes were used to determine the anticancer activity against the previously mentioned cancer cell lines (**Table 11**). Biological studies revealed that the osmium complexes exhibited greater cytotoxic activity on the CH1/PA-1 cell line and lower activity on the



A549 cell line. The analysis of cell cycle interaction performed using propidium iodide staining, followed by flow cytometry, indicated that the osmium complex **6c-Os** induces significant disturbances in the cell cycle at IC_{50} levels, resulting in a 10-16% decrease of cells in the G1/G0 phase. Finally, osmacycles **6c-Os** and **6d-Os** showed an induction of apoptosis in SW480 cells after 48 hours, with 25% and 14% respectively, at concentrations twice their IC_{50} values.¹¹⁶

Ruiz *et al.* synthesized a series of osmium complexes featuring functionalized 2-arylbenzimidazole as the cyclometalating ligand (**7a-f-Os**). These compounds were used on different cancer cell lines, demonstrating an elevated activity against cancer cell lines A2780 and A2780cisR (**Table 12**). All complexes were more active in A2780cisR cell line compared to *cisplatin*, with RF values ranging from 0.9 to 1.9, in contrast to *cisplatin* (RF = 30.6). Finally, flow cytometry analysis showed that **7b-Os** and **7c-Os** caused a dose-dependent cell cycle arrest in the G0/G1 phase, and apoptosis as mechanisms of cell death induction.¹¹⁷

Table 12. IC_{50} (μ M) of **7a-f-Os** complexes on A2780 and A2780Ra cancer cell lines^a

Compound	IC_{50} (μ M)		
	A2780	A2780cisR	RF ^b
7a-Os	3.6 \pm 0.7	3.4 \pm 0.1	0.9
7b-Os	2.0 \pm 0.2	1.8 \pm 0.1	0.9
7c-Os	1.9 \pm 0.1	1.89 \pm 0.09	1.0
7d-Os	2.5 \pm 0.5	3.0 \pm 0.5	1.2
7e-Os	2.0 \pm 0.1	3.7 \pm 0.2	1.9
7f-Os	0.98 \pm 0.03	1.0 \pm 0.1	1.0
<i>cisplatin</i>	1.5 \pm 0.2	44 \pm 4	30.6

^a Cell viability determined by MTT assay after treatment for 48 h

^b RF (Resistance Factor) = IC_{50} (A2780cisR)/ IC_{50} (A2780)

The Košmrlj group synthesized a series of osmium complexes using mesoionic carbenes functionalized with bidentate pyridyl type as ligands (**8a-Os** – **10-Os**) (**Figure 25**). The osmium complexes were evaluated against HeLa cell line and IC_{50} values in the range of 24 to 100 μ M were obtained for **8b-Os**, **8f-Os**, **9c-Os**, and **10-Os**, with **8f-Os** being the most active. The remaining complexes could not be evaluated due to their low solubility in DMSO.¹¹⁸

The **11a-c-Os** complexes exhibited good cytotoxic properties in human A549 cells with IC_{50} values down to 1.42 μ M. Complex **11c-Os** showed a notable cytotoxic behavior against the MCF-7,



MCF10A (non-tumorigenic breast epithelial), and MDA-MB-435 (melanoma) cell lines with IC_{50} values of 4.36, 4.71, and 2.32 μM , respectively.¹¹⁹

3.3.3. Pincer complexes

Wong *et al.* prepared a series of cyclometalated osmium complexes linked to a phosphonium ring (**12a-d-Os**) (**Figure 26**). These complexes were evaluated against HeLa, fibrosarcoma (HT1080), MCF-7, and A549 cell lines, exhibiting superior cytotoxic activities with IC_{50} values ranging from 0.02 to 4 μM . In relation to *cisplatin*'s cytotoxicity, a two-order-of-magnitude increase was observed. Flow cytometry studies demonstrated that **12a-Os** induced changes in mitochondrial membrane potential (MMP) in HeLa cells, suggesting that this complex could be a potential anticancer agent.¹²⁰

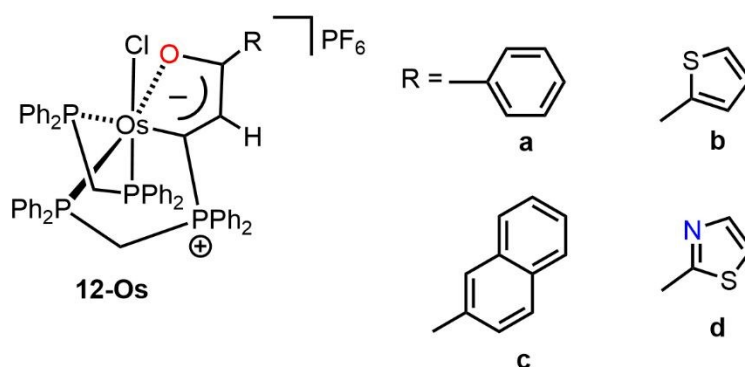


Figure 26. Pincer complexes of Os(II) with a tridentate cyclometalated ligand (**12-Os**).

4. Cyclometalated compounds of group 9

4.1. Rhodium

Various rhodium complexes have exhibited high antiproliferative activity against different cancer cell lines and can potentially inhibit enzymes involved in cancer cell growth.^{121,122} However, few studies have been conducted using cyclometalated complexes. For instance, the Sünkel's group has conducted extensive research on the anticancer activity of Rh(III) cyclometalated complexes containing a phenylpyridine ligand.^{86, 123-128} Complexes **1-15-Rh** (**Figure 27**) were evaluated against HT-29 (human colon carcinoma) and MCF-7 (human breast carcinoma) using MTT assays. The IC_{50} values ranged from 0.6 to 12.0 μM , with the most cytotoxic compound being the **14-Rh** complex, which showed IC_{50} values of $0.6 \pm 0.1 \mu\text{M}$ and $0.7 \pm 0.2 \mu\text{M}$ against HT-29 and MCF-7, respectively. These values were lower than those of cisplatin ($9.9 \pm 0.5 \mu\text{M}$ and $23.0 \pm 0.6 \mu\text{M}$ against HT-29 and MCF-7).



The García's group also evaluated the role of cyclometalated phenylpyridine by synthesizing complexes **16-Rh** and **17-Rh** (**Figure 27**).¹²⁹ Their cytotoxicity was assessed against human lung carcinoma (A549) and human colon adenocarcinoma (SW480). The highest cytotoxicity was observed with the **17-Rh** complex, which exhibited IC_{50} values of 4.1 ± 0.2 and 3.3 ± 0.1 μ M against A549 and SW480, respectively. The higher antiproliferative activity in A549 cells could be related to a higher cellular uptake of **17-Rh** compared to **16-Rh** ($23.3\% \pm 2$ higher). Additional studies showed that **17-Rh** may induce mitochondrial depolarization and an increase in intracellular ROS species concentration (likely superoxide radicals).

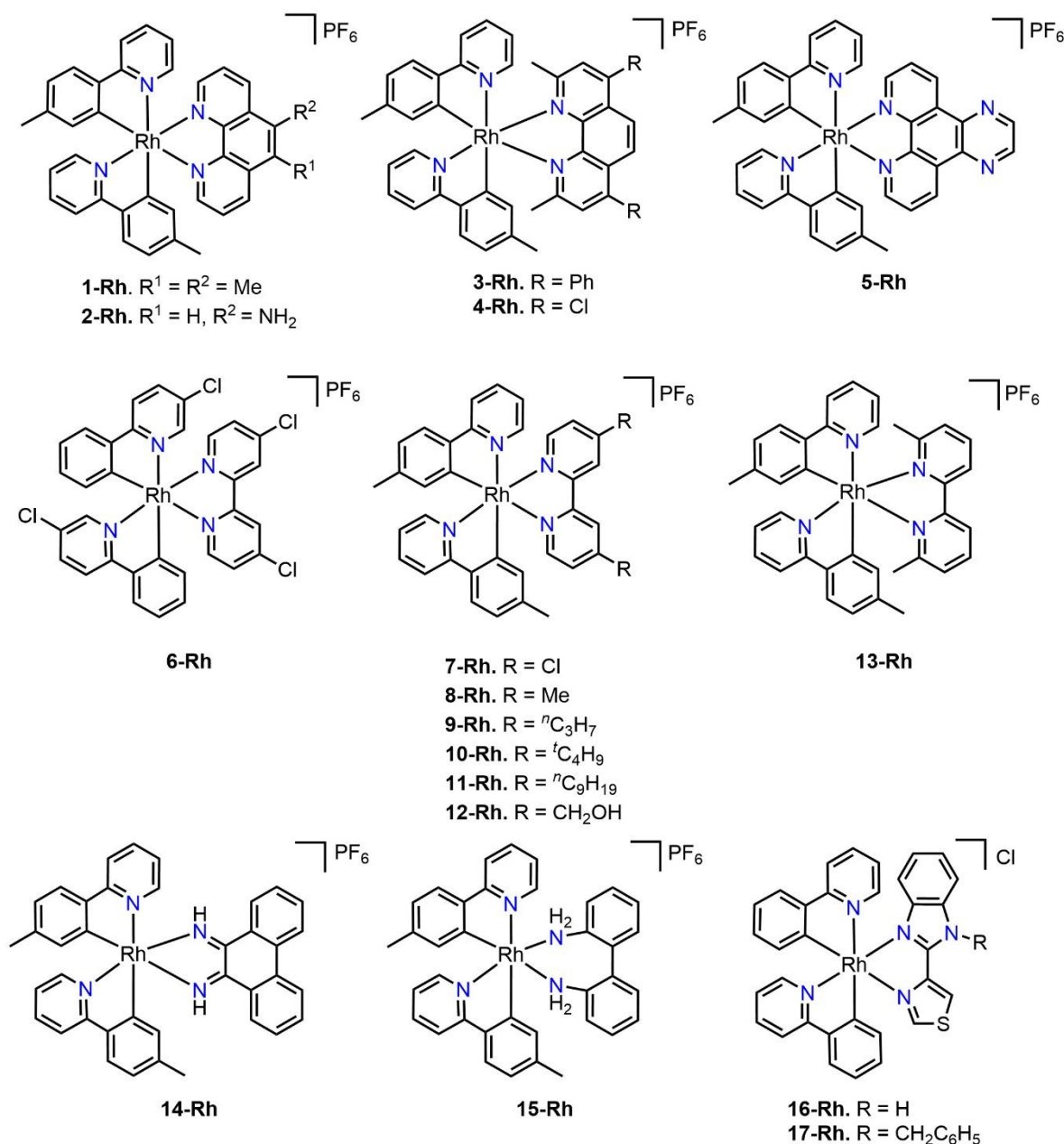


Figure 27. Rh(III) cyclometalated compounds used as potential anticancer agents (**1-Rh - 17-Rh**).

4.2. Iridium

Due to their fluorescence properties, the most common cyclometalated iridium(III) complexes possess a C^N type chelating ligand. Among the most widely used ligands are derivatives of 2-phenylpyridine (ppy), benzoquinoline (bzq), 2-phenylquinoline (pql), and 1-phenylisoquinoline (piq), which have been employed in studies as anticancer agents. The cytotoxic properties exhibited by these compounds will be discussed below.

4.2.1. Derivatives of phenylpyridine, benzoquinoline, 2-phenylquinoline, and 1-phenylisoquinoline

Liu's group has conducted cytotoxicity studies on different cell lines as well as various biochemical assays, aiming to explain the mechanisms of action of different cyclometalated C^N Ir(III) complexes.¹³⁰ Initially, **1a-c-Ir** complexes showed higher selectivity against the A549 cell line (**Table 13, Figure 28**), being **1c-Ir** the most active in this series. Using fluorescence microscopy, they determined that all complexes localized in the lysosomes (**Figure 29a**), which were initially stained red, while the complexes emitted green fluorescence. Through image overlay, it was suggested that the compounds could enter the lysosomes. Additionally, the complexes were also observed in the ER, inducing the opening of Ca²⁺ channels, which was reflected in the appearance of multiple bright green fluorescence spots (**Figure 29b**, far right). This resulted in changes in mitochondrial and ER Ca²⁺ levels, ultimately triggering apoptosis. In *in vivo* studies conducted on nude mice, doses of 2.0 mg/kg of cisplatin and 1.14 mg/kg and 2.28 mg/kg of **1c-Ir** were administered. It was observed that at a dose of 2.28 mg/kg, tumor size was reduced more significantly compared to cisplatin (**Figure 29c and 29d**). In a subsequent study, **2a-c-Ir** showed notable activity against the human gastric cancer cell line (SGC-7901), with **2c-Ir** being the most effective (**Table 13**). They determined that these complexes induce apoptosis through three pathways: first, the complexes act on lysosomal permeability and triggering apoptosis. Second, the complexes cause an intracellular increase in ROS and Ca²⁺ levels, leading to a decrease in mitochondrial membrane potential, promoting the release of cytochrome c into the cytosol, and activating caspase-3 production, thereby inducing apoptosis. Finally, the complexes cause DNA damage, inhibiting cell growth in the G0/G1 or S phases.¹³¹

Complexes **3a-c-Ir** (**Figure 28**) were evaluated in several lines and were most active against the HeLa cell line (IC₅₀ = 2.4 ± 0.2 (**3a-Ir**), 2.4 ± 0.1 (**3b-Ir**), 0.5 ± 0.1 μM (**3c-Ir**). In addition, These complexes induce apoptosis in HeLa cell through the following three pathways: activate caspase 3, induce DNA



damage, and induce autophagy by up-regulating the level of Beclin-1 expression and enhance the transform of LC3-I to LC3-II.¹³² Later, the same group reported similar complexes, but with chlorine (**4a-c-Ir**) or bromine (**5a-c-Ir**) at positions 11 and 12 of the phenazine moiety. For complexes **5a-c-Ir**, the results against the SGC-7901 cell line showed the same trend as mentioned before ($IC_{50} = 1.53 \pm 0.10$, 0.17 ± 0.05 , 0.30 ± 0.03 μ M, respectively). However, the chlorine derivatives (**4a-c-Ir**) showed an opposite trend, with the piq derivative being the least active ($IC_{50} = 1.3 \pm 0.2$, 6.2 ± 1.1 , 10.8 ± 0.5 μ M, respectively), suggesting that the presence of chlorine atoms significantly influences the cytotoxic activity.^{133,134} Likewise, this tendency was observed with imidazo-phenanthroline ligands (**6a-c-Ir**), where **6a-Ir** displayed the highest activity in most of the tested cancer cell lines, particularly against A549 cell line ($IC_{50} = 4.9 \pm 0.5$ μ M).¹³⁵

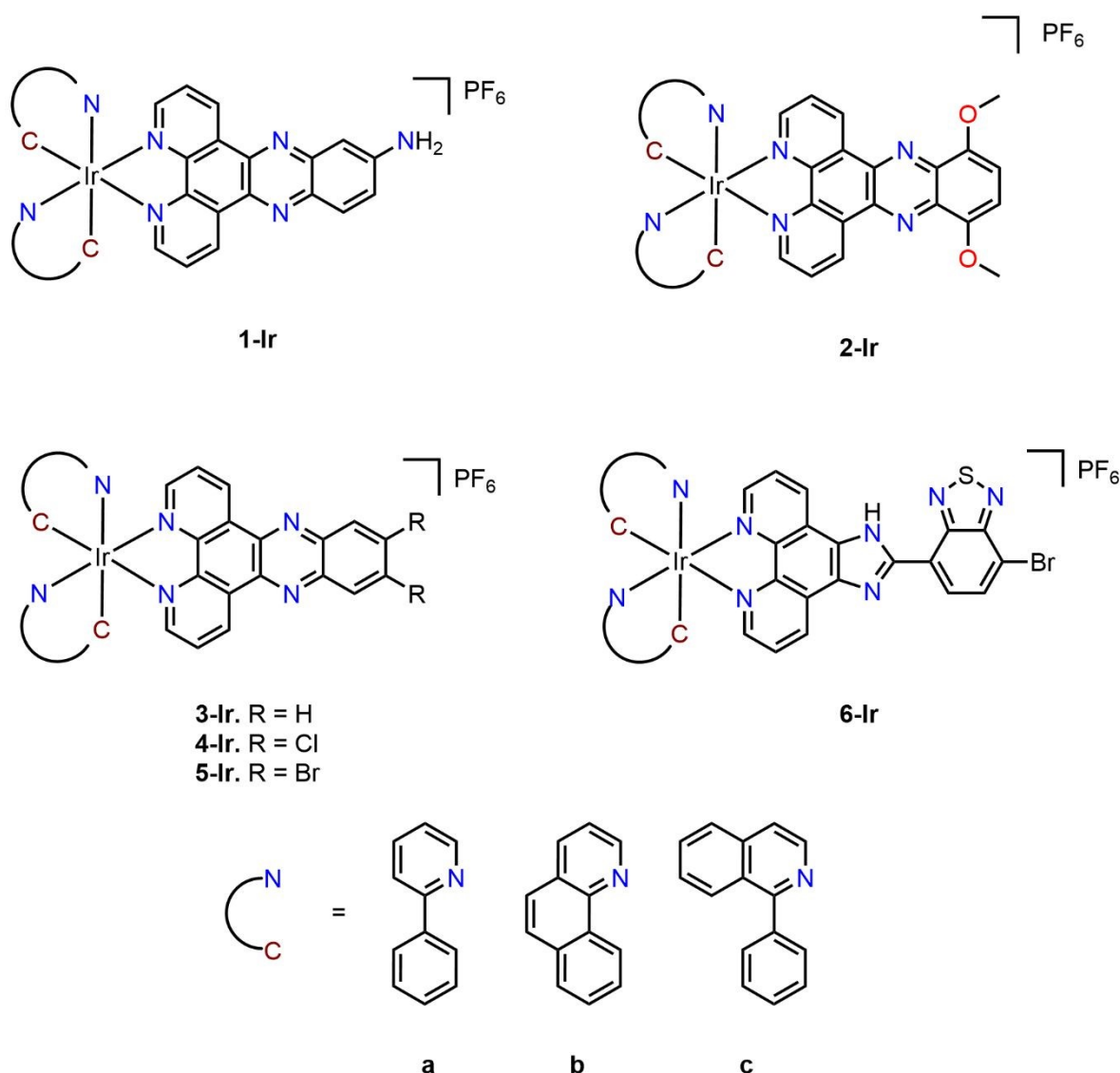
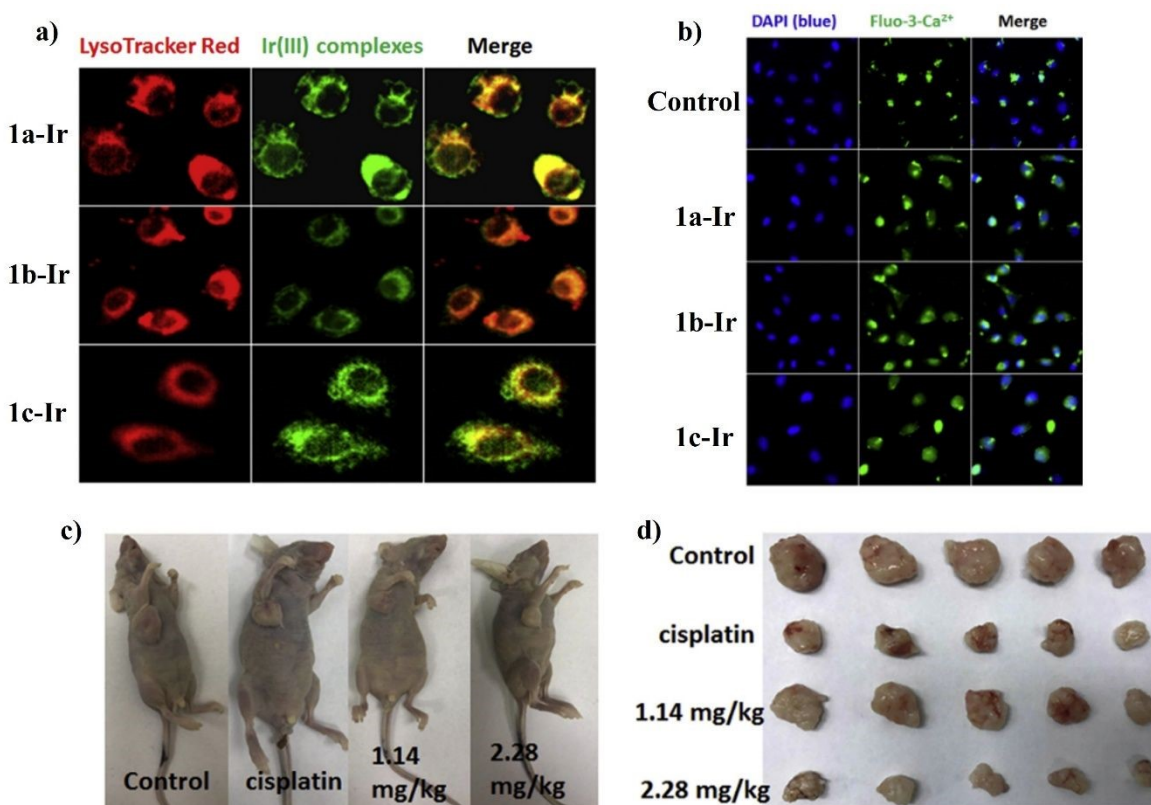


Figure 28. Structures of C^N cyclometalated Ir(III) compounds (**1a-Ir – 6c-Ir**).



Table 13. IC₅₀ (μM) of the **1a-Ir** - **2c-Ir** complexes on A549 and SGC-7901 cell lines^a

Compound	IC ₅₀ (μM)	
	A549	SGC-7901
1a-Ir	3.2 ± 0.4	-
1b-Ir	4.8 ± 0.5	-
1c-Ir	1.2 ± 0.2	-
2a-Ir	-	4.1 ± 0.5
2b-Ir	-	0.7 ± 0.1
2c-Ir	-	0.6 ± 0.2
<i>cisplatin</i>	7.5 ± 1.3	3.6 ± 0.5

^a Cell viability determined by MTT assay after treatment for 48 h**Figure 29.** Localization studies of complexes **1a-Ir** – **1b-Ir** using fluorescence microscopy in **a)** lysosomes and **b)** ER. **c)** and **d)** *in vivo* studies in nude mice with **1c-Ir**. (Reproduce with permission from ref. 130 Copyright 2019, Elsevier).

On the other hand, the antiproliferative activity of complexes **7a,b-Ir** and **8a,b-Ir** was evaluated against SGC-7901 and human hepatocellular carcinoma cell line BEL-7402 (**Figure 30**). Compound **7a-Ir** was the most cytotoxic against SGC-7901 ($IC_{50} = 0.5 \pm 0.1 \mu M$) and BEL-7402 ($1.0 \pm 0.1 \mu M$) and **8b-Ir** against BEL-7402 ($IC_{50} = 9.8 \pm 1.8 \mu M$)^{136,137} It was confirmed that these complexes could decrease GSH activity and lead to the accumulation of toxic lipid peroxidation products, such as malondialdehyde (MDA), resulting in increased ROS levels and intracellular calcium ion concentrations. Additionally, the complexes caused a reduction in mitochondrial membrane potential (MMP) and decreased the expression of caspase-3 and PARP proteins. Moreover, they reduced the levels of PI3K, AKT, VEGF, and mTOR proteins, inducing apoptosis through ROS-mediated mitochondrial dysfunction. The complexes also promoted autophagy by increasing the expression of Beclin-1, leading to the conversion of LC3-I to LC3-II. Furthermore, they were able to block the cell cycle at the S phase. These findings suggest that, collectively, the compounds can modulate the PI3K/AKT/mTOR pathway, ultimately triggering the activation of the Bcl-2 protein family, thereby inducing both apoptosis and autophagy (**Figure 31**).

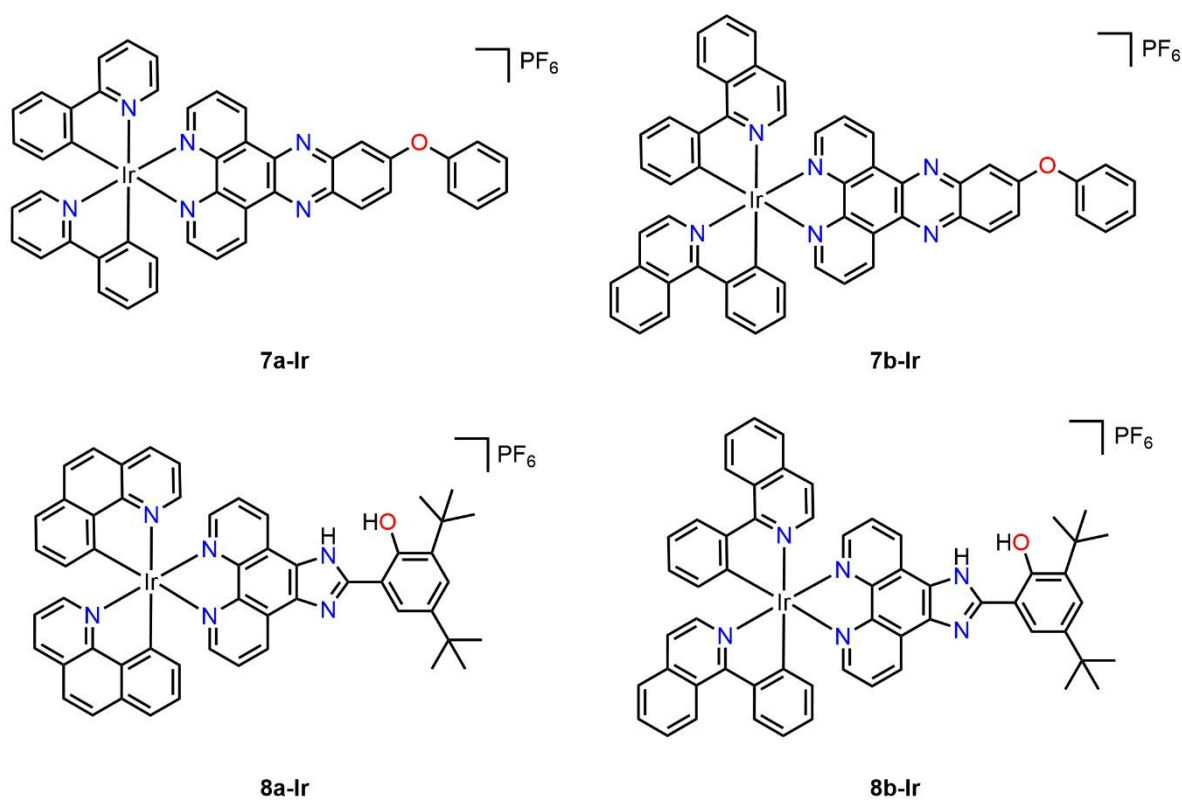


Figure 30. Ir(III) cyclometalated compounds (**7a-Ir** – **8b-Ir**) used as potential anticancer agents.



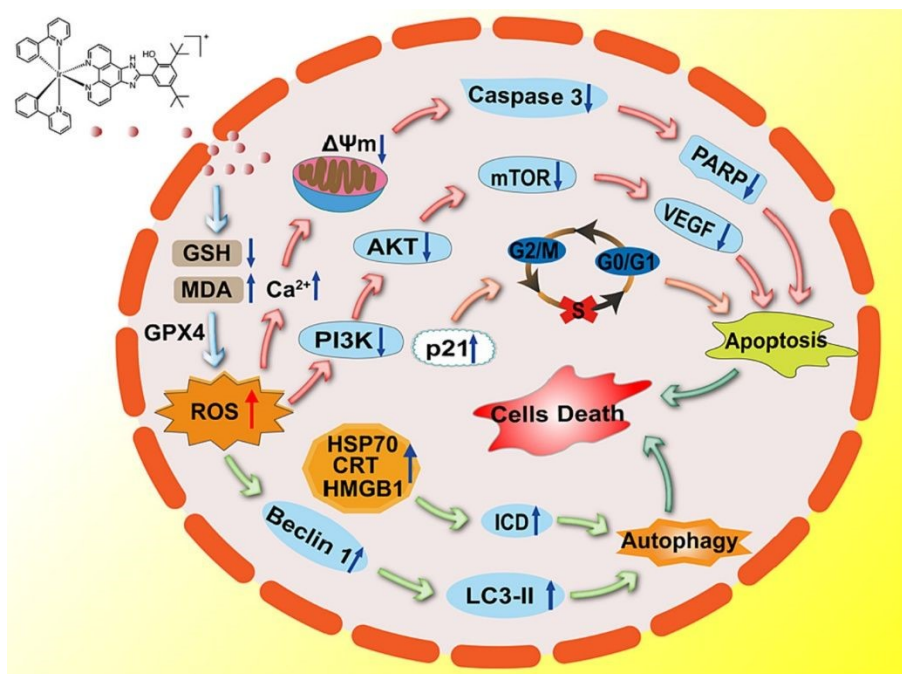


Figure 31. Proposed mechanism of action for complexes **8a-Ir** and **8b-Ir**, promoting cell death through apoptosis and autophagy. (Reproduce with permission from ref. 137 Copyright 2023, Elsevier).

Li and collaborators synthesized a series of cyclometalated Ir(III) complexes (**9a-c-Ir**) (**Figure 32**), which were tested against A549 and A549R cell lines. IC₅₀ values of the compounds ranged from 0.23 to 1.1 μM , which were lower than that of *cisplatin* ($18.2 \pm 1.3 \mu\text{M}$). Cytotoxicity was not altered against the resistant cell line (A549R) unlike *cisplatin*.¹³⁸ Confocal microscopy was used to determine the distribution and cellular uptake of cyclometalated iridium complexes in A549 cells (**Figure 33a** and **b**). The cells were incubated with MTDR (MitoTracker Deep Red) followed by iridium complexes **9a-c-Ir**, which were identified as being localized in the mitochondria (**Figure 33a**). Additionally, A549 cells were pretreated under different conditions to determine the cellular uptake mechanism. Cells were incubated with complex **9a-Ir** at different temperatures (**Figure 33b**). At 25 °C and 4 °C, cellular uptake efficiency was reduced using m-chlorophenylhydrazine (CCCP), whereas at 37 °C, the uptake of **9a-Ir** was significantly higher, indicating that the cellular uptake of this complex is energy-dependent. Furthermore, the ability of **9a-Ir** to cross the cell membrane was minimally affected when cells were treated with chloroquine at 37 °C, demonstrating that the cellular uptake of the complex is independent of endocytosis.



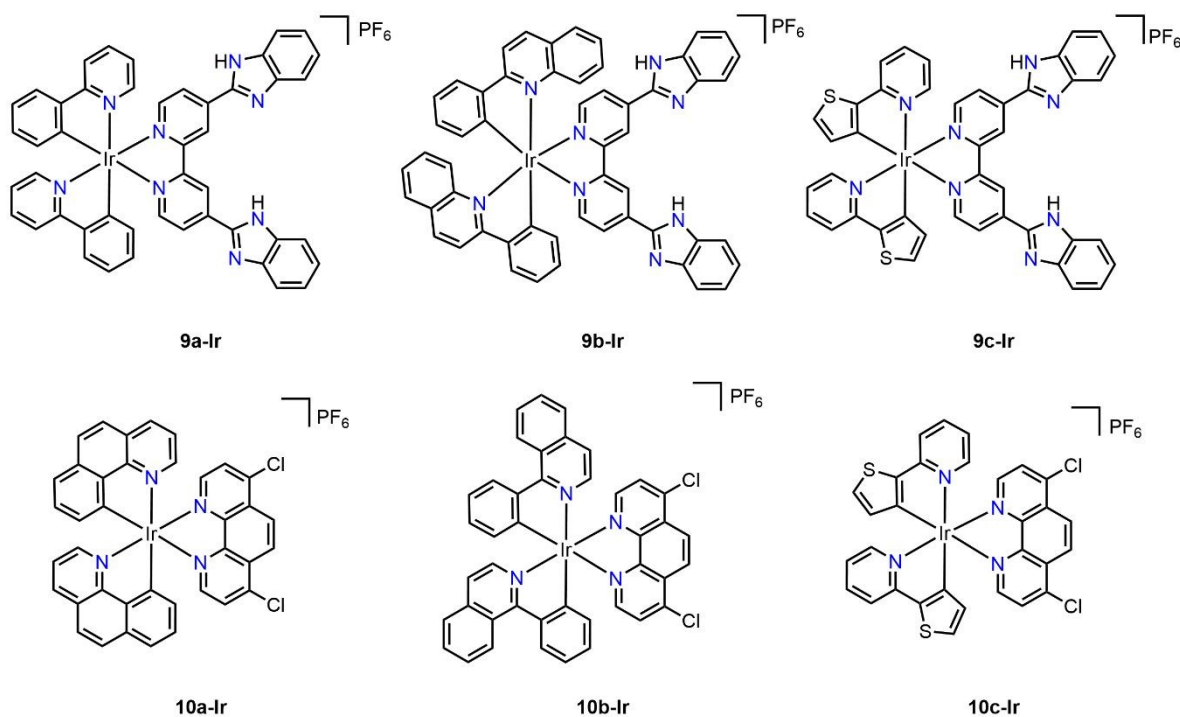


Figure 32. Ir(III) cyclometalated compounds (**9a-Ir** – **10c-Ir**) used as potential anticancer agents.

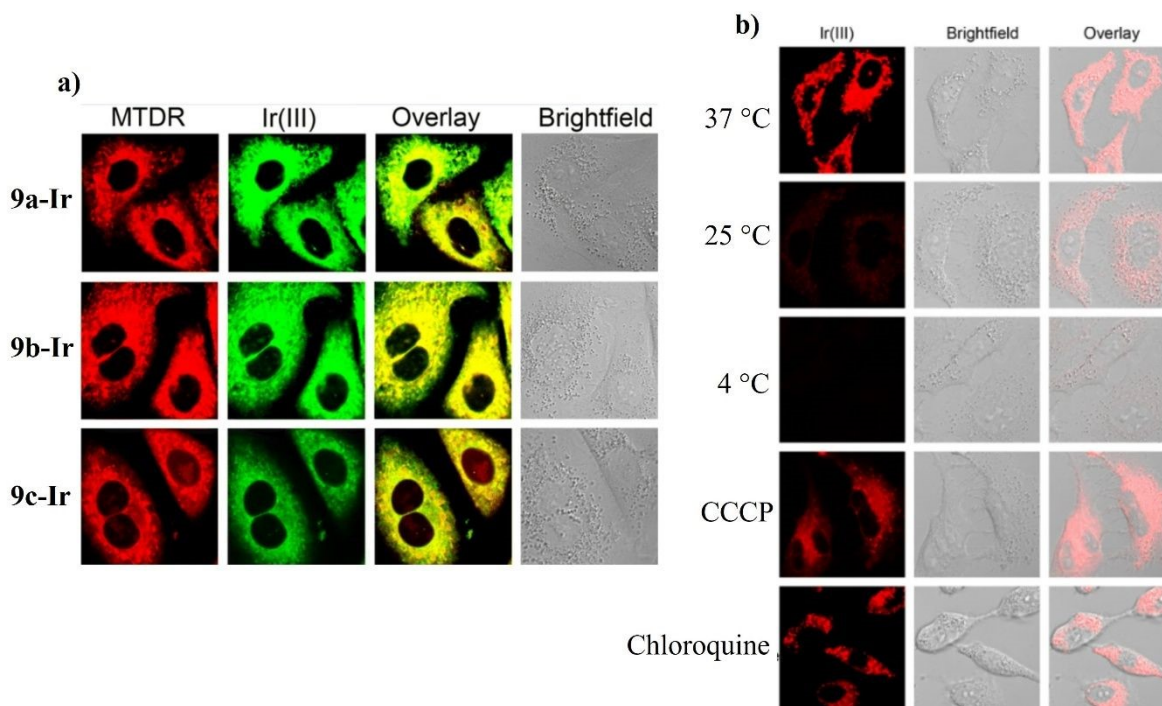


Figure 33. a) Cellular distribution of complexes **9a-c-Ir** and b) cellular uptake of complex **9a-Ir** in A549 cells through confocal microscopy. (Reproduce with permission from ref. 138 Copyright 2020, Springer).

Similar bis-cyclometalated compounds (**10a-c-Ir**) were tested by the Sun's group against a series of cancer cell lines, with HeLa being the most sensitive. The IC_{50} values obtained for the complexes in the HeLa cell line were $0.83 \pm 0.06 \mu\text{M}$ (**10a-Ir**), $4.73 \pm 0.11 \mu\text{M}$ (**10b-Ir**), and $4.95 \pm 0.62 \mu\text{M}$ (**10c-Ir**), respectively.¹³⁹ They investigated the ability of **10a-Ir** to induce apoptosis in HeLa cells using flow cytometry (**Figure 34a**) and laser confocal microscopy (**Figure 34b**). As the concentration of **10a-Ir** increased, the number of HeLa cells undergoing early and late apoptosis was significantly higher, indicating that the iridium complex primarily induces cell death through apoptosis (**Figure 34a**). Furthermore, confocal microscopy revealed that HeLa cells exhibited reduced cell size and membrane vesiculation as the concentration of **10a-Ir** increased, demonstrating its concentration-dependent efficiency in inducing apoptosis (**Figure 34b**). Molecular docking studies suggested that **10a-Ir** could interact with the PI3K receptor protein, which is typically overexpressed in HeLa cells. This study identified hydrophobic interactions between the protein and the complex, specifically involving ARG849 (**Figure 34c**).

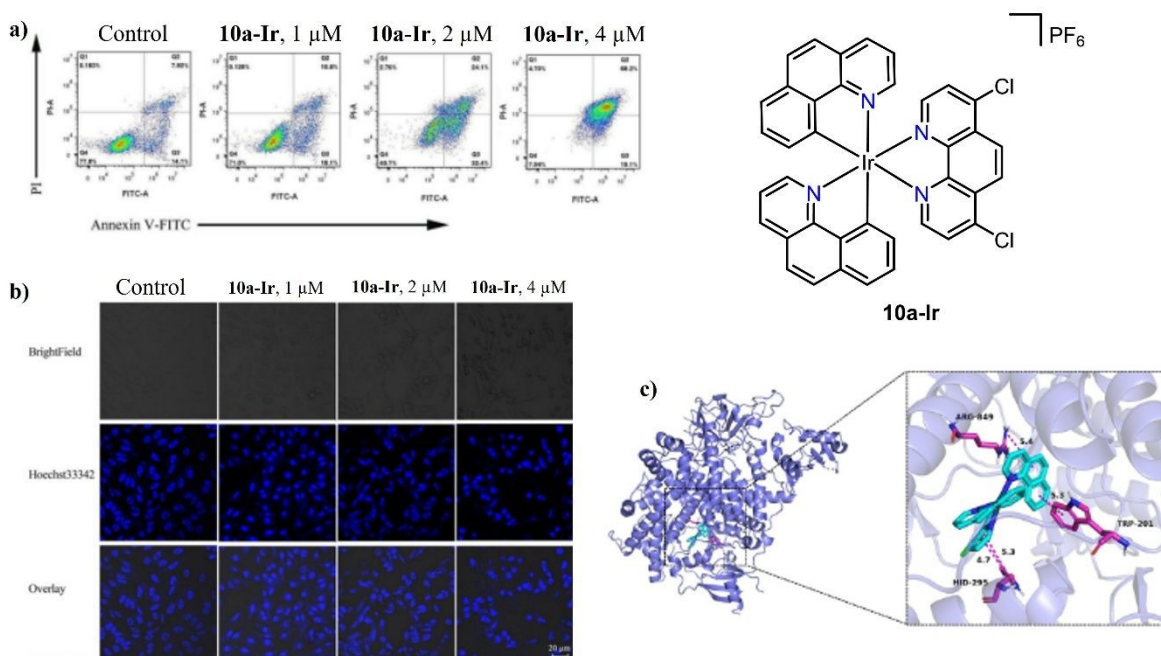


Figure 34. Apoptosis study of **10a-Ir** on HeLa cells through **a)** flow cytometry and **b)** laser confocal microscopy at different concentrations. **c)** Molecular docking study of the PI3K receptor protein with the **10a-Ir** complex. (Reproduce with permission from ref. 139 Copyright 2023, Elsevier).

The Chen's group synthesized complexes **11a-d-Ir** (**Figure 35**). Their activity against A549 ($IC_{50} = 3.3 \pm 0.5$ (**a**), 1.6 ± 0.2 (**b**), 5.2 ± 0.2 (**c**), 4.3 ± 0.4 (**d**) μM , respectively) showed the following trend: **11b-Ir** > **11a-Ir** > **11d-Ir** > **11c-Ir**.¹⁴⁰ It was observed that complex **11b-Ir** induced apoptosis and autophagy as mechanism of cell death. Qin reported four neutral Ir(III) complexes (**12a-d-Ir**) using a quinoline derivative as an auxiliary ligand and compared a series of C^N ligands, including a phenyl pyrazole (ppy). Activity against HeLa showed the following trend: **12d-Ir** > **12b-Ir** > **12c-Ir** > **12a-Ir** ($IC_{50} = 0.035 \pm 0.002$, 0.170 ± 0.05 , 2.14 ± 0.19 , 3.26 ± 0.78 μM , respectively), indicating that ppy ligand was the least active derivative, and the phenyl pyrazole ligand was the highest.¹⁴¹ Considering that ppy derivatives showed good cytotoxic activity, the impact of functionalizing this fragment on the cytotoxic activity needs to be further evaluated.

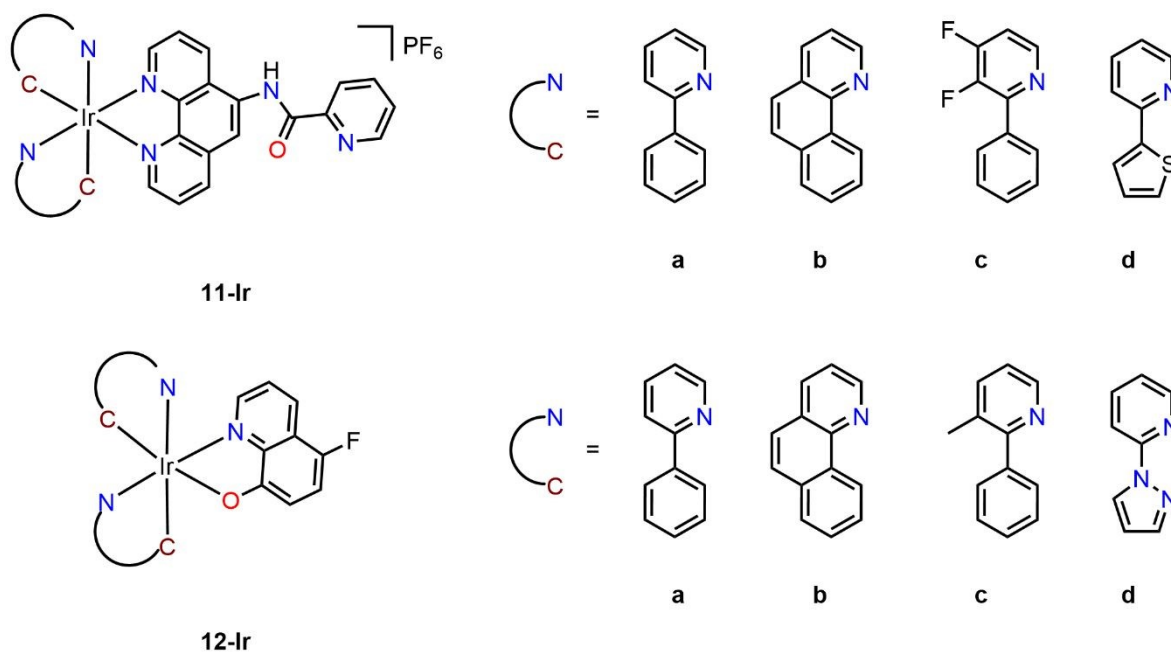


Figure 35. Ir(III) cyclometalated compounds (**11a-Ir – 12d-Ir**) used as potential anticancer agents.

Graf and collaborators reported a series of complexes derived from 2-(p-tolyl)pyridine (ptp) and from 2-(4-chlorophenyl)pyridine (**14-Ir**) with different N^N auxiliary ligands (**13a-g-Ir**) (**Figure 36**). The IC_{50} values against HT-29 (0.55 ± 0.10 (**a**), 0.21 ± 0.01 (**b**), 0.19 ± 0.04 (**c**), 0.12 ± 0.02 (**d**), 0.18 ± 0.02 (**e**), 6.8 ± 1.1 (**f**), 12.2 ± 1.5 (**g**) μM , respectively) of the ptp derivatives show that short chains increase cytotoxicity (**d** > **e** \approx **c** >> **f**). In addition, substituting one hydrogen atom by a methyl group



in R1 does not modify significantly the cytotoxic activity (**b** \approx **c**). The IC₅₀ values of chloride derivatives, long-chain and alcohol (**a** \gg **f** $>$ **g**) show low potency, suggesting they are not good substituents. Finally, the derivative of 2-(4-chlorophenyl)pyridine (**14-Ir**) showed similar activity to **13a-Ir**, indicating that no improvement was observed using a chlorine atom in the ppy fragment.^{86,126,127}

Another type of auxiliary N^N ligands explored by Graf are derivatives of 1,10-phenanthroline (**15a-e-Ir**). IC₅₀ values against HT-29 (0.2 ± 0.1 (**a**), 0.48 ± 0.26 (**b**), 0.61 ± 0.10 (**c**), 1.33 ± 0.45 (**d**), 1.76 ± 0.27 (**e**) μ M) indicate that methyl groups at positions 1 and 8 improve the cytotoxicity (**c** and **a**). On the other hand, substituents at positions 4 and 5 decrease the potency (**b** and **e**) (**Figure 36**).^{124,125}

Yang and coworkers synthesized a family of compounds (**16a-h-Ir**) and evaluated the relationship between the number and position of methyl groups and their cytotoxicity. All compounds exhibited low IC₅₀ values, mainly against the NCI-H460 cancer cell line. The increase in cytotoxicity was proportional to the number of methyl groups (IC₅₀ = 0.00505 ± 0.22 (**h**), 0.125 ± 0.5 (**f**) and 0.520 ± 0.95 (**d**) μ M, 1.09 ± 1.02 (**b**), 2.81 ± 1.02 (**g**), 2.52 ± 0.71 (**c**), 4.53 ± 0.86 (**e**), and 6.61 ± 0.93 (**a**) μ M). However, the most active compounds were those without functionalization in the ppy backbone.¹⁴²



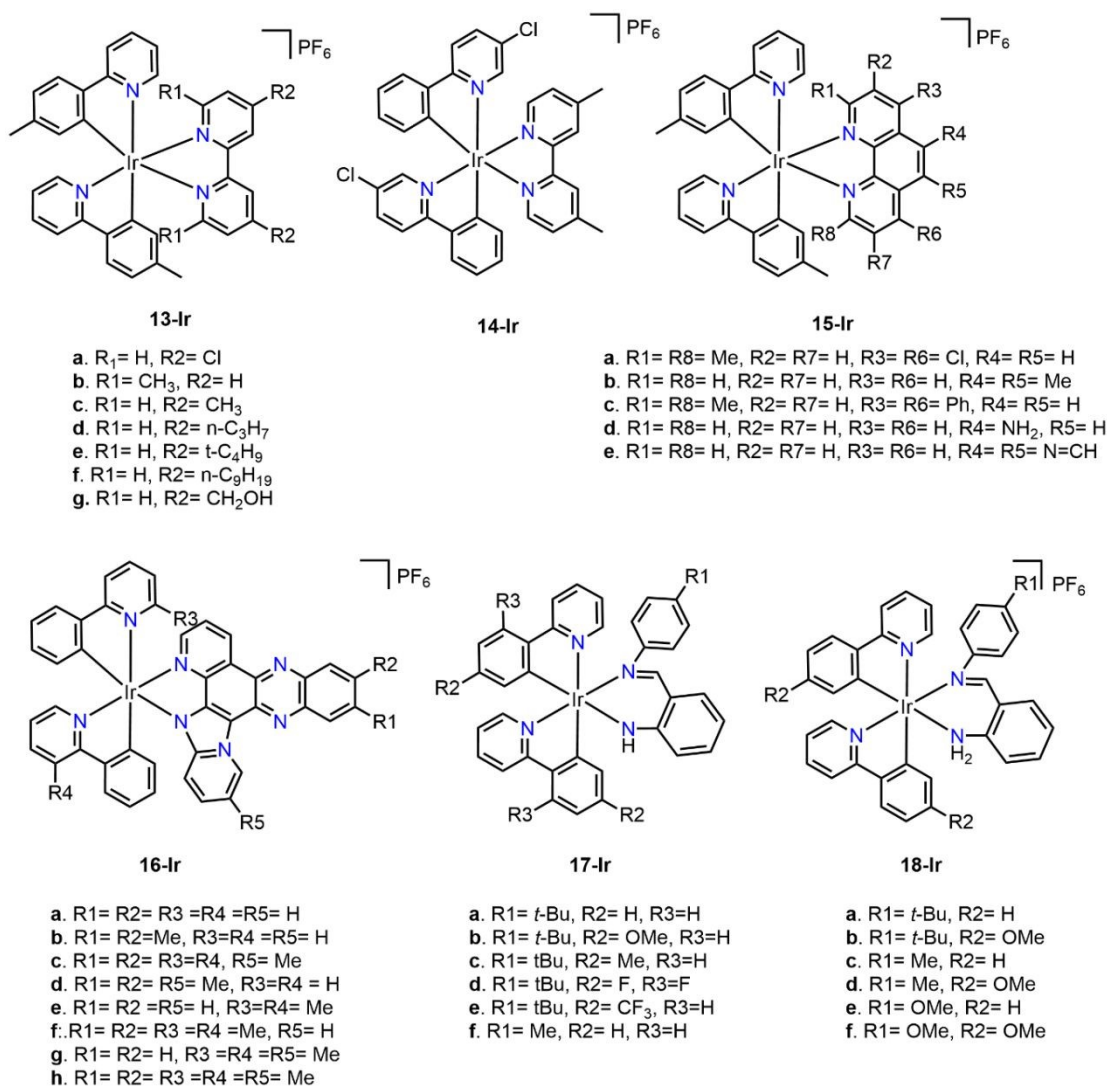


Figure 36. Ir(III) cyclometalated compounds (**13-Ir** - **18-Ir**) used as potential anticancer agents.

Li reported two series of compounds: neutral (**17a-f-Ir**) and cationic (**18a-f-Ir**), exploring the effect of different functional groups on the ppy fragment. When comparing both series, the IC₅₀ values between the cationic and neutral compounds were very similar, concluding that no improvement was observed. The most sensitive cell line was HeLa, where **17d-Ir** and **18c-Ir** were the most cytotoxic compounds in their respective groups, with IC₅₀ values of 10.16 ± 0.13 and 9.98 ± 0.03 μM.¹⁴³

4.2.2. Benzimidazole and carbene derivatives

Yellol reported a series of new complexes using different benzimidazoles (bim) and phenylpyrazoles (ppr) as either C[^]N or N[^]N ligands (**19-Ir** – **21-Ir**) (**Figure 37**). Complexes with bim as a N[^]N ligand (**19c-Ir**, **20c-Ir**, **21c-Ir**) showed the lowest cytotoxic performance against all tested cell lines (IC₅₀ > 10 μM). On the other hand, C[^]N ligands did not show an obvious trend, with **20a-Ir** and **21b-Ir** being



the most potent complexes against A2780 ($IC_{50} = 0.197 \pm 0.037$, 0.184 ± 0.008 μ M, respectively) and A2780cisR ($IC_{50} = 0.261 \pm 0.011$, 0.077 ± 0.015 μ M, respectively), which again suggests that no improvement was achieved with the unsubstituted bim fragment.¹⁴⁴

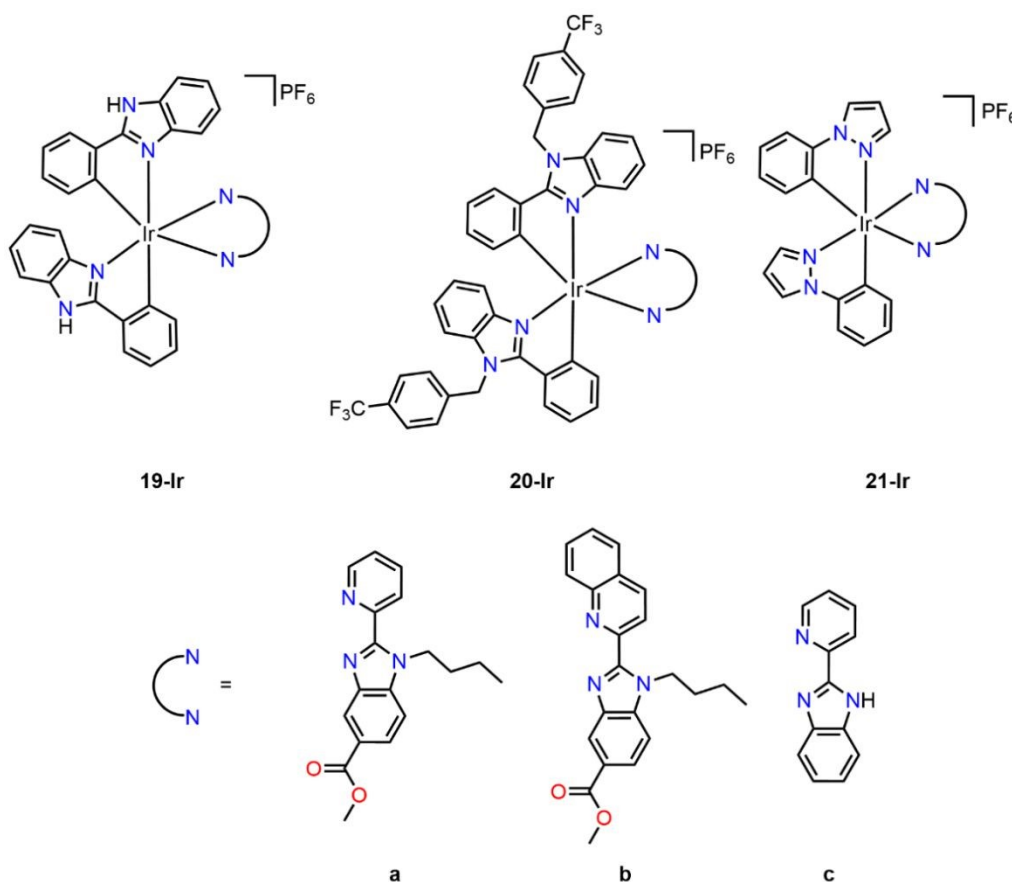


Figure 37. Ir(III) cyclometalated compounds (**19-Ir** – **21-Ir**) with benzimidazole ligands used as potential anticancer agents.

Laha and collaborators reported a series of Ir(III) complexes (**22a-Ir** – **23b-Ir**) (**Figure 38**), in which they varied the auxiliary N^N ligand and the length of the aliphatic chain attached to N in the C^NN bim ligand. Complexes with the shortest aliphatic chains (**23a-Ir** and **23b-Ir**) showed high cytotoxicity against MCF-7 ($IC_{50} = 0.4 \pm 0.22$, 0.4 ± 0.24 μ M, respectively), and no difference was observed between the N^N ligands, suggesting that the improvement in cytotoxic activity depends on the length of the aliphatic chains attached to N in the bim ligand.¹⁴⁵

N-heterocyclic carbenes (NHC) have also been explored as C^NN ligands. Bonfiglio's group carried out the synthesis of complexes **24a-d-Ir**, using an imidazolylpyridine and a series of C^NN ligands. Cytotoxicity against HCT116 ($IC_{50} = 2.3 \pm 1.4$, 2.1 ± 1.2 , 1 ± 1.1 , 1.7 ± 1.1 μ M, respectively) showed the following trend: **24c-Ir** > **24d-Ir** > **24b-Ir** > **24a-Ir**, indicating that benzothiazole improves



activity, while fluorinated derivatives reduce it.¹⁴⁶ Likewise, Ir(III) cyclometalated complexes with a series of C[^]N ligands derived from imine-NHC (**25a-e-Ir**) (**Figure 36**) have also been reported. These compounds were active against the A549 cell line, with IC₅₀ values ranging from 1.78 ± 0.30 to 4.95 ± 0.45 μ M, following the trend: **a** > **b** > **c** > **d** > **e**, indicating that increasing the size of the aryl substituent (**a-c** to **d-e**) enhances cytotoxicity. Additionally, increasing the length of the N substituent chain in the imidazole also produces the same effect (**a** vs **d** and **b** vs **e**).¹⁴⁷

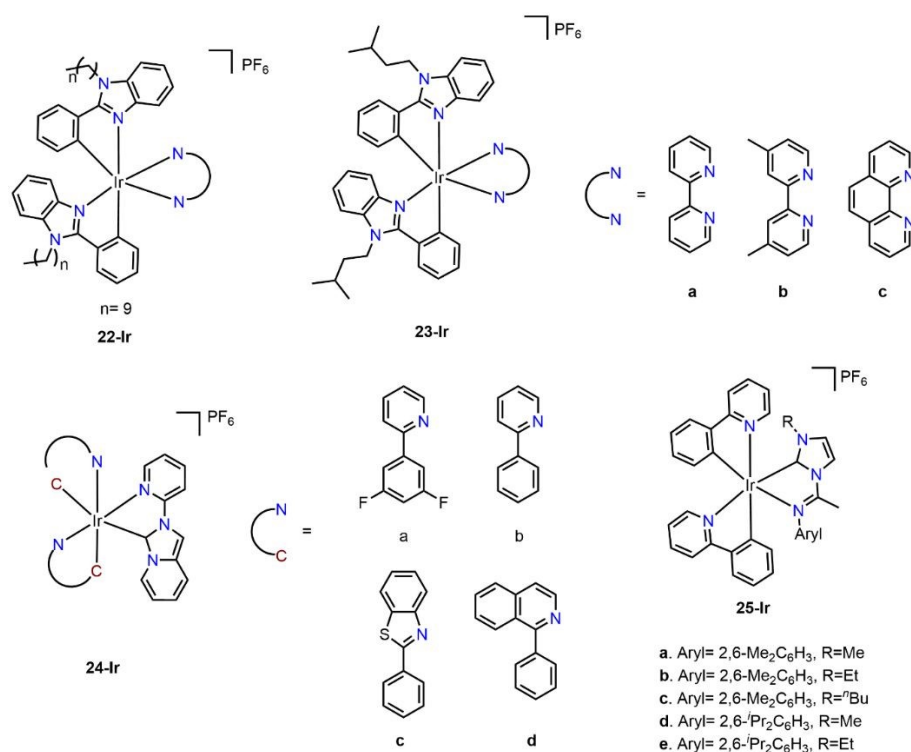


Figure 38. Ir(III) cyclometalated compounds (**22-Ir** – **25-Ir**) with carbene ligand used as potential anticancer agents.

4.2.3. Derivatives of 2,2'-bipyridine (bipy)

Mukhopadhyay and collaborators evaluated the antiproliferative activity of the **26a-c-Ir** complexes (**Figure 39**). All complexes showed similar log_{p_{0/w}} values (1.19, 1.17, and 1.13, respectively) and binding constant (K_{app}) displacement studies (K_{app} = 6.25, 5.08, and 4.54×10^7 M⁻¹, respectively). Complex **26a-c-Ir** presented the lowest IC₅₀ values against HeLa cells (3.46 ± 0.62 , 6.82 ± 1.02 , and 7.46 ± 0.6 μ M, respectively), suggesting that the –SCH₃ group is essential for the biological activity.¹⁴⁸ They also evaluated the type of cell death induced by the **26a-Ir** complex by analyzing nuclear morphological characteristics and distinguishing between apoptotic, necrotic, and viable cells using fluorescence microscopy (**Figure 40a**). Healthy cells exhibited uniformly shaped nuclei with



homogeneous blue fluorescence, whereas cells treated with **26a-Ir** displayed intensely blue fluorescent nuclei, indicative of early apoptotic cells with condensed nuclei. An increase in the complex concentration led to a higher population of early apoptotic cells (blue fluorescence) and late apoptotic cells with fragmented nuclei (red fluorescence). This suggests that **26a-Ir** effectively induces apoptosis. Furthermore, intracellular oxygen levels were assessed using fluorescent staining to detect ROS (**Figure 40b**), revealing a concentration-dependent increase in intracellular ROS levels. This observation suggests that apoptosis is induced via the oxidative pathway.

In another study, Liu explored the effect of bulky substituents with complexes **27a-d-Ir**. The most cytotoxic complexes against A549 cells were **27b-Ir** and **27c-Ir**, with IC_{50} values of 4.34 ± 0.01 and 5.8 ± 0.21 μ M, respectively. Complex **27d-Ir** showed some selectivity toward A549, indicating that the introduction of a double bond in the connector may be responsible for this selectivity.¹⁴⁹ A family of fluorinated Ir(III) cyclometalated complexes (**28a-f-Ir**) (**Figure 39**) showed elevated cytotoxicity against the HeLa cell line, with **28f-Ir** being the most effective (**Table 14**).¹⁵⁰

Table 14. IC_{50} (μ M) of the **28a-f-Ir** complexes against HeLa cells^a

Compound	IC_{50} (μ M)
	HeLa
28a-Ir	1.9 ± 0.5
28b-Ir	2.5 ± 0.3
28c-Ir	3.1 ± 0.2
28d-Ir	3.4 ± 0.5
28e-Ir	1.2 ± 0.3
28f-Ir	0.5 ± 0.1
<i>cisplatin</i>	21.4 ± 1.2

^a Cell viability determined by MTT assay after treatment for 48 h



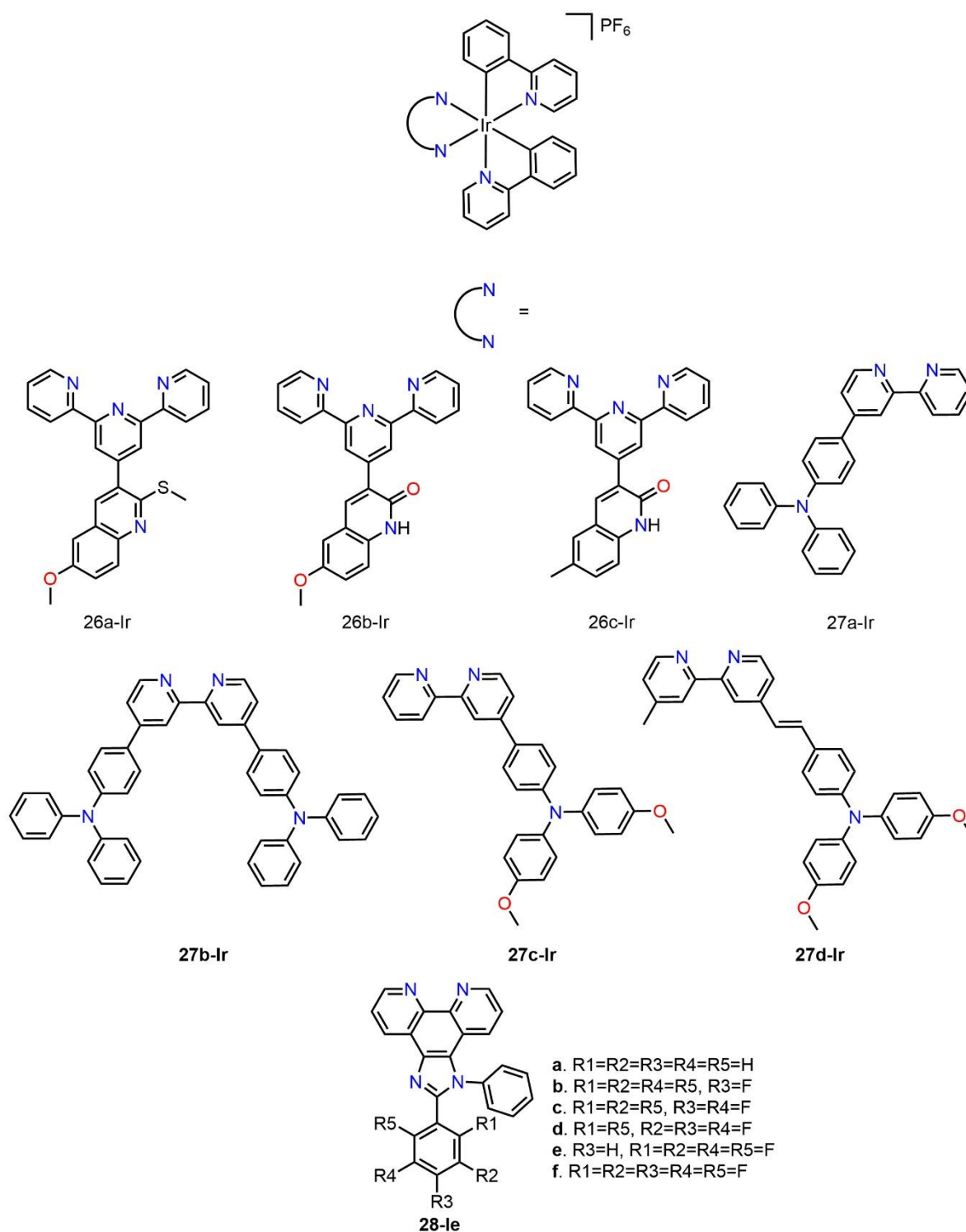


Figure 39. Ir(III) cyclometalated compounds (**26a-Ir** – **28f-Ir**) with 2,2'-bipyridine ligands used as potential anticancer agents.



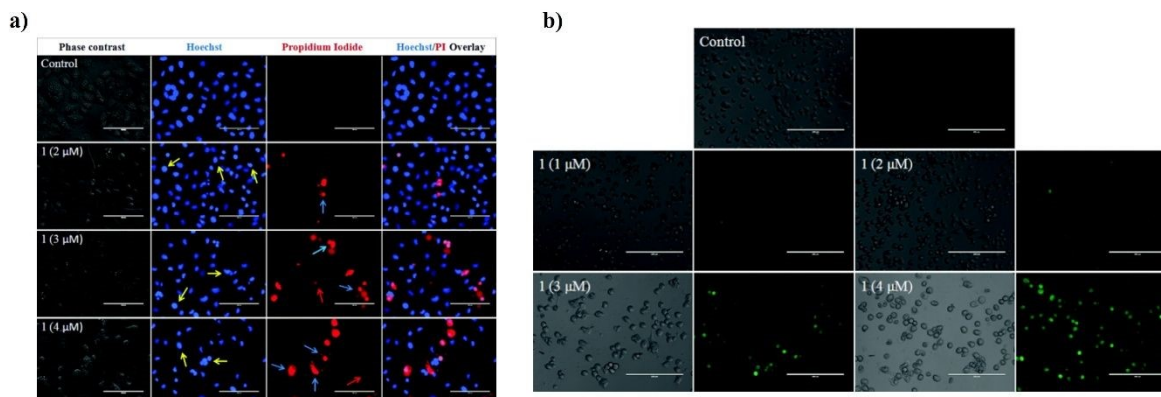


Figure 40. a) Morphological changes in HeLa cells treated with **26a-Ir** at different concentrations. Yellow, blue, and red arrows indicate early apoptotic cells (bright blue nuclei), late apoptotic cells (fragmented nuclei), and necrotic cells, respectively. b) HeLa cells treated for the detection of intracellular ROS generation using fluorescence staining. (Reproduce with permission from ref. 148 Copyright 2017, Royal Society of Chemistry).

Additionally, Yi and collaborators¹⁵¹ reported complex **29-Ir** (**Figure 41**) showing an IC_{50} of $3.6 \pm 0.3 \mu M$ against A549. Similar compounds were tested by Wang (**30-32-Ir**) against different cancer cell lines. Complex **32-Ir**, which features an alkyne group as a connector, was the most active against the gastric cell line SGC-7901 ($IC_{50} = 4.4 \pm 0.1 \mu M$) and a low cytotoxicity in normal cell line (NIH3T3, $IC_{50} = >100 \mu M$). The cytotoxicity of all these compounds was similar to or better than that of *cisplatin*, and they showed medium to good selectivity toward the healthy mouse fibroblast cell lines tested (NIH3T3).¹⁵² Complexes **33-Ir** and **34-Ir** were reported by Tang *et al.*, and by Wang *et al.*^{153,154} Subsequently, **35a-c-Ir** complexes were reported by Liu *et al.* These compounds can be considered a family of compounds which variations depend on the functionalization of the phenanthroline moiety. Compound **33-Ir** was the first reported and bears the bulkiest ligand of all. This complex showed high cytotoxic activity against all tested cancer cell lines, with a notable IC_{50} value of $1.0 \pm 0.02 \mu M$ against B16 (human skin cancer). Additionally, it exhibited great selectivity toward the normal cell lines tested (NIH3T3, $IC_{50} = 68.9 \pm 1.5 \mu M$). The cytotoxicity of **34-Ir** against BEL-7402 (cervical adenocarcinoma from human papillomavirus) was similar that of *cisplatin*. The **35a-Ir** complex was the most effective with an IC_{50} of $3.6 \pm 0.1 \mu M$ against SGC-7901 (human gastric cancer). However, complex **35c-Ir**, bearing the smallest ligand among this family of complexes, showed the best selectivity toward the normal cell lines tested (NIH3T3).¹⁵⁵ All these complexes (**29a-Ir – 35c-Ir**) exhibit similar mechanisms of action, which involve DNA damage leading to cell cycle arrest. Additionally, they localize to the ER, inducing an increase in Ca^{2+} ion production, which subsequently triggers enhanced intracellular ROS generation. This results in a decrease in MMP and



an increase in cytosolic cytochrome c, leading to caspase-3 activation and ultimately inducing apoptotic cell death (**Figure 42**).

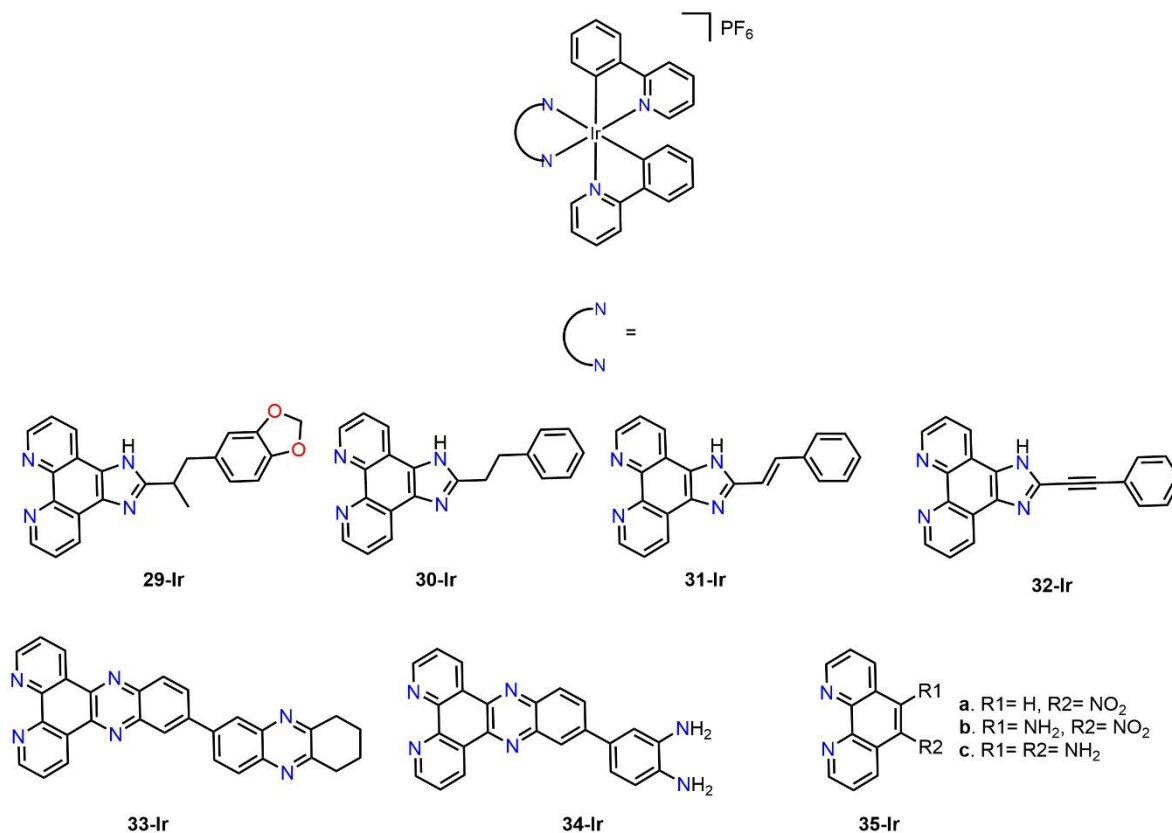


Figure 41. Ir(III) cyclometalated compounds (**29-Ir – 35-Ir**) with 2,2'-bipyridine ligands used as potential anticancer agents.

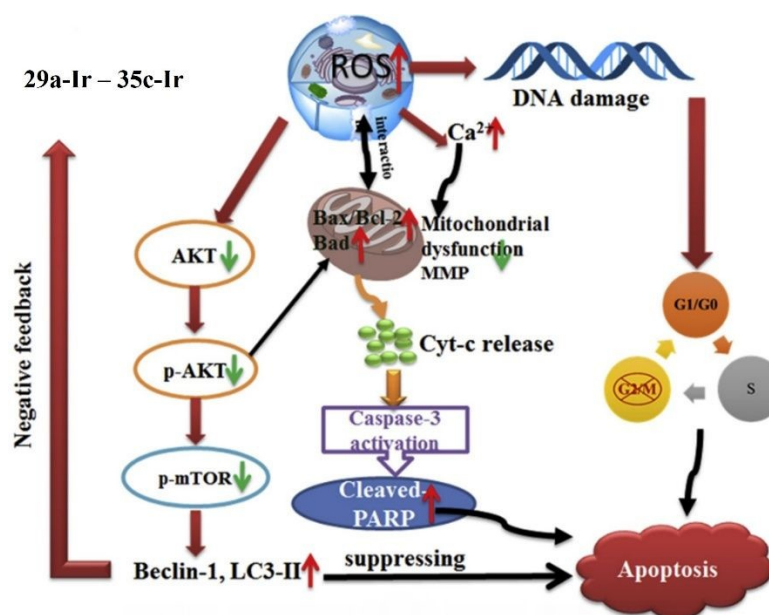


Figure 42. Plausible mechanism of action followed by the **29a-Ir – 35c-Ir** complexes. (Reproduce with permission from ref. 154 Copyright 2018, Elsevier).

4.2.4. Other auxiliary ligands

Two iridium(III) complexes have been reported using 2,2'-biphenyldiamine (**36a-Ir**) and 9,10-diaminophenanthrene (**36b-Ir**) as N^N ligands (**Figure 43**). These complexes were found to be selective against MCF-7, with IC₅₀ values of 7.8 ± 0.4 and 0.9 ± 0.2 μM , showing a significant improvement when using the phenanthrene derivative, as previously reported by the same research group.^{123,128}

Pérez-Arnaiz reported the use of thiabendazole (**37a-Ir**) and *N*-benzylthiabendazole (**37-Ir**) (**Figure 43**). Like other compounds, the *N*-substituted complex showed better cytotoxic activity against A549 (IC₅₀ = 18.9 ± 0.2 , 4.0 ± 0.4 μM , respectively). The pK_a value of **37a-Ir** (6.76 ± 0.03) suggests that at physiological pH partial deprotonation occurs, affecting the charge and thus the cellular uptake, thereby reducing its activity.¹²⁹

Yang and coworkers evaluated two new complexes bearing 5-bromo-8-quinolinoline and varying the C^N ligand (**38a-Ir** and **38b-Ir**) against different cell lines. Against the HeLa cell line, the IC₅₀ values (3.59 ± 0.44 μM and 0.50 ± 0.39 μM) indicate that the pyrazole derivative (**38b-Ir**) was the most active.¹⁵⁶ The cytotoxicity against A549 and A549/DDP of a pair of neutral compounds as O^N ligands (**38c** and **39-Ir**) was then evaluated. Both complexes showed high cytotoxicity, with A549/DDP being the most sensitive cell line (IC₅₀ = 0.53 ± 0.11 and 0.09 ± 0.03 μM , respectively). Importantly, complex **38c-Ir** was 737 times more active than *cisplatin* (IC₅₀ = 66.34 ± 1.21 μM), indicating that the position of the bromine is crucial for the cytotoxic performance.¹⁵⁷

Recently, Temram *et al.* synthesized two neutral complexes with monodentate cyano ligands (**40a-Ir** and **40b-Ir**). The resulting IC₅₀ values against MDA-MB-231 (triple-negative breast cancer) and HCC1937 (breast cancer) showed that compound **40b-Ir** (IC₅₀ = 72.8 ± 3.0 and 13.5 ± 2.8 μM , respectively) was more active than *cisplatin*. In contrast, **40a-Ir** was less active (223.9 ± 7.0 and 107.5 ± 3.5 μM), suggesting that the amine fragment improves the activity.¹⁵⁸

Kuang *et al.* reported a complex with a ppy derivative (**41a-Ir**), with a peculiar feature. The catechol fragment can easily be oxidized with two equivalents of Fe(III) to form a Schiff base, which, in an acidic environment, hydrolyzes to produce 2-hydroxy-1,4-benzoquinone and **41b-Ir**, a potent fluorophore. Such property allowed monitoring the complex in Fe(III)-rich cancer cells.¹⁵⁹ Initially, the phosphorescence of the complex is quenched as a result of photoinduced electron transfer (PET) from the catechol group. However, catechol can be chelated or oxidized by two equivalents of Fe(III)



via a two-electron pathway, forming a Schiff base, which subsequently undergoes hydrolysis to generate **41b-Ir**. **41a-Ir** enters the cells through endocytosis and localizes in the lysosomes, where the labile iron pool (LIP) is active and the microenvironment is acidic. Under these conditions, **41a-Ir** reacts in situ with Fe(III) to release hydroxybenzoquinone (BQ) and **41b-Ir**. This process leads to lysosomal damage and the release of **41b-Ir**, which subsequently localizes in the mitochondria, exhibiting strong fluorescence. The mitochondrial membrane potential (MMP) decreases, ultimately leading to cell death (**Figure 44**).

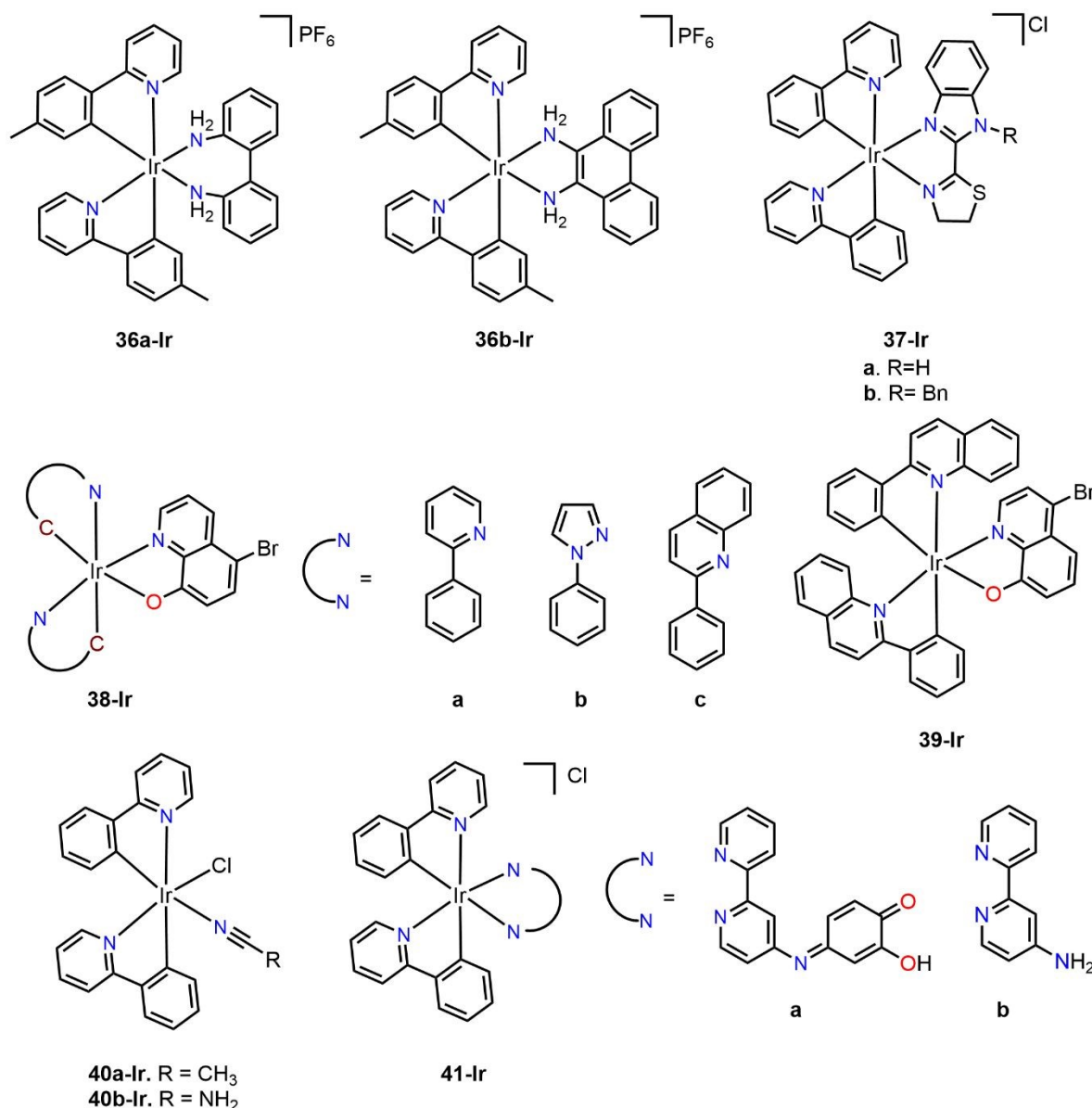


Figure 43. Ir(III) cyclometalated compounds (**36a-Ir** – **41-Ir**) with different ligands used as potential anticancer agents.



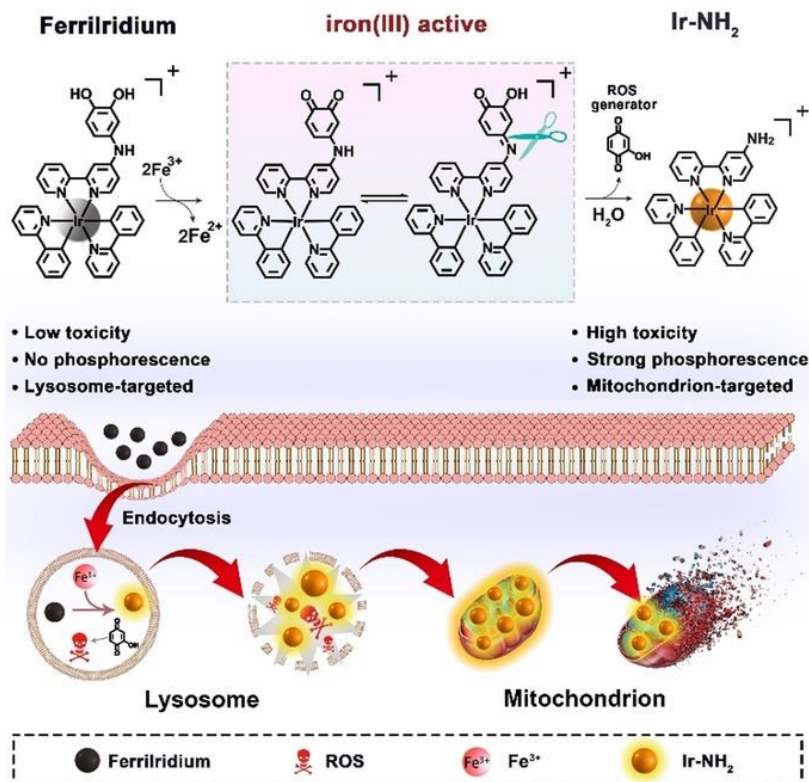


Figure 44. Proposed mechanism of action for Fe(III)-mediated activation in the reduction of **41a-Ir** to **41b-Ir**, leading to the subsequent cell death mechanism. (Reproduce with permission from ref.

159 Copyright 2018, Wiley-VCH).

4.2.5. C^N and Cp* complexes

Other common organometallic complexes of Ir(III) are those derived from the cyclopentadienyl (Cp) or pentamethylcyclopentadienyl (Cp*) ligands. In the literature, there are comparisons regarding the impact of Cp* and ppy ligands on the cytotoxic activity of Ir(III) complexes. For example, Liu's group carried out the synthesis of a group of cyclometalated Ir(III) complexes (**42a,b-Ir**) (**Figure 45**), using bipy derivatives (**43a,b-Ir**) as auxiliary ligands and comparing the cytotoxicity of the ligands (Cp* or ppy) on the A549 cancer cell line. It was found that bulky N^N ligands reduce the activity of the complexes, but more importantly, changing the C^N ligand shows a large variation, with Cp* complexes being the most potent: **42a-Ir** > **42b-Ir** > **43a-Ir** > **43b-Ir** (IC₅₀ = 3.56 ± 0.5, 17.27 ± 0.1, 32.73 ± 0.5, and >100 μM). Although the log*p*_{o/w} values suggest an explanation related to lipophilicity, the ability of Cp* derivatives to lose a chloride ion is favorable for cytotoxicity.¹⁶⁰



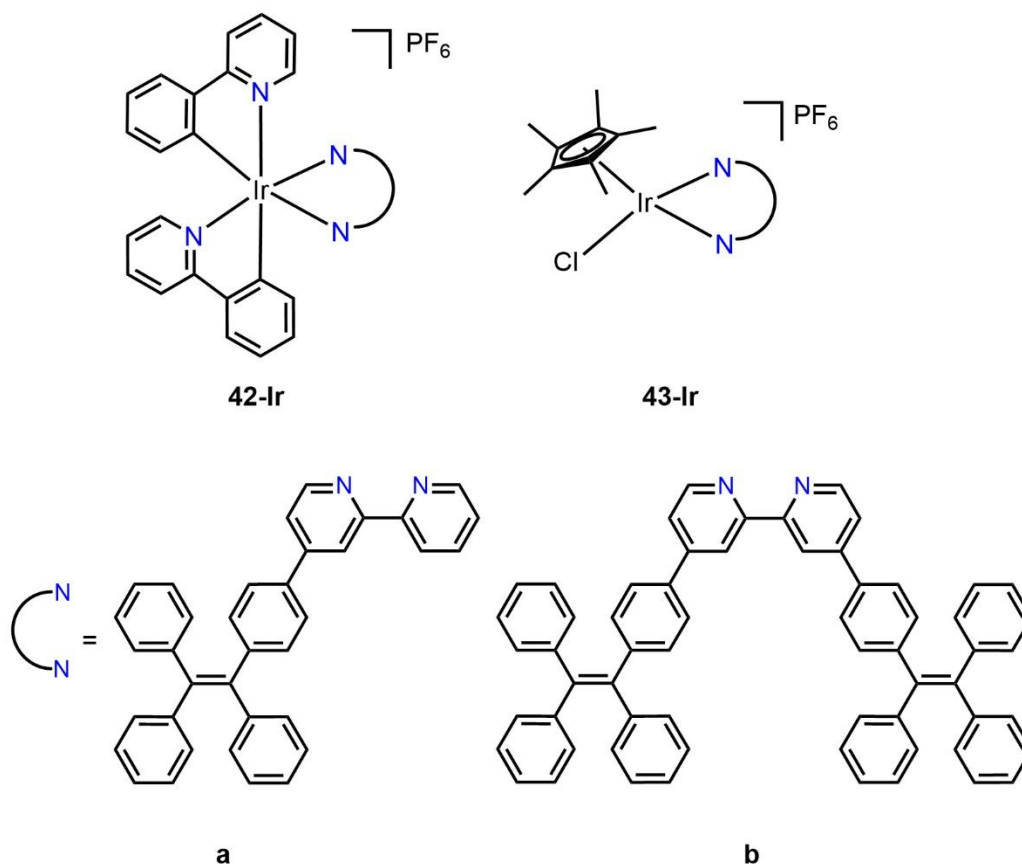


Figure 45. Ir(III) cyclometalated compounds (**42-Ir** – **43-Ir**) reported by Liu group as potential anticancer agents.

Wang reported two iridium(III) complexes with a phen ligand functionalized with alpha-lipoic acid. In this case, the ppy derivative (**44-Ir**) was more potent in all tested cell lines than its Cp^* (**45-Ir**) analog (**Figure 46**). The $\log p_{o/w}$ values (-1.06 and 1.39, respectively) show a significant difference, indicating that **44-Ir** was hydrophilic, while **45-Ir** was lipophilic, which could improve processes such as cellular uptake.¹⁶¹ Since both ligands have shown good results as cytotoxic agents, some research groups, instead of making a direct comparison, have used them in combination, suggesting synergy. The complexes **46a-h-Ir** (**Figure 46**) with functionalized pyridines as auxiliary ligands were tested against three cancer cell lines, with MCF-7 being the most sensitive to these compounds. The IC_{50} values ranged from $0.20 \pm 0.04 \mu\text{M}$ for **46e-Ir** to $8.8 \pm 0.8 \mu\text{M}$ for **46h-Ir**, suggesting that electron-donating substituents, such as $-\text{NEt}_2$, enhance the cytotoxicity, while electron-withdrawing substituents, such as $-\text{CON}(\text{CH}_2\text{CH}_3)$, decrease it.¹⁶²

Likewise, Zimbron reported the cytotoxic activity of **47a-Ir** and **47b-Ir** complexes using BODIPY-type ligands as auxiliaries. Their IC_{50} values ranged from 0.52 ± 0.03 to $1.08 \pm 0.05 \mu\text{M}$. In both



studies, the high IC_{50} values indicate good cytotoxic performance of the complexes with both ligands.¹⁶³ Additionally, through a study of cellular images obtained using a wide-field epifluorescence microscope, fluorescence emission was observed in most cells exposed to **47a-Ir** (**Figure 47a**) and 3-pyridyl-BODIPY (**Figure 47b**) as large diffuse areas and small bright spots in the cytoplasm, confirming that **47a-Ir** can permeate the membrane and accumulate within the cells. Thanks to its remarkable photostability, it was possible to monitor the uptake of the complex in real time (**Figure 47b**). Within less than 10 seconds, **47a-Ir** was detected emitting fluorescence inside the cells, with the intensity increasing over time and reaching a maximum after 90 seconds. This observation indicates that the internalization of **47a-Ir** occurs very rapidly.

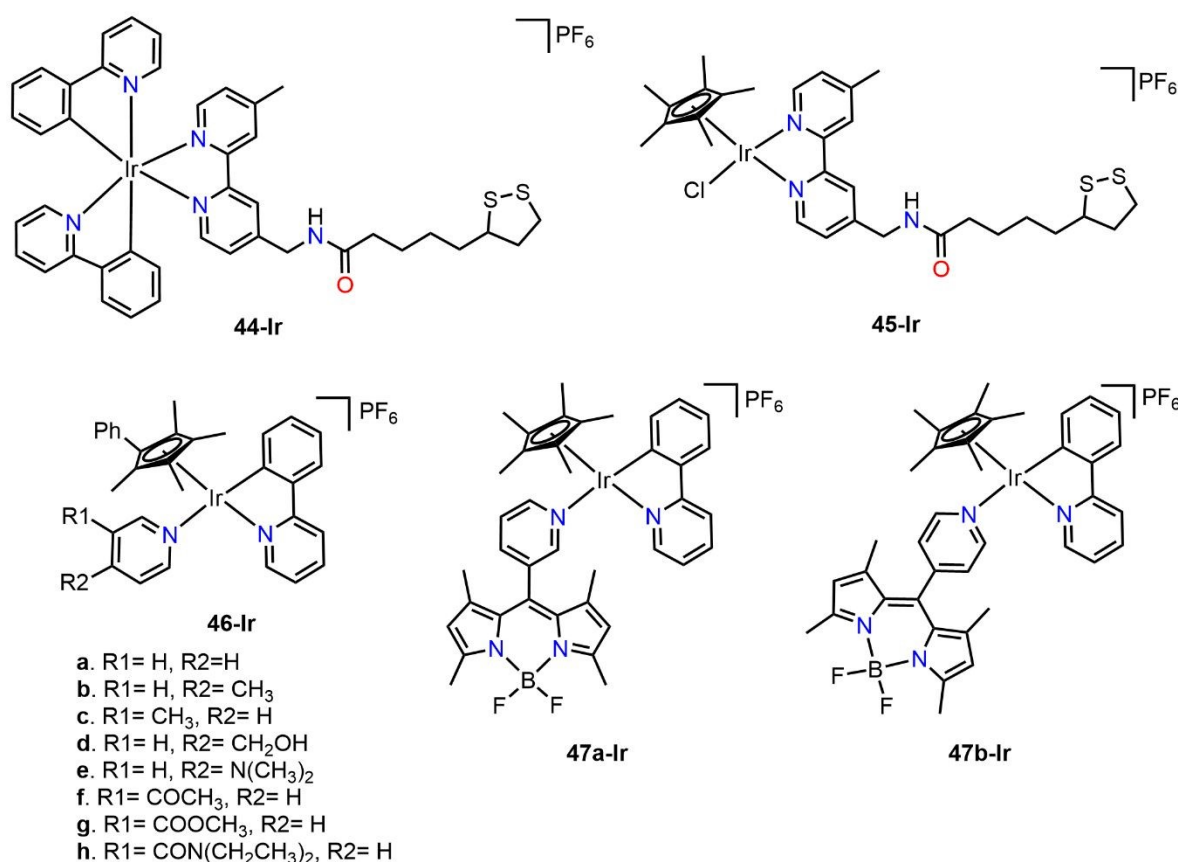


Figure 46. Cyclometalated Ir(III) complexes (**44-Ir** – **47b-Ir**) with C^N and Cp* ligands as potential anticancer agents.



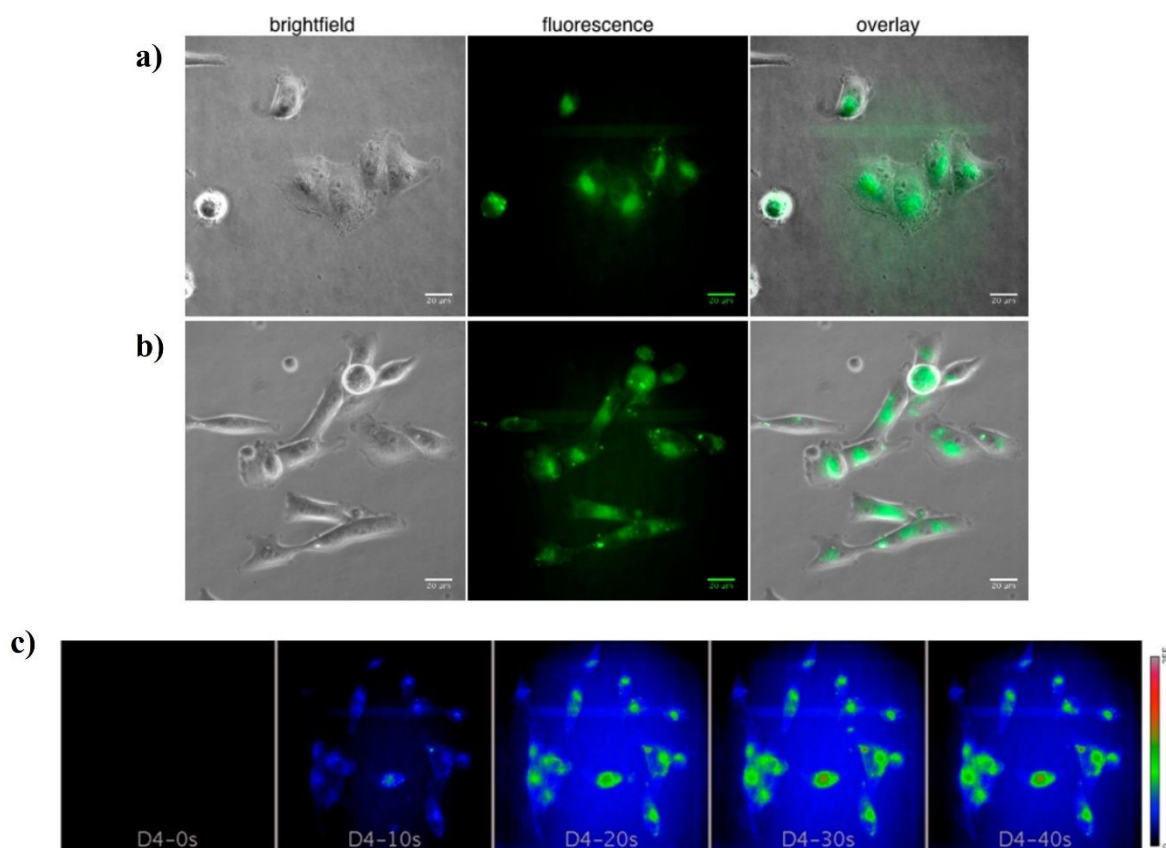


Figure 47. MDA-MB-231 cells treated with a) **47a-Ir** and b) 3-pyridyl-BODIPY, and c) real-time monitoring of **47a-Ir** uptake by MDA-MB-231 cells. (Reproduce with permission from ref. 163

Copyright 2017, American Chemical Society).

Variations in the ppy ligand have also been explored. For instance, the **48a-o-Ir** complexes (**Figure 48**) were evaluated towards four cancer cell lines, with A2780 being the most sensitive. The presence and positioning of substituents significantly affected the activity of the complexes, showing IC_{50} values ranging from $1.18 \pm 0.08 \mu M$ to $> 60 \mu M$, being complex **48m-Ir** the most cytotoxic.¹⁶⁴ Chen tested bulkier substituents in the ppy N^N ligand (**49a-Ir** – **51-Ir**). Complexes with Me and MeO substituents (**49a-Ir** and **49b-Ir**) showed the lowest IC_{50} values against A549 ($IC_{50} = 3.9 \pm 0.1 \mu M$ for both complexes). Meanwhile, **50-Ir** and **51-Ir**, with larger substituents, were the least active ($IC_{50} = 12.8 \pm 0.6$ and $8.6 \pm 0.3 \mu M$, respectively).¹⁶⁵ Liu *et al.* not only varied the substituents on the ppy ligand but also tested their impact on the Cp ring (**52a-Ir** – **53d-Ir**) (**Figure 48**). When comparing ppy ligands, there is no clear pattern regarding their IC_{50} values against A549 (2.8 ± 0.8 , 23.0 ± 0.7 , 7.4 ± 0.1 , 39.5 ± 2.7 , 3.5 ± 0.1 , 13.0 ± 0.5 , 27.6 ± 0.6 , $8.5 \pm 1.4 \mu M$, respectively). However, when comparing the substituted cyclopentadienyl ligands, the trend is clear: complexes with $R = C_6H_5$ were less active than those with $R = CH_3$. At first glance, steric hindrance could explain these results, but



computational NPA (Natural Population Analysis) of **52a-Ir** and **52b-Ir** showed that Ir was less charged in **52a-Ir**, facilitating the loss of the chloride atom and improving its cytotoxic activity.¹⁶⁶

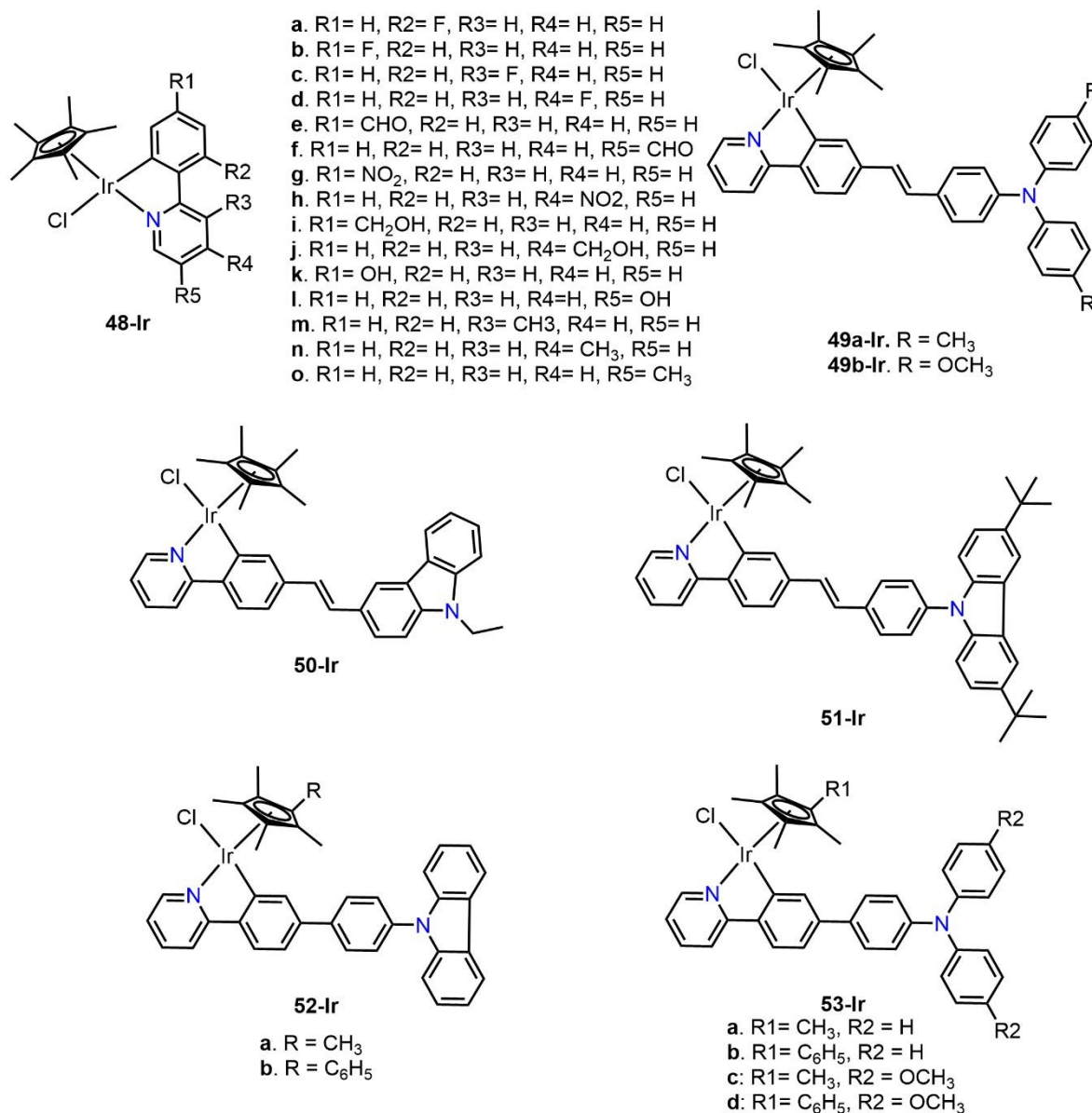


Figure 48. Cyclometalated Ir(III) compounds (**48-Ir** – **53-Ir**) with C^N, Cp, and Cp* ligands as potential anticancer agents.

Rao *et al.* synthesized two indazole-derived compounds (**54a,b-Ir**) (Figure 49). In this case, the 'Pr substituent improved the cytotoxic activity against HeLa (IC₅₀ = 6.0 ± 0.79 μM **54a-Ir** and 3.9 ± 0.36 μM **54b-Ir**), likely influenced by lipophilicity.¹⁶⁷ Furthermore, Yang reported a series of imine-NHC compounds (such as complexes **25a-e-Ir**), including a Cp* fragment (**55a-Ir**). Changes in the substituents resulted in a significant shift in cytotoxic performance against A549 (IC₅₀ = >100 μM



55a-c-Ir, $25.86 \pm 1.2 \mu\text{M}$ **55d-Ir**, $14.05 \pm 0.1 \mu\text{M}$ **55e-Ir**, $9.15 \pm 0.2 \mu\text{M}$ **55f-Ir**, $3.04 \pm 0.5 \mu\text{M}$ **55g-Ir**, $2.21 \pm 0.2 \mu\text{M}$ **55h-Ir**, $1.99 \pm 0.1 \mu\text{M}$ **55i-Ir**, $3.94 \pm 0.3 \mu\text{M}$ **55j-Ir**, $3.64 \pm 0.3 \mu\text{M}$ **55k-Ir**, $7.44 \pm 0.3 \mu\text{M}$ **55l-Ir**). The complexes **55g-Ir** and **55h-Ir** showed the lowest IC_{50} values, contrasting with **55a-Ir**, **55b-Ir**, and **56k-Ir**, which had the highest IC_{50} values. Increasing the steric hindrance in the *ortho* substituents of the aniline fragment leads to a proportional increase in cytotoxic effects IC_{50} (**55a-Ir** vs **55e-Ir**). However, the most significant impact was observed with the imidazole substituent, following the same trend: the bulkier the substituent, the more potent the complex (e.g., **55a-Ir** < **55b-Ir** < **55c-Ir** < **55d-Ir**).¹⁶⁸

Kralj *et al.* reported a group of pyridyl derivatives and explored substitutions on the nitrogen atom. Unfortunately, due to solubility issues, only the **56-Ir** complex could be tested. Similar compounds **57a-d-Ir** were evaluated by Yang and coworkers (**Figure 49**). The best cytotoxic performance against HeLa was shown by **57d-Ir** ($\text{IC}_{50} = 2.01 \pm 0.28 \mu\text{M}$).¹¹⁸

A series of Schiff base complexes with a Cp^* fragment has been reported by Mou *et al.* and was tested against A562 cells (**58a-o-Ir**). The IC_{50} values obtained were 1.10 **58a-Ir**, 0.73 **58b-Ir**, 0.26 **58c-Ir**, 0.95 **58d-Ir**, 0.67 **58e-Ir**, 1.06 **58f-Ir**, 0.53 **58g-Ir**, 1.00 **58h-Ir**, 0.62 **58i-Ir**, 0.94 **58j-Ir**, 4.77 **58k-Ir**, 1.13 **58l-Ir**, 0.61 **58m-Ir**, 1.20 **58n-Ir**, and 0.87 **58o-Ir** μM . Comparing compounds **58j-Ir** and **58e-Ir** showed that the most potent electron-donating group (Me) improves the cytotoxicity; the same behavior is maintained when comparing **58i-Ir**, **58h-Ir**, and **58g-Ir**, or **58d**, **58k-Ir**, and **58n-Ir**, indicating a correlation between electronic effects and the cytotoxic activity. On the contrary, no clear correlation was obtained with the R_2 substituent. When comparing the different substituents (R) located on the aromatic rings, an influence on the electronic properties of these complexes can be observed, suggesting that there is a synergy between the electronic effects and the anticancer activities of the cyclometalated iridium complexes (**58a-o-Ir**).¹⁶⁹



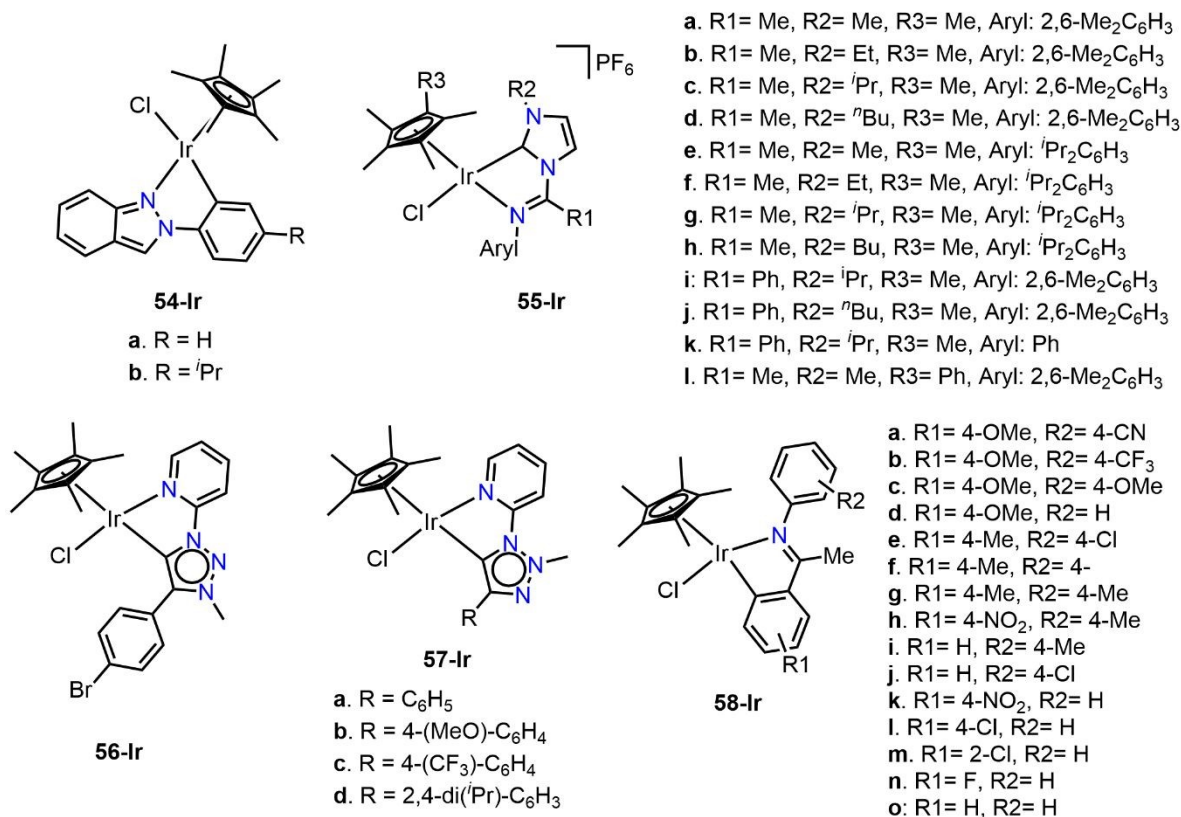


Figure 49. Cyclometalated Ir(III) complexes (**54-Ir** – **58-Ir**) with C^N and Cp* ligands as potential anticancer agents.

4.2.6. Photodynamic therapy (PDT)

Iridium(III) cyclometalated complexes exhibit great versatility in their photophysical properties, due to a high spin-orbit coupling constant that promotes intersystem crossing and results in long-lived triplet excited states of the photosensitizer (PS), as well as to an appropriate energy gap for the excitation of ³O₂ and the generation of highly toxic ¹O₂ molecules. These characteristics reveal their significant potential as single-photon and two-photon PS in PDT.^{170,171}

Zang *et al.* reported the cytotoxic activity of complex **59-Ir** (**Figure 50**). In the absence of light, the complex showed IC₅₀ values higher than 100 μM against seven tested cancer cell lines. However, after 45 minutes of irradiation, there was an improvement in cytotoxicity, particularly in SGC-7901 cells (IC₅₀ in dark > 200 μM vs IC₅₀ under light = 6.1 ± 0.6 μM, PI (phototoxicity index) > 32). The effect of light on ROS production was evaluated using the DCFH-DA fluorescent probe. Cells treated with 6.25 μM of **59-Ir**, with or without light irradiation, showed approximately seven times more fluorescence, indicating an increase in ROS concentration. However, no specific test was performed to detect the presence of ¹O₂.¹⁷²



Using the same imidazophenanthroline (imph) scaffold as an N^N auxiliary ligand, Zang synthesized a family of complexes (**60a-c-Ir**) by varying the N^C ligand (ppy, bzq, pig). In the absence of light, the IC₅₀ values were >200 μM against a series of cancer cell lines. However, after irradiation with white light, the cytotoxicity improved, particularly against BEL-7402 (**Table 15**). In the presence of superoxide radical (O₂^{•-}), dihydroethidium (DHE) can be converted to ethidium, which binds to DNA, producing fluorescence. The three complexes were tested in this assay, and the fluorescence intensity followed the trend **60c-Ir** > **60b-Ir** > **60a-Ir**, indicating that the complexes can increase intracellular O₂^{•-} levels.¹⁷³

Table 15. IC₅₀ values for complexes **60a-c-Ir** after 48 h under dark conditions and light exposure for 40 min^a

Compound	IC ₅₀ (μM)	
	BEL-7402 (dark)	BEL-7402 (light) (PI ^b)
60a-c	>200	5.5 ± 0.8 (>36)
60b-Ir	>200	7.3 ± 1.3 (>27)
60c-Ir	>200	11.5 ± 1.6 (>17)
<i>cisplatin</i>	10.8 ± 1.4	-

^a Cell viability determined by MTT assay after treatment for 48 h under dark and cells irradiated for 40 min

^b PI (Phototoxic Index) = IC₅₀ dark/IC₅₀ light

In this context, Song synthesized and tested the cytotoxic activity of **61a-c-Ir** (**Figure 50**), derived from imph, varying the N^C ligand (bzq, ptp, ppy) against six cancer cell lines. The IC₅₀ values in the dark ranged from 12.5 to 139.20 μM. However, after irradiation with light, those values decreased to 0.25 - 1.75 μM, indicating a significant enhancement in cytotoxicity. The PI values obtained against HepG2 cells were 386.7 **61a-Ir**, 51.2 **61b-Ir**, and 132.2 **61c-Ir** μM, indicating that the complexes are moderate PS.¹⁷⁴



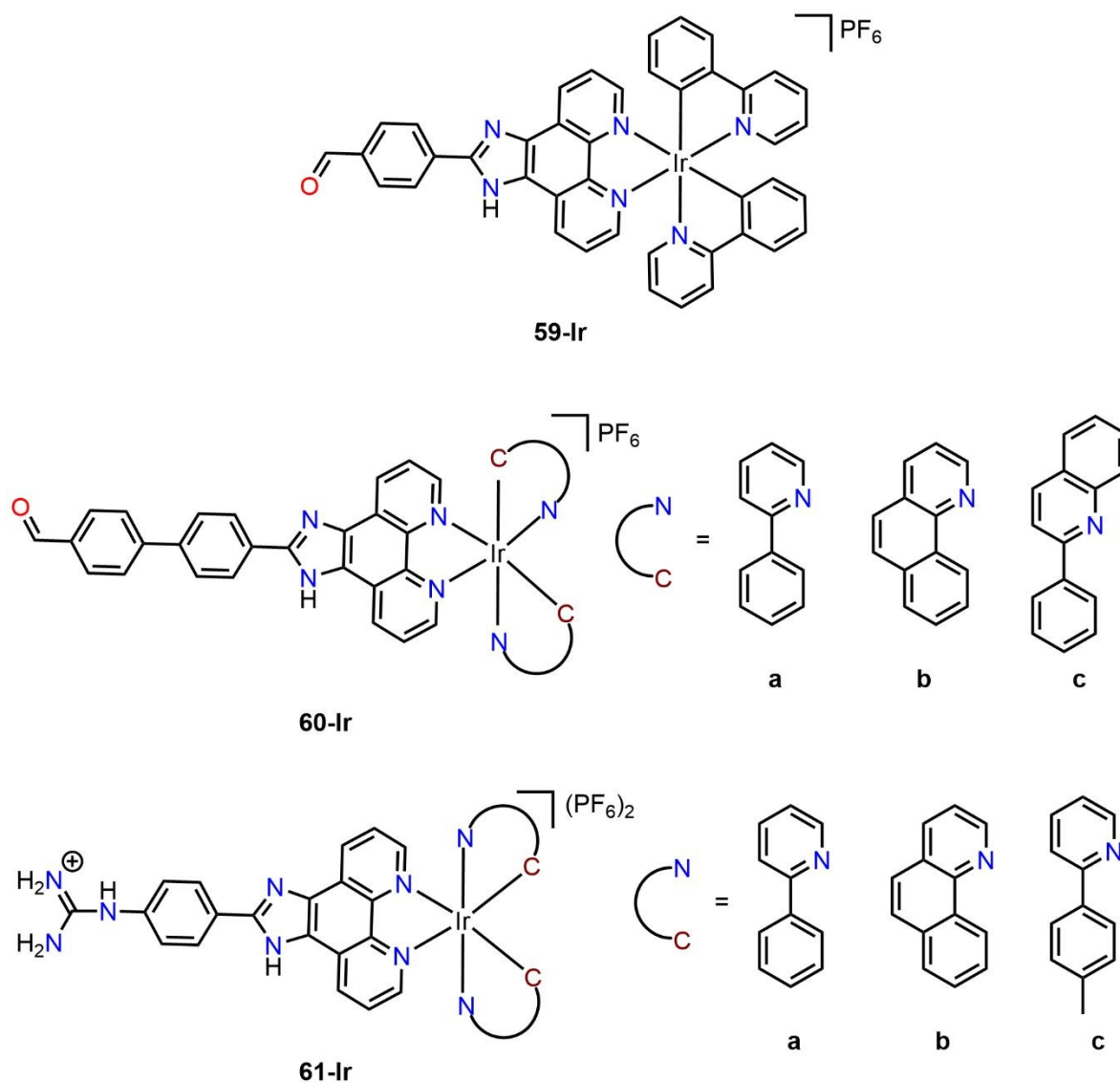


Figure 50. Cyclometalated Ir(III) complexes (**59-Ir** – **61-Ir**) used as potential photosensitizers for PDT.

Li *et al.* reported two new iridium(III) cyclometalated complexes (**62a-Ir** and **62b-Ir**) (**Figure 51**), where they incorporated a hexose into the imph fragment and varied the N[^]C ligand (ppy, pig). The cytotoxicity in the presence or absence of light was evaluated against four cancer cell lines. For A549, the PI values were >6.0 and 500. To determine ROS formation, the DCFH-DA test was performed under both dark and light conditions. In the dark, no significant change in fluorescence was observed. However, after irradiation, the fluorescence increased by 18.3 and 20.1 times, respectively. Another test for measuring ROS is lipid peroxidation, assessing malondialdehyde (MDA) formation. Under dark conditions, a slight increase in MDA content was observed. However, after irradiation, MDA production was greater, with values of 6.00 μ M and 8.32 μ M.¹⁷⁵ Through various biochemical studies,



it was determined that **62a-Ir** and **62b-Ir** localize in the endoplasmic reticulum (ER), inducing ER stress and triggering immunogenic cell death. Additionally, these complexes also act on the mitochondria, increasing intracellular reactive oxygen species (ROS) levels and reducing mitochondrial membrane potential (MMP). Moreover, the iridium complexes were able to increase the Bax/Bcl-2 ratio and caspase-3 activity while decreasing PARP (poly(ADP-ribose) polymerase), PI3K, and AKT (protein kinase B) levels. Furthermore, they caused DNA damage by increasing the expression of the γ -H2AX protein, leading to cell cycle arrest in the S phase (**Figure 52a**). Wound healing assays revealed that **62a-Ir** and **62b-Ir** can attenuate wound closure to some extent. However, upon irradiation, these complexes effectively inhibit cell migration, as the wound edge width remained largely unchanged. This demonstrates that **62a-Ir** and **62b-Ir** significantly reduce the wound closure percentage in A549 cells when photoactivated, whereas their ability to prevent cell migration without irradiation remains weak (**Figure 52b**).

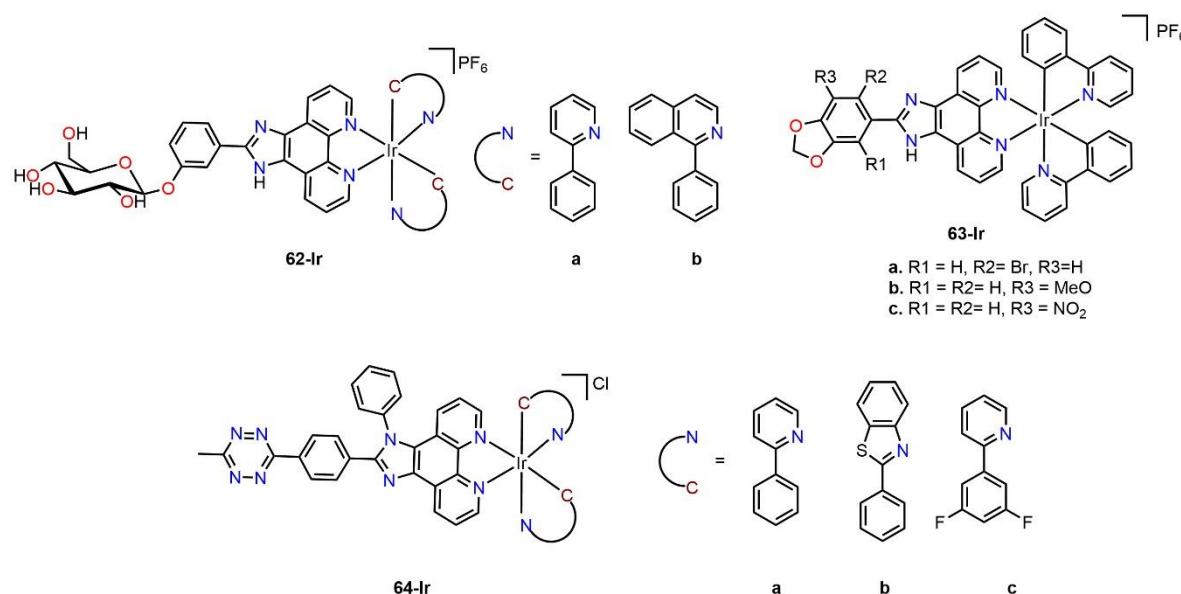


Figure 51. Cyclometalated Ir(III) complexes (**62-Ir** – **64-Ir**) used as potential photosensitizers for PDT.



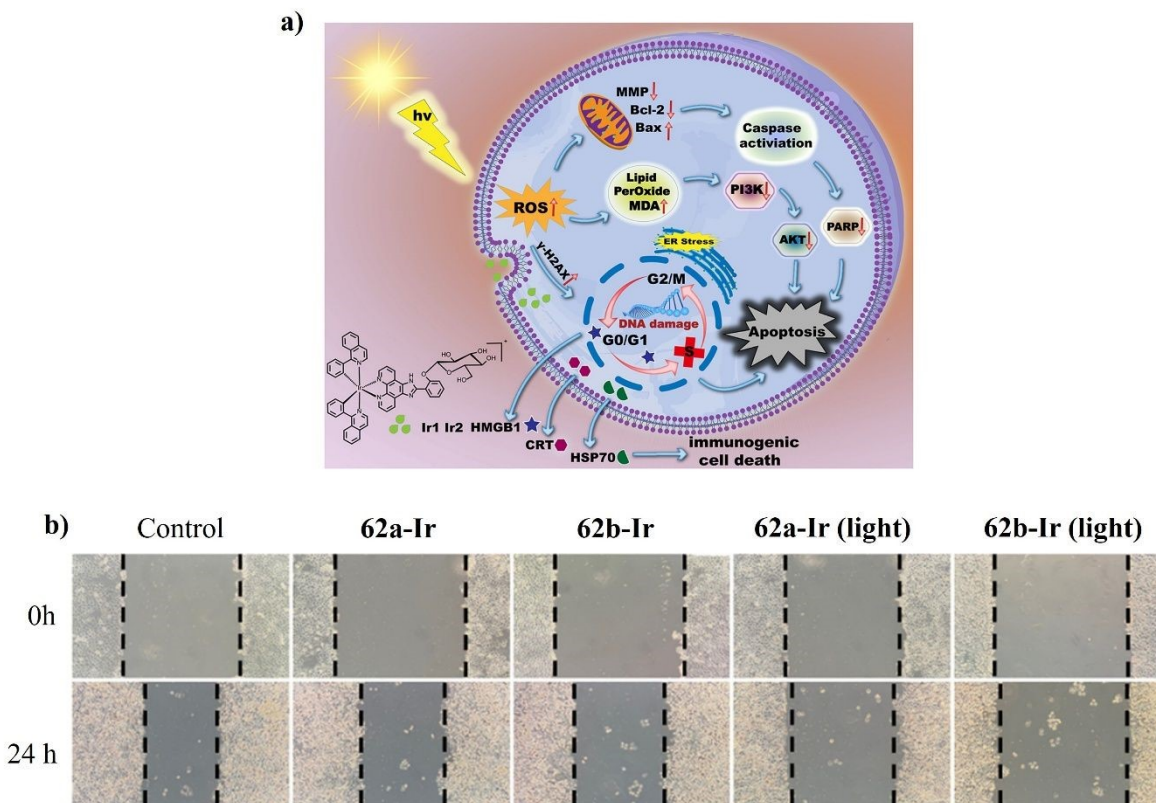


Figure 52. a) Plausible mechanism of action of **62a-Ir** and **62b-Ir** in inducing apoptosis in A549 cells. b) Wound healing studies after A549 cells were treated with and without irradiation.

(Reproduce with permission from ref. 175 Copyright 2022, Elsevier).

In another study, the cytotoxicity of **63a-c-Ir** was evaluated against five cancer cell lines. Complex **63a-Ir** showed high anticancer efficacy against A549 (IC_{50} dark = $4.0 \pm 0.6 \mu M$). However, the remaining complexes displayed moderate or negligible cytotoxic activity. After exposure to white light, the IC_{50} values for all cell lines treated with the three compounds decreased significantly, yielding a PI = 5.7 (IC_{50} light = $0.7 \pm 0.3 \mu M$) for the best compound (**63a-Ir**). The presence of 1O_2 was determined using 1,3-diphenylisobenzofuran (DPBF), which irreversibly oxidizes to 1,2-dibenzoylbenzene. The absorbance of DPBF at 411 nm in the presence of **63a-c-Ir** decreased, confirming the production of 1O_2 . The trend observed was **a** > **b** > **c** (76.0, 66.3, and 48.6%, respectively), correlating with their IC_{50} values under light against A549 (0.7 ± 0.3 , 1.8 ± 0.1 , $34.3 \pm 1.8 \mu M$, respectively).¹⁷⁶

Tan *et al.* evaluated the singlet oxygen quantum yields ($\phi\Delta$) of **64a-c-Ir** (Figure 51), derived from triazine, using the DPBF test. The trend of results was as follows: **64a-Ir** > **64b-Ir** > **64c-Ir** (72.0, 62.0, and 56.0%). In cytotoxic assays against four cancer cell lines, irradiation again improved the



IC₅₀ values, yielding PI values = 115.6, 350.0, and 185.2 for the A549 cell line (IC₅₀ light = 0.096, 0.024, and 0.058 μM, and IC₅₀ dark = 11.1, 8.1, and 10.8 μM), suggesting that the thiazole N[^]C ligand improves cytotoxicity.¹⁷²

In the same context, Yuan *et al.* reported a series of complexes using a tridentate auxiliary ligand and a set of N[^]C bzq ligands (**65a-c-Ir**) (**Figure 53**). The φΔ values obtained in DMSO were 39%, 45%, and 49%, indicating a relationship between ¹O₂ production and the length of the N[^]C ligand. The PI values obtained against the A549 cell line were >4.1, 94, and 45 (**Table 16**), suggesting that cytotoxicity can also be correlated with the length of the N[^]C ligand. Since **65b-Ir** showed the best PI, ¹O₂ production *in vitro* was determined using DCFH-DA. Cells treated with **65b-Ir** showed a clear increase in fluorescence after irradiation, suggesting its promising ability to generate ¹O₂ in A549 cells.¹⁷⁷

Table 16. IC₅₀ values of the complexes **65a-c-Ir** after 48 h under dark conditions and 4 h of light exposure

Compound	IC ₅₀ (μM)	
	A549 (dark)	A549 (light) (PI ^b)
65a-Ir	>100	24.3 ± 0.3 (>4.1)
65b-Ir	56.6 ± 0.2	0.6 ± 0.1 (94)
65c-Ir	22.3 ± 0.3	0.5 ± 0.1 (45)
<i>cisplatin</i>	18.4 ± 0.5	17.5 ± 0.6 (1.0)

^a Cell viability determined by MTT assay after treatment for 48 h under dark and cells irradiated for 4 h

^b PI (Phototoxic Index) = IC₅₀ dark/IC₅₀ light



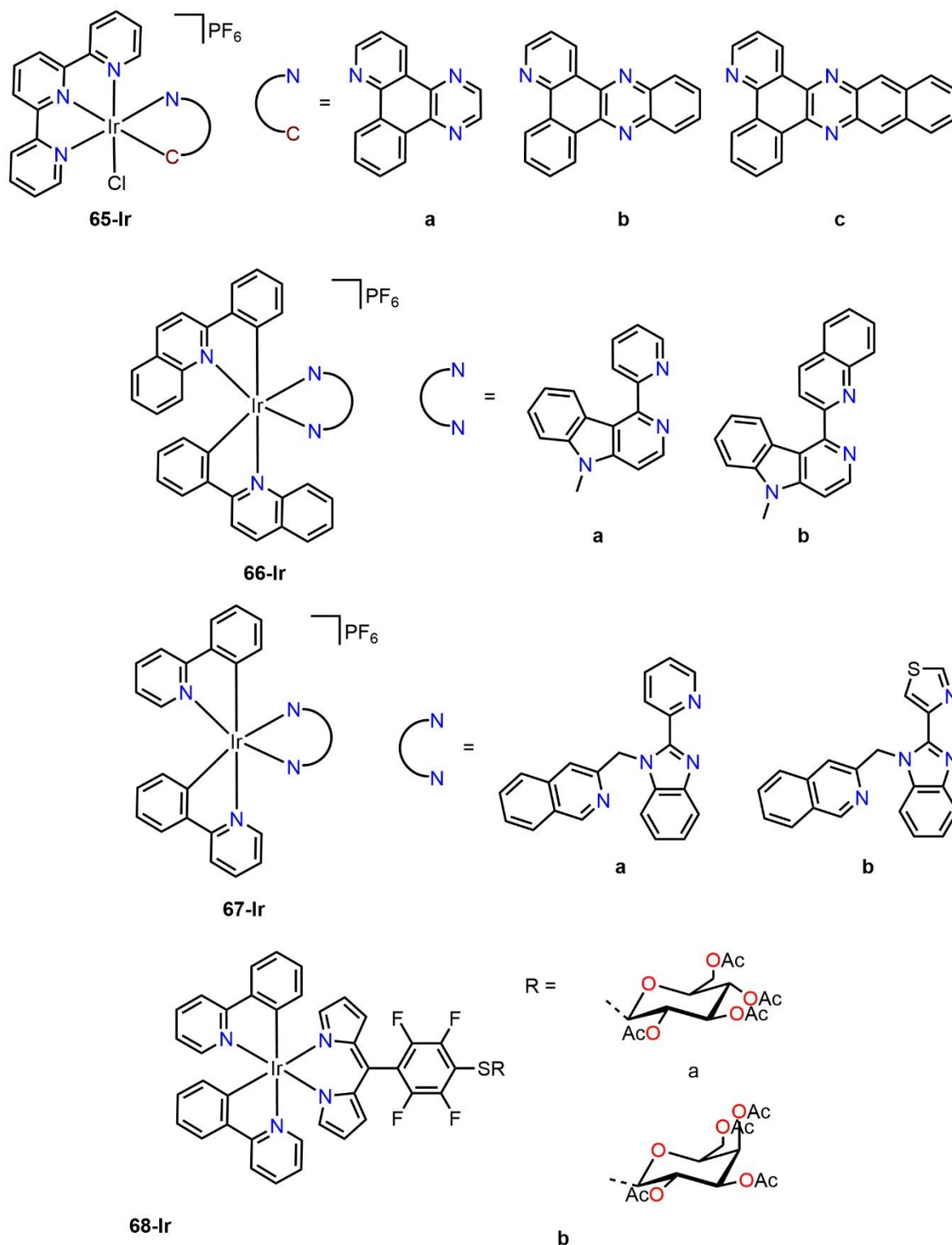


Figure 53. Cyclometalated Ir(III) complexes (**65-Ir** – **68-Ir**) used as potential photosensitizers for PDT.



Qin *et al.* reported complexes using pql as C^N ligands and ppy-derived auxiliary ligands (**66a-Ir**, **66b-Ir**) (**Figure 53**). Using the DPBF protocol, $\phi\Delta$ values of 94% and 88% were obtained, suggesting that the smallest ligand enhances the ¹O₂ production. Cytotoxicity assays against A549 showed PI values of 120 and 93, correlating with the $\phi\Delta$ values. To determine if the type I mechanism (oxygen-independent mechanism) was also involved, the MitoSOX-Red fluorescent protocol (a superoxide indicator) was performed. Without light irradiation, no significant signal was observed. After irradiation with light, the intracellular fluorescence signal of MitoSOX-Red increased considerably, suggesting the presence and thus involvement of superoxide anion in the cytotoxic activity.¹⁷⁸ Similarly, Redrado reported a pair of benzimidazole derivatives (**67a,b-Ir**) (**Figure 53**) with PI values (15.3, 13.5) against A549. Due to its IC₅₀ value under light, **67b-Ir** was tested for ROS levels in vitro using DHE. Under dark conditions, ROS generation was insignificant compared to when light exposure was applied, where a very significant increase in ROS production was observed.¹⁷⁰

Manav *et al.* measured the singlet oxygen quantum yields ($\phi\Delta$) of **68a-Ir** and **68b-Ir** using the DPBF test. In water, the obtained values were 70% and 78%, respectively, indicating that these complexes could be effective PS. Subsequently, the cytotoxic activity was evaluated against A549 cancer cell line, in the presence and absence of light. As expected, the IC₅₀ values after irradiation were the lowest (IC₅₀ dark= 88.5 (**a**) and 84.3 (**b**) μ M; IC₅₀ light= 25.5 (**a**) and 17.8 (**b**) μ M).¹⁷⁹

4.2.7. Other attempts to improve cytotoxicity

Currently, to enhance the cytotoxic activity, the use of biological fragments or delivery systems has been proposed. Thus, Zang reported complex **69-Ir** and its functionalization with Human Serum Albumin (HSA) (**70-Ir**) (**Figure 54**), and its use as a photosensitizer. The EPR signal generated by **70-Ir** using 2,2,6,6-tetramethylpiperidine (TEMP) as a spin trap to detect singlet oxygen (¹O₂) indicated a significant increase in its singlet oxygen quantum yields ($\phi\Delta$) compared to **69-Ir**. The evaluation of the cytotoxicity against four cancer cell lines showed a low cytotoxic activity for both complexes. However, after light irradiation, the IC₅₀ values improved as expected, with the A549 cell line being the most sensitive (53.3 \pm 4.5 and 1.1 \pm 0.3 μ M, respectively), which correlates with the $\phi\Delta$ values. Further evaluation against A549 multicellular 3D spheroids showed ineffective cytotoxicity in the dark (IC₅₀ = 65.6 \pm 5.9 μ M **70-Ir**), but again, after irradiation, the IC₅₀ value improved (4.8 \pm 0.2 μ M).¹⁸⁰



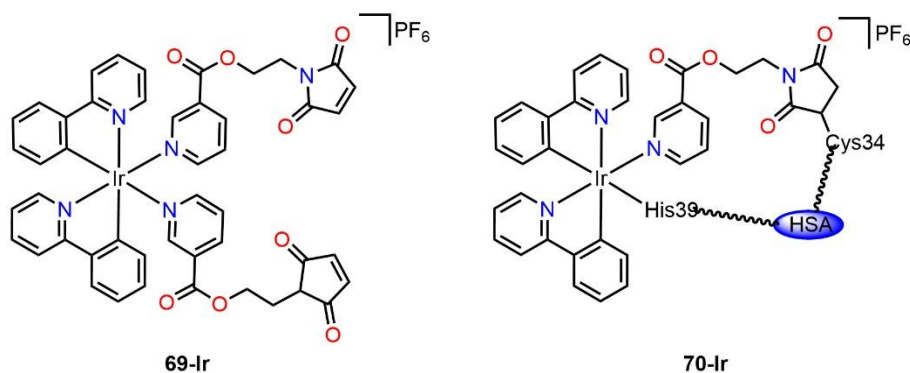


Figure 54. Ir(III) cyclometalated compounds (**69-Ir** and **70-Ir**) reported by Zang as potential anticancer agents.

Zang and coworkers also explored the use of liposomes as a delivery system. In this study, the complexes **71a-Ir** and **71b-Ir** (**Figure 55**) were encapsulated in liposomes (**Lipo-71a-Ir** and **Lipo-71b-Ir**) with encapsulation efficiencies (EE%) of 83.0 and 70.0%, respectively. *In vitro* drug release studies using the dialysis method confirmed a sustained release of liposomal derivatives, with accumulated release after 48 hours of 18.8% (**Lipo-71a-Ir**) and 13.8% (**Lipo-71b-Ir**). The cytotoxic assay showed high IC_{50} values for **71a-Ir** and **71b-Ir** in five cancer cell lines ($> 200 \mu\text{M}$). In contrast, the liposomal derivatives exhibited IC_{50} values (5.2 ± 0.8 , $10.8 \pm 1.5 \mu\text{M}$, respectively), which were more than nine times lower than their precursors.¹⁸¹

Similarly, Bai et al. evaluated the cytotoxic activity of **71c-Ir** – **71e-Ir** (**Figure 55**), varying the number and position of chlorine atoms, and their liposomes (**Lipo-71c-Ir** - **Lipo-71e-Ir**). After 30 minutes of *in vitro* release testing, no drastic release of the cyclometalated complexes was observed, but after 96 hours, the percentages of free compounds were $15.97 \pm 1.73\%$, $19.57 \pm 1.63\%$, and $30.77\% \pm 2.56\%$, respectively, indicating a relationship between drug release and the number of chlorine atoms. The cytotoxicity was determined against eight cancer cell lines. Compound **71c-Ir** was the only free complex to show a significant IC_{50} value against A549 ($15.1 \pm 1.6 \mu\text{M}$), indicating that, as a free system, the monosubstituted complex is the most potent. In contrast, the encapsulated systems showed a significant increase in activity against all cancer cell lines, with A549 being the most sensitive ($IC_{50} = 3.1 \pm 0.3$ **Lipo-71c-Ir**, 1.2 ± 0.4 **Lipo-71d-Ir**, $14.1 \pm 1.8 \mu\text{M}$ **Lipo-71e-Ir**).¹⁸²

A pyrene derivative and its respective liposome (**72-Ir** and **Lipo-72-Ir**) were reported by Zhang. After determining their EE% (97.06%) and knowing that the drug release at 96 hours was 21.25%, with no drastic release observed (**Lipo-72-Ir**), a cytotoxic assay was conducted against seven cancer cell lines. Like previous results, the delivery system improved the cytotoxicity, mainly in BEL-7402 cells ($IC_{50} > 200$ **72-Ir**, $IC_{50} = 2.6 \pm 0.03 \mu\text{M}$ **Lipo-72-Ir**).¹⁸³



On the other hand, Xie *et al.* reported the synthesis of **73a-Ir**, **73b-Ir** (**Figure 55**), and their liposomal derivatives, **Lipo-73a-Ir** and **Lipo-73b-Ir**. The EE% was 70.3 and 82.5%, respectively. In the first 24 hours, the release occurred rapidly, reaching percentages around 25%, and thereafter, the release slowed down. The cytotoxic assay for **73a-Ir** and **73b-Ir** showed poor performance against five cancer cell lines, with SGC-7901 being the most sensitive (20.9 ± 2.7 and 36.8 ± 6.1 μM , respectively), but the IC_{50} values of the derivatives, **Lipo-73a-Ir** and **Lipo-73b-Ir**, improved by about four times (5.8 ± 0.2 and 9.1 ± 1.9 μM , respectively).¹⁸⁴ Three complexes including the $-\text{CF}_3$ fragment (**74a-c-Ir**) were synthesized by Zhang and encapsulated (**Lipo-74a-Ir** - **Lipo-74c-Ir**). The EE% was 88.9 ± 6.2 , 91.9 ± 5.3 , $94.4 \pm 5.2\%$, and the drug release after 100 hours was 43%, 20%, and 35%, respectively. The free complexes showed IC_{50} values >100 μM against all tested cancer cell lines. However, the liposomal systems improved the cytotoxicity, with BEL-7402 being the most sensitive cell line ($\text{IC}_{50} = 5.8 \pm 0.16$, 18.1 ± 0.89 and 13.0 ± 0.42 μM).¹⁸⁵

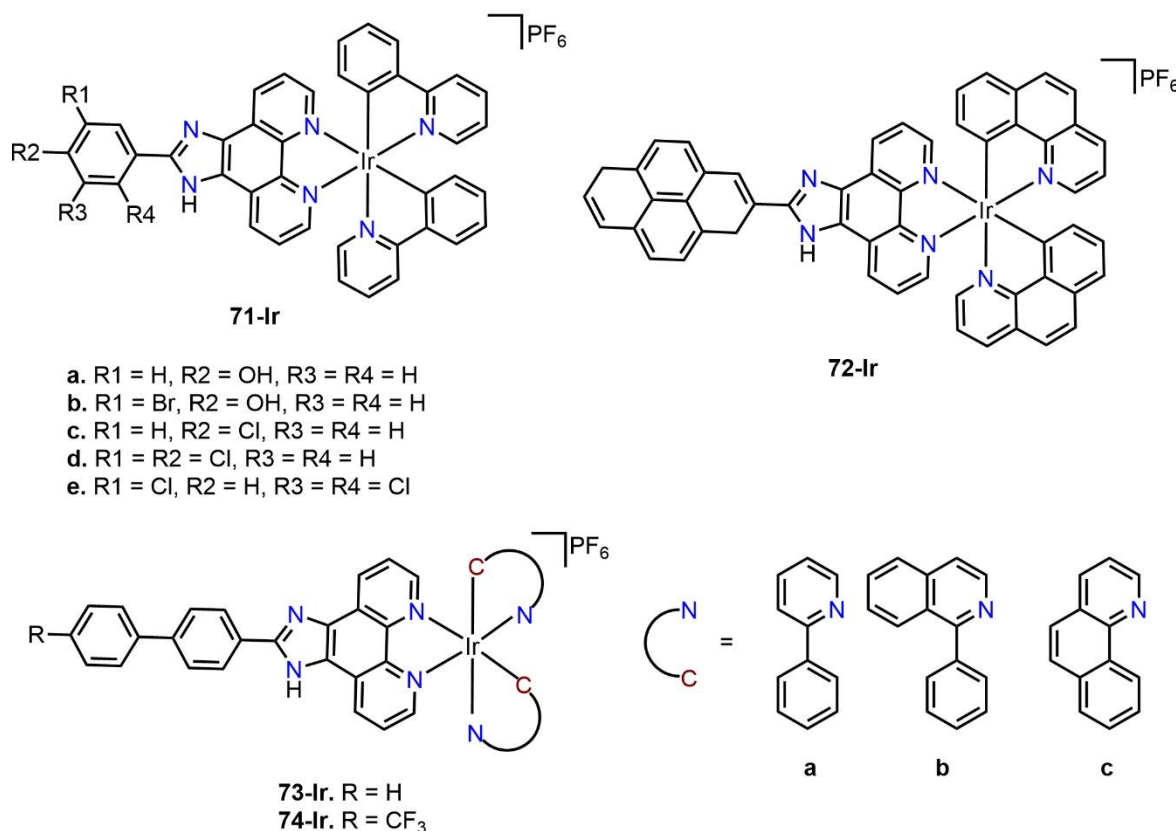


Figure 55. Ir(III) cyclometalated compounds (**71-Ir** – **74-Ir**) encapsulated in liposomes for their study as anticancer agents.



5. Cyclometalated compounds of group 10

5.1. Nickel

Nickel is an abundant element on Earth and has been extensively employed in industrial processes. Prolonged exposure to this metal leads to carcinogenesis mainly by epigenetic damage.¹⁸⁶ However, Ni-dependent metalloenzymes have been observed in unicellular organisms like bacteria, regulating vital processes for life.¹⁸⁷ An example is the lactate racemase (LarA) of *Lactobacillus plantarum*, which requires a cyclometalated SCS-Ni pincer for the racemization of lactate.^{188,189} Therefore, an investigation could be focused on tuning the toxicity of nickel derivatives to treat diseases such as cancer, employing a metal compatible with biomolecules.

5.1.1. Pincer complexes

Zargarian and collaborators have synthesized a series of SCS-Ni(II) pincer complexes (**1-3-Ni**) (**Figure 56**), which were subjected to cytotoxic studies. In these studies, complexes **1a-Ni** – **1c-Ni** were evaluated *in vitro* against the MCF-7 cancer cell line. It was found that all three complexes inhibited MCF-7 cell proliferation in a dose- and time-dependent manner (**Table 17**). Complex **1a-Ni** was slightly more active than the other two at shorter incubation times, but after 72 hours all three showed a similar activity. Due to the promising antitumor activity shown *in vitro* by **1a-Ni**, its ability to inhibit tumor growth was tested *in vivo* against estrogen-dependent cancer cells (MC4L2) in female BALB/c mice, showing significant inhibition of tumor growth compared to the control group. Additionally, these compounds exhibited an affinity for bovine serum albumin (BSA), forming stable adducts in a 1:1 ratio. The preferred binding site for all the complexes was toward site II of BSA, with **1a-Ni** showing the greatest displacement capacity.¹⁹⁰

Table 17. IC₅₀ values of **1a-Ni** – **1c-Ni** complexes against MCF-7 cells^a

Compound	IC ₅₀ (μM)		
	24 h	48 h	72 h
1a-Ni	100	40	20
1b-Ni	>200	40	20
1c-Ni	>200	200	20
<i>cisplatin</i>	40	10	10

^a Cell viability determined by MTT assay



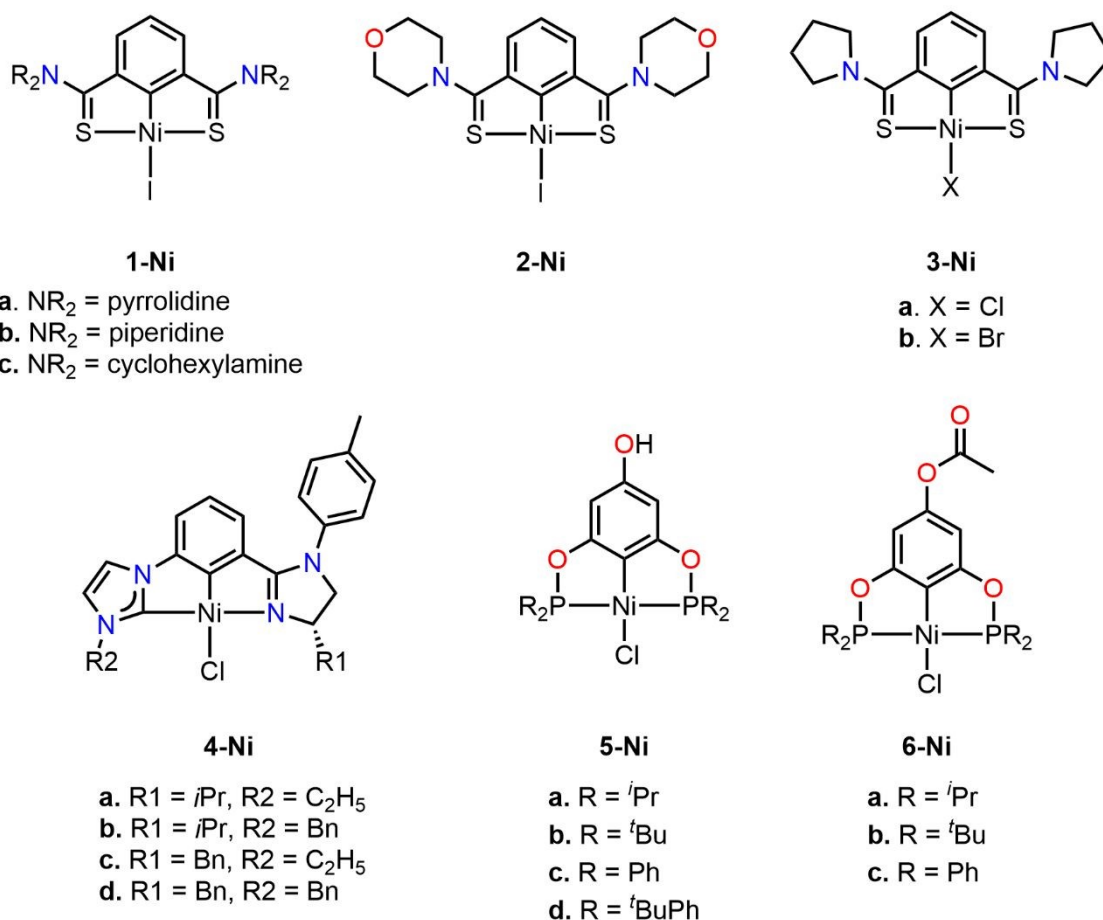


Figure 56. Nickel pincer-type cyclometalated complexes (**1-Ni** – **6-Ni**).

Complex **2-Ni** was evaluated against two cancer cell lines: MCF-7 and colon carcinoma cells (C26), as well as normal fibroblast cells (NIH-3T3) (**Table 18**). Complex **2-Ni** showed significantly lower toxicity than *cisplatin*, almost five times less against the control cell line, and showed some selectivity towards the MCF-7 cell line. A DNA-binding study using UV-vis spectroscopy revealed that **2-Ni** spontaneously interacted with DNA, forming an adduct. Competitive displacement studies confirmed that the complex could intercalate with DNA. Complex **2-Ni** also attenuated the intrinsic fluorescence of BSA through a static quenching mechanism. A DNA thermal denaturation study indicated that **2-Ni**'s interaction with CT-type DNA stabilizes the DNA double helix, suggesting non-covalent interactions and supporting the possibility of DNA intercalation. The complex likely has a single binding site in BSA, binding to site II.¹⁹¹

Table 18. IC_{50} and SI values of **2-Ni** against cancer cell lines MCF-7 and C26^a

Compound	IC_{50} (μM) (SI)		
	MCF-7	C26	NIH-3T3



4-Ni	76.94 (2.22)	88.67 (1.93)	170.81
cisplatin	40.99 (0.85)	27.66 (1.27)	34.99

^a Cell viability determined by MTT assay after treatment for 48 h

In a subsequent study, Zargarian *et al.*¹⁹² prepared a series of nickel pincer complexes analogous to **1a-Ni** – **2-Ni**, modifying the auxiliary ligand to chloride in **3a-Ni** or bromide in **3b-Ni**. *In vitro* cytotoxicity of these complexes was evaluated against three breast cancer cell lines (MCF-7, MC4L2, and 4T1), as well as against the human MF cell line as a control. Compound **3a-Ni** showed the highest cytotoxic activity in 4T1 cell line ($IC_{50} = 19 \pm 0.60 \mu M$).

Song and collaborators reported a series of asymmetric chiral CCN pincer complexes (**4a-Ni** – **4d-Ni**) which were tested on two prostate cancer cell lines, LNCaP (androgen-sensitive) and PC-3 (androgen/*cisplatin*-resistant). All four compounds exhibited significant growth inhibition against the LNCaP cell line, with IC_{50} values ranging from $4.33 \mu M$ to $5.33 \mu M$. It was observed that these complexes could induce cell cycle arrest followed by apoptosis, specifically arresting the S phase for **4a-Ni**, **4b-Ni**, and **4d-Ni**, and the G2/M phase for **4c-Ni**.¹⁹³

Our research group (Morales' group) has also contributed to the study of the cytotoxic effect of Ni(II) pincers compounds, specifically with POCOP-type complexes (**5a-Ni** – **6c-Ni**) (**Figure 56**).^{194,195} Complexes **5a-d-Ni** were evaluated against six cancer cell lines, where a preliminary study showed that **5a-Ni** and **5c-Ni** complexes were the most active. IC_{50} values revealed that **5c-Ni** was the most efficient complex in the family, primarily against the lung cancer cell line (SKLU-1) ($IC_{50} = 2.59 \pm 0.2 \mu M$). Fluorescence displacement studies using ethidium bromide (EB) as the intercalating agent showed that all POCOP-Ni(II) complexes had the ability to intercalate with DNA (**Figure 57a**). Such intercalation was corroborated through *in silico* studies (**Figure 57b**), as well as the ability of the complexes to interact with another biological target, such as topoisomerase I (**Figure 57c**). Likewise, a series of *para*-acetylated POCOP-Ni(II) complexes (**6a-c-Ni**) was evaluated, being complex **6b-Ni** the most active against leukemia (K-562) and MCF-7 cancer cell lines ($IC_{50} = 7.32 \pm 0.06 \mu M$ and $14.36 \pm 0.02 \mu M$).



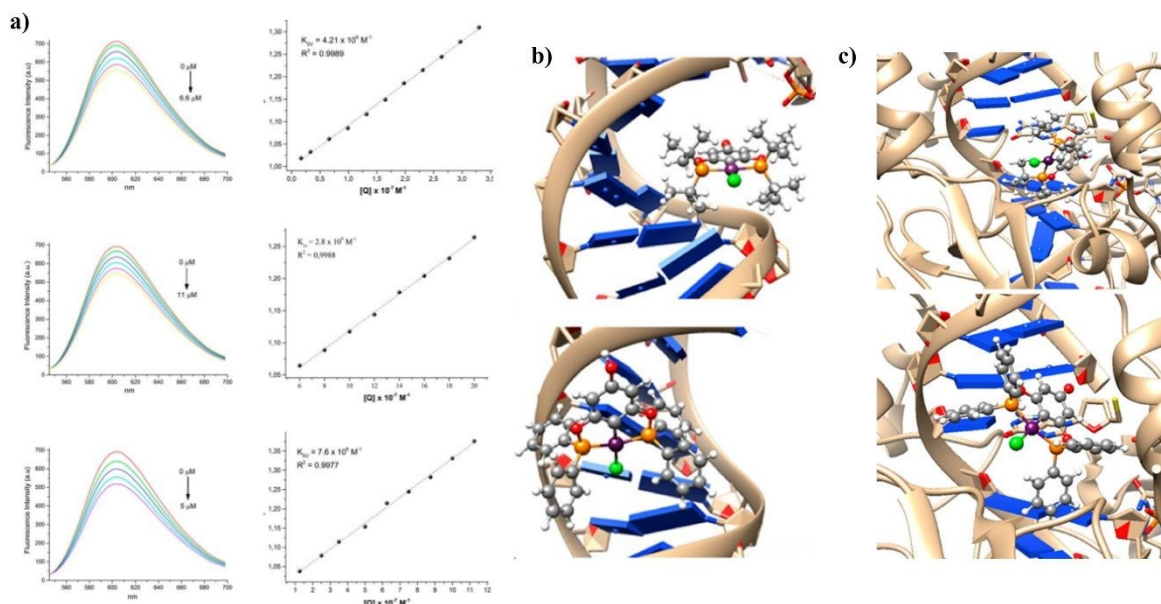


Figure 57. a) Fluorescence displacement study of complexes **5a-c-Ni**. b) DNA intercalation analysis via molecular docking of complexes **5b-Ni** and **5c-Ni**. c) Interaction with topoisomerase I through molecular docking of **5b-Ni** and **5c-Ni**. (Reproduce with permission from ref. 194 Copyright 2023 without license, open access Frontiers).

5.2. Palladium

Palladium complexes are a promising alternative for typical platinum complexes against cancer since they both possess a similar structure. In addition, different mechanisms of action would be available, reducing side effects.⁵⁵ Nevertheless, a rapid ligand exchange of palladium complexes in comparison to that of platinum complexes can alter the structure of palladium complexes inside the cell.^{196,197} Thus, continuous investigation is carried out to synthesize stable palladium complexes, employing strong ligands such as cyclometalated ligands.

5.2.1. C^N, C^C and C^P-type ligands

Albert and collaborators synthesized a series of C^N-type cyclopalladated complexes **1-Pd** – **6-Pd** (Figure 58), which were applied in cytotoxic assays. Complexes **1a-Pd** and **1b-Pd** were evaluated against the MCF-7 and MDA-MB-231 cancer cell lines and a *cisplatin*-resistant colon cancer line (HCT-116). The stability of **1a-Pd** and **1b-Pd** in biological media was investigated, revealing their conversion to ionic species through the substitution of auxiliary ligands (X, PPh₃, or both) with water molecules. These aqueous complexes could be responsible for the antiproliferative effects, suggesting a mechanism similar to *cisplatin*. Cytotoxicity assays (Table 19) indicate that these complexes exhibit a greater activity against all three cell lines compared to *cisplatin*, with the highest cytotoxicity



observed against the MDA-MB-231 cell line. Gel electrophoresis revealed that the complexes could alter the tertiary structure of DNA similarly to *cisplatin*, but only at much higher concentrations (100 μM - 200 μM). Additionally, these complexes demonstrated a limited activity as cathepsin B inhibitors, where **1b-Pd** inhibited more than 50% of enzyme activity at a concentration of 100 μM . Hence, the compounds would work through a different pharmacological mechanism, where DNA and cathepsin B are not the primary targets.^{198,199}

Table 19. IC₅₀ values of **1a-Pd** and **1b-Pd** complexes against cancer cell lines^a

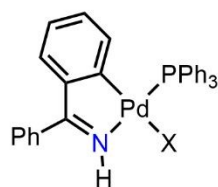
Compound	IC ₅₀ (μM)		
	MDA-MB-231	MCF-7	HCT-116
1a-Pd	1.1 \pm 0.3	4.0 \pm 0.5	18 \pm 2
1b-Pd	1.1 \pm 0.1	4.1 \pm 0.9	20 \pm 5
<i>cisplatin</i>	6.5 \pm 2.4	19.0 \pm 4.5	40.0 \pm 4.4

^a Cell viability determined by MTT assay after treatment for 72 h

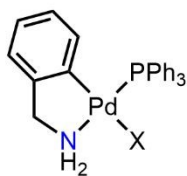
Likewise, a series of primary amine cyclopalladated complexes (**2a-Pd** – **4b-Pd**) were tested against different cancer cell lines (A549, MDA-MB-231, MCF-7, and HCT-116). Antiproliferative studies revealed high activity of almost all complexes against MDA-MB-231 (IC₅₀ = 1.0 μM to 13 μM) and HCT-116 (IC₅₀ = 2.1 μM to 16 μM), particularly **4a-Pd** and **4b-Pd**, which were 14 and 19 times more active than *cisplatin* against HCT-116 cell line. Palladium complexes induced subtle changes in the electrophoretic migration of plasmid DNA at high concentrations, at 100 μM for **2a-Pd** and 200 μM for **2b-Pd** and **3a-Pd**. For **3b-Pd**, the coalescence point occurred at 50 μM . After treating A549 cancer cells with **4a-Pd** or **4b-Pd** at a concentration equivalent to their IC₅₀ values, no notable effects were observed on cell cycle distribution.²⁰⁰

Subsequently, a series of six-membered palladacycles derived from amines or imines (**5-Pd** – **7-Pd**) were evaluated for their cytotoxic activities. Compared to *cisplatin*, the compounds with an imine moiety in their structure, **5-Pd** and **6-Pd**, exhibited a lower cytotoxicity toward normal cells; with **5-Pd** being practically non-cytotoxic toward any cell line. Interestingly, **6-Pd** showed a greater selectivity towards cancer cells, displaying a selectivity index (SI) of 11.2 on the HCT-116 cell line. In contrast, compounds with an amine group in their structure, such as **7-Pd**, exhibited higher toxicity towards all cell lines; particularly, **7-Pd** was highly toxic to normal cells (IC₅₀ = 0.9 \pm 0.1 μM). It appears that the halogen exchange facilitates the formation of aqueous species responsible for cytotoxic activity. DNA interaction studies showed that the complexes are unable to alter the tertiary structure or to inhibit cathepsin B, suggesting that the molecular target of these palladacycles is likely different from DNA and cathepsin B.²⁰¹

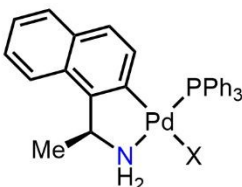


**1-Pd**

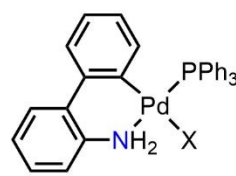
- a. X = OAc
b. X = Cl

**2-Pd**

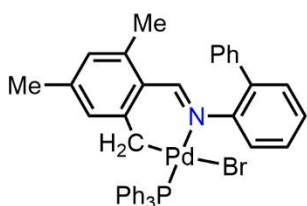
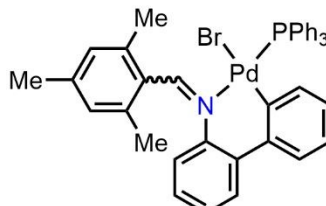
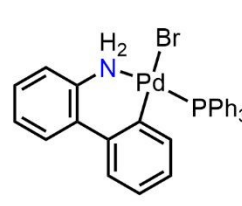
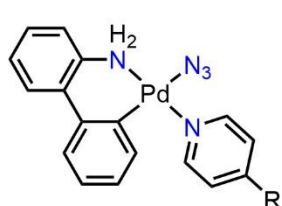
- a. X = OAc
b. X = Cl

**3-Pd**

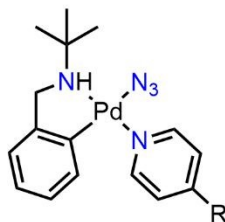
- a. X = OAc
b. X = Cl

**4-Pd**

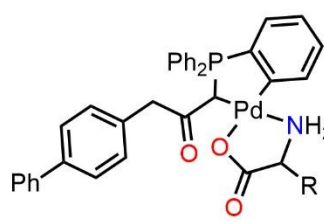
- a. X = OAc
b. X = Cl

**5-Pd****6-Pd****7-Pd****8-Pd**

- a. R = CONH₂
b. R = N(Me)₂

**9-Pd**

- a. R = CONH₂
b. R = N(Me)₂

**10-Pd**

- a. R = Me
b. R = *i*Pr
c. R = *i*Bu
d. R = *sec*-Bu
e. R = (CH₂)Ph

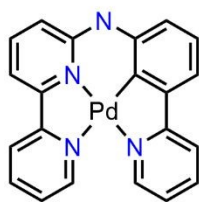
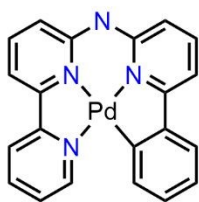
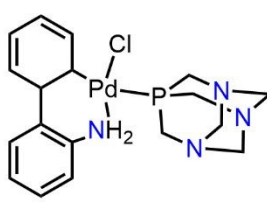
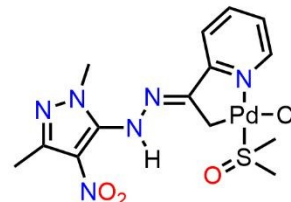
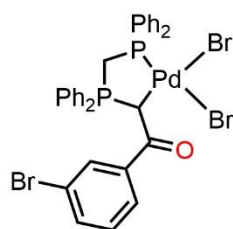
**11-Pd****12-Pd****13-Pd****14-Pd****15-Pd**

Figure 58. Pd(II) cyclometalated complexes: C^NN-Pd(II) (**1-Pd** – **9-Pd** and **11-Pd** – **14-Pd**), C^CC-Pd(II) (**10a-e-Pd**), and C^PP-Pd(II) (**15-Pd**).

Karami's group synthesized various cyclopalladated complexes (**8a-Pd** – **10e-Pd**) (**Figure 58**) and tested them in cytotoxicity studies. Those cytotoxicity assays revealed that the complexes showed comparable or superior values to *cisplatin*. Interestingly, complexes containing primary amines exhibited greater cytotoxicity, with **8a-Pd** being the most active compound, likely due to the ability of the -NH₂ ability group to form hydrogen bonds more efficiently. The interaction of these complexes with DNA was investigated using various techniques, including circular dichroism (CD). A decrease in the intensity of both positive and negative bands, without any shift in their positions, suggested that these complexes interact with DNA through groove binding (**Figure 59a**). Additionally, *in silico* studies indicated that the most favorable binding mode of these complexes with DNA is also through groove binding (**Figure 59b**). Complex **9a-Pd** exhibited the highest affinity for CT-DNA, attributed to its smaller size, greater rigidity, and planarity within the palladacycle. The binding mode was confirmed through competitive fluorescence displacement assays, revealing minimal displacement. Additionally, these complexes demonstrated interaction with BSA, where **8b-Pd** – **9b-Pd** complexes exhibited high binding affinity to BSA's site-I, while **8a-Pd** bound to site-III.²⁰²

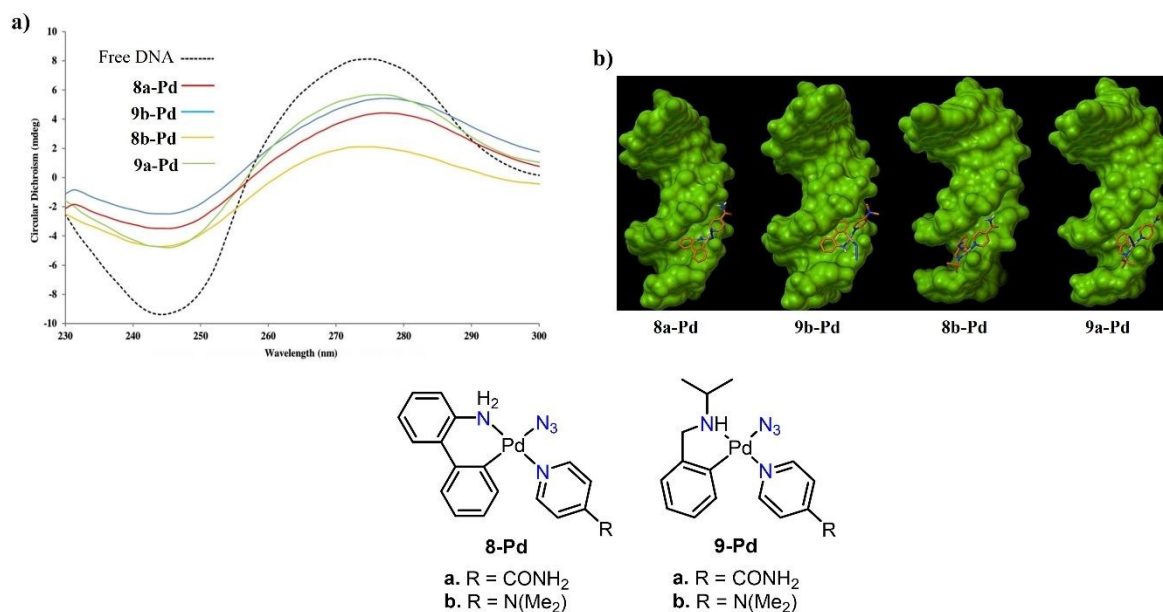


Figure 59. a) DNA interaction study using circular dichroism (CD). b) Molecular docking studies showing groove binding interaction of complexes **8a-b-Pd** and **9a-b-Pd** with DNA. (Reproduce with permission from ref. 202 Copyright 2018, Wiley-VCH).



In a subsequent study, palladium complexes bearing α -amino acids (**10a-e-Pd**) were evaluated against a leukemia cell line (K562). The results revealed that complexes with bulky alkyl substituents, such as **10c-Pd** ($IC_{50} = 23.84 \mu M$), **10d-Pd** ($IC_{50} = 34.53 \mu M$), and **10e-Pd** ($IC_{50} = 20.80 \mu M$), were twice to thrice more active than *cisplatin* ($IC_{50} = 64.66 \mu M$). The **10e-Pd** complex was shown to interact with BSA, effectively displacing warfarin, indicating that site I is its primary binding site.²⁰³

Two new isomers of polypyridyl cyclopalladated complexes, **11-Pd** and **12-Pd** (Figure 58), were reported by Bonnet and coworkers.²⁰⁴ The effective concentrations for cell growth inhibition (EC_{50}) against A549 and skin (A431) cell lines are shown in Table 20. Both compounds exhibited a significant increase in cytotoxicity after activation with blue light. Despite being isomers, **11-Pd** demonstrated significantly greater phototoxicity, particularly against A549 cells, with a PI of 13.

Table 20. EC_{50} of **11-Pd** and **12-Pd** complexes evaluated in darkness and light conditions^a

Compound	EC_{50} (μM)					
	A549			A431		
	Dark	Light	PI ^b	Dark	Light	PI ^b
11-Pd	12	0.9	13	20	5.0	4.0
12-Pd	8.0	6.0	1.3	14	10	1.4

^a Cell viability determined by MTT assay after treatment for 48 h under dark and cells irradiated blue light for 5 min
^b PI (Phototoxic Index) = $EC_{50} \text{ dark} / EC_{50} \text{ light}$

Lighvan's and Khonakdar's group evaluated the cytotoxic activity of a six-membered C^N cyclopalladated complex with a phosphadamantane ligand (PTA) (**13-Pd**) against MCF-7 cancer cells, leukemia (JURKAT), and normal fibroblasts. The complex exhibited moderate cytotoxic activity towards JURKAT cells ($IC_{50} = 51 \mu M$) and MCF-7 cells ($IC_{50} = 35 \mu M$), with an SI > 2. Notably, the coordination of phosphorus ligands favors hydrophobicity and promotes interactions with DNA, while the presence of amines with low steric hindrance favors the formation of hydrogen bonds. Additionally, the complex's interactions with DNA were studied, where it is highly likely that the complex binds to DNA via an intercalative mode. Furthermore, **13-Pd** caused a significant increase in the DNA melting temperature ($\Delta T_m = 5.25$), like classical intercalators.²⁰⁵

The Abushamleh's group evaluated the cytotoxic activity of a five-membered C^N palladacycle (**14-Pd**) against K562 cells.²⁰⁶ The compound showed moderate growth inhibition ($GI_{50} = 76.46 \mu M$), which was superior to that of *cisplatin* ($GI_{50} = 134.83 \mu M$). Moreover, **14-Pd** demonstrated a faster response time of 24 hours compared to *cisplatin*'s 48 hours. Regarding **14-Pd**'s structure, the cytotoxic activity could be attributed to the presence of a DMSO molecule and its likely dissociation inside the cell, or even to the hydrolysis of the azomethine bond in physiological media.



Sabounchei's group reported the cytotoxic activity of a five-membered palladacycle (**15-Pd**) against PC-3, MCF-7, and A2780 cancer cells, using normal rat cells (PC-12) as a control.²⁰⁷ In the MCF-7 cell line, the complex reduced cell viability by 35% at a concentration of 29.5 μM . Complex **15-Pd** showed higher cytotoxic activity than *cisplatin* and the ligand toward PC-3 cells ($\text{IC}_{50} = 2.06 \mu\text{M}$) and A2780 cells ($\text{IC}_{50} = 14.45 \mu\text{M}$), while not toxic to normal PC-12 cells or MCF-7 cancer cells. Treating PC-3 cells with **15-Pd** at different concentrations induced growth inhibition, shrinkage, vacuolization, and moderate cytoplasmic granulations. Due to the aromatic rings and flatness around the palladacycle, this complex could exhibit intercalation-type interactions with DNA. Additionally, the presence of auxiliary bromide ligands suggests that the complex may undergo aquation, making the aqueous complex likely to be active.

5.2.2. Pincer complexes

Casini *et al.* reported an iminophosphorane-based NNC-Pd(II) pincer complex (**16-Pd**) (**Figure 60**) and evaluated its antiproliferative activity against two cancer cell lines, A2780 and A549, with a non-tumorigenic human embryonic kidney cell line (HEK-293T) used as a control and *cisplatin* as a reference (**Table 21**).²⁰⁸ Complex **16-Pd** exhibited low cytotoxic activity towards A549 and HEK-293T cells. However, the antiproliferative study showed high activity against A2780 cells with an SI nearly double that of *cisplatin*. Gel electrophoresis assays showed no interaction with plasmid DNA, suggesting a different mechanism of action compared to *cisplatin*. Fluorescence quenching analysis revealed a single quenching mechanism, the presence of different binding sites on the protein, and a faster reactivity with HSA compared to *cisplatin*. These findings could explain the higher selectivity and efficacy of **16-Pd** against ovarian cancer cells.

Table 21. IC_{50} values of complex **16-Pd** against A2780 and A549 cancer cells^a

Compound	IC_{50} (μM) (SI ^b)		
	A2780	A549	HEK-293T
16-Pd	13.2 ± 2.1 (5.00)	86.5 ± 2.5 (0.76)	66.0 ± 5.5
<i>cisplatin</i>	3.90 ± 1.80 (2.82)	8.0 ± 0.5 1.38	11.0 ± 2.9

^a Cell viability determined by MTT assay after treatment for 72 h

^b SI (Selectivity Index) = IC_{50} (HEK-293T)/ IC_{50} (A2780 or A549)

The Che's group reported a series of CNN-Pd(II) pincer complexes (**17a-Pd** – **20-Pd**) (**Figure 60**), which are stable in the presence of biological thiols (glutathione, thioredoxin reductase) and ascorbic acid. The complexes showed promising cytotoxic activity against cancer cell lines, particularly **17d-Pd**, which exhibited high selectivity toward cancer cells (SI = 23.6-147.5). The activity of the other complexes was much lower, potentially due to lower stability under cellular conditions and higher



binding affinity to serum proteins. Complexes **17a-Pd** and **17d-Pd** showed low interaction with HSA, with over 60% and 55% of the compounds, respectively, remaining unbound; in contrast, less than 16% of the other complexes were unbound, indicating lower stability. HeLa cells treated with **17a-Pd** and **17d-Pd** showed induction of apoptosis, evidenced by an increase in the cell population in the sub-G1 phase, increased caspase-3 and caspase-9 enzymatic activity, and PARP-1 cleavage. Disruption of the mitochondrial membrane was also observed, although no ROS production was detected. The mechanism of action of the complexes involves mitochondrial dysfunction leading to apoptotic cell death.²⁰⁹

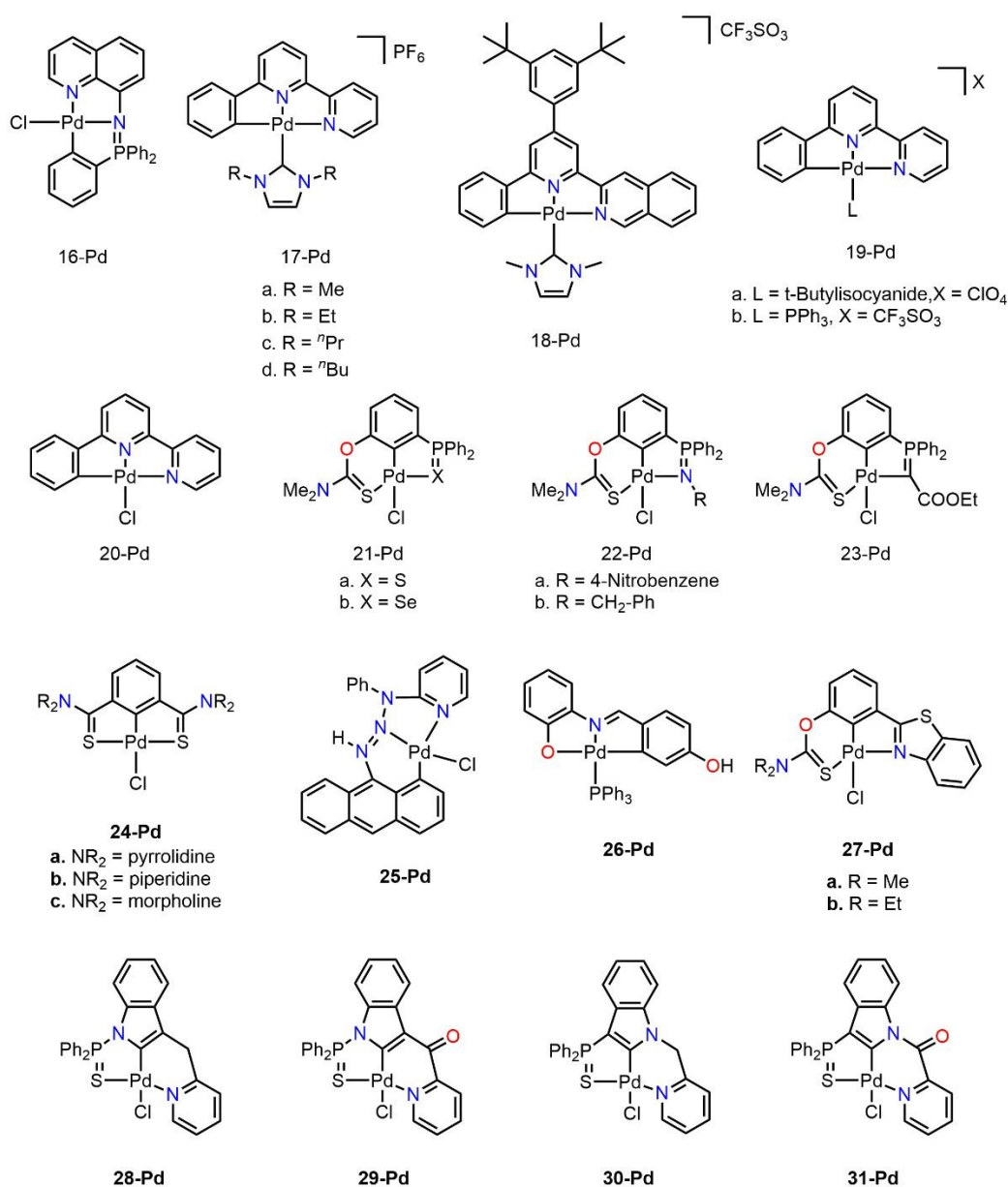


Figure 60. Pd(II) pincer complexes with different cyclometalated tridentate ligands (**16-Pd** – **31-Pd**).

A series of asymmetric five- and six-membered Pd(II) pincer complexes (**21-Pd** – **23-Pd**) was reported by Aleksanyan's group, and their cytotoxic activity against various cancer cell lines was evaluated. Only compounds **22a-Pd** ($IC_{50} = 7.5 \pm 1.5 \mu M$) and **22b-Pd** ($IC_{50} = 2.5 \pm 0.5 \mu M$) exhibited significant cytotoxic activity against the HCT-116 cell line. However, their activity against normal cell lines (HEK-293T) was high ($IC_{50} = 14.5 \pm 1.5 \mu M$ and $4 \pm 1 \mu M$, respectively), suggesting a lack of selectivity towards cancer cell lines. Notably, the high cytotoxic effect of **22b-Pd** could be attributed to the high electron density on the atom forming the five-membered palladacycle, which could make the Pd-L bond in the five-membered palladacycle less labile. In contrast, the other complexes, which have lower electron density, could undergo palladacycle breakage, making these complexes prone to side reactions in biological media.²¹⁰

Zargarian and collaborators reported a series of SCS-Pd(II) pincer complexes (**24a-c-Pd**) and studied their cytotoxic activity against three breast cancer cell lines: MCF-7, MC4L2, and 4T1, as well as their effects on tumor cell adhesion and migration. The cytotoxic profile of **24b-Pd** was notable, exhibiting slightly lower cytotoxicity than *cisplatin* against the three breast cancer cell lines evaluated, but almost no toxicity towards normal cells. In comparison, **24a-Pd** and **24c-Pd** showed lower activity. Notably, complex **24c-Pd** was more effective against cancer cells with short exposure times (24 hours) while maintaining its low toxicity toward normal cells. This efficacy could be attributed to the involvement of the oxygen atom in the morpholine ring in donor-acceptor-type interactions with the substrate, resulting in the formation of a robust complex with its target. All three complexes inhibited cell adhesion compared to the control, with **24c-Pd** being the most effective cell adhesion inhibitor (42.3%), indicating its potential to affect the metastatic capacity of cancer cells by inhibiting their adhesion properties. Studies on cell migration in triple-negative breast cancer (TNBC 4T1) were conducted using an *in vitro* scratch wound assay, and the inhibitory capacity of the palladium complexes demonstrated that treatment with the three complexes reduced the spread of cells along the wound edges compared to the control.¹⁹²

Gosh *et al.* synthesized an asymmetric CNN-Pd(II) pincer complex conjugated with anthracene (**25-Pd**), capable of specifically staining and visualizing the cell membrane through confocal microscopy and FLIM (fluorescence lifetime imaging). The complex showed the ability to stain the membrane of various cell lines, efficiently staining the membranes of cancer cell lines such as HeLa and MCF-7, as well as a normal cell line, HEK-293T. The longer lifetimes exhibited by **25-Pd** in the cancer cell lines HeLa and MCF-7 (1.77 ns and 1.69 ns, respectively), compared to the lifetime in the normal



cell line HEK-293T (1.54 ns) (**Figure 61**), suggest that the cancer cell membrane is slightly more rigid than the normal one. The efficient staining of the negatively charged membrane is likely due to the potential loss of the chloride ligand and the subsequent formation of a positively charged palladium complex.²¹¹

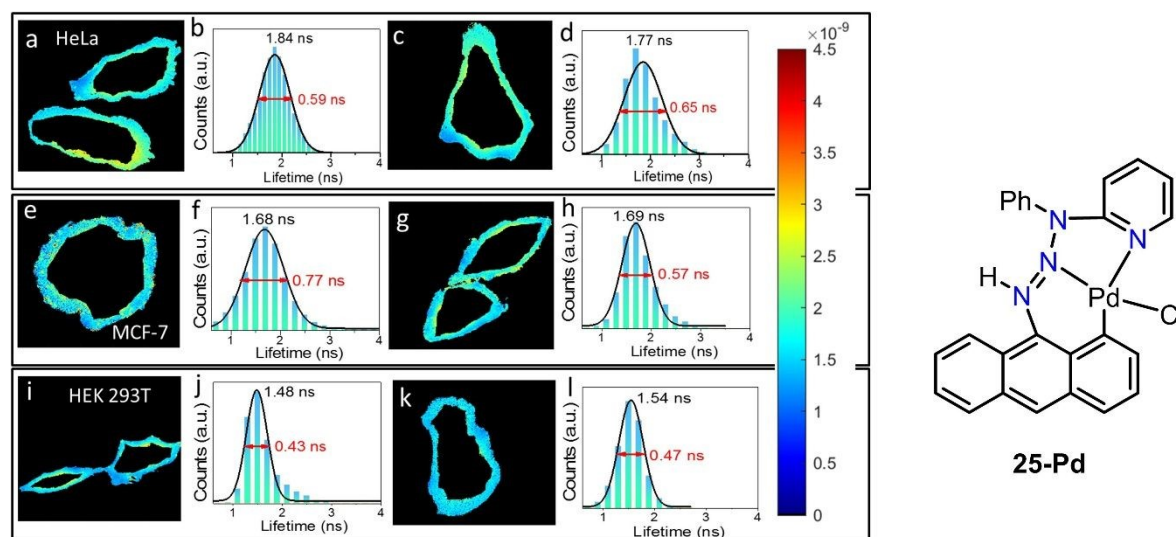


Figure 61. FLIM images (**a, c, e, g, i, and k**) and their corresponding lifetime distributions (**b, d, f, h, j, and l**) of HeLa, MCF-7, and HEK 293T cells stained with complex **25-Pd**. (Reproduce with permission from ref. 211 Copyright 2022, Elsevier).

Albert *et al.* reported an ONC-Pd(II) pincer complex (**26-Pd**) with an acceptable cytotoxic profile against MCF-7 and HCT-116 cancer cell lines and low toxicity towards normal cells (BJ) (**Table 22**). Complex **26-Pd** was highly selective towards MCF-7 cancer cells (SI = 11.03), being thirteen times more selective towards cancer cells and almost thirty times less toxic against healthy cells compared to *cisplatin*. The cytotoxic activity of **26-Pd** is likely due to the high lipophilic character imparted by the PPh₃ ligand, which could facilitate transport through passive diffusion. An electrophoretic DNA migration assay was performed with plasmid DNA using *cisplatin* and ethidium bromide as controls for a DNA-alkylating agent and a DNA-intercalating agent, respectively. The **26-Pd** compound did not act as an alkylating or intercalating agent, as no reduction in the mobility of the plasmid DNA bands was observed. Due to the lack of interaction between **26-Pd** and DNA, the complex's ability to inhibit topoisomerases (I and II α) was tested. The complex was unable to inhibit topoisomerase I but showed low inhibitory capacity against topoisomerase II α at 50 μ M, suggesting that this could be a potential biological target.²¹²



Table 22. IC₅₀ of **26-Pd** complex on MCF-7 and HCT-116 cancer cell lines^a

Compound	IC ₅₀ (μM)		
	MCF-7 (SI ^b)	HCT-116	BJ
26-Pd	7.8 ± 1.7 (11,03)	31 ± 6	86 ± nd
<i>cisplatin</i>	3.6 ± 1.7 (0.83)	19 ± 2	3 ± nd

^a Cell viability determined by MTT assay after treatment for 72 h^b SI (Selectivity Index) = IC₅₀ (BJ)/IC₅₀ (MCF-7)

Aleksanyan evaluated the cytotoxic activity of a series of asymmetric SCN-Pd(II) pincer complexes (**27-Pd** – **31-Pd**) against various cancer cell lines. Cancer cell proliferation was significantly inhibited, as seen in the H-9 cell line, where **27b-Pd** was highly active (IC₅₀ = 1.3 ± 0.1 μM). Specifically, the PC-3 cancer cell line was successfully inhibited by **27b-Pd** (IC₅₀ = 8.5 ± 2.5 μM), **28-Pd** (IC₅₀ = 4.8 ± 0.8 μM), and **30-Pd** (IC₅₀ = 3.6 ± 0.6 μM). These complexes were highly selective for PC-3 cells (SI > 3). Notably, the most active complexes in this series contain more lipophilic substituents than the less active ones, which could improve cellular uptake, thereby increasing their cytotoxicity. Complex **27b-Pd** was able to halt the cell cycle through early apoptosis in K562 leukemia cells (33.5%) and K562/iS9 cells (21.2%). On the other hand, **28-Pd** induced necrosis in PC-3 cells while 90% of normal cells remained alive, with no significant cell cycle arrest. Compound **30-Pd** induced both early apoptosis and necrosis in cancer cells, with the lowest percentage of normal cells remaining, and like **27b-Pd**, no significant cell cycle arrest was observed.^{213,214}

5.3. Platinum

Platinum-based compounds such as *cisplatin* are widely studied and applied in the treatment of cancer. *Cisplatin* is a wide-spectrum drug against several cancers such as ovarian, testicular, and colorectal among others.²¹⁵ However, side effects, including nephrotoxicity, ototoxicity, and neurotoxicity among others, arise due to a lack of selectivity.^{216,217} For that reason, further generations of drugs were developed yielding carboplatin, nedaplatin, oxaliplatin, lobaplatin, and heptaplatin, which are either regionally clinically approved or in clinical trials.^{218,219} Likewise, continuous research implies ligand modification, preparation of platinum(IV) compounds, and delivery systems.²²⁰⁻²²⁵

5.3.1. C^N, C^P, C^C and C^O complexes

Shahsavari and collaborators synthesized a series of C^N cyclometalated Pt(II) complexes, which were used in cytotoxicity assays. In an initial study, they reported the cytotoxic activity of a series of



thiolate-substituted Pt(II) complexes (**1a-e-Pt**) (**Figure 62**). Among these, **1a-Pt** exhibited higher antiproliferative activity against the SKOV3 ($IC_{50} = 4.58 \mu M$) and MCF-7 ($IC_{50} = 10.34 \mu M$) cell lines compared to *cisplatin* ($IC_{50} = 14.18 \mu M$ and $IC_{50} = 12.53 \mu M$, respectively). Complex **1b-Pt** showed high cytotoxicity against the MCF-7 cell line, while **1d-Pt** and **1e-Pt** were practically non-cytotoxic, and **1a-Pt** significantly increased its cytotoxicity.²²⁶ In a subsequent study, **2a-e-Pt** complexes derived from oxibipyridine were evaluated on different cancer cell lines. Complexes **2a-d-Pt** were minimally active, while **2e-Pt** was the most active complex of the series, particularly against the SKOV3 ($IC_{50} = 0.72 \pm 0.19 \mu M$) and MCF-7 ($IC_{50} = 1.23 \pm 0.34 \mu M$) cell lines.²²⁷

The cytotoxic evaluation of **3a-Pt** and **3b-Pt** complexes (**Figure 62**), coordinated with a 2-mercaptopyridine N-oxide (SpyO) ligand, was carried out. The results indicated that both complexes were less cytotoxic than *cisplatin* in most cancer cell lines. However, in the HT-29 cell line, both complexes demonstrated significantly higher activity compared to the reference metallodrug ($IC_{50} = 107.1 \pm 2.3 \mu M$), with **3b-Pt** showing more than a twenty-fold increase in toxicity ($IC_{50} = 5.3 \pm 0.7 \mu M$) and exhibiting minimal cytotoxicity against the normal MCF-12A cell line. Notably, both complexes showed a lack of cytotoxicity against the SKOV3 cell line, particularly **3a-Pt** ($IC_{50} = 166.2 \pm 2.5 \mu M$). Complex **3a-Pt** was shown to induce apoptotic cell death in SKOV3 cells, and *in silico* assays confirmed that both complexes could interact with DNA in the minor groove (**Figure 63a and b**).²²⁸

Ruiz *et al.* have reported the cytotoxic activity of a series of C^N Pt(II) complexes (**4-Pt – 8-Pt**) in human ovarian carcinoma cell lines. Compound **4-Pt – 8-Pt** complexes showed high activity against the A2780 cell line, with **4b-Pt** and **5-Pt** being the most active (**Table 23**).^{229,230} These two complexes were able to overcome *cisplatin* resistance in the A2780cisR cell line, exhibiting resistance factors (RF) lower than 2. To understand the mode of action of **4b-Pt** and **5-Pt** complexes, apoptosis induction studies were conducted in treated A2780 cells. The results showed a high incidence of apoptosis (58.9% and 76.6%, respectively) without an increase in the necrotic population. It was found that neither **4b-Pt** nor **5-Pt** increased caspase-3 activity after the treatment of A2780 cells, suggesting that these complexes promote cell death through a caspase-independent pathway. Additionally, the *in vivo* antivasular activity of **4b-Pt** and **5-Pt** was tested in chicken embryos at 5 and 10 nmol. After six hours, both complexes exhibited antivasular effects on blood vessels (**Figure 64**). Subsequently, the **8-Pt** complex derived from the integrin receptor $\alpha_5\beta_1$ (RGDFK) was tested on different cancer cell lines. Although **8-Pt** showed minimal cytotoxicity against all the tested cell lines, it induced morphological changes in the cells.



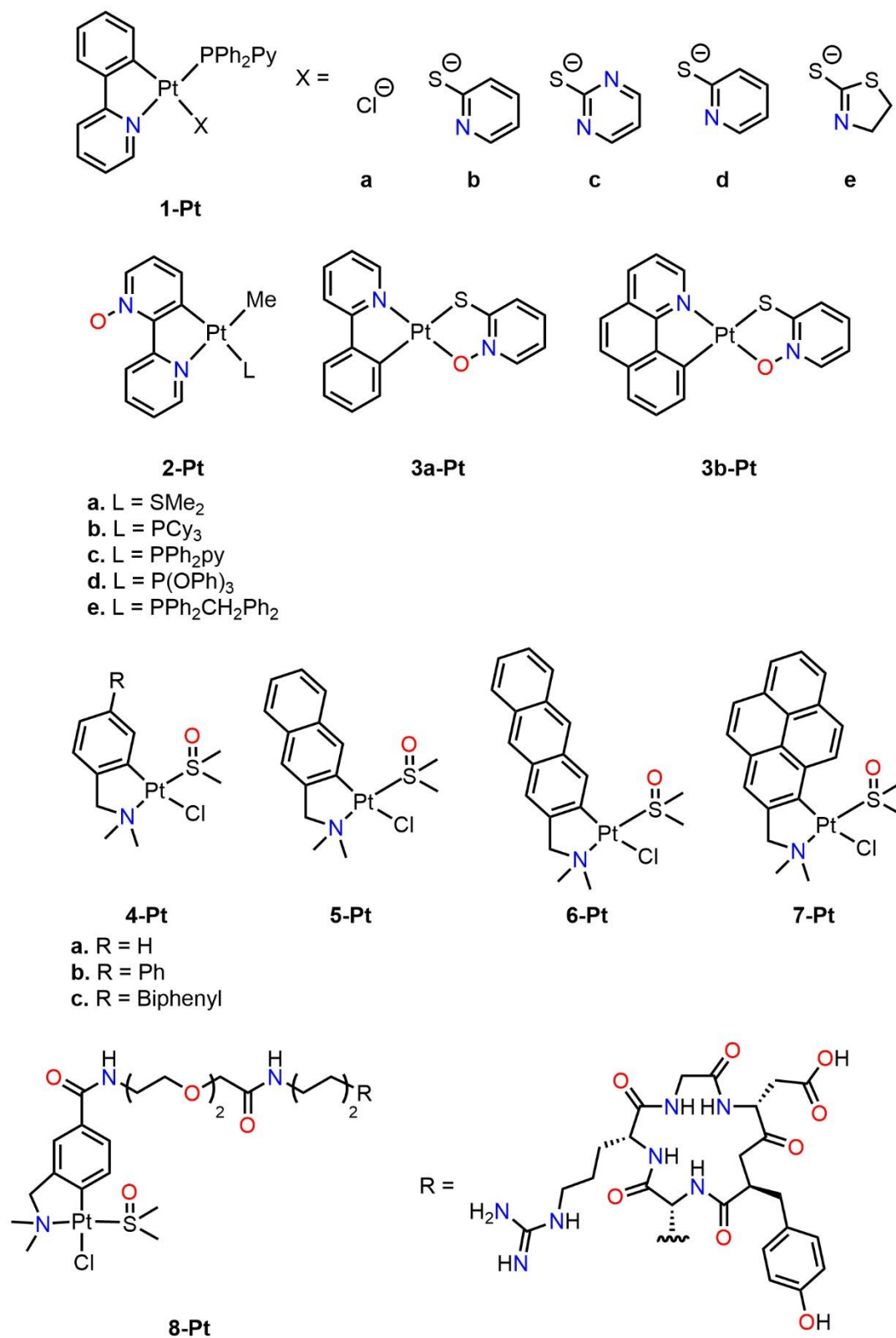


Figure 62. Cyclometalated C^N-type Pt(II) complexes (1-Pt – 8-Pt).

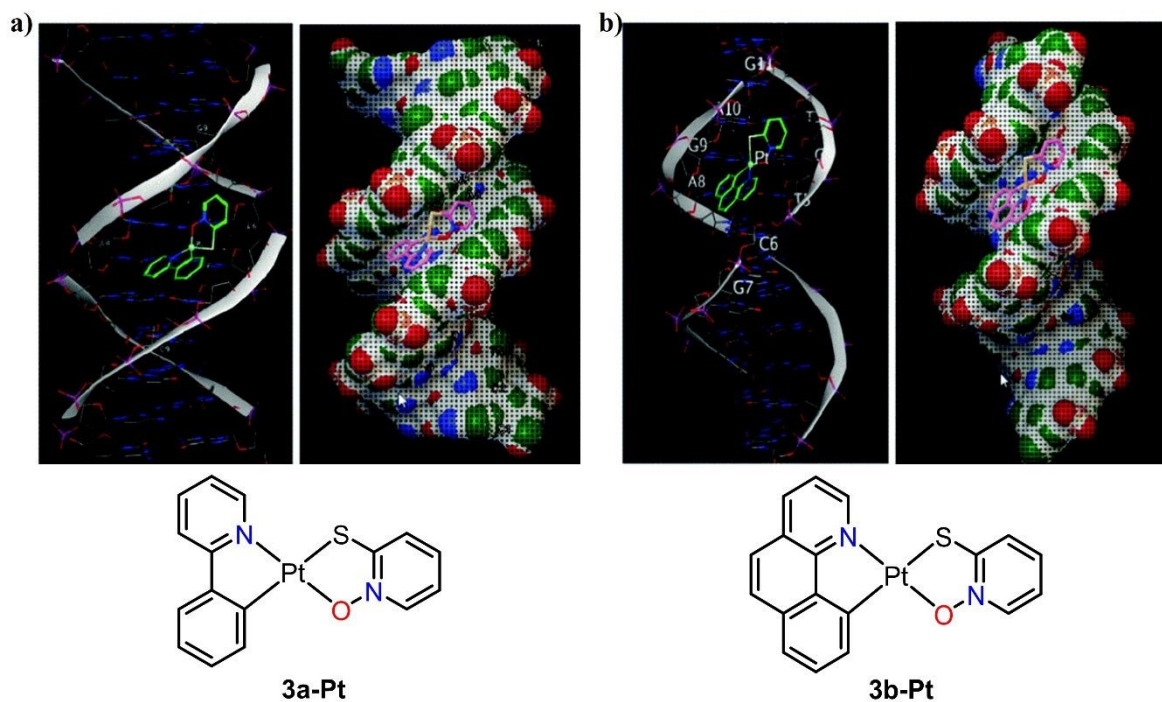


Figure 63. Molecular docking studies of complexes **a) 3a-Pt** and **b) 3b-Pt** with DNA, demonstrating their interaction within the minor groove. (Reproduce with permission from ref. 228 Copyright 2018, American Chemical Society).

Table 23. IC₅₀ of **4a-Pt** – **7-Pt** complexes evaluated against the A2780 and A2780cisR cancer cell lines^a

Compound	IC ₅₀ (μM)	
	A2780	A2780cisR (RF ^b)
4a-Pt	1.38 ± 0.37	2.05 ± 0.24 (1.49)
4b-Pt	1.18 ± 0.10	1.51 ± 0.34 (1.29)
4c-Pt	2.08 ± 0.16	2.61 ± 0.39 (1.25)
5-Pt	1.29 ± 0.09	1.97 ± 0.24 (1.53)
6-Pt	2.10 ± 0.08	2.34 ± 0.39 (1.12)
7-Pt	2.04 (0.25)	2.38 ± 0.18 (1.16)
cisplatin	1.63 ± 0.35	24.13 ± 2.88 (14.80)

^a Cell viability determined by MTT assay after treatment for 48 h

^b RF (Resistance Factor) = IC₅₀ (A2780cisR)/IC₅₀ (A2780)



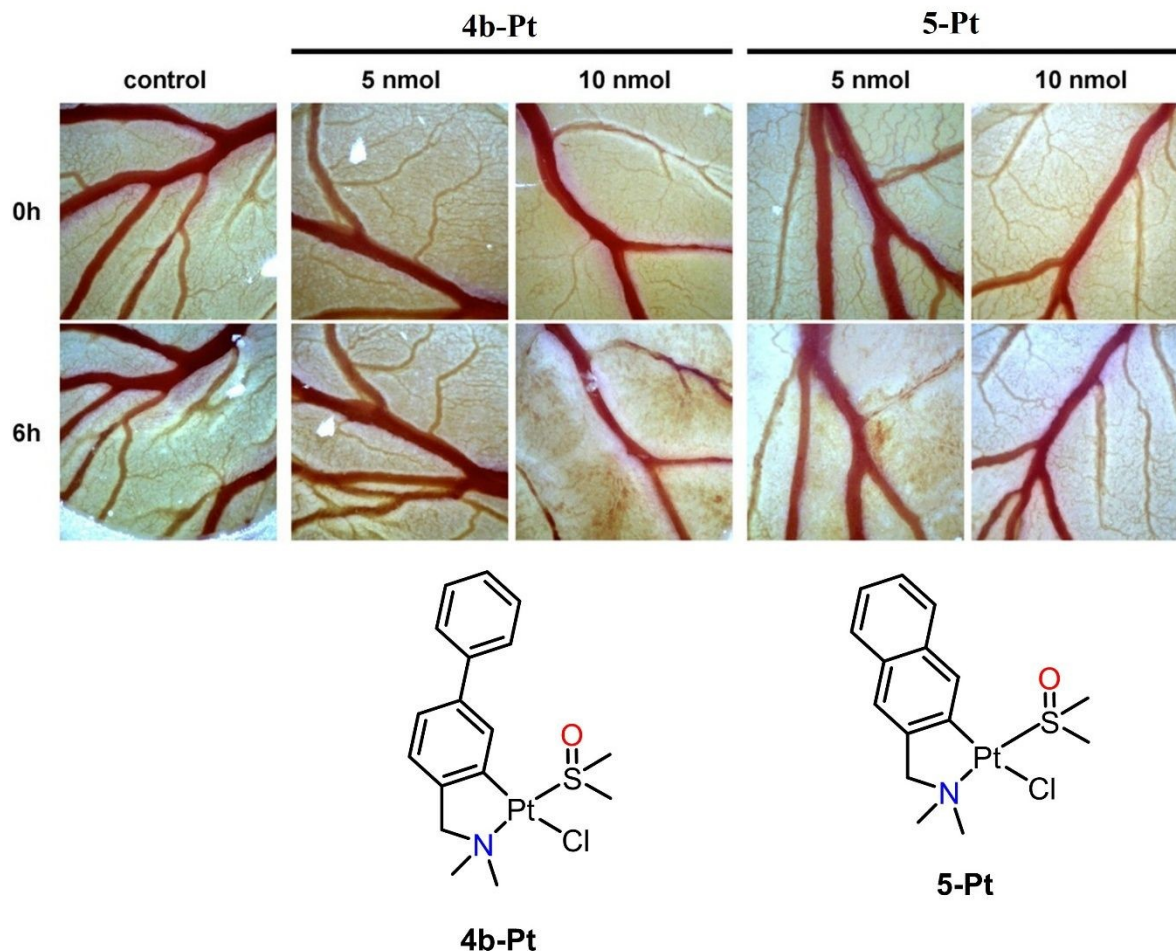


Figure 64. Effects of treatment with **4b-Pt** and **5-Pt** at 5 and 10 nmol on the chorioallantoic membrane of fertilized chicken embryos after six hours. (Reproduce with permission from ref. 229 Copyright 2017, Wiley-VCH).

Rashidi and collaborators evaluated the cytotoxic activity of complexes **9-11-Pt** (**Figure 65**). While **9a-Pt** was practically inactive against any cell line, **9b-Pt** was highly water-soluble and showed cytotoxic activity ($IC_{50} = 0.84 \pm 0.19 \mu M$) comparable to *cisplatin* ($IC_{50} = 0.16 \pm 0.03 \mu M$) against CH1 cancer cells. In contrast, **10-Pt** showed greater cytotoxic activity ($IC_{50} = 6.6 \mu M$) against the Jurkat cancer cell line compared to **11-Pt** ($IC_{50} = 16.4 \mu M$) and *cisplatin* ($IC_{50} > 100 \mu M$). Complexes **10-Pt** and **11-Pt** are capable of inducing apoptosis, while **11-Pt** can also induce necrosis, which could contribute to its greater potential to generate various side effects compared to **10-Pt**. Additionally, both complexes can stimulate caspase 3 activity.^{231,232}

Complex **12-Pt** was stable in DMSO and undergoes aquation in physiological media, probably generating the species responsible for its cytotoxic activity. The platinum complex showed high



cytotoxicity toward normal cells and low selectivity compared to *cisplatin*. Since the free imine ligand was not cytotoxic, **12-Pt**'s activity could be attributed to the metal center or the release and subsequent oxidation of the phosphine ligand.¹⁹⁹

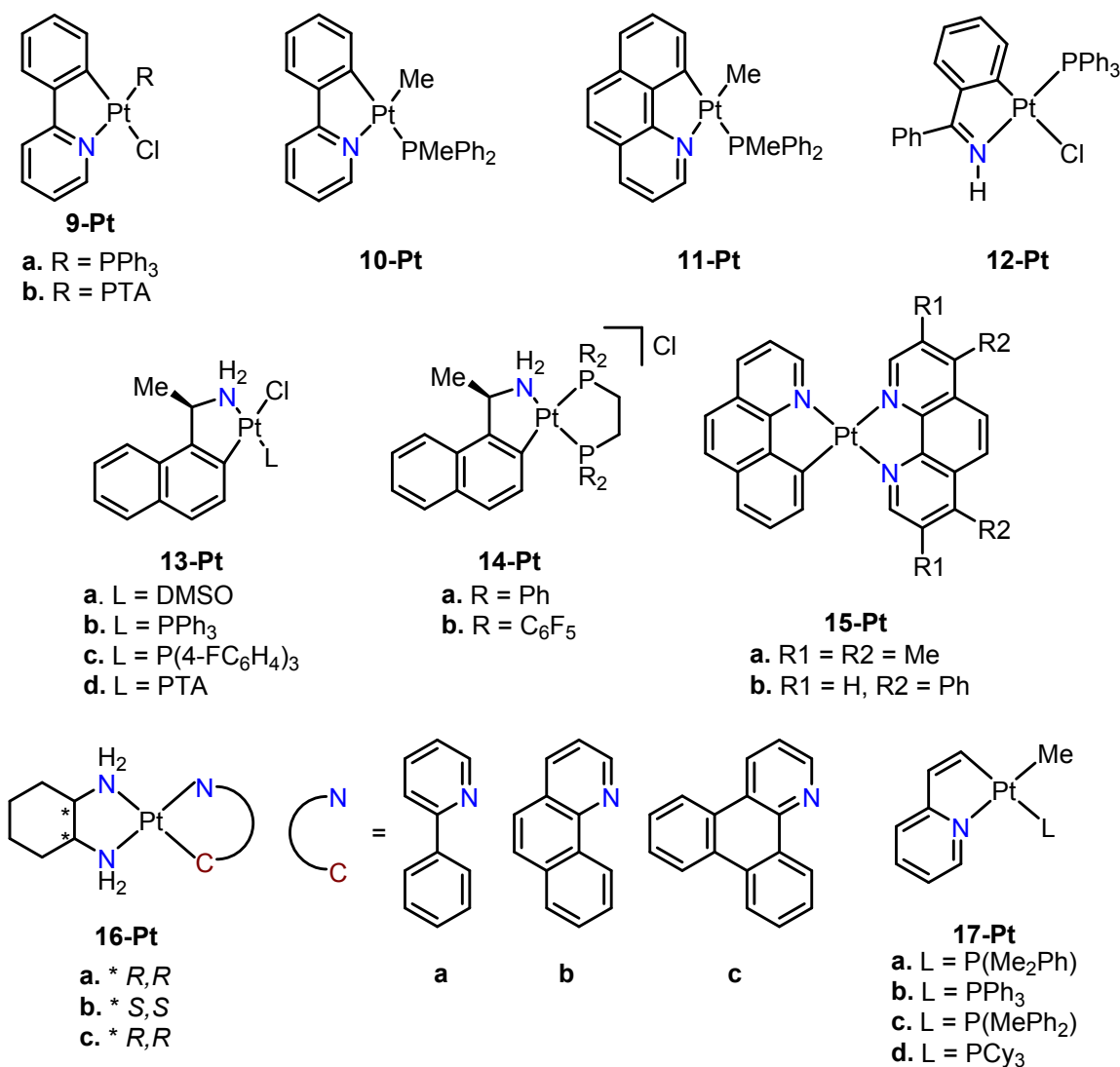


Figure 65. Cyclometalated C^N-Pt(II) complexes (**9-Pt** – **17-Pt**).

Likewise, the cytotoxicity of a series of platinum complexes, both neutral (**13a-d-Pt**) and ionic (**14a,b-Pt**), was studied. Notably, the **13b-Pt** complex ($IC_{50} = 0.27 \pm 0.1 \mu M$ against HCT-116), **14a-Pt** ($IC_{50} = 1.2 \pm 0.4 \mu M$ against A549), and **14b-Pd** ($IC_{50} = 0.82 \pm 0.08 \mu M$ against MDA-MB-231) exhibited higher activity compared to *cisplatin*. Complex **13d-Pt** was practically non-cytotoxic against any cell line, possibly due to its low solubility. Meanwhile, the ionic complexes **14a-Pt** and **14b-Pt** demonstrated notable activity against all evaluated cell lines, being up to 25 times more active



than *cisplatin*. However, the addition of a fluorinated substituent to the ligand did not improve cytotoxicity.²³³

Aldrich *et al.* synthesized a series of cyclometalated C^N complexes (**15a,b-Pt**) (**Figure 65**) able to interact with G-quadruplex DNA (QDNA).^{234,235} Notably, **15b-Pt** showed strong stabilization of QDNA, suggesting its potential for targeted DNA interactions. Lipophilicity was identified as the most significant predictor of cytotoxic activity for these complexes, with strong correlations ($R^2 > 0.98$), indicating that their hydrophobic nature enhances cellular interactions. Furthermore, the cytotoxicity of **16a-c-Pt** complexes was evaluated, showing a significant selectivity towards MCF-7 compared to the normal cell line MCF-10A with SI values of 2.46, 3.70, and 2.02, respectively, compared to an SI of 0.64 for 56MESS (platinum-based metallodrug).

Fereidoon nezhad and collaborators prepared a series of cyclometalated platinum complexes (**17a-d-Pt**) (**Figure 65**) and evaluated their cytotoxic activities. Among the complexes tested, **17c-Pt** showed the highest cytotoxic activity, surpassing that of *cisplatin*. Notably, **17a-Pt** and **17c-Pd**, which contain methyl and phenyl substituents on the phosphine ligand, showed higher cytotoxic activity compared to **17b-Pt** and **17d-Pt**, which bear phenyl and cyclohexyl substituents (**Table 24**).²³⁶ Genotoxicity studies and DNA interaction analysis of **17b-Pt** against MDA-MB-231 cells were conducted using the comet assay. Treatment with **17b-Pt** resulted in a relatively long comet tail in electrophoresis assays (**Figure 66c**) compared to *cisplatin* (**Figure 66b**), demonstrating that **17b-Pt** exhibits strong genotoxic potential. Additionally, the DNA-binding activity of **17b-Pt** was assessed through electrophoretic mobility shift assays, where the complex induced a significant change in plasmid mobility compared to untreated DNA at higher concentrations (400 μM) (**Figure 66d**). Although these changes were less pronounced than those induced by *cisplatin*, the results suggest that the activity of **17b-Pt** is exerted through direct interaction with DNA.

Table 24. IC₅₀ of **17a-d-Pt** complexes on the MDA-MB-231 cancer cell line^a

Compound	IC ₅₀ (μM)	
	MDA-MB-231	MCF-10 A (SI ^b)
17a-Pt	21.96 \pm 0.32	42.36 \pm 0.87 (1.92)
17b-Pt	36.18 \pm 1.19	75.32 \pm 1.54 (2.08)
17c-Pt	12.96 \pm 0.90	29.84 \pm 1.23 (2.30)
17d-Pt	44.08 \pm 0.65	96.16 \pm 1.49 (2.18)
<i>cisplatin</i>	19.50 \pm 1.30	28.73 \pm 1.55 (1.47)

^a Cell viability determined by MTT assay after treatment for 72 h



$$^b \text{ SI (Selectivity Index) = IC}_{50} (\text{MDA-MB-231})/\text{IC}_{50} (\text{MCF-10 A})$$

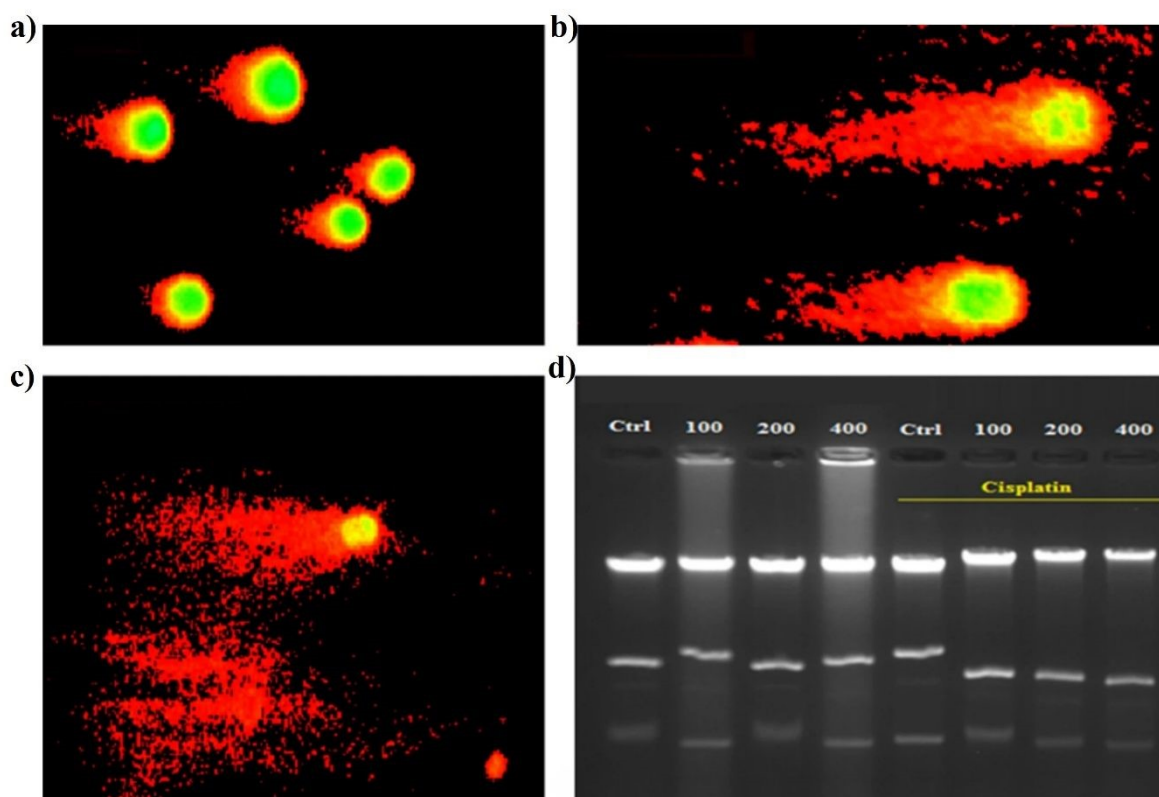


Figure 66. Genotoxic effect of **17b-Pt** on MDA-MB-231 cells compared to a) untreated cells, b) DNA-cisplatin, and c) DNA-**17b-Pt**. d) Treatment of a circular plasmid with various doses of cisplatin and **17b-Pt**. (Reproduce with permission from ref. 236 Copyright 2022, Springer).

Contel evaluated the cytotoxic activity of a series of ionic platinumacycles (**18-Pt** – **19b-Pt**) (**Figure 67**) against various cancerous and normal cell lines. The complexes exhibited significantly higher cytotoxicity compared to *cisplatin* in several cell lines (**Table 25**). Despite sharing the same cation, **19a-Pt** was twice as active as **Pt43** in the A549 and MDA-MB-231 cell lines. When tested on non-tumorigenic HEK293T cells, all compounds showed cytotoxicity comparable to that observed in cancer cells. The three evaluated complexes induced apoptosis through caspase-dependent mechanisms. The lack of interaction of **19b-Pt** with plasmid DNA (pBR322) and CT-DNA suggests a different mode of action compared to *cisplatin*. Permeability studies indicate that **19b-Pt** has a high permeability profile, like metoprolol or caffeine, and an estimated oral absorption fraction of 100%, making it a strong candidate for oral administration.²³⁷

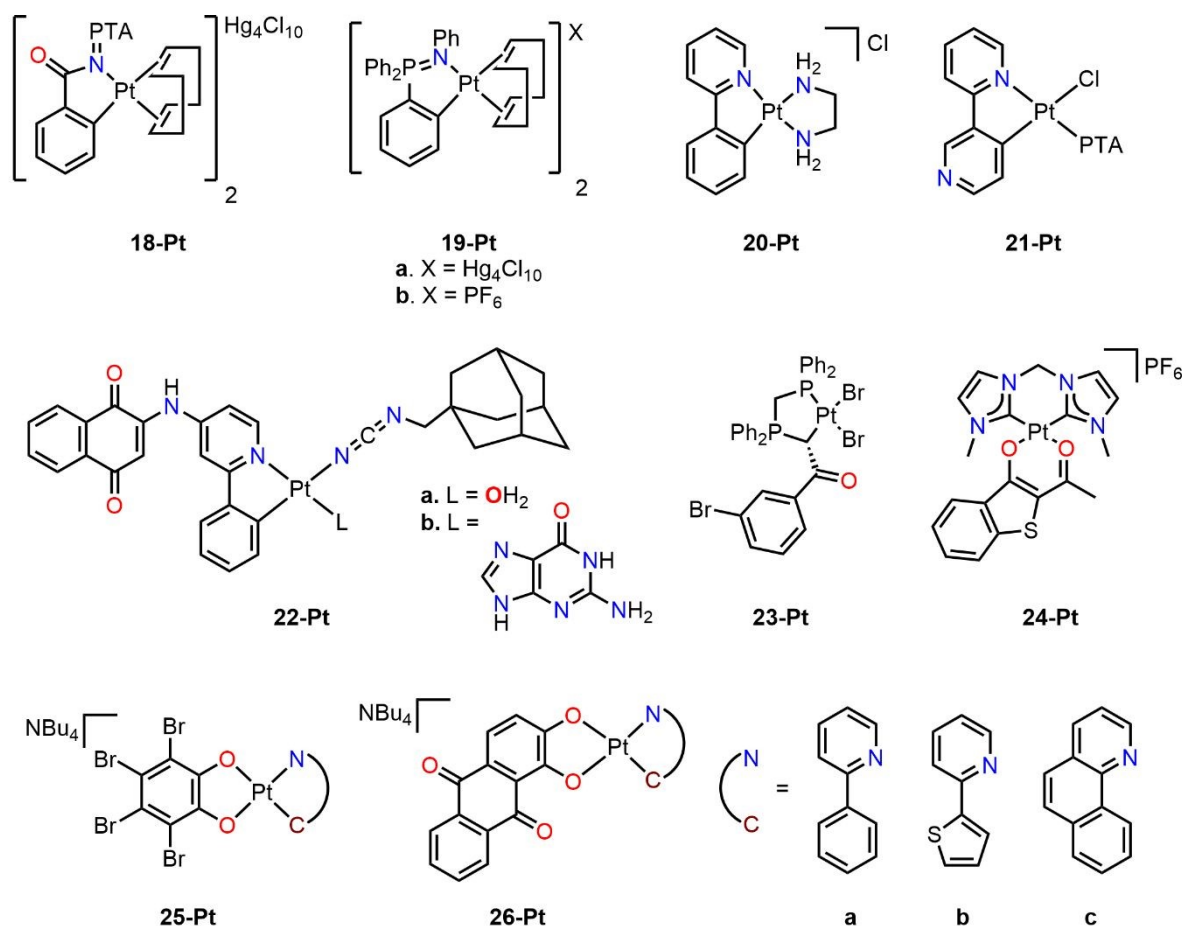
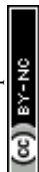


Table 25. IC₅₀ of **18-Pt** and **19a,b-Pt** complexes on A549 and MDA-MB-231 cancer cell lines^a

Compound	IC ₅₀ (μM)		
	A549	MDA-MB-231	HEK293T
18-Pt	20.8 ± 1.7	14.6 ± 3.7	4.0 ± 0.42
19a-Pt	0.85 ± 0.29	0.39 ± 0.05	1.25 ± 0.25
19b-Pt	2.01 ± 0.89	0.84 ± 0.29	0.94 ± 0.07
<i>cisplatin</i>	114.2 ± 9.1	131.2 ± 18	69.0 ± 6.7

^a Cell viability determined by MTT assay after treatment for 24 h

Complex **20-Pt** was water-soluble and showed suitable characteristics for use as a bioimaging probe, spontaneously entering the cytoplasm and preferentially localizing in the cell nucleus. Cellular uptake studies indicated that the compound is absorbed by both cancerous and normal cells, with greater uptake in cancer cells. Complex **20-Pt** was mostly localized in the cytoplasm and nucleus.²³⁸

**Figure 67.** Cyclometalated Pt(II) complexes (**18-Pt** – **26-Pt**).

Complex **21-Pt** was evaluated in cytotoxicity studies, demonstrating slightly higher activity ($IC_{50} = 1.4 \pm 0.2 \mu M$) compared to *cisplatin* ($IC_{50} = 3.3 \pm 0.4 \mu M$) against the SW480 cancer cell line. Complex **21-Pt** was found to alter the electrophoretic mobility of plasmid DNA at low concentrations, suggesting the formation of mono- and/or bifunctional DNA adducts. The DNA damage induced by **21-Pt** could occur in a p53-dependent way.²³⁹

Tabrizi and collaborators synthesized two C^N cyclometalated Pt(II) complexes derived from 1,4-naphthoquinone (**22a-Pt** and **22b-Pt**) (Figure 67) and evaluated their cellular uptake, DNA platination, and cytotoxicity. Compound **22a-Pt** demonstrated a remarkable cytotoxic activity against the HT-29 cancer cell line with an IC_{50} value of $0.56 \mu M$, significantly surpassing that of *cisplatin*. Additionally, **22a-Pt** showed greater accumulation in cancer cells compared to *cisplatin* and exhibited a high degree of DNA platination.²⁴⁰

Sabounchei reported the platinum derivative of **15-Pd**, designated as **23-Pt** (Figure 67). Unlike **15-Pd**, complex **23-Pt** showed insignificant cytotoxicity against the evaluated cancer cell lines. Furthermore, **23-Pt** did not affect the viability of normal PC-12 cells.²⁰⁷

Che and collaborators reported a bis-NHC cyclometalated platinum complex (**24-Pt**), which cytotoxic activity was studied against *cisplatin*-sensitive and *cisplatin*-resistant cancer cell lines. Complex **24-Pt** showed cytotoxicity comparable to *cisplatin* in sensitive cell lines and was less toxic toward normal cells ($IC_{50} = 54.6 \pm 3.64 \mu M$). In contrast, the activity of **24-Pt** against *cisplatin*-resistant cell lines was much higher, with RF values in A2780CisR and A549CisR of 1 and 0.7, respectively. *In vivo* studies of the complex demonstrated 70% tumor growth inhibition with reduced side effects. A greater accumulation of platinum was observed in the cells for **24-Pt**, probably due to the increased lipophilicity of the ligand. However, the complex induced less platination than *cisplatin* or oxaliplatin, suggesting a different mechanism of action.²⁴¹

Ionescu and collaborators studied the cytotoxic activity of cyclometalated anionic complexes (**25a-c-Pt** and **26a-c-Pt**). All the complexes exhibited significant cytotoxic effects on the MDA-MB-231 cell line, with IC_{50} values ranging from $1.9 \mu M$ to $127 \mu M$. Complexes **25a-c-Pt** showed consistent cytotoxic activity regardless of the ligand. In contrast, **26a-c-Pt** displayed variable cytotoxicity depending on the cyclometalated ligand. Compounds **26a-Pt**, bearing a cyclometalated phenylpyridine, showed the highest cytotoxicity, with an IC_{50} of $1.9 \pm 1.6 \mu M$. It was ten times more potent against MDA-MB-231 cells than against normal vascular smooth muscle cells. Complex **26a-Pt** caused cellular accumulation in the S phase and reduced the population in the G2/M phase, indicating its antiproliferative effect by blocking S phase progression.²⁴²



García *et al.* reported a series of five-membered Pt(II) complexes containing various aromatic fragments (**27a-d-Pt**) (**Figure 68**) and evaluated their cytotoxic activity and mechanisms of action. The complexes were found to be unstable in DMSO solution, dissociating after 3 hours. Neither **27c-Pt** nor **27d-Pt** exhibited any cytotoxic effect against the SW480 colon cancer cell line. In contrast, **27a-Pt** and **27b-Pt** were twice as active as *cisplatin* and induced morphological changes such as apoptotic body and vacuole formation. Complexes **27a-Pt** and **27b-Pt** showed significant intracellular accumulation, correlating with their cytotoxicity. Interestingly, **27d-Pt** exhibited high levels of accumulation despite being non-cytotoxic. Compounds **27a-Pt** and **27b-Pt** interacted with DNA through covalent interactions, forming adducts with N7 of deoxyguanosine monophosphate (dGMP). In contrast, **27c-Pt** and **27d-Pt** interacted through intercalation, likely due to the high steric hindrance associated with the bulky condensed aromatic rings.²⁴³

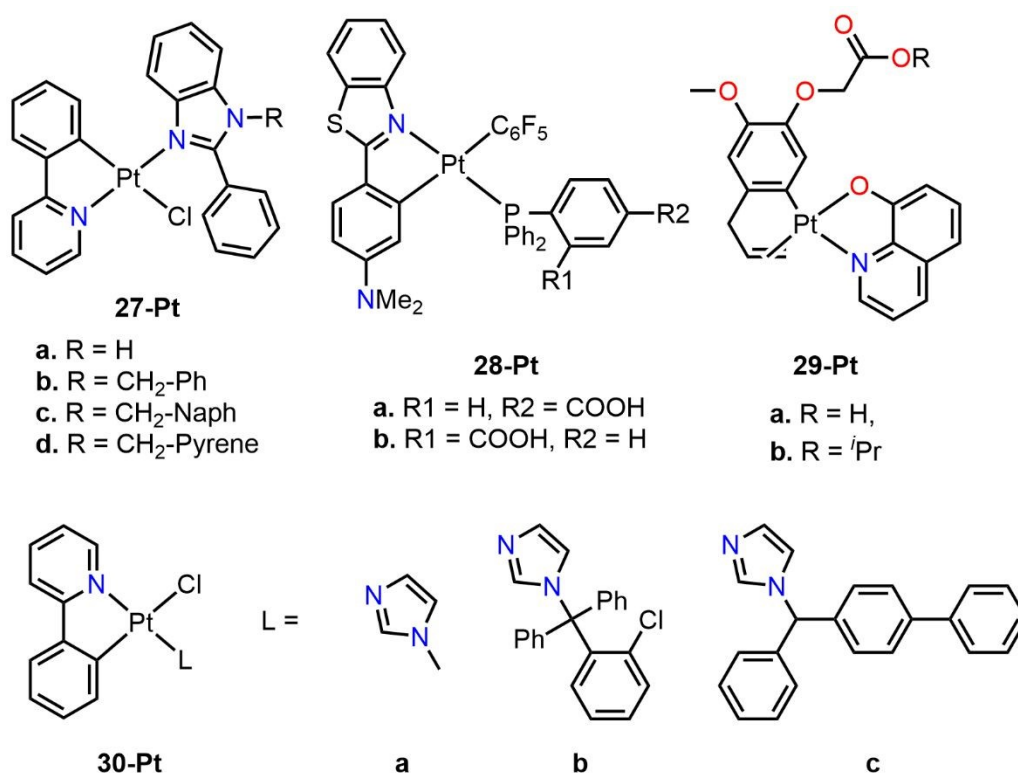


Figure 68. Cyclometalated Pt(II) complexes (**27-Pt** – **30-Pt**).

Larráyo and collaborators reported the cytotoxic activity of a series of C^N cyclometalated Pt(II) complexes based on benzothiazole (**28a,b-Pt**) (**Figure 68**, **Table 26**). Against healthy mammary epithelial cells (184B5), **28a,b-Pt** showed lower cytotoxic effects (SI = 2.80 and 0.60) compared to *cisplatin* (SI = 0.89 and 0.42).²⁴⁴ Additionally, cellular localization studies were performed using confocal fluorescence imaging in mouse lung embryonic fibroblasts (LMEF) and A549 cells with the



organic ligand (Me₂N-pbtH) and **28a-Pt**. Upon the addition of **28a-Pt**, an intracellular green fluorescence signal was observed, indicating the successful internalization of the complex. Furthermore, the complex was not localized in the nucleus, suggesting that it does not interact with DNA (**Figure69a**). Moreover, it was determined that **28a-Pt** does not localize in the mitochondria, as this organelle did not exhibit green fluorescence (**Figure69b**). However, **28a-Pt** was found to accumulate in the Golgi apparatus at a concentration of 10 μ M, indicating its preferential localization in this organelle (**Figure69c**).

Table 26. IC₅₀ of **28a,b-Pt** complexes against A549 and HeLa cancer cell lines^a

Compound	IC ₅₀ (μ M)		
	A549 (SI ^b)	HeLa (SI ^c)	184B5
28a-Pt	8.39 \pm 0.75 (2.80)	38.82 \pm 1.05 (0.60)	23.46 \pm 0.46
28b-Pt	11.59 \pm 1.40 (1.60)	16.51 \pm 0.57 (1.13)	18.60 \pm 1.63
<i>cisplatin</i>	6.45 \pm 0.47 (0.89)	13.60 \pm 0.99 (0.42)	5.73 \pm 0.45

^a Cell viability determined by MTT assay after treatment for 72 h

^b SI (Selectivity Index) = IC₅₀ (184B5)/IC₅₀ (A549)

^c SI (Selectivity Index) = IC₅₀ (184B5)/IC₅₀ (HeLa)

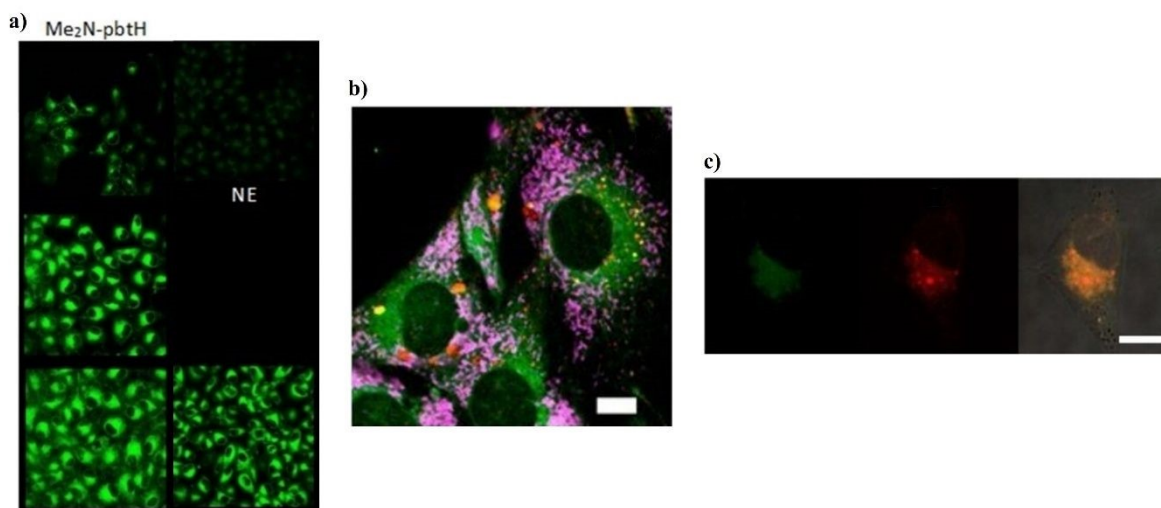


Figure 69. Cellular localization of **28a-Pt** using laser scanning confocal microscopy in **a**) LMEF cells, **b**) mitochondria, and **c**) Golgi apparatus in A549 cells. (Reproduce with permission from ref.

244 Copyright 2021, Wiley-VCH).

Chi *et al.* evaluated the cytotoxic activity of compounds **29a,b-Pt** against epidermal carcinoma (KB) and lung (Lu) cell lines. Both complexes displayed high cytotoxicity against the Lu and KB cell lines,

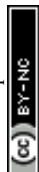


making them 6 and 4 times, respectively, more effective than *cisplatin* (Table 27). Both **29a-Pt** and **29b-Pt** exhibited enhanced cytotoxicity compared to their free ligands, with **29b-Pt** being approximately 9 times more potent against the KB cell line than the free ligand, indicating that complexation with Pt(II) significantly improves its cytotoxicity.²⁴⁵

Table 27. IC₅₀ of **29a,b-Pt** complexes against KB and Lu cell lines^a

Compound	IC ₅₀ (μM)	
	KB	Lu
29a-Pt	18.3 ± 0.6	7.1 ± 0.4
29b-Pt	4.1 ± 0.2	27.9 ± 1.1
<i>cisplatin</i>	15.2	42.9

Busto and coworkers reported a series of C^N metallacycles (**30a-c-Pt**) capable of covalently interacting with DNA and exhibiting different mechanisms of action. These complexes showed a low degree of dissociation in DMSO after 24 hours, with Cl⁻ being replaced by DMSO. Among them, **30b-Pt** was the least cytotoxic, while **30a-Pt** and **30c-Pt** demonstrated higher activity than *cisplatin* against all tested tumor cell lines. Complex **30a-Pt** exhibited the highest activity against the SW480 cell line, while **30bc-Pt** was equally cytotoxic against A549 and A2780 cells. Notably, photoactivation of these Pt(II) complexes via UV and blue light irradiation did not significantly affect their cytotoxicity. Complex **30a-Pt** showed the highest level of internalization in A549 cells, consistent with its high cytotoxicity. In contrast, **30c-Pt** exhibited lower cellular accumulation despite its effectiveness, and **30b-Pt** showed high uptake but was almost inactive. Despite its lower uptake and moderate interaction with DNA, compound **30c-Pt** maintained high cytotoxicity, suggesting additional mechanisms beyond Pt-DNA binding. All platinum complexes were capable of interacting with DNA via covalent bonds, causing similar conformational changes in the DNA double helix. However, only **30a-Pt** and **30c-Pt** induced cell cycle alterations, leading to significant accumulation of cells in the G0/G1 phase. Both complexes also induced changes in mitochondrial membrane potential and appeared to trigger apoptosis through the mitochondrial pathway, while **30b-Pt** may induce apoptosis via a different pathway. Additionally, only **30a-Pt** and **30c-Pt** increased ROS levels. Complex **30c-Pt**, despite its lower accumulation, exhibited a marked increase in ROS levels compared to **30a-Pt**. Notably, **30b-Pt** is the only complex that increases superoxide levels, suggesting that ROS generation is a crucial factor in its biological activity.²⁴⁶



Yang and collaborators reported a series of platinum complexes (**31a-c-Pt** and **32a-c-Pt**) (**Figure 70**), capable of inhibiting carbonic anhydrase IX (CAIX) and studied their cytotoxic activity. Compounds **31a-c-Pt** effectively inhibited CAIX activity, particularly **31b-Pt**, which showed excellent inhibitory activity with an IC_{50} value of 6.57 μ M. Complexes **31a-Pt** and **31c-Pt** were more lipophobic, particularly **31c-Pt**, and thus cannot be efficiently absorbed by cells and mainly accumulate in the cytoplasmic membrane. In contrast, **31b-Pt** was lipophilic and was able to penetrate cells through an energy-dependent mechanism, selectively localizing in the cytoplasm. Furthermore, the metformin derivatives (**32a-c-Pt**) were all lipophilic, which could be attributed to their modified molecular structure. Complexes **32a-Pt** and **32b-Pt** mainly accumulated in the endoplasmic reticulum, while **32c-Pt** accumulated in the mitochondria, indicating that the structure of the auxiliary ligand greatly influences organelle-targeted selectivity. Compound **32c-Pt** showed a much higher activity than the other complexes, with cytotoxicity up to 588 times superior to *cisplatin*. Complexes **32b-Pt** and **32c-Pt** significantly induced ROS levels and only **32c-Pt** caused a significant loss of mitochondrial membrane potential (MMP).^{247,248}

A tyrosinase-activated cyclometalated platinum complex (**33a-Pt**) and its metabolite (**33b-Pt**) were evaluated against melanoma in photodynamic therapy (PDT). Complex **33a-Pt** was highly specific for tyrosinase and reacted to generate the **33b-Pt** metabolite. A375 cells were treated with both **33a-Pt** and **33b-Pt**, followed by irradiation with white light. Both complexes exhibited high activity with IC_{50} values of approximately 0.4 μ M. However, **33b-Pt** showed higher phototoxicity, requiring only 30 minutes of irradiation to kill A375 cells, whereas the **33a-Pt** prodrug required 3 hours of irradiation to achieve a similar effect.²⁴⁹



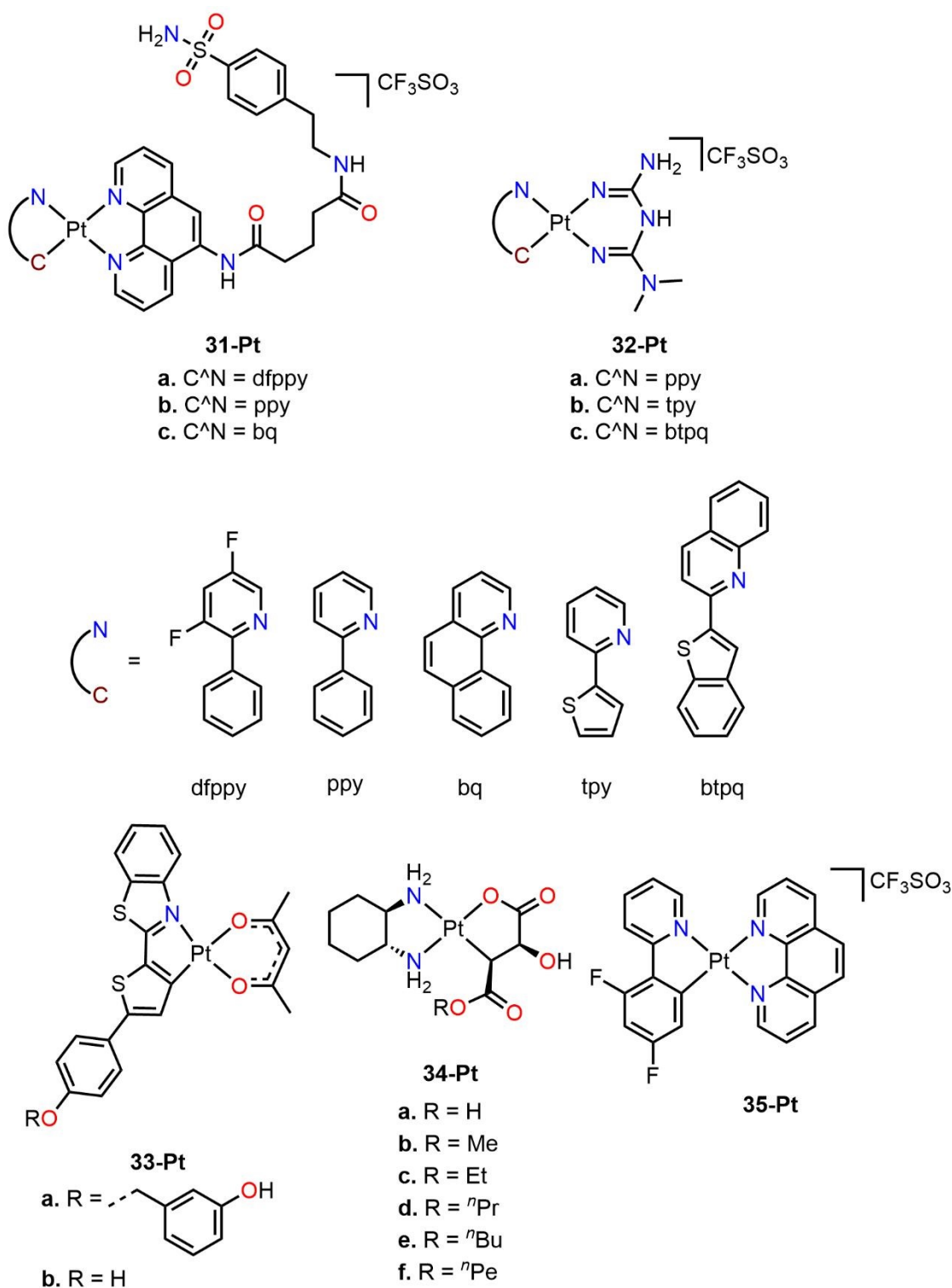


Figure 70. Cyclometalated Pt(II) complexes (**31-Pt** – **35-Pt**).

The Keppler group synthesized a series of five-membered C^O platinacycles (**34a-f-Pt**) (**Figure 70**), derived from oxaliplatin, bearing different alkyl substituents in the maleic acid structure to investigate



the impact of lipophilicity on the cytotoxic activity. All the complexes showed low activity. For example, the deprotonation of **34a-Pt** under physiological conditions could prevent its interaction with negatively charged DNA due to electrostatic repulsion. None of the complexes induced DNA crosslinking or strand breaks, indicating limited interaction with DNA.²⁵⁰

In a separate study, Shen and collaborators reported a cationic C^N cyclometalated complex (**35-Pt**). The uptake mechanism of **35-Pt** is mainly through endocytosis, and it showed greater selectivity towards HeLa cells compared to *cisplatin*. Furthermore, **35-Pt** rapidly penetrated cells, inducing significant alterations in mitochondrial membrane potential (MMP), and causing an increase in cell volume without significant morphological changes in the nucleus.²⁵¹

5.3.2. Pt(II) pincer complexes

Casini and collaborators reported the platinum analog of **16-Pd** (**36-Pt**) (**Figure 71**), which is highly cytotoxic but with poor selectivity, as its toxicity toward the normal HEK-293T cell line is higher than toward tumor cells (A2780 and A549). Furthermore, this toxicity toward normal cells is significantly higher ($IC_{50} = 2.64 \pm 0.87 \mu M$) compared to **16-Pd** and *cisplatin* (**Table 28**). The complex did not exhibit interactions with plasmid DNA or fluorescence quenching in the HAS spectra. Thus, the cytotoxic activity could be attributed to interactions with a molecular target different from DNA. The higher cytotoxicity exhibited by **36-Pt** compared to **16-Pd** could be due to the faster ligand substitution kinetics of the chloride, making the platinum complex more reactive than palladium.²⁰⁸

Table 28. IC_{50} of the **36-Pt** complex on A2780 and A549 cancer cell lines^a

Compound	IC_{50} (μM)		
	A2780	A549	HEK-293T
36-Pt	3.56 ± 0.70	4.60 ± 0.50	2.64 ± 0.87
<i>cisplatin</i>	3.90 ± 1.80	8.0 ± 0.5	11.0 ± 2.9

^a Cell viability determined by MTT assay after treatment for 72 h

The Che group reported a series of luminescent C^NN platinum pincer complexes and evaluated the cytotoxic activity and ability to form adducts with DNA and RNA of **37-Pt**. Upon adding **37-Pt**, the viscosity of a CT-DNA solution increased, indicating intercalation stabilized by π interactions with adenine-thymine (A-T) bases. Complex **37-Pt** increased the double-stranded DNA fragmentation similarly to camptothecin (CPT, used as control) and was able to form a ternary complex with



Topoisomerase I (TopoI) and DNA (TopoI-DNA-**37-Pt**). Additionally, **37-Pt** exhibited high cytotoxicity toward several cancer cell lines such as human oral squamous carcinoma (KB, $IC_{50} = 0.009 \mu\text{M}$), neuroblastoma (SH-5YSY, $IC_{50} = 0.010 \mu\text{M}$), non-small cell lung carcinoma (NCI-H460, $IC_{50} = 0.110 \mu\text{M}$), and nasopharyngeal carcinoma (SUNE1, $IC_{50} = 0.130 \mu\text{M}$). Notably, **37-Pt** accumulated in the nuclei of KB cancer cells. In an *in vivo* assay, **37-Pt** showed the ability to inhibit tumor growth by 60% in nude mice implanted with NCI-H460 cancer cells.²⁵²

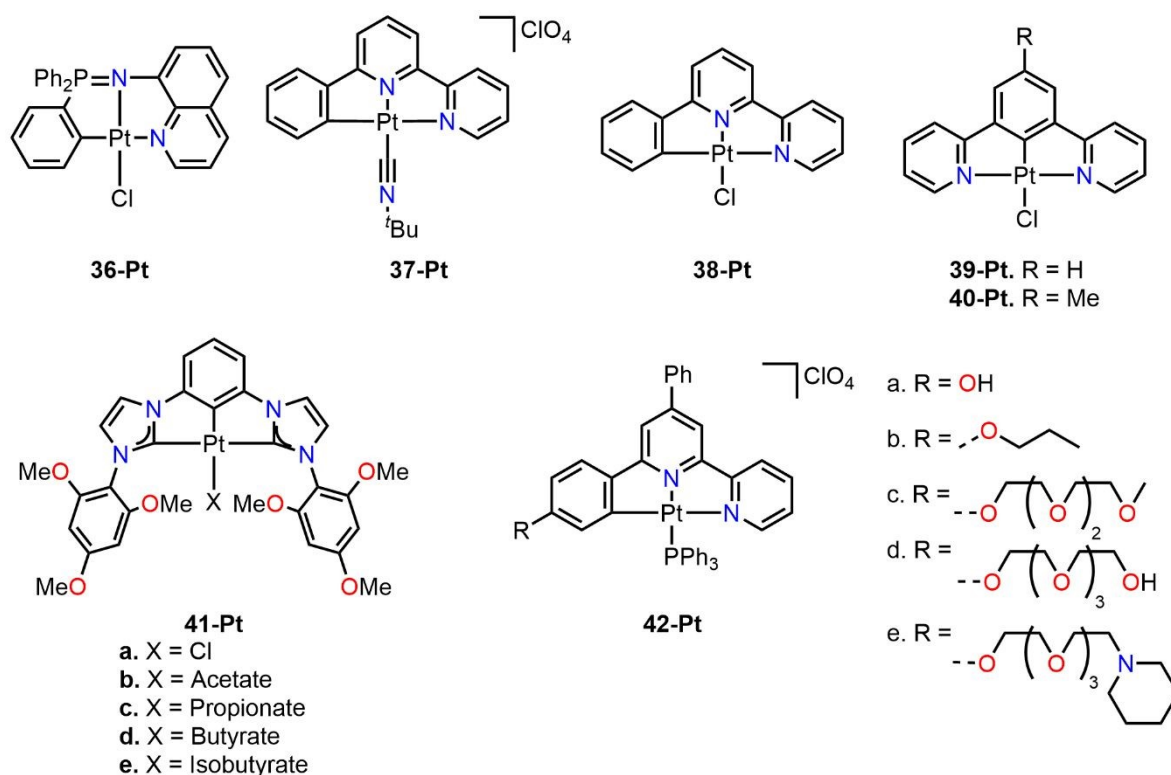


Figure 71. Cyclometalated pincer Pt(II) complexes (**36-Pt** – **42-Pt**).

Chen *et al.* evaluated the cytotoxicity of two isomeric C^NN and N^CN pincer complexes (**38-Pt** and **39-Pt**) (**Figure 71**) against three lung cancer cell lines (NCI-H522, NCI-H1299, and HCC827) and one prostate cancer cell line (RV-1). Compound **39-Pt** showed high cytotoxic activity in all tested cell lines, with efficacy several times greater than *cisplatin*. In contrast, **38-Pt** was practically non-cytotoxic against any cell line (**Table 29**). This disparity in cytotoxicity could be attributed to the stronger *trans* influence exerted by the carbon donor in **39-Pt** compared to the nitrogen donor in **38-Pt**. The consequent *trans* effect in **39-Pt** would make the chloride ligand more susceptible to dissociation.²⁵³



Table 29. IC₅₀ of **38-Pt** and **39-Pt** complexes on lung and prostate cancer cell lines^a

Compound	IC ₅₀ (μM)			
	NCI-H522	NCI-H1299	HCC827	RV-1
38-Pt	85.6 ± 4.3	-	-	> 240
39-Pt	21.5 ± 2.1	19.4 ± 2.2	22.4 ± 2.0	37.7 ± 3.2
cisplatin	49.8 ± 1.6	163.0 ± 4.1	> 666	> 333

^a Cell viability determined by MTT assay after treatment for 48 h

Bryant *et al.* evaluated the photosensitizing ability of a previously reported platinum N[^]C[^]N pincer complex (**40-Pt**) against a series of cancer cell lines, including a *cisplatin*-resistant bladder line (EJ-R).²⁵⁴ Complex **40-Pt** remained non-cytotoxic against HeLa cells at concentrations from 0.1 μM to 1 μM in the absence of light. In contrast, its cytotoxic effect increased significantly upon light exposure. HeLa cell survival was unaffected by the presence or absence of light, with no significant difference in survival fractions. However, cancer cell lines treated with 0.4 μM of **40-Pt** and exposed to 405 nm light showed a significant reduction in survival fractions compared to non-light-exposed cells. Complex **40-Pt** exhibited an LD₅₀ of 0.2 μM upon light irradiation and 1.6 μM in darkness against HeLa cells, with a phototoxicity index (PI) of 8, indicating relatively low photocytotoxicity.²⁵⁵

A series of Pt(II) C[^]C[^]C pincer complexes (**41a-e-Pt**) (**Figure 71**) were evaluated for their cytotoxic activity against various cancer cell lines by the Tabrizi group. All complexes were stable for up to 3 days under physiological conditions. The carboxylate-substituted complexes (**41a-e-Pt**) exhibited both high activity and selectivity toward cancer cell lines, with **41e-Pt** being the most active compound (IC₅₀ = 0.18 ± 0.03 μM against A549) with an SI of 234.7 (**Table 30**). This behavior can be attributed to increased lipophilicity due to the auxiliary ligand (Cl < acetate < propionate < butyrate < isobutyrate). Furthermore, the substitution of the chlorine ligand with carboxylate derivatives probably reduces aquation kinetics, leading to higher cytotoxicity and selectivity. All complexes tended to accumulate in the nucleus, and total cellular uptake decreased in the order **41e-Pt** > **41d-Pt** > **41c-Pt** > **41b-Pt** > **41a-Pt**, consistent with decreasing lipophilicity. Compounds **41b-e-Pt** induced more efficiently apoptosis in A549 cells compared to **41a-Pt** and *cisplatin*, with **41d-Pt** and **41e-Pt** expressing APO2.7 antigen at 81% and 86%, respectively.²⁵⁶



Table 30. IC₅₀ of **41a-e-Pt** complexes on SK-OV-3, MCF7, HT29, and A549 cancer cell lines^a

Compound	IC ₅₀ (μM)				
	SK-OV-3	MCF7	HT29	A549	LLC-PK1 ^b
41a-Pt	10.32 ± 0.09	6.92 ± 0.10	8.25 ± 0.10	1.55 ± 0.05	16.41 ± 0.20
41b-Pt	4.61 ± 0.20	3.89 ± 0.15	5.37 ± 0.20	1.04 ± 0.02	22.23 ± 0.20
41c-Pt	2.24 ± 0.32	2.41 ± 0.12	3.74 ± 0.17	0.98 ± 0.03	27.07 ± 0.10
41d-Pt	1.13 ± 0.12	0.97 ± 0.03	1.48 ± 0.15	0.51 ± 0.02	37.87 ± 0.10
41e-Pt	0.64 ± 0.05	0.33 ± 0.05	0.71 ± 0.04	0.18 ± 0.03	42.25 ± 0.20
<i>cisplatin</i>	5.20 ± 0.70	5.30 ± 0.87	6.30 ± 0.23	1.50 ± 0.10	6.95 ± 0.20

^a Cell viability determined by MTT assay after treatment for 48 h.^b Complexes 1-5 and cisplatin evaluated in non-tumor LLC-PK1 renal cells.

Guo and collaborators evaluated the cytotoxicity of a series of ionic platinum C^NN pincer complexes (**42a-e-Pt**). The complexes were slightly more cytotoxic than *cisplatin*. Notably, **42e-Pt** exhibited greater selectivity toward cancer cells than the other complexes, with an SI ranging from 2.3 to 3.8. Nevertheless, **42e-Pt** was unable to overcome drug resistance in the A549DDP resistant cell line. Despite this, it was able to inhibit tumor growth in *in vivo* studies without causing death. After treating A549 cells with **42e-Pt**, a significant accumulation of platinum was observed in the mitochondria, and **42e-Pt** was found to increase cell adhesion and effectively inhibit cell migration.²⁵⁷

The Tian group synthesized a C^NC-Pt(II) pincer complex (**43-Pt**) able to bind NF-κB and inhibit tumor growth (**Figure 72**). Complex **43-Pt** showed a distinct intracellular distribution pattern between normal and cancerous cells, likely due to interaction with the NF-κB protein. Immunofluorescence analysis demonstrated a strong co-localization of **43-Pt** with NF-κB in HepG2 cells. Additional experiments using the RAW264.7 inflammation cell line confirmed that **43-Pt** transport is NF-κB-dependent. Direct binding interactions between **43-Pt** and NF-κB were confirmed through protein electrophoresis and fluorescence emission spectra with purified NF-κB protein, supporting the hypothesis that cellular uptake is mediated by protein interactions. The complex's ability to penetrate 3D tumor spheroids and its reduced side effects suggest that **43-Pt** could offer a more effective and safer alternative to current platinum-based chemotherapeutic agents.²⁵⁸

Sarli and collaborators reported an N^CN-Pt(II) pincer complex (**44-Pt**) (**Figure 72**) *para*-substituted with c(RGDyK), known for its high affinity for integrin αvβ3 receptors and its ability to develop molecular imaging compounds for determining αvβ3 expression. Complex **44-Pt** mainly



exhibited cytostatic rather than cytotoxic activity against the PC-3 and A549 cell lines, with a notable activity against the metastatic MDA-MB-231 cell line. Furthermore, the complex reduced cell survival by 50% in rat bladder cancer AY27 cells after exposure to blue light. The cellular uptake of complex **44-Pt** occurred via receptor-mediated endocytosis, and singlet oxygen was effectively generated upon irradiation.²⁵⁹

A series of C^NN-Pt(II) pincer complexes (**45a,b-Pt** and **46a,b-Pt**) exhibited epidermal growth factor receptor (EGFR) inhibitory activity. All complexes demonstrated the ability to discriminate between G4-DNA and double-stranded DNA, with **45b-Pt** showing the highest binding affinities to CT-DNA and G4-DNA. Confocal fluorescence microscopy was used to investigate the DNA interaction properties of complexes **45a,b-Pt** in HeLa cells. Both complexes exhibited rapid internalization at an early stage, progressively penetrating the cells over time (**Figure 73a**). Additionally, **45a-Pt** was observed to accumulate in the cell membrane shortly after administration. As the incubation period increased, **45a-Pt** gradually localized in the nucleus. The deeper the complex penetrated the nucleus (**Figure 73b**), the stronger the fluorescence signal became, eventually overshadowing the dye's fluorescence. This suggests that **45a-Pt** could serve as a luminescent DNA probe for live-cell imaging (**Figure 73c**). In silico studies further revealed that **45a-Pt** has a strong affinity for DNA intercalation (**Figure 73d**) as well as minor groove binding interactions (**Figure 73e**).²⁶⁰

The Che group reported a series of cationic C^NN/N^CN pincer complexes coordinated with NHC (**47a-Pt** – **50-Pt**) and evaluated their cytotoxic activity against a panel of cancer cell lines. All complexes exhibited significant cytotoxic activity, with IC₅₀ values ranging from 0.03 to 1.49 μM. Notably, **47a-Pt** showed particularly high selectivity toward cancer cell lines compared to normal lung fibroblasts (CCD-19Lu, IC₅₀=4.74±0.28), with SI values of 30 in lung cancer NCI-H460 and 79 in ovarian cancer A2780. The change of the counterion from PF₆⁻ in **47a-Pt** to Cl⁻ in **47c-Pt** resulted in insignificant differences in cytotoxic activity. Lipophilicity played an important role in cytotoxic activity, as **47b-Pt**, with two methyl groups, was at least three-fold less potent than **47a-Pt**, which contains two butyl chains. Complex **50-Pt**, which features a benzimidazole group in the auxiliary ligand instead of an imidazole showed greater cytotoxicity and selectivity toward cancer cells, with SI values of 54.3 and 108.7 in ovarian cancer and *cisplatin*-resistant ovarian cancer cell lines, respectively.²⁶¹



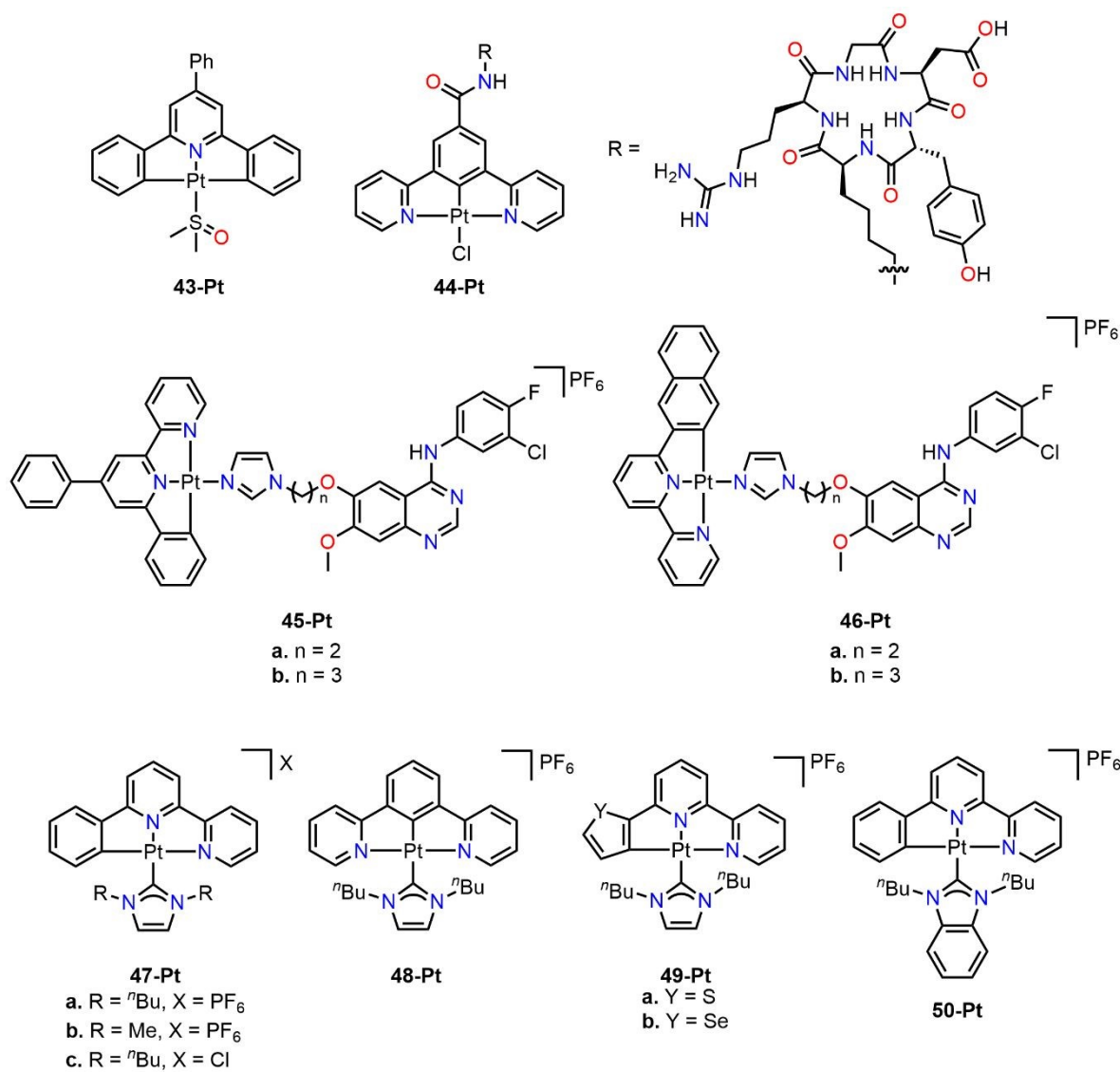


Figure 72. Cyclometalated Pt(II) pincer complexes (43-Pt – 50-Pt).

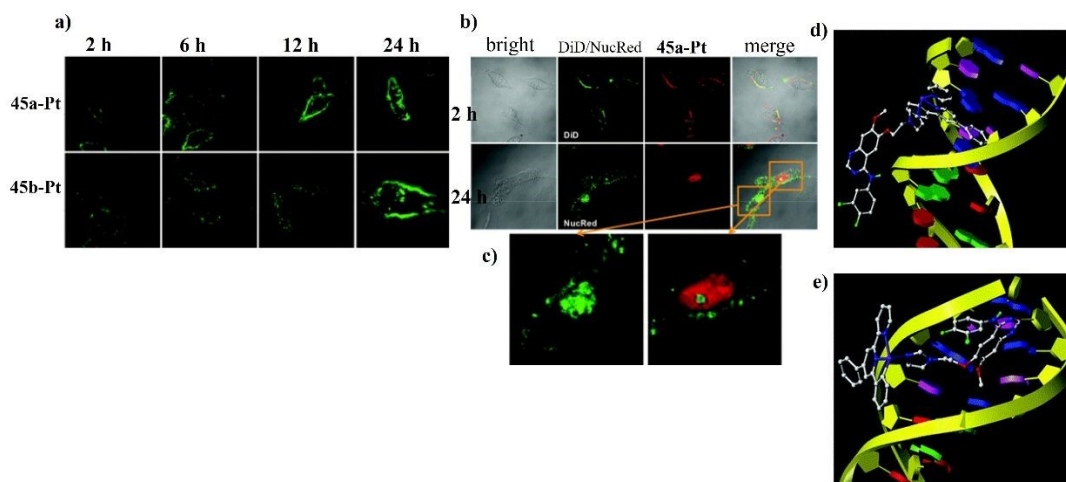


Figure 73. Cellular localization studies using confocal fluorescence microscopy of HeLa cells exposed to **a) 45a-Pt** and **45b-Pt**, and **b) 45a-Pt**. **c)** Magnified fluorescence images of HeLa cells treated with **45a-Pt** for 24 hours. **d)** Interaction of **45a-Pt** with DNA through intercalation. **e)** Interaction of **45a-Pt** with DNA via minor groove binding. (Reproduce with permission from ref. 260 Copyright 2017, Royal Society of Chemistry).

5.3.3. Platinum(IV) cyclometalated complexes

Crespo et al. have reported on a series of Pt(IV) complexes studied as potential anticancer agents (**Pt115-135**) (**Figure 74**). First, **51-Pt** and **52a,b-Pt** compounds were tested against the A549 cancer cell line. All three complexes showed moderate toxicity compared to *cisplatin*, with **52b-Pt** being the most active, showing little difference from its chloride analog **52a-Pt** (**Table 31**). This difference could be attributed to the higher lipophilicity imparted by the fluoro substituent or its ability to promote DNA binding. Noteworthy, these complexes present a seven-membered metallacycle, which exhibits lower stability than five- and six-membered metallacycles. This destabilization could be responsible for their higher cytotoxicity. Complex **51-Pt** was one of the first C^NN-Pt(IV) pincer complexes with asymmetric axial ligands evaluated as a cytotoxic agent and showed a moderate activity (**Table 31**) similar to that of *cisplatin*. Both Pt(II) and Pt(IV) complexes exhibited low or very low DNA binding, respectively. Since the complexes only altered the electrophoretic mobility of plasmid DNA at high concentrations compared to *cisplatin*, this suggests that DNA is unlikely the main molecular target of these complexes.²⁶²

Table 31. IC₅₀ of **51-Pt** and **52a,b-Pt** complexes on the A549 cell line^a

Compound	IC ₅₀ (μM)
	A549
51-Pt	11.6 ± 2.2
52a-Pt	2.8 ± 0.5
52b-Pt	2.5 ± 0.1
<i>cisplatin</i>	14.1 ± 1.3

^a Cell viability determined by MTT assay after treatment for 72 h

In a subsequent study, the cytotoxic activity of a series of C^NN-Pt(IV) pincer complexes with an axial aryl ligand (**53a-c-Pt**) was evaluated. Cyclic voltammetry studies revealed that all three complexes were reluctant to be reduced, with **53b-Pt** being the most susceptible to reduction. The cytotoxic activity of Pt(IV) compounds is related to the formation of biologically active Pt(II) species.



Given the significantly lower reduction potential of **53b-Pt**, the formation of Pt(II) species is highly unlikely. Complex **53c-Pt** emerged as the most lipophilic compound of the series and the most selective toward cancer cells (SI = 4.3 against A549). Complex **53c-Pt** induced G1 and G2 phase arrest, as well as early apoptosis in A549.²⁶³

Another series of C^NN-Pt(II) and C^NN-Pt(IV) pincer complexes and cyclometalated C^N-Pt(II) complexes (**54-Pt** – **57-Pt**) (**Figure 74**) were evaluated against a panel of human cancer cells. Among these complexes, **56a-Pt** exhibited the highest cytotoxicity, being several times more effective than *cisplatin* against all evaluated cancer cell lines. Notably, **55a-Pt** also demonstrated significant cytotoxic activity in all cell lines. Interestingly, complexes containing PPh₃ ligands were practically non-cytotoxic, and the Pt(IV) phosphine derivative was slightly more cytotoxic than the Pt(II) derivative, suggesting that the presence of a specific ligand does not necessarily enhance the cytotoxic profile of a compound.²⁶⁴

In a more recent study conducted by Crespo's group, a series of C^NN-Pt(II) and C^NN-Pt(IV) pincer complexes (**58a-d-Pt** and **59a-d-Pt**) derived from amine-imine ligands were synthesized and their cytotoxic activity was studied against various human cancer cell lines. All complexes, except **58c-Pt** and **58d-Pt**, displayed a cytotoxic activity comparable to oxaliplatin and superior to *cisplatin*. Some of the Pt(IV) complexes exhibited IC₅₀ values in the high nanomolar range. Specifically, **59a-Pt** was the most effective against PC-3 cells (IC₅₀ = 0.9 ± 0.2 μM) and **59c-Pt** showed the highest efficacy against SW620 (IC₅₀ = 0.41 ± 0.04 μM).²⁶⁵

Safari studied the cytotoxic activity of a five-member C^N-Pt(IV) complex (**60-Pt**) (**Figure 74**) in two colon cancer cell lines (Caco-2 and HT-29) and one breast cancer cell line (T47D). The results showed that the **60-Pt** complex was only cytotoxic against HT-29 and is not cytotoxic on normal NIH-3T3 cells (IC₅₀ = 357 ± 11.9 μM, **Table 32**).²⁶⁶

Table 32. IC₅₀ of **60-Pt** complex on NIH-3T3, HT29, and T47D cancer cell lines^a

Compound	IC ₅₀ (μM)			
	NIH-3T3	Caco ₂ ^b	HT29	T47D
60-Pt	357.4 ± 11.9	96.9 ± 3.5	19.9 ± 1.8	171.7 ± 0.4
<i>cisplatin</i>	19.5 ± 0.08	13.5 ± 0.05	34.23 ± 3.7	35.8 ± 0.21

^a Cell viability determined by MTT assay after treatment for 96 h and ^b 120 h for Caco₂



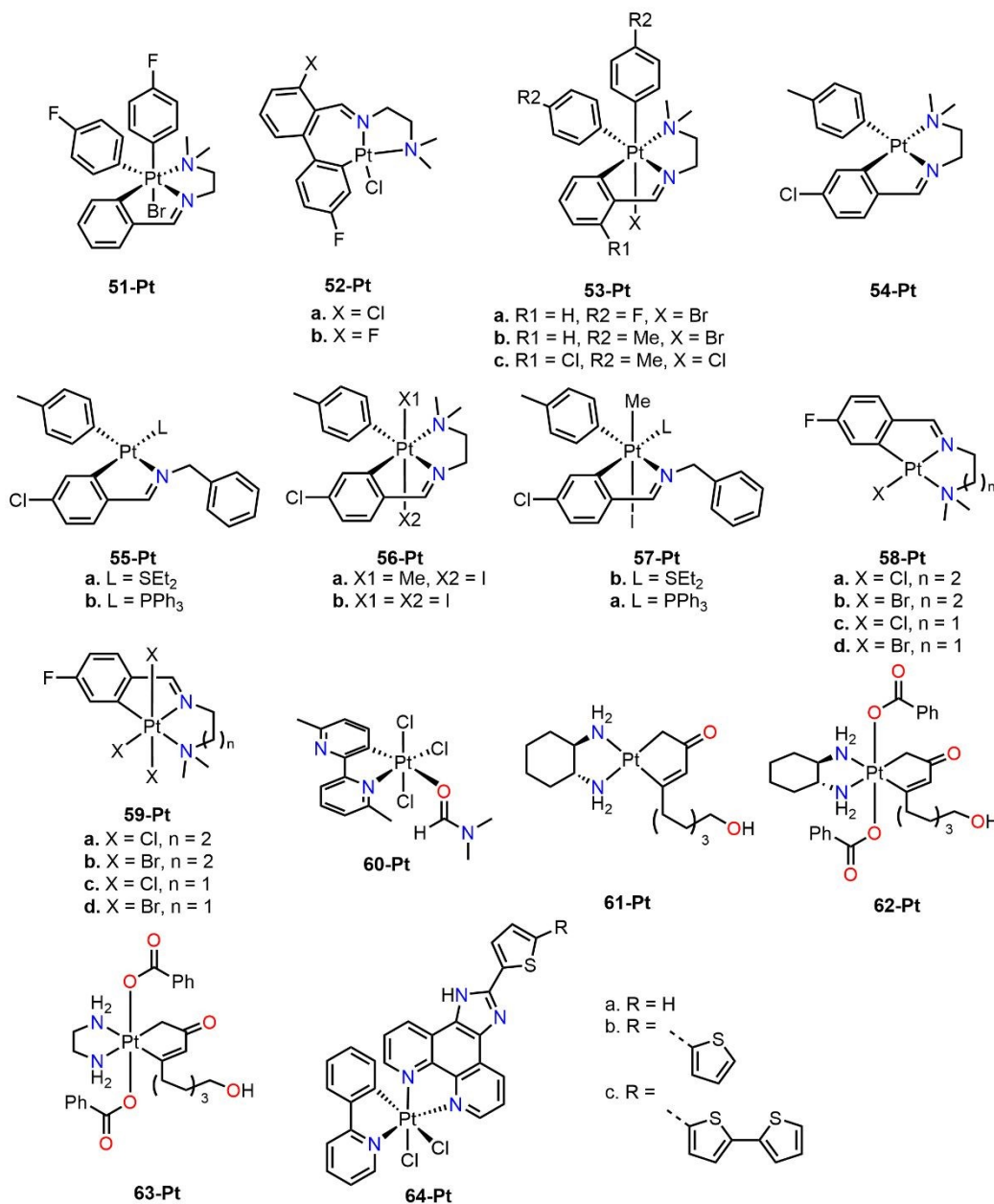


Figure 74. Cyclometalated Pt(IV) complexes (**51-Pt** – **64-Pt**).

Margiotta *et al.* evaluated the cytotoxic activity of cyclometalated Pt(II) and Pt(IV) complexes (**61-Pt** – **63-Pt**). Complex **61-Pt** showed significant efficacy against the PSN-1 pancreatic cancer cell line, surpassing the potency of *cisplatin* and oxaliplatin. In contrast, Pt(IV) benzoate derivatives **62-Pt** and **63-Pt** exhibited moderate cytotoxicity. However, **62-Pt** was twice as active as *cisplatin* against PSN-1 and comparable to oxaliplatin. This increased activity aligns with the established characteristics of Pt(IV) complexes containing benzoate groups, known for their ideal reduction potential and higher lipophilicity, facilitating cell entry through passive diffusion.²⁶⁷ Additionally, **62-**



Pt with a chiral chelating diamine ligand showed greater potency than its ethylenediamine analogue **63-Pt**.²⁶⁸

Cao and collaborators reported a series of cyclometalated Pt(IV) complexes derived from terthiophene (**64a-c-Pt**) (**Figure 74**) capable of disrupting zinc homeostasis. Among these, **64c-Pt** was found to be the most cytotoxic, significantly surpassing *cisplatin* (**Table 33**). Despite its potent cytotoxicity, **64a-Pt** complex phototoxicity was low, reducing its potential for PDT. Complex **64c-Pt** primarily accumulated in the nucleus and, to a lesser extent, in the mitochondria. Its nuclear localization contributes to its ability to induce DNA damage, as evidenced by the increased expression of γ H2AX. Furthermore, the complex suppressed cellular respiration at low concentrations (0.1–0.2 μ M), altering cellular respiration and energy metabolism, as indicated by the increase in oxygen consumption rate (OCR), ATP production, and mitochondrial membrane potential (MMP).²⁶⁹ Based on these studies, a plausible mechanism was proposed for **64c-Pt**, suggesting that it disrupts zinc homeostasis while inducing DNA damage. This effect is attributed to abnormal transcriptional levels of zinc-regulating proteins such as ZIP and ZnT (zinc transporters) and metallothioneins (MT), leading to excessive accumulation of Zn^{2+} ions in the cytoplasm. Consequently, intracellular redox homeostasis is disrupted due to the downregulation of ROS scavengers (MT and SOD1), glutathione (GSH) depletion, and the inactivation of glutathione peroxidase 4 (GPX4). The simultaneous disruption of zinc and redox homeostasis results in inflammatory cell death pyroptosis rather than GPX4-mediated ferroptosis in cancer cells. This ultimately triggers an immune response, enhancing dendritic cell (DC) maturation and increasing T-cell infiltration within the tumor, thereby eliminating not only the primary tumor but also distant tumors in vivo (**Figure 75**).

Table 33. IC_{50} of **64a-c-Pt** complexes on MDA-MB-231 and MCF-7 cancer cell lines^a

Compound	IC_{50} (μ M)		
	MDA-MB-231	MCF-7	MCF-10A (SI ^b)
64a-Pt	6.5 ± 0.4	5.9 ± 0.3	38.4 ± 1.3 (6.5)
64b-Pt	0.17 ± 0.02	0.34 ± 0.01	0.48 ± 0.06 (1.4)
64c-Pt	0.11 ± 0.05	0.43 ± 0.07	0.49 ± 0.04 (1.1)
<i>cisplatin</i>	43.2 ± 2.5	40.7 ± 1.3	27.2 ± 1.7 (0.67)

^a Cell viability determined by MTT assay after treatment for 48 h

^b SI (Selectivity Index) = IC_{50} (MCF-10A)/ IC_{50} (MCF-7)



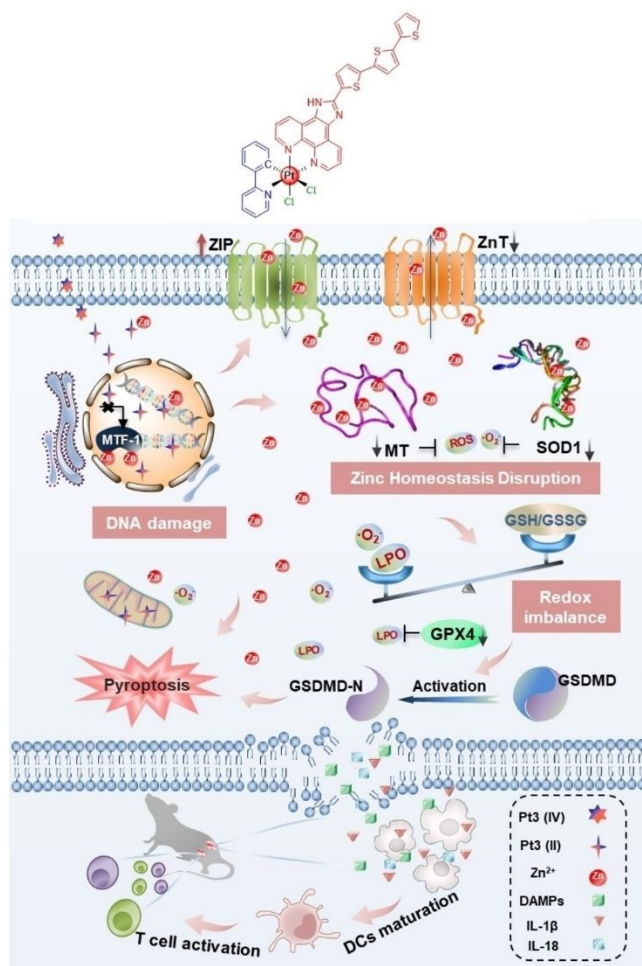


Figure 75. Proposed mechanism of action of complex **64c-Pt** in activating antitumor immunity through simultaneous disruption of zinc and redox homeostasis. (Reproduce with permission from ref. 269 Copyright 2023, Wiley-VCH).

Conclusions and future perspectives

This review summarizes recent advances in the cytotoxic effects of cyclometalated compounds as potential anticancer agents. Despite that such organometallic species are often viewed as air-sensitive, unstable under physiological conditions, and unsuitable for medicinal purposes, they can display superior activity compared to coordination compounds. Based on this review, it can clearly be stated that they possess greater stability, better lipophilicity, and are susceptible to derivatization reactions. This makes these compounds potentially valuable as future anticancer agents.

Undoubtedly, the advances made in recent years in the fight against cancer have been significant. Although a definitive cure for this disease has not yet been found, research has opened new avenues for identifying the most promising treatment alternatives. Certainly, the use of metallodrugs has



emerged as one of the most innovative approaches, as the combination of metal centers and organic ligands creates a synergistic effect that leads to unique properties in these compounds.

The development of metallodrugs still faces numerous challenges and limitations before they can be commercialized and used in humans. One of the main challenges remains the selectivity of these compounds. Although a few platinum-based drugs have been approved for cancer treatment, their lack of selectivity and associated toxicity still play a crucial role in limiting their application. Additionally, ligand synthesis often presents a significant challenge due to the large number of synthetic steps required before coordination to a specific metal center. The use of second- and third-row transition metals is also currently limited due to high costs, low availability in the Earth's crust, and, in some cases, significant toxicity, which necessitates the search for alternative options. Furthermore, *in vivo* testing presents another major limitation, as the use of animal models in these studies remains a subject of global debate.

However, significant progress has been made in improving the anticancer activity of these compounds. For instance, the use of first-row transition metals has increased biocompatibility in biochemical processes, leading to reduced side effects.²⁷⁰⁻²⁷² Drug delivery and transport mechanisms have also improved, with research focusing on micellar and dendrimeric systems that enhance the bioavailability and selectivity of metallodrugs.²⁷³⁻²⁷⁵ Moreover, *in vitro* assays using solid tumor models have emerged as an innovative alternative to *in vivo* studies. Cancer cell-derived spheroids can mimic the physiological environment of a tumor, making them a compelling strategy to reduce reliance on animal testing.^{276,277} Additionally, the incorporation of natural products as ligands has facilitated the development of novel metallodrugs. These natural structures enhance cytotoxic activity, promote reactive oxygen species (ROS) formation to combat cancer cells, and exhibit antioxidant properties that help prevent malignant tumor formation.^{278,279}

Cancer treatments vary depending on the type and stage of the disease. Among these, chemotherapy remains the most used approach. However, this treatment has several limitations, including non-selective drug distribution via the bloodstream, which affects both healthy and malignant cells, leading to significant side effects. More recent and less harmful therapeutic strategies have been developed, such as photodynamic therapy (PDT), which stands out for its localized drug administration, selectively targeting cancer cells. Various coordination and organometallic complexes have demonstrated promising photosensitizing properties for use in PDT.^{280,281} Additionally, theranostic therapy enables the use of drugs that function as biomarkers to determine drug localization, a field where metallodrugs have gained significant importance due to the ability to combine the photophysical and photochemical properties of metal centers and ligands.²⁸²⁻²⁸⁴ In this



same context, the development of metallodrugs with cytostatic properties as angiogenesis inhibitors offers the potential to halt cancer cell growth, allowing tumors to be subsequently removed through surgery.²⁸⁵⁻²⁸⁸

Furthermore, thanks to current synthetic strategies, the diversity of organometallic structures that can be achieved is almost limitless, further increasing the potential to improve the anticancer activities of these compounds. Moreover, the support from other disciplines such as biology, biochemistry, and computational chemistry has led to a better understanding of the mechanisms of action of these compounds, their potential cellular targets, and how they interact with them. This progress has allowed *in vivo* studies to become more detailed, serving as one of the first steps before entering clinical phases and, potentially, reaching commercialization and clinical applications.

Therefore, it is expected that future research focusing on the anticancer properties of cyclometalated compounds will attract greater attention, enabling more of these compounds to reach clinical phases and spark the interest of pharmaceutical industries that could support future research focused on organometallic metallodrugs.

Author Contributions: Writing-original draft preparation, A.A-F., J.R-G., E.S-Y., A.R-M., J.S.S-G., A.R-P., P.C-S., V.R-M., R.L.L and D.M-M.; execution drawing, A.A-F., J.R-G., E.S-Y., A.R-M., J.S.S-G., A.R-P., P.C-S., V.R-M., R.L.L and D.M-M.; writing-review and editing A.A-F., J.R-G., E.S-Y., A.R-M., J.S.S-G., A.R-P., P.C-S., V.R-M., R.L.L and D.M-M.; visualization and supervision, A. A-F., J.S.S-G., R.L.L and D.M-M. All authors have read and agreed to the published version of the manuscript.

Acknowledgment: A.A-F., J.R-G., E.S-Y., J.S.S-G. are grateful for the Doctoral Fellowships with CVU 1032866, 1099989, 997936, and 997800 respectively. D.M-M. would like to thank UNAM-DGAPA-PAPIIT IN223323 and CONAHCYT A1-S-033933 for their generous financial support.

Conflicts of interest: The authors declare no conflicts of interest.

References

- 1 J. S. Thayer, *J Chem Educ*, 1969, **46**, 442–443, DOI: 10.1021/ed046p442.
- 2 J. S. Serrano-García, A. Amaya-Flórez, J. R.-Galindo, L. González-Sebastián, L. H. Delgado-Rangel and D. Morales-Morales, *Inorganics*, 2024, **12**, 221, DOI: 10.3390/inorganics12080221.
- 3 J. A. Cruz-Navarro, A. Sánchez-Mora, J. S. Serrano-García, A. Amaya-Flórez, R. Colorado-Peralta, V. Reyes-Márquez and D. Morales-Morales, *Catalysts*, 2024, **14**, 69, DOI: 10.3390/catal14010069.



- 4 L. E. López-Robledo, E. E. Ortiz-Fuentes, E. Rufino-Felipe, J. S. Serrano-García, A. Arenaza-Corona, S. Hernandez-Ortega, H. Valdés, L. Gonzalez-Sebastian, V. Reyes-Márquez and D. Morales-Morales, *New J. Chem*, 2025, **49**, 3426–3435, DOI: 10.1039/D4NJ03776F.
- 5 T. Yang, A. Zhou, Y. He, Z. Yao, X. Song, X. Tao and Y. Tao, *Mater Adv*, 2023, **4**, 631–640, DOI: 10.1039/D2MA00999D.
- 6 M. K. Salomón-Flores, I. J. Bazany-Rodríguez, D. Martínez-Otero, M. A. García-Eleno, J. J. Guerra-García, D. Morales-Morales and A. Dorazco-González, *Dalton Trans*, 2017, **46**, 4950–4959, DOI: 10.1039/C6DT04897H.
- 7 H. Leopold, A. Tronnier, G. Wagenblast, I. Münster and T. Strassner, *Organometallics*, 2016, **35**, 959–971, DOI: 10.1021/acs.organomet.5b00991.
- 8 A. Y. Gitlina, A. Surkova, M. V. Ivonina, V. V. Sizov, S. K. Petrovskii, A. Legin, G. L. Starova, I. O. Koshevoy, E. V. Grachova and D. O. Kirsanov, *Dyes and Pigments*, 2020, **180**, 108428, DOI: 10.1016/j.dyepig.2020.108428.
- 9 H. Leopold, M. Tenne, A. Tronnier, S. Metz, I. Münster, G. Wagenblast and T. Strassner, *Angew. Chem., Int. Ed. Engl*, 2016, **55**, 15779–15782. DOI: 10.1002/anie.201607075.
- 10 T. Funaki, H. Kusama, N. Onozawa-Komatsuzaki, K. Kasuga, K. Sayama and H. Sugihara, *Eur. J. Inorg. Chem.*, 2014, 1303–1311, DOI: 10.1002/ejic.201301459.
- 11 M. Mbaba, T. M. Golding and G. S. Smith, *Molecules*, 2020, **25**, 5276, DOI: 10.3390/molecules25225276.
- 12 M. A. Sierra, L. Casarrubios and M. C. de la Torre, *Chem. Eur. J.*, 2019, **25**, 7232–7242, DOI: 10.1002/chem.201805985.
- 13 Y. C. Ong and G. Gasser, *Drug Discov. Today Technol*, 2020, **37**, 117–124, DOI: 10.1016/j.ddtec.2019.06.001.
- 14 B. S. Ludwig, J. D. G. Correia and F. E. Kühn, *Coord. Chem. Rev.*, 2019, **396**, 22–48, DOI: 10.1016/j.ccr.2019.06.004.
- 15 C. Mu, K. E. Prosser, S. Harrypersad, G. A. Macneil, R. Panchmatia, J. R. Thompson, S. Sinha, J. J. Warren and C. J. Walsby, *Inorg Chem*, 2018, **57**, 15247–15261, DOI: 10.1021/acs.inorgchem.8b02542.
- 16 J. P. Bugarinović, M. S. Pešić, A. Minić, J. Katanić, D. Ilić-Komatina, A. Pejović, V. Mihailović, D. Stevanović, B. Nastasijević and I. Damljanović, *J. Inorg. Biochem.*, 2018, **189**, 134–142, DOI: 10.1016/j.jinorgbio.2018.09.015.
- 17 L. Tabrizi, T. L. A. Nguyen, H. D. T. Tran, M. Q. Pham and D. Q. Dao, *J. Chem. Inf. Model.*, 2020, **60**, 6185–6203, DOI: 10.1021/acs.jcim.0c00730.
- 18 V. Kovač, T. Lukačević, D. Jadreško, J. Mrvčić, D. Stanzer, K. Hanousek-Čiča, T. Murati, M. Miletić and I. Kmetić, *Appl. Organomet. Chem.*, 2025, **39**, e7753, DOI: 10.1002/aoc.7753.
- 19 V. Tomar, P. Kumar, D. Sharma, R. K. Joshi and M. Nemiwal, *J. Mol. Struct.*, 2025, **1319**, 139589, DOI: 10.1016/j.molstruc.2024.139589.



- 20 A. Chaudhary and K. Poonia, *Inorg. Chem. Commun.*, 2021, **134**, 109044, DOI: 10.1016/j.inoche.2021.109044.
- 21 K. M. Deo, D. L. Ang, B. McGhie, A. Rajamanickam, A. Dhiman, A. Khoury, J. Holland, A. Bjelosevic, B. Pages, C. Gordon and J. R. Aldrich-Wright, *Coord. Chem. Rev.*, 2018, **375**, 148-163 DOI: 10.1016/j.ccr.2017.11.014.
- 22 Z. Xu, Z. Wang, Z. Deng and G. Zhu, *Coord. Chem. Rev.*, 2021, **442**, 213991, DOI: 10.1016/j.ccr.2021.213991.
- 23 A. Bergamo and G. Sava, *Chem. Soc. Rev.*, 2015, **44**, 8818-8835, DOI: 10.1039/C5CS00134J.
- 24 R. C. Todd and S. J. Lippard, *Metallomics*, 2009, **1**, 280-291, DOI: 10.1039/B907567D.
- 25 F. Trudu, F. Amato, P. Vaňhara, T. Pivetta, E. M. Peña-Méndez and J. Havel, *J. Appl. Biomed.*, 2015, **13**, 79-103, DOI: 10.1016/j.jab.2015.03.003.
- 26 K. Peng, Y. Zheng, W. Xia and Z. W. Mao, *Chem. Soc. Rev.*, 2023, **52**, 2790-2832, DOI: 10.1039/D2CS00757F.
- 27 E. J. Anthony, E. M. Bolitho, H. E. Bridgewater, O. W. L. Carter, J. M. Donnelly, C. Imberti, E. C. Lant, F. Lermite, R. J. Needham, M. Palau, P. J. Sadler, H. Shi, F. X. Wang, W. Y. Zhang and Z. Zhang, *Chem. Sci.*, 2020, **11**, 12888-12917, DOI: 10.1039/D0SC04082G.
- 28 S. Komeda and A. Casini, *Curr. Top. Med. Chem.*, 2012, **12**, 219-235, DOI: 10.2174/156802612799078964.
- 29 G. Gasser, I. Ott and N. Metzler-Nolte, *J. Med. Chem.*, 2011, **54**, 3-25, DOI: 10.1021/jm100020w.
- 30 S. Swaminathan, J. Haribabu, N. Balakrishnan, P. Vasanthakumar, R. Karvembu, *Coord. Chem. Rev.*, 2022, **459**, 214403, DOI: 10.1016/j.ccr.2021.214403.
- 31 L. Zeng, P. Gupta, Y. Chen, E. Wang, L. Ji, H. Chao, Z. S. Chen, *Chem. Soc. Rev.*, 2017, **46**, 5771-5804, DOI: 10.1039/C7CS00195A.
- 32 P. Chellan, P. J. Sadler, *Chem. Eur. J.*, 2020, **26**, 8676-8688. DOI: 10.1002/chem.201904699.
- 33 W. Liu, R. Gust, *Coord. Chem. Rev.*, 2016, **329**, 191-213, DOI: 10.1016/j.ccr.2016.09.004.
- 34 I. Chakraborty, S. J. Carrington, G. Roseman, P. K. Mascharak, *Inorg. Chem.*, 2017, **56**, 1534-1545, DOI: 10.1021/acs.inorgchem.6b02623.
- 35 S. Bhowmick, A. Jana, K. Singh, P. Gupta, A. Gangrade, B. B. Mandal, N. Das, *Inorg. Chem.*, 2018, **57**, 3615-3625, DOI: 10.1021/acs.inorgchem.5b01156.
- 36 A. Haque, R. A. Al-Balushi, M. S. Khan, *J. Organomet. Chem.*, 2019, **897**, 95-106, DOI: 10.1016/j.jorganchem.2019.06.026.



- 37 S. Hostachy, C. Policar, N. Delsuc, *Coord. Chem. Rev.*, 2017, **351**, 172–188, DOI: 10.1016/j.ccr.2017.05.004.
- 38 U. Schatzschneider, *Bri. J. Pharmacol.*, 2014, **172**, 1638–1650, DOI: 10.1111/bph.12688.
- 39 J. Jimenez, I. Chakraborty, A. Dominguez, J. Martinez-Gonzalez, W. M. C. Sameera, P. K. Mascharak, *Inorg. Chem* 2018, **57**, 1766–1773, DOI: 10.1021/acs.inorgchem.7b02480.
- 40 M. Porchia, M. Pelli, M. Marinelli, F. Tisato, F. Del Bello, C. Santini, *Eur. J. Med. Chem.*, 2018, **146**, 709–746, DOI: 10.1016/j.ejmech.2018.01.065.
- 41 T. Nabyeva, C. Marschner, B. Blom, *Eur. J. Med. Chem.*, 2020, **201**, 112483, DOI: 10.1016/j.ejmech.2020.112483.
- 42 A. Chakraborty, K. Singh, P. Vaswani, A. Gangrade, D. Bhatia, N. Das, *Appl. Organomet. Chem.*, 2023, **37**, e7172, DOI: 10.1002/aoc.7172.
- 43 A. P. Carnizello, M. I. F. Barbosa, M. Martins, N. H. Ferreira, P. F. Oliveira, G. M. Magalhães, A. A. Batista, D. C. Tavares, *J. Inorg. Biochem.*, 2016, **164**, 42–48, DOI: 10.1016/j.jinorgbio.2016.08.010.
- 44 T. Zou, C. N. Lok, P. K. Wan, Z. F. Zhang, S. K. Fung, C. M. Che, *Curr. Opin. Chem. Biol.* 2018, **43**, 30–36, DOI: 10.1016/j.cbpa.2017.10.014.
- 45 P. Zhang, P. J. Sadler, *J. Organomet. Chem.*, 2017, **839**, 5–14, DOI: 10.1016/j.jorganchem.2017.03.038.
- 46 V. Chandrasekhar, T. Hajra, J. K. Bera, S. M. W. Rahaman, N. Satumtira, O. Elbjeirami, M. A. Omary, *Inorg. Chem.*, 2012, **51**, 1319–1329, DOI: 10.1021/ic2012952.
- 47 H. Qian, Z. Yin, T. Zhang, S. Yan, Q. Wang, C. Zhang, *Organometallics* 2014, **33**, 6241–6246, DOI: 10.1021/om5008924.
- 48 I. Omae, *Coord. Chem. Rev.*, 2014, **280**, 84–95, DOI: 10.1016/j.ccr.2014.07.019.
- 49 P. Zhang, H. Huang, *Dalton Trans.*, 2018, **47**, 14841–14854, DOI: 10.1039/C8DT03432J.
- 50 Z. Deng, P. Gao, L. Yu, B. Ma, Y. You, L. Chan, C. Mei, T. Chen, *Biomaterials*, 2017, **129**, 111–12, DOI: 10.1016/j.biomaterials.2017.03.017.



- 51 A. Valente, A. M. Santos, L. Côrte-Real, M. P. Robalo, V. Moreno, M. Font-Bardia, T. Calvet, J. Lorenzo, M. H. Garcia, *J. Organomet. Chem.*, 2014, **756**, 52–60, DOI: 10.1016/j.jorganchem.2014.01.027.
- 52 M. Sohrabi, M. Bikhof Torbati, M. Lutz, S. Meghdadi, H. Farrokhpour, A. Amiri, M. Amirnasr, *J. Photochem. Photobiol. A. Chem.*, 2022, **423**, 113573, DOI: 10.1016/j.jphotochem.2021.113573.
- 53 B. F. Hohlfeld, B. Gitter, C. J. Kingsbury, K. J. Flanagan, D. Steen, G. D. Wieland, N. Kulak, M. O. Senge, A. Wiehe, *Chem. Eur. J.*, 2021, **27**, 6440–6459, DOI: 10.1002/chem.202004776.
- 54 P. Szymaszek, M. Tyszka-Czochara, J. Ortyl, *Eur. J. Med. Chem.*, 2024, **276**, 116648, DOI: 10.1016/j.ejmech.2024.116648.
- 55 E. Z. Jahromi, A. Divsalar, A. A. Saboury, S. Khaleghizadeh, H. Mansouri-Torshizi, I. Kostova, *J. Iran. Chem. Soc.*, 2016, **13**, 967–989, DOI: 10.1007/s13738-015-0804-8.
- 56 B. Ay, O. Şahin, B. Saygideğer Demir, Y. Saygideger, J. M. López-De-Luzuriaga, G. Mahmoudi, D. A. Safin, *New J. Chem.*, 2020, **44**, 9064–9072, DOI: 10.1039/D0NJ00921K.
- 57 T. C. Johnstone, K. Suntharalingam, S. J. Lippard, *Chem. Rev.*, 2016, **116**, 3436–3486, DOI: 10.1021/acs.chemrev.5b00597.
- 58 C. Imberti, P. Zhang, H. Huang, P. J. Sadler, *Angew. Chem.*, 2020, **132**, 61–73, DOI: 10.1002/ange.201905171.
- 59 M. Albrecht, *Chem. Rev.*, 2010, **110**, 576–623, DOI: 10.1021/cr900279a.
- 60 B. Bertrand and A. Casini, *Dalton Trans.*, 2014, **43**, 4209–4219, DOI: 10.1039/C3DT52524D.
- 61 G. C. Dickmu and I. P. Smoliakova, *Coord. Chem. Rev.*, 2020, **409**, 213203, DOI: 10.1016/j.ccr.2020.213203.
- 62 B. T. Paul, D. H. Manz, F. M. Torti and S. V. Torti. *Expert Rev. Hematol.* 2017, **10**, 65–79, DOI: 10.1080/17474086.2016.1268047.
- 63 W. Szlasa, Mr. Gachowska, K. Kiszka, K. Rakoczy, A. Kielbik., K. Wala, J. Puchala, K. Chorążykiewicz, J. Saczko and J. Kulbacka. *Chem. Pap.* 2022, **76**, 1285–1294, DOI: 10.1007/s11696-021-02001-2.
- 64 Y. Liu, S. Lu, L. Wu, L. Yang, L. Yang and J. Wang. *Cell Death Dis.* 2023, **14**, 519, DOI: 10.1038/s41419-023-06045-y
- 65 A. S. Estrada-Montaña, A. D. Ryabov, A. Gries, C. Gaidon and R. Le Lagadec, *Eur. J. Inorg. Chem.*, 2017, **2017**, 1673–1678, DOI: 10.1002/ejic.201601350.



- 66 A. S. Estrada-Montaña, A. Gries, J. A. Oviedo-Fortino, C. Torres-Gutierrez, A. Grain-Hayton, R. Marcial-Hernández, L. Shen, A. D. Ryabov, C. Gaiddon and R. Le Lagadec, *Organometallics*, 2020, **39**, 1842–1854, DOI: 10.1021/acs.organomet.0c00107.
- 67 L. Tabrizi, *Appl. Organomet. Chem.*, 2018, **32**, e4161, DOI: 10.1002/aoc.4161.
- 68 K. Lin, Z.-Z. Zhao, H.-B. Bo, X.-J. Hao and J.-Q. Wang, *Front. Pharmacol.* 2018, **9**, 1323. DOI: 10.3389/fphar.2018.01323
- 69 J. Liu, H. Lai, Z. Xiong, B. Chen and T. Chen, *Chem. Commun.* 2019, **55**, 9904, DOI: 10.1039/C9CC04098F.
- 70 M. Bashir, I. A. Mantoo, F. Arjmand, S. Tabassum, I. Yousuf, *Coord. Chem. Rev.* 2023, **487**, 215169. DOI: 10.1016/j.ccr.2023.215169.
- 71 M. Pal, U. Nandi and D. Mukherjee, *Eur. J. Med. Chem.* 2018, **150**, 419–445. DOI: 10.1016/j.ejmech.2018.03.015.
- 72 J. A. Solís-Ruiz, A. Barthe, G. Riegel, R. O. Saavedra-Díaz, C. Gaiddon and R. Le Lagadec, *J. Inorg. Biochem.*, 2020, **208**, 111080, DOI: 10.1016/j.jinorgbio.2020.111080.
- 73 H. Rico Bautista, R. O. Saavedra Díaz, L. Q. Shen, C. Orvain, C. Gaiddon, R. Le Lagadec and A. D. Ryabov, *J. Inorg. Biochem.*, 2016, **163**, 28–38. DOI: 10.1016/j.jinorgbio.2016.07.014.
- 74 C. Licon, J. B. Delhorme, G. Riegel, V. Vidimar, R. Cerón-Camacho, B. Boff, A. Venkatasamy, C. Tomasetto, P. Da Silva Figueiredo Celestino Gomes, D. Rognan, J. N. Freund, R. Le Lagadec, M. Pfeffer, I. Gross, G. Mellitzer and C. Gaiddon, *Inorg. Chem. Front.*, 2020, **7**, 678–688, DOI: 10.1039/C9QI01148J.
- 75 G. Riegel, C. Orvain, S. Recberlik, M. E. Spaety, G. Poschet, A. Venkatasamy, M. Yamamoto, S. Nomura, T. Tsukamoto, M. Masson, I. Gross, R. Le Lagadec, G. Mellitzer and C. Gaiddon, *Cancer Lett.*, 2024, **585**, 216671, DOI: 10.1016/j.canlet.2024.216671.
- 76 T. Sainuddin, J. McCain, M. Pinto, H. Yin, J. Gibson, M. Hetu and S. A. McFarland, *Inorg. Chem.*, 2016, **55**, 83–95, DOI: 10.1021/acs.inorgchem.5b01838.
- 77 G. Ghosh, K. L. Colón, A. Fuller, T. Sainuddin, E. Bradner, J. McCain, S. M. A. Monroe, H. Yin, M. W. Hetu, C. G. Cameron and S. A. McFarland, *Inorg. Chem.*, 2018, **57**, 7694–7712, DOI: 10.1021/acs.inorgchem.8b00689.
- 78 J. McCain, K. L. Colón, P. C. Barrett, S. M. A. Monroe, T. Sainuddin, J. Roque, M. Pinto, H. Yin, C. G. Cameron and S. A. McFarland, *Inorg. Chem.*, 2019, **58**, 10778–10790, DOI: 10.1021/acs.inorgchem.9b01044.
- 79 J. Chen, F. Peng, Y. Zhang, B. Li, J. She, X. Jie, Z. Zou, M. Chen and L. Chen, *Eur. J. Med. Chem.*, 2017, **140**, 104–117, DOI: 10.1016/j.ejmech.2017.09.007.
- 80 J. Chen, Y. Deng, J. Wang, S. Chen, F. Peng, X. He, M. Liu, H. Luo, J. Zhang and L. Chen, *J. Biol. Inorg. Chem.*, 2021, **26**, 793–808. DOI: 10.1007/s00775-021-01894-4.
- 81 X. Zhu, Q. Sun, X. Guo, C. Liang, Y. Zhang, W. Huang, W. Pei, Z. Huang, L. Chen and J. Chen, *J. Inorg. Biochem.*, 2023, **247**, 112333, DOI: 10.1016/j.jinorgbio.2023.112333.



- 82 J. Chen, J. Wang, Y. Deng, B. Li, C. Li, Y. Lin, D. Yang, H. Zhang, L. Chen and T. Wang, *Eur. J. Med. Chem.*, 2020, **203**, 112562, DOI: 10.1016/j.ejmech.2020.112562.
- 83 L. Chen, J. Wang, X. Cai, S. Chen, J. Zhang, B. Li, W. Chen, X. Guo, H. Luo and J. Chen, *Bioorg. Chem.*, 2022, **119**, 105516, DOI: 10.1016/j.bioorg.2021.105516.
- 84 L. Chen, W. Yu, H. Tang, S. Zhang, J. Wang, Q. Ouyang, M. Guo, X. Zhu, Z. Huang and J. Chen, *Metallomics*, 2024, **16**, mfae002, DOI: 10.1093/mtomcs/mfae002.
- 85 Z. Lv, H. Wei, Q. Li, X. Su, S. Liu, K. Y. Zhang, W. Lv, Q. Zhao, X. Li and W. Huang, *Chem. Sci.*, 2018, **9**, 502–512, DOI: 10.1039/C7SC03765A.
- 86 M. Graf, D. Siegmund, N. Metzler-Nolte, K. Sünkel and H. C. Böttcher, *Inorg. Chim. Acta.*, 2019, **487**, 9–14, DOI: 10.1016/j.ica.2018.11.050.
- 87 L. Xie, L. Wang, R. Guan, L. Ji and H. Chao, *J. Inorg. Biochem.*, 2021, **217**, 111380 DOI: 10.1016/j.jinorgbio.2021.111380.
- 88 Y. Wang, J. Jin, L. Shu, T. Li, S. Lu, M. K. M. Subarkhan, C. Chen and H. Wang, *Chem. Eur. J.*, 2020, **26**, 15170–15182, DOI: 10.1002/chem.202002970.
- 89 J. Cervinka, A. Hernández-García, D. Bautista, L. Marková, H. Kostrhunova, J. Malina, J. Kasparkova, M. D. Santana, V. Brabec and J. Ruiz, *Inorg. Chem. Front.*, 2024, **11**, 3855–3876, DOI: 10.1039/D4QI00732H.
- 90 M. Klajner, C. Licon, L. Fetzter, P. Hebraud, G. Mellitzer, M. Pfeffer, S. Harlepp and C. Gaidon, *Inorg. Chem.*, 2014, **53**, 5150–5158, DOI: 10.1021/ic500250e.
- 91 V. Novohradsky, J. Yellol, O. Stuchlikova, M. D. Santana, H. Kostrhunova, G. Yellol, J. Kasparkova, D. Bautista, J. Ruiz and V. Brabec, *Chem. Eur. J.*, 2017, **23**, 15294–15299, DOI: 10.1002/chem.201703581.
- 92 V. Vidimar, C. Licon, R. Cerón-Camacho, E. Guerin, P. Coliat, A. Venkatasamy, M. Ali, D. Guenot, R. Le Lagadec, A. C. Jung, J. N. Freund, M. Pfeffer, G. Mellitzer, G. Sava and C. Gaidon, *Cancer. Lett.*, 2019, **440–441**, 145–155, DOI: 10.1016/j.canlet.2018.09.029.
- 93 M. Martínez-Alonso, A. Gandioso, C. Thibaudeau, X. Qin, P. Arnoux, N. Demeubayeva, V. Guérineau, C. Frochot, A. C. Jung, C. Gaidon and G. Gasser, *Chem. Bio. Chem.*, 2023, **24**, e202300203, DOI: 10.1002/cbic.202300203.
- 94 H. Huang, P. Zhang, B. Yu, Y. Chen, J. Wang, L. Ji and H. Chao, *J. Med. Chem.*, 2014, **57**, 8971–8983, DOI: 10.1021/jm501095r.
- 95 H. Huang, P. Zhang, H. Chen, L. Ji and H. Chao, *Chem. Eur. J.*, 2015, **21**, 715–725, DOI: 10.1002/chem.201404922.
- 96 L. Zeng, Y. Chen, J. Liu, H. Huang, R. Guan, L. Ji and H. Chao, *Sci. Rep.*, 2016, **6**, 19449, DOI: 10.1038/srep19449.
- 97 J. Li, L. Zeng, Z. Wang, H. Chen, S. Fang, J. Wang, C. Y. Cai, E. Xing, X. Liao, Z. W. Li, C. R. Ashby, Z. S. Chen, H. Chao and Y. Pan, *Adv. Mater.*, 2022, **34**, 2100245, DOI: 10.1002/adma.202100245.



- 98 F. J. Ballester, E. Ortega, D. Bautista, M. D. Santana and J. Ruiz, *Chem. Commun.*, 2020, **56**, 10301–10304, DOI: 10.1039/D0CC02417A.
- 99 J. Yellol, S. A. Pérez, A. Buceta, G. Yellol, A. Donaire, P. Szumlas, P. J. Bednarski, G. Makhoulfi, C. Janiak, A. Espinosa and J. Ruiz, *J. Med. Chem.*, 2015, **58**, 7310–7327, DOI: 10.1021/acs.jmedchem.5b01194.
- 100 F. J. Ballester, E. Ortega, V. Porto, H. Kostrhunova, N. Davila-Ferreira, D. Bautista, V. Brabec, F. Domínguez, M. D. Santana and J. Ruiz, *ChemComm*, 2019, **55**, 1140–1143, DOI: 10.1039/C8CC09211G.
- 101 R. N. Rao, R. L. Panchangam, V. Manickam, M. M. Balamurali and K. Chanda, *Chempluschem*, 2020, **85**, 1800–1812, DOI: 10.1002/cplu.202000516.
- 102 R. L. Panchangam, R. N. Rao, M. M. Balamurali, T. B. Hingamire, D. Shanmugam, V. Manickam and K. Chanda, *Inorg. Chem.*, 2021, **60**, 17593–17607, DOI: 10.1021/acs.inorgchem.1c02193.
- 103 V. Koch, A. Meschkov, W. Feuerstein, J. Pfeifer, O. Fuhr, M. Nieger, U. Schepers and S. Bräse, *Inorg. Chem.*, 2019, **58**, 15917–15926, DOI: 10.1021/acs.inorgchem.9b02402.
- 104 C. A. Riedl, L. S. Flocke, M. Hejl, A. Roller, M. H. M. Klose, M. A. Jakupec, W. Kandioller and B. K. Keppler, *Inorg. Chem.*, 2017, **56**, 528–541, DOI: 10.1021/acs.inorgchem.6b02430.
- 105 L. Rafols, D. Josa, D. Aguilà, L. A. Barrios, O. Roubeau, J. Cirera, V. Soto-Cerrato, R. Pérez-Tomás, M. Martínez, A. Grabulosa and P. Gamez, *Inorg. Chem.*, 2021, **60**, 7974–7990, DOI: 10.1021/acs.inorgchem.1c00507.
- 106 K. Kumarasamy, T. Devendhiran, S. M. Asokan, R. Mahendran, M. C. Lin, W. J. Chien, S. K. Ramasamy and C. Y. Huang, *Inorg. Chem. Commun.*, 2023, **152**, 110662, DOI: 10.1016/j.inoche.2023.110662.
- 107 L. Zeng, Y. Chen, H. Huang, J. Wang, D. Zhao, L. Ji and H. Chao, *Chem. Eur. J.*, 2015, **21**, 15308–15319, DOI: 10.1002/chem.201502154.
- 108 Y. Wen, C. Ouyang, Q. Li, T. W. Rees, K. Qiu, L. Ji and H. Chao, *Dalton Trans*, 2020, **49**, 7044–7052, DOI: 10.1039/D0DT01412E.
- 109 L. Tabrizi, L. O. Olasunkanmi and O. A. Fadare, *Dalton Trans.*, 2019, **48**, 728–740, DOI: 10.1039/C8DT03266A.
- 110 D. Alessi, P. Del Mestre, E. Aneggi, M. Ballico, A. P. Beltrami, M. Busato, D. Cesselli, A. A. Heidecker, D. Zuccaccia and W. Baratta, *Catal. Sci. Technol.*, 2023, **13**, 5267–5279, DOI: 10.1039/D3CY00676J.
- 111 M. Ballico, D. Alessi, E. Aneggi, M. Busato, D. Zuccaccia, L. Allegri, G. Damante, C. Jandl and W. Baratta, *Molecules*, 2024, **29**, 2146, DOI: 10.3390/molecules29092146.
- 112 R. Kumar, A. Yadav, A. Ratnam, S. Kumar, M. Bala, D. Sur, S. Narang, U. P. Singh, P. K. Mandal and K. Ghosh, *Eur. J. Inorg. Chem.*, 2017, **2017**, 5334–5343, DOI: 10.1002/ejic.201700839.
- 113 M. Hanif, M. V. Babak and C. G. Hartinger. *Drug Discov. Today*. 2014, **19**, 1640–1648, DOI: 10.1016/j.drudis.2014.06.016.



- 114 R. Kushwaha, A. Kumar, S. Saha, S. Bajpai, A. K. Yadav and S. Banerjee, *Chem. Commun.*, 2022, **58**, 4825–4836, DOI: 10.1039/D2CC00341D.
- 115 A. Hernández-García, L. Marková, M. D. Santana, J. Prachařová, D. Bautista, H. Kostrhunová, V. Novohradský, V. Brabec, J. Ruiz and J. Kašpárková, *Inorg. Chem.*, 2023, **62**, 6474–6487, DOI: 10.1021/acs.inorgchem.3c00501.
- 116 P. Getreuer, L. Marretta, E. Toyoglu, O. Dömötör, M. Hejl, A. Prado-Roller, K. Cseh, A. A. Legin, M. A. Jakupec, G. Barone, A. Terenzi, B. K. Keppler and W. Kandioller, *Dalton Trans.*, 2024, **53**, 5567–5579, DOI: 10.1039/D4DT00245H.
- 117 E. Ortega, J. G. Yellol, M. Rothmund, F. J. Ballester, V. Rodríguez, G. Yellol, C. Janiak, R. Schobert and J. Ruiz, *Chem. Commun.*, 2018, **54**, 11120–11123, DOI: 10.1039/C8CC06427J.
- 118 J. Kralj, A. Bolje, D. S. Polančec, I. Steiner, T. Gržan, A. Tupek, N. Stojanović, S. Hohloch, D. Urankar, M. Osmak, B. Sarkar, A. Brozovic and J. Košmrlj, *Organometallics*, 2019, **38**, 4082–4092, DOI: 10.1021/acs.organomet.9b00327.
- 119 D. Josa, D. Aguilà, P. Fontova, V. Soto-Cerrato, P. Herrera-Ramírez, L. Rafols, A. Grabulosa and P. Gamez, *Dalton Trans.*, 2023, **52**, 8391–8401, DOI: 10.1039/D3DT00743J.
- 120 C. F. Yeung, L. H. Chung, S. W. Ng, H. L. Shek, S. Y. Tse, S. C. Chan, M. K. Tse, S. M. Yiu and C. Y. Wong, *Chem. Eur. J.*, 2019, **25**, 9159–9163, DOI: 10.1002/chem.201901080.
- 121 M. Sohrabi, M. Saeedi, B. Larijani and M. Mahdavi, *Eur. J. Med. Chem.*, 2021, **216**, 113308, DOI: 10.1016/j.ejmech.2021.113308.
- 122 C.-H. Leung, H.-J. Zhong, D. S.-H. Chan and D.-L. Ma, *Coord. Chem. Rev.*, 2013, **257**, 1764–1776, DOI: 10.1016/j.ccr.2013.01.034.
- 123 M. Graf, D. Siegmund, N. Metzler-Nolte and K. Sünkel, *Z. Anorg. Allg. Chem.*, 2019, **645**, 1068–1071, DOI: 10.1002/zaac.201900147.
- 124 M. Graf, D. Siegmund, Y. Gothe, N. Metzler-Nolte and K. Sünkel, *Z. Anorg. Allg. Chem.*, 2020, **646**, 665–669, DOI: 10.1002/zaac.201900317.
- 125 M. Graf, Y. Gothe, N. Metzler-Nolte, R. Czerwieniec and K. Sünkel, *J. Organomet. Chem.*, 2014, **765**, 46–52, DOI: 10.1016/j.jorganchem.2014.04.031.
- 126 M. Graf, Y. Gothe, N. Metzler-Nolte, R. Czerwieniec and K. Sünkel, *Inorg. Chim. Acta.*, 2017, **463**, 36–43, DOI: 10.1016/j.ica.2017.04.006.
- 127 M. Graf, Y. Gothe, D. Siegmund, N. Metzler-Nolte and K. Sünkel, *Inorg. Chim. Acta.*, 2018, **471**, 265–271, DOI: 10.1016/j.ica.2017.11.003.
- 128 M. Graf, H. Böttcher, N. Metzler-Nolte, K. Sünkel, S. Thavalingam and R. Czerwieniec, *Z. Anorg. Allg. Chem.*, 2021, **647**, 519–524, DOI: 10.1002/zaac.202000460.
- 129 C. Pérez-Arnaiz, M. I. Acuña, N. Busto, I. Echevarría, M. Martínez-Alonso, G. Espino, B. García and F. Domínguez, *Eur. J. Med. Chem.*, 2018, **157**, 279–293, DOI: 10.1016/j.ejmech.2018.07.065.
- 130 F. Du, L. Bai, M. He, W. Y. Zhang, Y. Y. Gu, H. Yin and Y. J. Liu, *J. Inorg. Biochem.*, 2019, **201**, 110822, DOI: 10.1016/j.jinorgbio.2019.110822.



- 131 M. He, Q. Y. Yi, W. Y. Zhang, L. Bai, F. Du, Y. Y. Gu, Y. J. Liu and P. Wei, *New J. Chem.*, 2019, **43**, 8566–8579, DOI: 10.1039/C9NJ01001G.
- 132 J. Xu, L. Bai, Y. Y. Gu, F. Du, W. Y. Zhang, M. He and Y. J. Liu, *Inorg. Chem. Commun.*, 2020, **111**, 107594, DOI: 10.1016/j.inoche.2019.107594.
- 133 H. Zhang, L. Tian, R. Xiao, Y. Zhou, Y. Zhang, J. Hao, Y. Liu and J. Wang, *Bioorg. Chem.*, 2021, **115**, 105290, DOI: 10.1016/j.bioorg.2021.105290.
- 134 Y. Zhou, L. Bai, Y. Y. Gu, L. Tian, H. Yin, Y. Y. Zhang, H. W. Zhang, D. G. Xing and Y. J. Liu, *Inorg. Chem. Commun.*, 2020, **118**, 108012, DOI: 10.1016/j.inoche.2020.108012.
- 135 Y. Zhou, L. Bai, L. Tian, L. Yang, H. Zhang, Y. Zhang, J. Hao, Y. Gu and Y. Liu, *J. Inorg. Biochem.*, 2021, **223**, 111550, DOI: 10.1016/j.jinorgbio.2021.111550.
- 136 L. Tian, Y. Zhang, H. Zhang, Y. Zhou, W. Li, Y. Yuan, J. Hao, L. Yang and Y. Liu, *J. Biol. Inorg. Chem.*, 2021, **26**, 705–714, DOI: 10.1007/s00775-021-01895-3.
- 137 J. Chen, H. Liu, Y. Chen, H. Hu, C. Huang, Y. Wang, L. Liang and Y. Liu, *J. Inorg. Biochem.*, 2023, **241**, 112145, DOI: 10.1016/j.jinorgbio.2023.112145.
- 138 Y. Li, B. Liu, C. X. Xu, L. He, Y. C. Wan, L. N. Ji and Z. W. Mao, *J. Biol. Inorg. Chem.*, 2020, **25**, 597–607, DOI: 10.1007/s00775-020-01783-2.
- 139 S. fen He, W. chao Han, Y. ying Shao, H. bin Zhang, W. xin Hong, Q. hong Yang, Y. qing Zhang, R. rong He and J. Sun, *Bioorg. Chem.*, 2023, **141**, 106867, DOI: 10.1016/j.bioorg.2023.106867.
- 140 L. Chen, H. Tang, W. Chen, J. Wang, S. Zhang, J. Gao, Y. Chen, X. Zhu, Z. Huang and J. Chen, *J. Inorg. Biochem.*, 2023, **249**, 112397, DOI: 10.1016/j.jinorgbio.2023.112397.
- 141 L. Q. Qin, B. Q. Zou, Q. P. Qin, Z. F. Wang, L. Yang, M. X. Tan, C. J. Liang and H. Liang, *New J. Chem.*, 2020, **44**, 7832–7837, DOI: 10.1039/D0NJ00465K.
- 142 Y. Yang, Y. D. Bin, Q. P. Qin, X. J. Luo, B. Q. Zou and H. X. Zhang, *ACS Med. Chem. Lett.*, 2019, **10**, 1614–1619, DOI: 10.1021/acsmmedchemlett.9b00337.
- 143 P. Li, L. Guo, J. Li, Z. Yang, H. Fu, K. Lai, H. Dong, C. Fan and Z. Liu, *Dalton Trans.*, 2024, **53**, 1977–1988, DOI: 10.1039/D3DT03700B.
- 144 J. Yellol, S. A. Pérez, G. Yellol, J. Zajac, A. Donaire, G. Vigueras, V. Novohradsky, C. Janiak, V. Brabec and J. Ruiz, *Chem. Commun.*, 2016, **52**, 14165–14168, DOI: 10.1039/C6CC07909A.
- 145 P. Laha, U. De, F. Chandra, N. Dehury, S. Khullar, H. S. Kim and S. Patra, *Dalton Trans.*, 2018, **47**, 15873–15881, DOI: 10.1039/C8DT02461H.
- 146 A. Bonfiglio, C. McCartin, U. Carrillo, C. Cebrián, P. C. Gros, S. Fournel, A. Kichler, C. Daniel and M. Mauro, *Eur. J. Inorg. Chem.*, 2021, **2021**, 1551–1564, DOI: 10.1002/ejic.202100132.
- 147 Y. Yang, L. Guo, X. Ge, Z. Tian, Y. Gong, H. Zheng, Q. Du, X. Zheng and Z. Liu, *Dyes and Pigm.*, 2019, **161**, 119–129, DOI: 10.1016/j.dyepig.2018.09.044.
- 148 S. Mukhopadhyay, R. S. Singh, R. P. Paitandi, G. Sharma, B. Koch and D. S. Pandey, *Dalton Trans.*, 2017, **46**, 8572–8585, DOI: 10.1039/C7DT01015J.



- 149 X. Liu, H. Hao, X. Ge, X. He, Y. Liu, Y. Wang, H. Wang, M. Shao, Z. Jing, L. Tian and Z. Liu, *J. Inorg. Biochem.*, 2019, **199**, 110757, DOI: 10.1016/j.jinorgbio.2019.110757.
- 150 M. Ouyang, L. Zeng, H. Huang, C. Jin, J. Liu, Y. Chen, L. Ji and H. Chao, *Dalton Trans.*, 2017, **46**, 6734–6744, DOI: 10.1039/C7DT01043E.
- 151 Q. Y. Yi, D. Wan, B. Tang, Y. J. Wang, W. Y. Zhang, F. Du, M. He and Y. J. Liu, *Eur. J. Med. Chem.*, 2018, **145**, 338–349, DOI: 10.1016/j.ejmech.2017.11.091.
- 152 J. Wang, H. Liu, X. Wu, C. Shi, W. Li, Y. Yuan, Y. Liu and D. Xing, *J. Biol. Inorg. Chem.*, 2022, **27**, 455–469, DOI: 10.1007/s00775-022-01943-6.
- 153 Y. J. Wang, Q. Y. Yi, W. Y. Zhang, F. Du, M. He and Y. J. Liu, *Polyhedron*, 2018, **156**, 320–331, DOI: 10.1016/j.poly.2018.09.057.
- 154 B. Tang, D. Wan, Y. J. Wang, Q. Y. Yi, B. H. Guo and Y. J. Liu, *Eur. J. Med. Chem.*, 2018, **145**, 302–314, DOI: 10.1016/j.ejmech.2017.12.087.
- 155 L. X. Zhang, Y. Y. Gu, Y. J. Wang, L. Bai, F. Du, W. Y. Zhang, M. He, Y. J. Liu and Y. Z. Chen, *Molecules*, 2019, **24**, 3129, DOI: 10.3390/molecules24173129.
- 156 Z. L. Chen, B. Q. Zou, Q. P. Qin, Z. F. Wang, M. X. Tan, X. L. Huang, C. J. Liang and H. Liang, *Inorg. Chem. Commun.*, 2020, **115**, 107854, DOI: 10.1016/j.inoche.2020.107854.
- 157 Y. Yang, C. M. Wang, H. S. Cao, Z. Zhou, Q. J. Xie, Q. P. Qin and Q. Chen, *Inorg. Chem. Commun.*, 2022, **142**, 109609, DOI: 10.1016/j.inoche.2022.109609.
- 158 T. Temram, E. Klaimanee, S. Saithong, P. Amornpitoksuk, S. Phongpaichit, A. Ratanaphan, Y. Tantirungrotechai and N. Leesakul, *Polyhedron*, 2023, **243**, 116540, DOI: 10.1016/j.poly.2023.116540.
- 159 S. Kuang, X. Liao, X. Zhang, T. W. Rees, R. Guan, K. Xiong, Y. Chen, L. Ji and H. Chao, *Angew. Chem., Int. Ed. Engl.*, 2020, **132**, 3341–3347, DOI: 10.1002/anie.201915828.
- 160 X. Liu, X. He, X. Zhang, Y. Wang, J. Liu, X. Hao, Y. Zhang, X. A. Yuan, L. Tian and Z. Liu, *ChemBioChem*, 2019, **20**, 2767–2776, DOI: 10.1002/cbic.201900268.
- 161 M. M. Wang, X. L. Xue, X. X. Sheng, Y. Su, Y. Q. Kong, Y. Qian, J. C. Bao, Z. Su and H. K. Liu, *RSC Adv.*, 2020, **10**, 5392–5398, DOI: 10.1039/C9RA10357K.
- 162 Z. Liu, I. Romero-Canelón, A. Habtemariam, G. J. Clarkson and P. J. Sadler, *Organometallics*, 2014, **33**, 5324–5333, DOI: 10.1021/om500644f.
- 163 J. M. Zimbron, K. Passador, B. Gatin-Fraudet, C. M. Bachelet, D. Plazuk, L. M. Chamoreau, C. Botuha, S. Thorimbert and M. Salmay, *Organometallics*, 2017, **36**, 3435–3442, DOI: 10.1021/acs.organomet.7b00250.
- 164 A. J. Millett, A. Habtemariam, I. Romero-Canelón, G. J. Clarkson and P. J. Sadler, *Organometallics*, 2015, **34**, 2683–2694, DOI: 10.1021/acs.organomet.5b00097.
- 165 S. Chen, X. Liu, Z. Tian, X. Ge, H. Hao, Y. Hao, Y. Zhang, Y. Xie, L. Tian and Z. Liu, *Appl. Organomet. Chem.*, 2019, **33**, e5053, DOI: 10.1002/aoc.5053.



- 166 X. Liu, S. Chen, X. Ge, Y. Zhang, Y. Xie, Y. Hao, D. Wu, J. Zhao, X. A. Yuan, L. Tian and Z. Liu, *J Inorg. Biochem.*, 2020, **205**, 110983, DOI: 10.1016/j.jinorgbio.2019.110983.
- 167 R. N. Rao, R. L. Panchangam, V. Manickam, M. M. Balamurali and K. Chanda, *Chempluschem*, 2020, **85**, 1800–1812, DOI: 10.1002/cplu.202000516.
- 168 Y. Yang, L. Guo, Z. Tian, Y. Gong, H. Zheng, S. Zhang, Z. Xu, X. Ge and Z. Liu, *Inorg. Chem.*, 2018, **57**, 11087–11098, DOI: 10.1021/acs.inorgchem.8b01656.
- 169 Z. dong Mou, N. Deng, F. Zhang, J. Zhang, J. Cen and X. Zhang, *Eur. J. Med. Chem.*, 2017, **138**, 72–82, DOI: 10.1016/j.ejmech.2017.06.027.
- 170 M. Redrado, M. Miñana, M. P. Coogan, M. Concepción Gimeno and V. Fernández-Moreira, *ChemMedChem.*, 2022, **17**, e202200244, DOI: 10.1002/cmdc.202200244.
- 171 Z. Tan, M. Lin, J. Liu, H. Wu and H. Chao, *Dalton Trans.*, 2024, **53**, 12917–12926, DOI: 10.1039/D4DT01665C.
- 172 C. Zhang, S. H. Lai, H. H. Yang, D. G. Xing, C. C. Zeng, B. Tang, D. Wan and Y. J. Liu, *RSC Adv*, 2017, **7**, 17752–17762, DOI: 10.1039/C7RA00732A.
- 173 W. Y. Zhang, Q. Y. Yi, Y. J. Wang, F. Du, M. He, B. Tang, D. Wan, Y. J. Liu and H. L. Huang, *Eur. J. Med. Chem.*, 2018, **151**, 568–584, DOI: 10.1016/j.ejmech.2018.04.013.
- 174 X. D. Song, B. B. Chen, S. F. He, N. L. Pan, J. X. Liao, J. X. Chen, G. H. Wang and J. Sun, *Eur. J. Med. Chem.*, 2019, **179**, 26–37, DOI: 10.1016/j.ejmech.2019.06.045.
- 175 W. Li, C. Shi, X. Wu, Y. Zhang, H. Liu, X. Wang, C. Huang, L. Liang and Y. Liu, *J. Inorg. Biochem.*, 2022, **236**, 111977, DOI: 10.1016/j.jinorgbio.2022.111977.
- 176 G. Li, J. Chen, Y. Xie, Y. Yang, Y. Niu, X. Chen, X. Zeng, L. Zhou and Y. Liu, *J. Inorg. Biochem.*, 2024, **259**, 112652, DOI: 10.1016/j.jinorgbio.2024.112652.
- 177 B. Yuan, J. Liu, R. Guan, C. Jin, L. Ji and H. Chao, *Dalton Trans.*, 2019, **48**, 6408–6415, DOI: 10.1039/C9DT01072F.
- 178 W. W. Qin, Z. Y. Pan, D. H. Cai, Y. Li and L. He, *Dalton Trans.*, 2020, **49**, 3562–3569, DOI: 10.1039/D0DT00180E.
- 179 N. Manav, M. Y. Lone, M. K. Raza, J. Chavda, S. Mori and I. Gupta, *Dalton Trans.*, 2022, **51**, 3849–3863, DOI: 10.1039/D1DT04218A.
- 180 P. Zhang, H. Huang, S. Banerjee, G. J. Clarkson, C. Ge, C. Imberti and P. J. Sadler, *Angew. Chem., Int. Ed. Engl.*, 2019, **131**, 2372–2376, DOI: 10.1002/ange.201813002.
- 180 W. Y. Zhang, F. Du, M. He, L. Bai, Y. Y. Gu, L. L. Yang and Y. J. Liu, *Eur. J. Med. Chem.*, 2019, **178**, 390–400, DOI: 10.1016/j.ejmech.2019.06.009.
- 182 L. Bai, W. D. Fei, Y. Y. Gu, M. He, F. Du, W. Y. Zhang, L. L. Yang and Y. J. Liu, *J. Inorg. Biochem.*, 2020, **205**, 111014, DOI: 10.1016/j.jinorgbio.2020.111014.
- 183 Y. Zhang, W. Fei, H. Zhang, Y. Zhou, L. Tian, J. Hao, Y. Yuan, W. Li and Y. Liu, *J. Inorg. Biochem.*, 2021, **225**, 111622, DOI: 10.1016/j.jinorgbio.2021.111622.



- 184 F. L. Xie, Z. T. Huang, L. Bai, J. W. Zhu, H. H. Xu, Q. Q. Long, Q. F. Guo, Y. Wu and S. H. Liu, *J. Inorg. Biochem.*, 2021, **225**, 111603, DOI: 10.1016/j.jinorgbio.2021.111603.
- 185 H. Zhang, X. Liao, X. Wu, C. Shi, Y. Zhang, Y. Yuan, W. Li, J. Wang and Y. Liu, *J. Inorg. Biochem.*, 2022, **228**, 111706, DOI: 10.1016/j.jinorgbio.2021.111706.
- 186 H. Sun, M. Shamy and M. Costa. *Genes*, 2013, **4**, 583-595. DOI: 10.3390/genes4040583.
- 187 J. L. Boer, S. B. Mulrooney and R. P. Hausinger. *Arch. Biochem. Biophys.* 2014, **544**, 142-152. DOI: 10.1016/j.abb.2013.09.002.
- 188 J. L. Nevarez, A. Turmo, J. Hu and R. P. Hausinger. *ChemCatChem*, 2020, **12**, 4242-4254. DOI: 10.1002/cctc.202000575.
- 189 R. P. Hausinger, B. Desguin, M. Fellner, J. A. Rankin and J. Hu. *Curr. Opin. Chem. Biol.* 2018, **47**, 18-23. DOI: doi.org/10.1016/j.cbpa.2018.06.019.
- 190 M. Hosseini-Kharat, D. Zargarian, A. M. Alizadeh, K. Karami, M. Saeidifar, S. Khalighfard, L. Dubrulle, M. Zakariazadeh, J. P. Cloutier and Z. Sohrabijam, *Dalton Trans.*, 2018, **47**, 16944–16957, DOI: 10.1039/C8DT03079K.
- 191 M. Hosseini-Kharat, R. Rahimi, D. Zargarian, Z. Mehri Lighvan, A. A. Momtazi-Borojeni, T. Sharifi, E. Abdollahi, H. Tavakol and T. Mohammadi, *J. Biomol. Struct. Dyn.*, 2019, **37**, 3788–3802, DOI: 10.1080/07391102.2018.1527724.
- 192 M. Hosseini-Kharat, R. Rahimi, A. M. Alizadeh, D. Zargarian, S. Khalighfard, L. P. Mangin, N. Mahigir, S. H. Ayati and A. A. Momtazi-Borojeni, *Bioorg. Med. Chem. Lett.*, 2021, **43**, 128107, DOI: 10.1016/j.bmcl.2021.128107.
- 193 J.-J. ; Qu, L.-L. ; Shi, Y.-B. ; Wang, J. ; Yan, T. ; Shao, X.-Q. ; Hao, J.-X. ; Wang, H.-Y. ; Zhang, J.-F. ; Gong, J.-J. Qu, L.-L. Shi, Y.-B. Wang, J. Yan, T. Shao, X.-Q. Hao, J.-X. Wang, H.-Y. Zhang, J.-F. Gong and B. Song, *Molecules*, 2022, **27**, 3106, DOI: 10.3390/molecules27103106.
- 194 A. Amaya-Flórez, J. S. Serrano-García, J. Ruiz-Galindo, A. Arenaza-Corona, J. A. Cruz-Navarro, A. L. Orjuela, J. Alí-Torres, M. Flores-Alamo, P. Cano-Sanchez, V. Reyes-Márquez and D. Morales-Morales, *Front. Chem.*, 2024, **12**, 1483999, DOI: 10.3389/fchem.2024.1483999.
- 195 A. Sánchez-Mora, E. Briñez, A. Pico, L. González-Sebastián, J. Antonio Cruz-Navarro, A. Arenaza-Corona, N. Puentes-Díaz, J. Alí-Torres, V. Reyes-Márquez and D. Morales-Morales, *Chem. Biodivers.*, 2024, **21**, e202400995, DOI: 10.1002/cbdv.202400995.
- 196 A. R. Kapdi and I. J. S. Fairlamb. *Chem. Soc. Rev.*, 2014, **43**, 4751-4777. DOI: 10.1039/C4CS00063C.
- 197 T. J. Carneiro, A. S. Martins, M. P. M. Marques and A. M. Gil. *Front. Oncol.*, 2020, **10**, 590970. DOI: 10.3389/fonc.2020.590970.
- 198 J. Albert, S. García, J. Granell, A. Llorca, M. V. Lovelle, V. Moreno, A. Presa, L. Rodríguez, J. Quirante, C. Calvis, R. Messeguer, J. Badía and L. Baldomà, *J. Organomet. Chem.*, 2013, **724**, 289–296, DOI: 10.1016/j.jorganchem.2012.11.034.



- 199 J. Albert, L. D'Andrea, J. Granell, P. Pla-Vilanova, J. Quirante, M. K. Khosa, C. Calvis, R. Messeguer, J. Badía, L. Baldomà, M. Font-Bardia and T. Calvet, *J. Inorg. Biochem.*, 2014, **140**, 80–88, DOI: 10.1016/j.jinorgbio.2014.07.001.
- 200 J. Albert, R. Bosque, M. Crespo, G. García, J. Granell, C. López, M. V. Lovelle, R. Qadir, A. González, A. Jayaraman, E. Mila, R. Cortés, J. Quirante, C. Calvis, R. Messeguer, J. Badía, L. Baldomà and M. Cascante, *Eur. J. Med. Chem.*, 2014, **84**, 530–536, DOI: 10.1016/j.ejmech.2014.07.046.
- 201 J. Albert, J. Granell, J. A. Durán, A. Lozano, A. Luque, A. Mate, J. Quirante, M. K. Khosa, C. Calvis, R. Messeguer, L. Baldomà and J. Badia, *J. Organomet. Chem.*, 2017, **839**, 116–125, DOI: 10.1016/j.jorganchem.2017.04.002.
- 202 K. Karami, N. Jamshidian and M. Zakariazadeh, *Appl. Organomet. Chem.*, 2019, **33**, e4728, DOI: 10.1002/aoc.4728.
- 203 S. Abedanzadeh, K. Karami, M. Rahimi, M. Edalati, M. Abedanzadeh, A. M. Tamaddon, M. D. Jahromi, Z. Amirghofran, J. Lipkowski and K. Lyczko, *Dalton Trans.*, 2020, **49**, 14891–14907, DOI: 10.1039/D0DT02304C.
- 204 X. Q. Zhou, A. Busemann, M. S. Meijer, M. A. Siegler and S. Bonnet, *Chem. Commun.*, 2019, **55**, 4695–4698, DOI: 10.1039/C8CC10134E.
- 205 Z. M. Lighvan, H. A. Khonakdar, A. Heydari, M. Rafiee, M. D. Jahromi, A. Derakhshani and A. A. Momtazi-Borojeni, *Appl. Organomet. Chem.*, 2020, **34**, e5839, DOI: 10.1002/aoc.5839.
- 206 A. S. Abushamleh, K. A. Abu-Safieh, M. A. Khanfar, D. Taher, L. Tahtamouni and N. J. Alwahsh, *J. Struct. Chem.*, 2021, **62**, 1112–1122, DOI: 10.1134/S0022476621070167.
- 207 K. Badpa, S. J. Sabounchei, L. Hosseinzadeh and R. W. Gable, *J. Coord. Chem.*, 2020, **73**, 2941–2962, DOI: 10.1080/00958972.2020.1836624.
- 208 M. Frik, J. Jiménez, V. Vasilevski, M. Carreira, A. De Almeida, E. Gascón, F. Benoit, M. Sanaú, A. Casini and M. Contel, *Inorg. Chem. Front.*, 2014, **1**, 231–241, DOI: 10.1039/C4QI00003J.
- 209 T. T. H. Fong, C. N. Lok, C. Y. S. Chung, Y. M. E. Fung, P. K. Chow, P. K. Wan and C. M. Che, *Angew. Chem., Int. Ed.*, 2016, **55**, 11935–11939, DOI: 10.1002/anie.201602814.
- 210 D. V. Aleksanyan, S. G. Churusova, Z. S. Klemenkova, R. R. Aysin, E. Y. Rybalkina, Y. V. Nelyubina, O. I. Artyushin, A. S. Peregudov and V. A. Kozlov, *Organometallics*, 2019, **38**, 1062–1080, DOI: 10.1021/acs.organomet.8b00867.
- 211 R. Saini, C. Rao, A. Maji, P. M. Mishra, A. Yadav, C. K. Nandi and K. Ghosh, *J. Inorg. Biochem.*, 2022, **237**, 112019, DOI: 10.1016/j.jinorgbio.2022.112019.
- 212 J. Albert, B. Al Janabi, J. Granell, M. S. Hashemi, D. Sainz, M. K. Khosa, C. Calvis, R. Messeguer, L. Baldomà, J. Badia and M. Font-Bardia, *J. Organomet. Chem.*, 2023, **983**, 122555, DOI: 10.1016/j.jorganchem.2022.122555.
- 213 V. A. Kozlov, D. V. Aleksanyan, S. G. Churusova, A. A. Spiridonov, E. Y. Rybalkina, E. I. Gutsul, S. A. Aksenova, A. A. Korlyukov, A. S. Peregudov and Z. S. Klemenkova, *Int. J. Mol. Sci.*, 2023, **24**, 17331, DOI: 10.3390/ijms242417331,



- 214 D. V. Aleksanyan, A. A. Spiridonov, S. G. Churusova, E. Y. Rybalkina, A. A. Danshina, A. S. Peregudov, Z. S. Klemenkova and V. A. Kozlov, *Inorg. Chim. Acta.*, 2023, **548**, 121369, DOI: 10.1016/j.ica.2022.121369.
- 215 S. Dirulba and G. V. Kalayda. *Cancer Chemother. Pharmacol.*, 2016, **77**, 1103-1124. DOI: 10.1007/s00280-016-2976-z.
- 216 M. G. Apps, E. H. Y. Choi and N. J. Wheate. *Endocrine-Related Cancer*. 2015, **22**, R219-R233. DOI: 10.1530/ERC-15-0237.
- 217 M. Fanelli, M. Formica, V. Fusi, L. Giorgi and M. Micheloni. *Coord. Chem. Rev.* 2016, **310**, 41-79. DOI: 10.1016/j.ccr.2015.11.004.
- 218 S. Jin, Y. Guo, Z. Guo and X. Wang. *Pharmaceuticals*, 2021, **14**, 133. DOI: 10.3390/ph14020133.
- 219 K. Peng, B.-B. Liang, W. Liu and Z.-W. Mao. *Coord. Chem. Rev.* 2021, **449**, 214210. DOI: 10.1016/j.ccr.2021.214210.
- 220 B. J. Pages, K. B. Garbutcheon-Singh and J. R. Aldrich-Wright. *Eur. J. Inorg. Chem.* 2017, **2017**, 1613-1624. DOI: 10.1002/ejic.201601204.
- 221 Y. Zhong, C. Jia, X. Zhang, X. Liao, B. Yang, Y. Cong, S. Pu and C. Gao. *Eur. J. Med. Chem.* 2020, **194**, 112229. DOI: 10.1016/j.ejmech.2020.112229.
- 222 P. Štarha and R. Křikavová. *Coord. Chem Rev.* 2024, **501**, 215578. DOI: /10.1016/j.ccr.2023.215578.
- 223 L. Cai, C. Yu, L. Ba, Q. Liu, Y. Qian, B. Yang and C. Gao. *Appl Organometal Chem.* 2018, **32**, e4228. DOI: 10.1002/aoc.4228.
- 224 C. Jia, G. B. Deacon, Y. Zhang and C. Gao. *Coord. Chem. Rev.* 2021, **429**, 213640. DOI: 0.1016/j.ccr.2020.213640.
- 225 N. Mohammadi, S. Abedanzadeh, R. Fereidonnejad, M. Mahdavinia and M. Fereidoonhezad, *J. Organomet. Chem.*, 2023, **996**, 122759, DOI: 10.1016/j.jorganchem.2023.122759.
- 226 M. Fereidoonhezad, M. Niazi, Z. Ahmadipour, T. Mirzaee, Z. Faghih, Z. Faghih and H. R. Shahsavari, *Eur. J. Inorg. Chem.*, 2017, **2017**, 2247–2254, DOI: 10.1002/ejic.201601521.
- 227 M. Fereidoonhezad, M. Niazi, M. Shahmohammadi Beni, S. Mohammadi, Z. Faghih, Z. Faghih and H. R. Shahsavari, *ChemMedChem*, 2017, **12**, 456–465, DOI: 10.1002/cmdc.201700007.
- 228 M. Fereidoonhezad, Z. Ramezani, M. Nikraves, J. Zangeneh, M. Golbon Haghighi, Z. Faghih, B. Notash and H. R. Shahsavari, *New J. Chem.*, 2018, **42**, 7177–7187, DOI: 10.1039/C8NJ01332B.
- 229 A. Zamora, S. A. Pérez, M. Rothenmund, V. Rodríguez, R. Schobert, C. Janiak and J. Ruiz, *Chem. Eur. J.*, 2017, **23**, 5614–5625, DOI: 10.1002/chem.201700717.
- 230 A. Zamora, A. Gandioso, A. Massaguer, S. Buenestado, C. Calvis, J. L. Hernández, F. Mitjans, V. Rodríguez, J. Ruiz and V. Marchán, *ChemMedChem*, 2018, **13**, 1755–1762, DOI: 10.1002/cmdc.201800282.
- 231 H. Samouei, M. Rashidi and F. W. Heinemann, *J. Iran. Chem. Soc.*, 2014, **11**, 1207–1216, DOI: 10.1007/s13738-013-0389-z.



- 232 R. Mohammadi, R. Yousefi, M. D. Aseman, S. M. Nabavizadeh and M. Rashidi, *Anticancer Agents. Med. Chem.*, 2014, **15**, 107–114. DOI: 10.2174/1871520614666141203143543.
- 233 J. Albert, R. Bosque, M. Crespo, J. Granell, C. López, R. Martín, A. González, A. Jayaraman, J. Quirante, C. Calvis, J. Badía, L. Baldomà, M. Font-Bardia, M. Cascante and R. Messeguer, *Dalton Trans.*, 2015, **44**, 13602–13614, DOI: 10.1039/C5DT01713K.
- 234 B. S. McGhie, J. Sakoff, J. Gilbert, C. P. Gordon and J. R. Aldrich-Wright, *Int J Mol Sci*, 2022, **23**, 10469, DOI: 10.3390/ijms231810469.
- 235 B. S. McGhie, J. Sakoff, J. Gilbert, C. P. Gordon and J. R. Aldrich-Wright, *Int. J. Mol. Sci.*, 2023, **24**, 8049, DOI: 10.3390/ijms24098049.
- 236 A. Mojaddami, A. Karimi, M. Mahdavinia and M. Fereidoonhezahad, *BioMetals*, 2022, **35**, 617–627, DOI: 10.1007/s10534-022-00392-7
- 237 M. Frik, J. Fernández-Gallardo, O. Gonzalo, V. Mangas-Sanjuan, M. González-Alvarez, A. Serrano Del Valle, C. Hu, I. González-Alvarez, M. Bermejo, I. Marzo and M. Contel, *J. Med. Chem.*, 2015, **58**, 5825–5841, DOI: 10.1021/acs.jmedchem.5b00427.
- 238 S. S. Pasha, P. Das, N. P. Rath, D. Bandyopadhyay, N. R. Jana and I. R. Laskar, *Inorg. Chem. Commun.*, 2016, **67**, 107–111, DOI: 10.1016/j.inoche.2016.03.017.
- 239 M. V. Babak, M. Pfaffeneder-Kmen, S. M. Meier-Menches, M. S. Legina, S. Theiner, C. Licon, C. Orvain, M. Hejl, M. Hanif, M. A. Jakupc, B. K. Keppler, C. Gaidon and C. G. Hartinger, *Inorg. Chem.*, 2018, **57**, 2851–2864, DOI: 10.1021/acs.inorgchem.7b03210.
- 240 L. Tabrizi, B. Zouchoune and A. Zaiter, *RSC Adv.*, 2018, **9**, 287–300, DOI: 10.1039/C8RA08739C.
- 241 D. Hu, C. Yang, C. Lok, F. Xing, P. Lee, Y. M. E. Fung, H. Jiang and C. Che, *Angew. Chem., Int. Ed. Engl.*, 2019, **58**, 10914–10918, DOI: 10.1002/anie.201904131.
- 242 A. Ionescu, R. Caligiuri, N. Godbert, L. Ricciardi, M. La Deda, M. Ghedini, N. Ferri, M. G. Lupo, G. Facchetti, I. Rimoldi, *Appl Organometal Chem.*, 2020, **46**, e5455, DOI: 10.1002/aoc.5455.
- 243 M. Vaquero, N. Busto, N. Fernández-Pampín, G. Espino and B. García, *Inorg. Chem.*, 2020, **59**, 4961–4971, DOI: 10.1021/acs.inorgchem.0c00219.
- 244 R. Lara, G. Millán, M. T. Moreno, E. Lalinde, E. Alfaro-Arnedo, I. P. López, I. M. Larráyo and J. G. Pichel, *Chem. Eur. J.*, 2021, **27**, 15757–15772, DOI: 10.1002/chem.202102737.
- 245 P. Van Thong, L. Van Meervelt and N. T. T. Chi, *Polyhedron*, 2022, **228**, 116180, DOI: 10.1016/j.poly.2022.116180.
- 246 N. Fernández-Pampín, M. Vaquero, T. Gil, G. Espino, D. Fernández, B. García and N. Busto, *J. Inorg. Biochem.*, 2022, **226**, 111663, DOI: 10.1016/j.jinorgbio.2021.111663.
- 247 J. Yang, D. L. Chen, P. C. Wang, B. Yang and C. Z. Gao, *Eur. J. Med. Chem.*, 2022, **243**, 114702, DOI: 10.1016/j.ejmech.2022.114702.
- 248 J. Yang, W. T. Wang, Z. D. Shi, R. Yang, X. L. Liao, B. Yang and C. Z. Gao, *J. Inorg. Biochem.*, 2022, **237**, 111992, DOI: 10.1016/j.jinorgbio.2022.111992.



- 249 Y. Liu, H. Zhao, L. Li, B. Yang, Y. Yue, M. Li, X. Shi, B. Zhang, L. Wang, C. Qi, Y. Liu, S. Ren, K. Zhang and J. Yoon, *Sens Actuators B Chem*, 2023, **374**, 132836, DOI: 10.1016/j.snb.2022.132836.
- 250 T. Maier, J. Wutschitz, N. Gajic, M. Hejl, K. Cseh, S. Mai, M. A. Jakupc, M. S. Galanski and B. K. Keppler, *Dalton Trans.*, 2023, **52**, 16326–16335, DOI: 10.1039/D3DT01736B.
- 251 W. Wang, P. Wang, F. Shen, C. Gao and J. Yang, *ACS Nano*, 2024, **18**, 5656–5671, DOI: 10.1021/acsnano.3c11366.
- 252 T. Zou, J. Liu, C. T. Lum, C. Ma, R. C. T. Chan, C. N. Lok, W. M. Kwok and C. M. Che, *Angew. Chem., Int. Ed. Engl.*, 2014, **53**, 10119–10123, DOI: 10.1002/anie.201405384.
- 253 D. A. K. Vezzu, Q. Lu, Y. H. Chen and S. Huo, *J. Inorg. Biochem.*, 2014, **134**, 49–56, DOI: 10.1016/j.jinorgbio.2014.01.021.
- 254 J. A. Gareth Williams, A. Beeby, E. Stephen Davies, J. A. Weinstein and C. Wilson, *Inorg. Chem.*, 2003, **42**, 8609–8611, DOI: 10.1021/ic035083+.
- 255 R. E. Doherty, I. V. Sazanovich, L. K. McKenzie, A. S. Stasheuski, R. Coyle, E. Baggaley, S. Bottomley, J. A. Weinstein and H. E. Bryant, *Scientific Reports 2016 6:1*, 2016, **6**, 1–9, DOI: 10.1038/srep22668.
- 256 L. Tabrizi and H. Chiniforoshan, *J. Organomet. Chem.*, 2016, **818**, 98–105, DOI: 10.1016/j.jorganchem.2016.06.013.
- 257 J. Li, X. He, Y. Zou, D. Chen, L. Yang, J. Rao, H. Chen, M. C. W. Chan, L. Li, Z. Guo, L. W. Zhang and C. Chen, *Metallomics*, 2017, **9**, 726–733, DOI: 10.1039/c6mt00188b.
- 258 Y. Zhu, M. Zhang, L. Luo, M. R. Gill, C. De Pace, G. Battaglia, Q. Zhang, H. Zhou, J. Wu, Y. Tian and X. Tian, *Theranostics*, 2019, **9**, 2158–2166, DOI: 10.7150/thno.30886.
- 259 T. Chatzisideri, S. Thysiadis, S. Katsamakas, P. Dalezis, I. Sigala, T. Lazarides, E. Nikolakaki, D. Trafalis, O. A. Gederaas, M. Lindgren and V. Sarli, *Eur. J. Med. Chem.*, 2017, **141**, 221–231, DOI: 10.1016/j.ejmech.2017.09.058.
- 260 Y. Zhang, Q. Luo, W. Zheng, Z. Wang, Y. Lin, E. Zhang, S. Lü, J. Xiang, Y. Zhao and F. Wang, *Inorg. Chem. Front.*, 2018, **5**, 413–424, DOI: 10.1039/C7QI00346C.
- 261 P. K. Wan, K. C. Tong, C. N. Lok, C. Zhang, X. Y. Chang, K. H. Sze, A. S. Tsai Wong and C. M. Che, *Proc. Natl. Acad. Sci U S A.*, 2021, **118**, e2025806118, DOI: 10.1073/pnas.2025806118.
- 262 A. Escolà, M. Crespo, J. Quirante, R. Cortés, A. Jayaraman, J. Badía, L. Baldomà, T. Calvet, M. Font-Bardía and M. Cascante, *Organometallics*, 2014, **33**, 1740–1750, DOI: 10.1021/om5000908.
- 263 A. Escolà, M. Crespo, C. López, J. Quirante, A. Jayaraman, I. H. Polat, J. Badía, L. Baldomà and M. Cascante, *Bioorg. Med. Chem.*, 2016, **24**, 5804–5815, DOI: 10.1016/j.bmc.2016.09.037.
- 264 M. Solé, C. Balcells, M. Crespo, J. Quirante, J. Badia, L. Baldomà, M. Font-Bardia and M. Cascante, *Dalton Trans*, 2018, **47**, 8956–8971, DOI: 10.1039/C8DT01124A.
- 265 A. Lázaro, C. Balcells, J. Quirante, J. Badia, L. Baldomà, J. S. Ward, K. Rissanen, M. Font-Bardia, L. Rodriguez, M. Crespo and M. Cascante, *Chem. Eur. J.* 2020, **26**, 1947–1952, DOI: 10.1002/chem.201905325.



- 266 A. Abedi, V. Amani, N. Safari, S. N. Ostad and B. Notash, *J. Organomet. Chem.*, 2015, **799**–**800**, 30–37, DOI: 10.1016/j.jorganchem.2015.08.023.
- 267 P. Papadia, K. Micoli, A. Barbanente, N. Ditaranto, J. D. Hoeschele, G. Natile, C. Marzano, V. Gandin and N. Margiotta, *Int. J. Mol. Sci.*, 2020, **21**, 2325, DOI: 10.3390/ijms21072325.
- 268 A. Barbanente, V. Gandin, C. Donati, C. I. Pierro, G. Natile and N. Margiotta, *New J. Chem.*, 2023, **47**, 18386–18399, DOI: 10.1039/D3NJ03617K.
- 269 X. Su, B. Liu, W. J. Wang, K. Peng, B. B. Liang, Y. Zheng, Q. Cao and Z. W. Mao, *Angew. Chem., Int. Ed. Engl.*, 2023, **62**, e202216917 DOI: 10.1002/anie.202216917.
- 270 O. Mallick Ganguly, S. Moulik, *Dalton Trans*, 2023, **52**, 10639–10656, DOI: 10.1039/D3DT00659J.
- 271 D. A. da Silva, A. De Luca, R. Squitti, M. Rongioletti, L. Rossi, C. M. L. Machado, G. Cerchiaro, *J. Inorg. Biochem*, 2022, **226**, 111634, DOI: 10.1016/j.jinorgbio.2021.111634.
- 272 C. R. Munteanu, K. Suntharalingam, *Dalton Trans*, 2015, **44**, 13796–1380, DOI: 10.1039/C5DT02101D.
- 273 A. Prabhakar, R. Banerjee, *ACS Omega*, 2019, **4**, 15567–15580, DOI: 10.1021/acsomega.9b01924.
- 274 M. Callari, J. R. Aldrich-Wright, P. L. De Souza, M. H. Stenzel, *Prog. Polym. Sci*, 2014, **39**, 1614–1643, DOI: 10.1016/j.progpolymsci.2014.05.002.
- 275 Y. Dang, J. Guan, *Smart Mater Med*, 2020, **1**, 10–19, DOI: 10.1016/j.smaim.2020.04.001.
- 276 W. H. Abuwatfa, W. G. Pitt, G. A. Hussein, *J. Biomed. Sci*, 2024, **31**, 31:7, DOI: 10.1186/s12929-024-00994-y.
- 277 H. Lu, M. H. Stenzel, *Small*, 2018, **14**, 1702858, DOI: 10.1002/smll.201702858.
- 278 S. Salunke-Gawali, E. Pereira, U. A. Dar, S. Bhand, *J. Mol. Struct*, 2017, **1148**, 435–458, DOI: 10.1016/j.molstruc.2017.06.130.
- 279 S. Banerjee, A. R. Chakravarty, *Acc. Chem. Res*, 2015, **48**, 2075–2083, DOI: 10.1021/acs.accounts.5b00127.
- 280 S. Monro, K. L. Colón, H. Yin, J. Roque, P. Konda, S. Gujar, R. P. Thummel, L. Lilge, C. G. Cameron, S. A. McFarland, *Chem. Rev*, 2019, **119**, 797–828, DOI: 10.1021/acs.chemrev.8b00211.
- 281 Y. Wu, S. Li, Y. Chen, W. He, Z. Guo, *Chem. Sci*, 2022, **13**, 5085–5106, DOI: 10.1039/d1sc05478c.
- 282 J. Xu, J. Wang, J. Ye, J. Jiao, Z. Liu, C. Zhao, B. Li, Y. Fu, *Adv. Sci*, 2021, **8**, 2101101, DOI: 10.1002/advs.202101101.



- 283 M. Redrado, V. Fernández-Moreira, M. C. Gimeno, *ChemMedChem*, 2021, **16**, 932–941, DOI: 10.1002/cmdc.202000833.
- 284 Z. Zhu, X. Wang, T. Li, S. Aime, P. J. Sadler, Z. Guo, *Angew. Chem*, 2014, **126**, 13441–13444, DOI: 10.1002/ange.201407406.
- 285 P. Nagababu, A. K. Barui, B. Thulasiram, C. S. Devi, S. Satyanarayana, C. R. Patra, B. Sreedhar, *J. Med. Chem.* 2015, **58**, 5226–5241, DOI: 10.1021/acs.jmedchem.5b00651.
- 286 B. T. Elie, Y. Pechenyy, F. Uddin, M. Contel, *JBIC*, 2018, **23**, 399–411, DOI: 10.1007/s00775-018-1546-8.
- 287 T. S. Morais, Y. Jousseume, M. F. M. Piedade, C. Roma-Rodrigues, A. R. Fernandes, F. Marques, M. J. Villa De Brito, M. Helena Garcia, *Dalton Trans*, 2018, **47**, 7819–7829, DOI: 10.1039/c8dt01653d.
- 288 H. H. Repich, V. V. Orysyk, L. G. Palchykovska, S. I. Orysyk, Y. L. Zborovskii, O. V. Vasylenko, O. V. Storozhuk, A. A. Biluk, V. V. Nikulina, L. V. Garmanchuk, V. I. Pekhnyo, M. V. Vovk, *J. Inorg. Biochem*, 2017, **168**, 98–106, DOI: 10.1016/j.jinorgbio.2016.12.004.



Data Availability Statement

No primary research results, software or code have been included and no new data were generated or analysed as part of this review.

